DRUG RELEASE USING pH-RESPONSIVE DRUG DELIVERY SYSTEM

TAN PANG KERN JEREMY

SCHOOL OF MECHANICAL AND AEROSPACE ENGINEERING

A thesis submitted to the Nanyang Technological University
in partial fulfillment of the requirement for the degree of
Doctor of Philosophy

2009

ACKNOWLEDGEMENTS

I would like to express my gratitude to Professor Tam Kam Chiu and Professor Yue Chee Yoon for their continuous guidance, support and encouragement during my experimental studies and interpretation of results. I would like to acknowledge Dr. Maureen Tan, Dr. P. Ravi, Dr. Dai Sheng, Dr. Wang Chang, Ms Brenda Liu, Ms Ai Hwa and Ms Elaine He for their assistance, supports and advice, which are vital to the successful progress of this research. I also like to extend my sincere thanks to all the technical staff and friends in Materials Laboratory for their kind support. Lastly, I would like to thank Nanyang Technological University for providing the financial support to pursue this research project.

On this occasion, I am thankful to my family and wife, Melissa Lim, for their constant encouragement and for giving me their blessing to pursue my studies.

TABLE OF CONTENTS

ABSTRACT

The colloid phenomenon of soft particles is becoming an important area of research due to the growing interest in using polymeric systems for drug delivery applications. The former studies have focused on techniques that required the intermediate steps of dialysis or centrifugation, whereas, in this study, a drug selective electrode (DSE) was used to directly measure the concentration of procaine (PrHy) or imipramine (IMI) hydrochloride released from pH-responsive colloidal particles, thereby eliminating the intermediate step. The PrHy and IMI selective membrane exhibited excellent reproducibility and stability.

With a single drug delivery system (methacrylic acid-ethyl acrylate (MAA-EA) nanogel), release of two different drugs loaded by distinctly different interactions was demonstrated. PrHy was found to be hydrophobically bounded, while IMI was bounded electrostatically to the MAA–EA nanogels, which were further enhanced by hydrogen bonding. The different kinds of interactions produced different release kinetic profiles. Mathematical fitting of the release kinetic profiles to the Berens and Hopfenberg model allowed the quantification of parameters that describe the contributions of chain relaxation and diffusion process. A balance between chain relaxation and Fickian diffusion process controls the release of drugs from these pH-responsive nanogels.

The coated nanogels with encapsulated drugs were successfully prepared by layer by layer (LBL) assembly approach. The initial burst release behavior observed in the nanoparticles was minimized and eliminated by the introduction of several

polyelectrolyte layers. Through this LBL approach, the permeability of nanogels was altered and with each additional polyelectrolyte layer, the time to achieve the steady state drug concentration increased linearly with the number of polyelectrolyte layer. LBL coating of responsive nanogels provided an elegant solution that may be suitable for designing nanoparticles for drug delivery applications, where the high initial burst release and short therapeutic time range can be adequately managed.

pH-responsive nanogels with varying glass transition temperature (T_g) were synthesized via emulsion polymerization for elucidating the effect of swelling on the drug release. With a higher chain rigidity (high T_g), the swelling ability of the nanogels was reduced, which would have a significant effect on the release of PrHy. With a lower swelling capacity (higher T_g), the porosity of the nanogels was minimized resulting in a slower release of the drugs from the nanogels. The DSE was proven to be a versatile and simple technique to quantify the release kinetic profiles of the cross-linked nanogel system.

LIST OF PUBLICATIONS

Jeremy P. K. Tan, K. C. Tam. Application of drug selective electrode in the drug release study of pH-responsive microgels. **Journal of Controlled Release.** 2007, 118, 87 – 94.

Jeremy P. K. Tan, C. H. Goh, K. C. Tam. Comparative drug release studies of two cationic drugs from pH-responsive nanogels. **European Journal of Pharmaceutical Sciences.** 2007, 32, 340 – 348.

Jeremy P. K. Tan, Angeline Q. F. Zeng, C. C. Chang, K. C. Tam. Release kinetics of procaine hydrochloride (PrHy) from pH-responsive nanogels: Theory and experiments. **International Journal of Pharmaceutics.** 2008, 357, 305 – 313.

Jeremy P. K. Tan, Q. Wang, K. C. Tam. Control of burst release from nanogels via layer by later assembly approach. **Journal of Controlled Release.** 2008, 128, 248 – 254.

B. S. Ho, B. H. Tan, Jeremy P. K. Tan, K. C. Tam. Inverse microemulsion polymerization of sterically stabilized polyampholyte microgels. **Langmuir.** 2008, 24, 7698 – 7703.

Jeremy P. K. Tan, Tam K. C. Microgels for drug delivery applications. Structure and functional properties of colloidal systems. Taylor and Francis Group. (In Press).

LIST OF FIGURES

LIST OF TABLES

LIST OF SYMBOLS

MAA	:	Methacrylic acid
EA	:	Ethyl acrylate
BMA	:	Butyl methacrylate
MMA	:	Methyl methacrylate
DAP	:	Di-allyl phthalate
PEGMA	:	Poly(ethylene glycol)methacrylate
α	:	Degree of neutralization
η	:	Intrinsic viscosity
R_g	:	Radius of gyration
R_h	:	Hydrodynamic radius
Π_{in}	:	Osmotic pressure of the mobile ions inside the microgel
Π_{out}	:	Osmotic pressure of the mobile ions in the bulk solution
Π_{el}	:	Elastic pressure of the polymeric network
Q	:	Swelling ratio at infinite dilution
N_x	:	Cross-linked density
c_0	:	Polymer concentration inside the particles at collapsed state
C_{in}	:	Concentration of counter ions inside microgel
C_{out}	:	Concentration of counter-ions outside microgel
c	:	Concentration of the polymer solution in grams per millimeter
c_{COOH}	:	Total concentration of methacrylic acid groups
x	:	Molar fraction of methacrylic acidic groups
y	:	Molar fraction of ethyl acrylate groups

z	:	Weight percent of cross-linker
κ_{in}^{-1}	:	Debye length
$\mathbf{l}_B$	:	Bjerrum length
N_A	:	Avogadro number
Γ	:	Fraction of counter-ions in the solution
$\tilde{Q}$	:	Swelling ratio at finite concentration
ϕ	:	Volume fraction of microgels in the solution
V_m	:	Molar volume of monomeric units
ρ_s	:	Specific mass of suspension in g/ml
ρ_p	:	Specific mass of polymer in g/ml
M_w	:	Weight average molecular weight
M_n	:	Number averaged molecular weight
A_2	:	Second virial coefficient
$\vec{k}$	:	Incident wave vector
n_0	:	Medium refractive index
ω_0	:	Circular frequency in vacuum
θ	:	Scattering angle
q	:	Magnitude of the scattering vector
λ	:	Wavelength
I	:	Intensity of scattered light
ε_0	:	Electric permittivity of vacuum
n_p	:	Number of polymer chains in the scattering volume
$S(q,c)$	:	Static structure factor
N	:	Monomer number of polymer chain

ρ	:	Local segment density
$f_D(x)$	:	Debye function
P(q)	:	Form factor or internal structure factor
K	:	Optical constant
R	:	Rayleigh ratio
dn/dc	:	Refractive index increment of the polymer solution
τ	:	Decay time
β	:	Coherence factor
$G_1(t)$	:	Field autocorrelation function
$g_1(t)$	:	Normalized field autocorrelation function
$G_2(t)$	:	Autocorrelation function of scattered intensity
$g_2(t)$	:	Normalized autocorrelation function of scattered intensity
$S(q,c,\tau)$	:	Dynamics structure factor
D	:	Translational diffusion coefficient
$w(\Gamma)$	:	Continuous distribution function of decay rate
k	:	Boltzmann constant
ΔE^o	:	Standard potential of the cell
a_i	:	Activity of ion *i*
R	:	Universal gas constant
n	:	Charge number of ion *i*
F	:	Faraday constant
$\Delta\Phi_M$	:	Membrane potential
E_{ISE}	:	Potential of ion selective electrode
v	:	Total volume of microgel sample
ΔH	:	Enthalpy

T	:	Transmittance
P	:	Radiant power leaving the sample
P_0	:	Radiant power directed at the sample
A	:	Absorbance
ε	:	Molar absorbtivity
b	:	Path length
$\bar{\Gamma}$	:	First cumulant
μ_2	:	Second cumulant
C_{Na^+}	:	Concentration of mobile sodium, Na^+ ions in bulk solution
C_{K^+}	:	Concentration of mobile potassium, K^+ ions in bulk solution
M_t	:	Amount of drugs released at time t
M_∞	:	Amount of drugs released at infinite time or total amount of drugs incorporated in the carrier
D_o	:	Diffusion coefficient
ϕ_F	:	Fractions of sorption contributed by Fickian diffusion
ϕ_R	:	Fractions of sorption contributed by chain relaxation
T_g	:	Glass transition temperature

1.0 INTRODUCTION

1.1 Background

Polymeric drug delivery systems in the form of beads, pellets, microspheres and nanospheres have been developed to supplement conventional single or multiple dosage delivery modes [Kumar et al., 2002]. Through this method, optimization of pharmacological activity of drug and reduction in toxicity level can be achieved and this will address some of the challenges in modern drug therapy, such as the optimization of pharmacological action of drug and reduction in toxicity level. Through the control of precise level or location of drug in the body, side effects are reduced, lower dosage is possible, toxicity level is reduced and new therapies are possible [Langer, 2001].

The criteria used for the design of a drug delivery system are commonly based on the drug's physicochemical and pharmacokinetic properties. Currently, significant efforts have been devoted to develop controlled release devices for the delivery of rapidly metabolized drugs [Lopez et al., 2005]. One strategy is to use colloidal drug carriers that can provide site specific or targeted drug delivery with an optimum drug release profile [Mathiowitz, 1999]. Release systems based on the swelling controlled of nanoparticles (like nanogels) seem to fit the above requirements. The colloidal phenomenon of soft particles is becoming an important field of research due to the growing interest in using polymeric system in drug delivery. New controlled release systems that respond to changes in the external environmental conditions like temperature, pH, light, electric fields and certain chemicals are developed. Such systems, which are useful in pulsed drug delivery, normally undergo changes in their structures or intra-molecular

interactions brought about by external stimuli. Nanoparticles have been widely reported to be ideal systems for such site specific delivery applications [Roman et al., 2004].

Various forms of controlled drug release formulations have been attempted, depending on the end-use specification, such as nanoparticles, microparticles, hydrogels and liposomes [Mathiowitz, 1999]. Nanoparticles or nanogels are solid colloidal particles with size ranging from 10 to below 1000 nm. The uptake of particles via the membranous-cells (M-cells) and peyer's patch will increase with decreasing particle sizes [Sahoo et al., 1998], which is the major reason for the popularity in using nanoparticles as drug carriers. Depending on the method of preparation, two different types of nanoparticles can be achieved, namely nanospheres and nanocapsules [Mathiowitz, 1999]. Nanospheres have a matrix typed structure in which a drug is dispersed whereas nanocapsules possess a membrane-like wall structure with a core containing the drugs. As these systems have high surface areas, drugs can be absorbed onto the surface leading to a phenomenon called burst release.

There are two goals that should be satisfied in the design of an efficient drug delivery system [Bruce et al., 1994], namely:

i. efficient binding of drugs to the polymeric matrix and the release of the drugs in a controlled manner,
ii. ability to release drugs through a local or externally applied trigger by changing the binding affinity between the drug and polymeric matrix.

Previous studies [Govender et al., 1999; Madeline and Peppas, 1999; Soppimath et al., 2001; Yang et al., 2004] on drug release using nanoparticles have focused on using

techniques like UV-spectrophotometer, fluorescence or high performance liquid chromatography (HPLC). All these techniques would require the use of a dialysis membrane or centrifugal machine to isolate the nanoparticles from free drugs prior to the quantification of the concentration of released drugs. Hence, the measurements of drug concentrations may be affected, as drug released from delivery vehicles may absorb on the dialysis membrane or the high centrifugal forces may expel drugs from the delivery vehicle. However, in this study, a novel technique making use of a drug selective electrode (DSE) to directly measure the concentration of free drugs without the need of a dialysis membrane or centrifugal machine is explored. The benefits of DSE are that intermediate steps, such as dialysis membrane or centrifugation machine can be eliminated and automation of the whole process is feasible. This method yields reproducible drug release profiles, and thus is more efficient. A comprehensive model that describes both the diffusion and relaxation contributions to the drug release kinetics has been proposed by Berens and Hopfenberg [Enscore et al., 1977; Berens and Hopfenberg, 1978]. Since this is a non-linear model, a larger number of data points would be required to generate a statistically meaningful model fitting, and hence this model was often not used. In most drug release kinetic studies, the release of drugs from the dialysis membrane and nanoparticles were measured. Hence, the relaxation contribution of drug release from the nanoparticles often cannot be observed. With the use of DSE in this study, dialysis membrane was not necessary, thus the relaxation contribution of drug release from nanoparticles can now be measured and DSE is the only method able to generate a large number of data points.

Particles in the range of below 500 nm are known to be able to diffuse through the submucosal layers but the large surface to volume ratio will promote higher burst release

[Arifin et al., 2006]. Hence, the control of burst release is essential. The layer by layer (LBL) coating can be used for drug release applications. By adopting this strategy in this study, the initial burst release was alleviated, and this technique offers potential advantages:

(1) simplicity as this only involves electrostatic attraction between oppositely charged polyelectrolyte and the layer thickness can be generated with nanometer precision,

(2) more cost efficient and practical than chemically modifying the surface of nanoparticles and,

(3) the release process can be extended by manipulating the number of polyelectrolyte layers.

pH responsive nanogels consisting of methacrylic acid-ethyl acrylate (MAA-EA), methacrylic acid-butyl methacrylate (MAA-BMA) and methacrylic acid-methyl methacrylate (MAA-MMA) cross-linked with di-allyl phthalate (DAP) were synthesized via emulsion polymerization technique. The nanogels are insoluble lattices at low pH and increasing the pH, the ionization of acid groups is enhanced, which increases the solubility and electrostatic repulsion between polymeric chains, yielding interesting changes in particle interaction potential. An advantage of using pH-responsive drug delivery carriers is that by varying pH or ionic strength, the release profile of drugs can be controlled.

1.2 Objectives

The objectives of the present research are:

1. To develop a drug selective membrane electrode for quantifying the kinetics of drug release from pH-responsive drug carriers,
2. To elucidate the drug loading mechanism and characteristics of drug carriers on the drug loading capability,
3. To lower or eliminate the burst release process through a simple layer by layer (LBL) coating process, and
4. To obtain the diffusion coefficient and characteristics relaxation time through a mathematical fitting of the data based on a diffusion model.

These are achieved by performing quantitative studies on the effect of different compositions of ion exchangers and solvent mediator on the sensitivity of the drug electrode. Laser scattering techniques (both static and dynamic) (LLS) were utilized to measure the hydrodynamics radius (R_h), radius of gyration (R_g) and molecular weight (M_w), which would provide insights into the neutralization and microstructure behavior of cross-linked nanogels. Isothermal titrating calorimeter (ITC), LLS and ζ-potential were utilized to elucidate the binding behavior of drug-polymer systems. Drug release using pH-responsive, chemically cross-linked nanogel particles would be conducted under different conditions (e.g. varying pH, salt concentration and concentration gradient) to obtain the diffusion coefficient and characteristics relaxation time. The drug release kinetic profiles for nanoparticles would be obtained using the drug selective electrode, and the use of dialysis membrane or centrifugal machine, which might not truly reflect the release of drugs from delivery systems would not be necessary.

1.3 Overview of thesis

Chapter 2 provides an overview of microgel and nanogel synthesis and fundamental knowledge of swelling and deswelling theories of pH-responsive microgels. In addition, the later parts of Chapter 2 provide an overview of drug release using microgel and nanogel based delivery vehicles. The use of drug selective electrodes for quantifying the drug release kinetics will be reviewed. Description of the chemical structures and synthesis procedures for the polymers and theories of related research techniques are documented in Chapter 3. Chapter 4 presents detailed characterizations on the reliability and reproducibility of the drug selective membrane. The effect of pH and selectivity of these drug selective membranes are also reported. Chapter 5 describes the drug and MAA-EA nanogels interaction and changes in particle sizes and drug loading capability with varying procaine hydrochloride (PrHy) concentration. Drug release under varying parameters (e.g. pH and drug loading) were performed using the DSE and modeled with Berens and Hopfenberg model. Chapter 6 illustrates the coating of MAA-EA nanogels using the LBL technique to eliminate or minimize the burst release phenomenon. PrHy interaction with nanogels with different glass transition temperature (T_g) was elucidated and the effects of polymeric T_g on the release behavior are discussed in Chapter 7. Berens and Hopfenberg model was used to extract the diffusion coefficient to clearly illustrate the effect of T_g. Chapter 8 describes the usefulness of MAA-EA nanogels in loading and releasing another cationic drug, imipramine hydrochloride (IMI). IMI interaction with MAA-EA nanogels and the effect on the particle size of MAA-EA nanogels will be discussed.

2.0 LITERATURE REVIEW

The literature review is divided into six separate parts. The first part summarizes the synthetic methods using emulsion and solution polymerization for producing the nanogels. The second section will describe the characteristics of anionic and polyampholyte nanogels and swelling theory of anionic nanogels, while the third section discusses the layer by layer coating method and its utility in drug release application. Controlled drug release using nanogels will be described in details in the fourth section, and the theory of laser light scattering and drug selective electrodes will be reviewed in section five and six respectively.

2.1 General aspect of microgel and nanogel synthesis

Gelation is the result of a cross-linking process of polymeric chains to produce a three-dimensional network of infinitely large size [Carothers, 1931]. The term “infinitely large”, according to Flory, refers to a molecule having dimensions of an order of magnitude that approaches the containing vessel [Flory, 1941]. Thus, such polymeric molecules are finite in size but by comparison with ordinary molecules, they may be considered infinitely large [Flory, 1941]. However, by decreasing the size of the vessel through decreasing the concentration of the emulsifier, the size of the microgel produced can be reduced to nano length scale.

Since microgels are intra-molecularly cross-linked macromolecules, the size of the growing cross-linked molecules must be controlled during synthesis. This can be

accomplished by carrying out the polymerization and cross-linking in a restricted volume, i.e., in a surfactant micelle acting as an emulsifier. Four methods have been reported for the preparation of microgel particles: namely emulsion polymerization [Clarke and Vincent, 1981; Pelton and Chibante, 1986], anionic co-polymerization [Okay and Funke, 1990; Okay and Funke, 1990; Antionietti et al., 1995], cross-linking of neighboring polymer chains [Frank and Burchard, 1991] and micro-emulsion polymerization [Neyret and Vincent, 1997].

For emulsion polymerization, each micelle in an emulsion behaves like a separate micro-continuous reactor that contains all the different monomers and radicals in aqueous phase, where the hydrophobic monomer will be emulsified by surfactants. Emulsion polymerization is a versatile technique that can give rise to particles with narrow size distributions. There are three regimes in emulsion polymerization: In Region I, initiation occurs where particles are nucleated. In Region II, the particles grow by diffusion of monomers from droplets through the aqueous phase to into the particles. When the monomers in the droplets have been consumed, Region III commences, where the residual monomer in the particles and any monomer dissolved in the aqueous phase are polymerized. The end of Region III corresponds to the completion of polymerization reaction. Emulsion polymerization can be performed in the presence of added surfactants, such as in the synthesis of MAA-EA nanogel [Cloitre et al., 2003; Tan et al., 2004], PNIPAM nanogel [Matsummura and Iwai, 2005] or in the absence of added surfactants (surfactant free emulsion polymerization) PMMA-MAA nanogel [Saunders et al., 1997]. In the latter method, the charged polymer chains formed during polymerization act as surfactant molecules that stabilize the growing particles. The inverse emulsion polymerization technique [Chen et al., 1997; Neyret and Vincent, 1997;

Zhang et al., 2005] is suitable for hydrophilic monomers, where the monomers are dispersed by emulsifiers in an organic solvent, instead of water.

This heterogeneous free-radical polymerization involves emulsification of hydrophobic monomers in water by an oil-in-water emulsifier followed by an initiation reaction via a water-soluble (sodium persulfate) or oil soluble initiator (2-20-azobisisobutyronitrile). During the polymerization, a large oil-water interfacial area is created as the nuclei are formed and grow in size as the polymerization progresses. Stabilizers, such as ionic or non-ionic surfactants and protective colloid (polyvinyl alcohol) can be either physically absorbed or chemically attached onto the particle surface to prevent coagulation of latex particles. The colloidal stability can be achieved by electrostatic stabilization, steric stabilization or a combination of both. Emulsion polymerization can be conducted in the absence of added surfactant (surfactant free emulsion polymerization), where the continuous phase will have a high dielectric constant and ionic initiators are used. The charged polymer chains formed during polymerization act as surfactant molecules that stabilize the growing particles. Surfactant free polymerization will not suffer from residual surfactant contamination unlike conventional emulsion polymerization. Thermal decomposition of the ionic initiator induces the free-radical polymerization process. The oligomers produced are surface active and form nuclei when the length of the oligomers exceeds the solubility limit of the solvent. The nuclei then undergo limited aggregation, thereby increasing the surface charge until electrostatic stabilization is achieved. The polymer growth is achieved through the absorption of monomers or oligomeric chains. Polymerization continues within the particles until another radical species enters the growing particle and termination occurs. Particle nucleation period is very short (of the order of minutes), which ensures a narrow particle size distribution. The final particle

size achieved increases with electrolyte concentration and decreasing initiator concentration.

An alternative method to prepare microgels involves anionic polymerization in the presence of a good solvent. However, the poor size uniformity due to a lack of electrostatic stabilization during polymerization limits the utility of this technique. From the work of Okay and Funke [Okay and Funke, 1990], pendant groups in divinylbenzene (DVB) are able to react with radical sites on neighboring polymeric chains resulting in network growth between neighboring particles. This will increase the polydispersity of the microgel particles. However, it is likely that particles formed using this method have a relatively uniform distribution of co-monomers because precipitation of high molecular weight chains does not occur. When a good solvent is used for both monomers, as demonstrated by Abrol and Solomon [Abrol and Solomon, 1999], a better control of the distribution of size was achieved.

An elegant approach to producing microgels is through cross-linking of neighboring particles. Since an increased in dilution during cross-linking increases the probability of intra-molecular cross-linking, the growing polymer chains in a highly diluted solution become intra-molecularly cross-linked and the structure approaches that of a microgel formed within the micelles, where the initial micelle size determines the microgel particle size. The method discussed above should produce monodispersed particle size distributions since micelles of block copolymers dispersed in hemi-solvents are usually narrow.

The concept of micro-emulsion first appeared around 1980s and this is relatively new compared to emulsion polymerization. Emulsion polymerization can be sub-divided into macroemulsion polymerization due to the large size of monomer droplets (hundreds of microns) and microemulsion polymerization due to the small size of monomer droplets (tens of nanometers). Briefly, micro-emulsion polymerization can be divided into oil-in-water (O/W) and water-in-oil (W/O) (also known as inverse micro-emulsion). The features of micro-emulsion are that they are isotropic and thermodynamically stable dispersions containing oil and water, where the stability is ensured by a very low interfacial tension capable of compensating for the dispersion entropy, which is very largely owing to the small droplet size. These interesting features of micro-emulsions result in a unique microenvironment that can be harnessed to produce novel materials with interesting morphologies or polymers with specific properties. The resulting product can be classified as nanogels. A major difference between normal and inverse emulsions comes from the amount of monomers and surfactant needed to stabilize the systems. The amount of monomer is usually restricted to 5-10 wt% with respect to the overall mass, and that of surfactants lies within the same range or greater. When emulsifier concentration exceeds a critical value, all the monomeric molecules are solubilized in the aqueous phase and the polymerization system becomes transparent, which is typical for microemulsion.

A different type of microgel can be obtained by free radical solution polymerization. Since an increased in dilution during cross-linking increases the probability of intra-molecular cross-linking, the growing polymer chains in a highly diluted solution become intra-molecularly cross-linked and the structure approaches that of a microgel formed within the micelles. Free radical solution polymerization has three important

reaction steps: chain initiation, chain propagation and chain termination. The polymerization involves at least two types of vinyl groups with different reactivities, those of monomers and pendant vinyl groups [Funke et al., 1998]. Two possible reactions of a pendant vinyl group may occur as shown in Figure 2.1: intra-molecular cross-linking (a and b) and inter-molecular cross-linking (c). Intra-molecular cross-linking occurs between pendant vinyls and radical centers located on the same macromolecule that results in the formation of cyclic chains and multiple cross-links. Inter-molecular cross-linking between pendant vinyl groups and radical centers located on different macromolecules produce cross-links that are responsible for the aggregation of macromolecules. Polyurethane nanogel prepared by Graham and Mao [Graham and Mao, 1996] and MAA-g-EG hydrogel prepared by Madeline and Peppas [Madeline and Peppas, 1999] were synthesized using this technique.

Microgels or nanogels prepared by these two methods exhibit different properties. Those prepared by emulsion polymerization with sufficient amounts of cross-linker behaves like a macroscopic globular gel with similar internal structure [Funke at al., 1998]. Microgels or nanogels prepared by solution polymerization may have various shapes depending on the relative contributions of intra-molecular and inter-molecular cross-linkings [Funke et al., 1998].

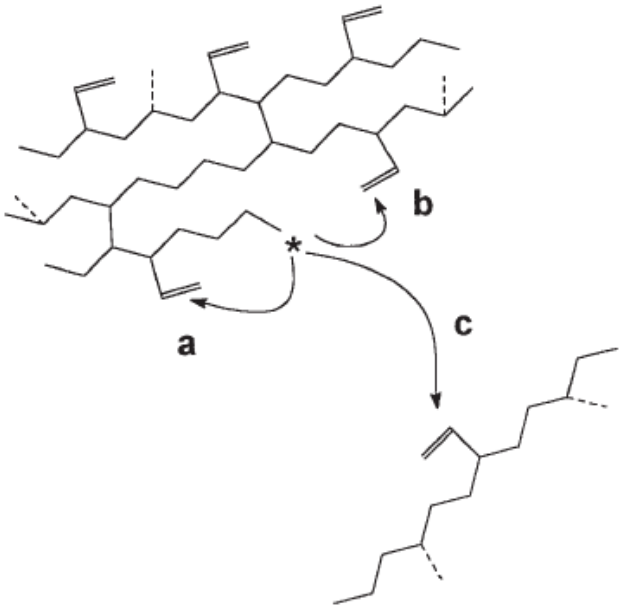

Figure 2.1 Schematic diagram showing intra-molecular cross-linking (a and b) and intermolecular cross-linking (c) [Funke et al., 1998].

2.2 Soft spherical colloidal particles

2.2.1 Characteristics of microgels

A microgel particle is an intra-molecularly cross-linked latex macromolecule, which is dispersed in a solvent and the degree of swelling depends on the degree of cross-linking and the characteristics of the solvent [Wolfe and Scopazzi, 1989; Rodriquez and Wolfe, 1994; Bartsch et al., 1997; Funke et al., 1998; Saunders and Vincent, 1999]. Staudinger and Husemann were the first to prepare microgels made of divinyl benzene (DVB) [Saunders and Vincent, 1999]. The particles are a dispersion consisting of discrete particles randomly distributed in a fluid medium [Tan Maureen, 2004]. Any dispersion containing small particles of less than 1 μm are often called colloids, a term used to describe a substance that could not diffuse through a membrane and is dictated by Brownian dynamics. Beside linear and branched macromolecules and cross-linked polymers, intra-molecularly cross-linked macromolecules (microgels) may be considered as a fourth class of macromolecules.

The soft-spherical particles in suspensions are stabilized through electrostatic charging of particles surfaces (electrostatic stabilization) or coating the particles with an absorbed layer of material (steric stabilization) [Barnes, 1989; Hunter, 2001]. The charges lead to long range repulsions that keep the particles apart so that they are not drawn together by van der Waals forces. The electrostatic interactions are long range and strong electrostatic interactions are possible even for very low particle volume fraction, as low as $\phi \approx 0.001$.

Nanogels or microgels swell considerably in good solvent and the turbidity of dispersions is observed to decrease on swelling. Due to the compact structure of nanogels or microgels, the intrinsic viscosities (η) are much smaller than linear or branched polymers. In Figure 2.2, intrinsic viscosity of copolymer divinyl benzene (DVB) and styrene (S) cross-linked with divinyl monomer (DVM) is plotted against the cross-link density (mole% DVM). The data points were taken from different sources [Shashoua and Beaman, 1958; Sieglaff, 1963; Hofmann, 1974; Antonietti et al., 1990; Bolle, 1993]. There is a reverse proportionality of η of cross-linked DVB/S to the molar ratio of cross-linker, DVM. The size of the microgel decreases rapidly with increasing cross-link density to about 3 mole% of cross-linking monomer.

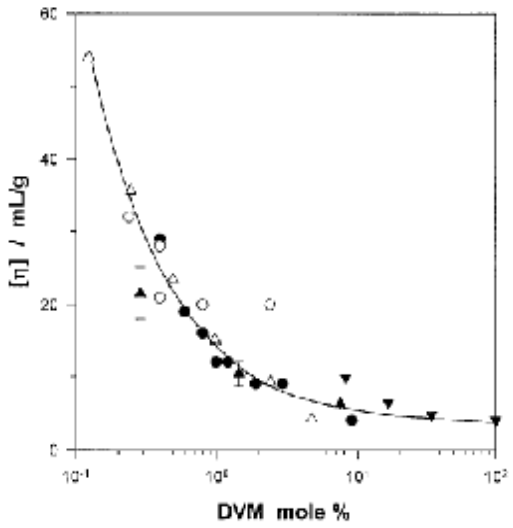

Figure 2.2 Variation of the [η] of microgels formed by emulsion polymerization with the amount of divinyl monomer (DVM) in the monomer mixture.

(˜): [Shashoua and Beaman, 1958]: technical-DVB/S microgels; measurements in benzene at 30°C.
(™): [Sieglaff, 1963]: technical-DVB/S microgels; measurements in toluene at 25°C.
(•): [Hofmann, 1974]: technical-DVB/S microgels; measurements in salt containing DMF at 25°C.
(r): [Antonietti et al., 1990]: 1,3-diisopropenylbenzene/S microgels; measurements in toluene at 20°C.
(q): [Bolle, 1993]: 1,4-DVB/S microgels; measurements in toluene at 25°C.

2.2.2 Swelling of stimuli-responsive nanogel

Nanogel particles are classified as “smart materials” because of their conformational changes in response to changes in environmental conditions (either physical or chemical) such as temperature [Senel et al., 1997], pH [Sen et al., 1999; Tan Maureen, 2004], ionic strength [Tan et al., 2004] or a change in solvent types. The extent of swelling and deswelling is an interesting property of nanogel [Benee et al., 2002]. Nanogels containing ionic co-monomers will exhibit pH-dependent swelling. The swelling of these particles are governed by the increase in internal osmotic pressure due to the mobile counter-ions contained within the nanogels, which balances the internal electrostatic repulsion [Saunders and Vincent, 1999]. The extent of swelling will depend on the quality of solvent, the ionization degree, cross-link density and ionic strength. In Figure 2.3, the hydrodynamic diameter (nm) of poly(methyl methacrylate-co-methacrylic acid) is plotted against pH [Saunders et al., 1997]. On increasing pH, swelling increases due to the ionizing of carboxylic acid groups. The rate of increase levels off at around pH 8 as the ionization attains a maximum value. The increase in ionic strength screens the internal repulsion or reduces the osmotic pressure difference inside and outside of the nanogels. Similar trends can be observed for methacrylic acid-ethyl acrylate (MAA-EA) cross-linked with di-allyl phthalate (DAP) [Tan et al., 2004; Tan et al., 2005], poly(methacrylic acid-co-acrylic acid) (PMAA-co-AA) [Eichenbaum et al., 1999] and poly(methacrylic acid-g-ethylene glycol) (PMAA-g-EG) [Madeline and Peppas, 1999].

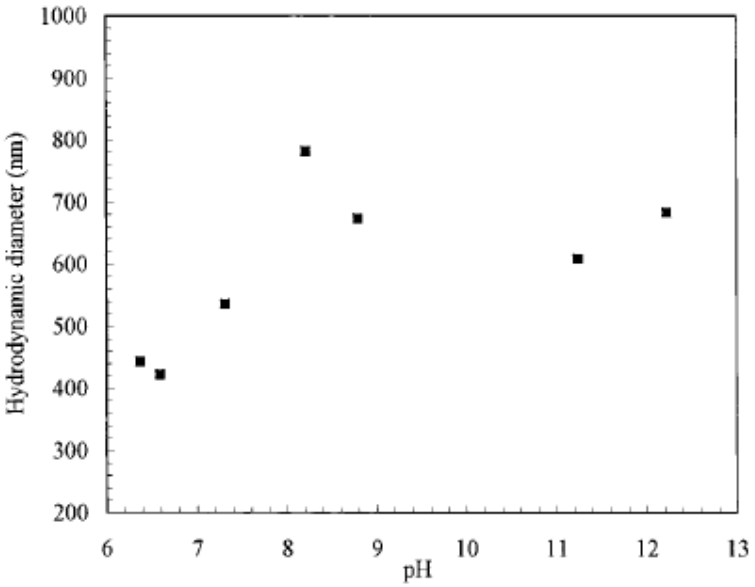

Figure 2.3 Effect of dispersion pH on the hydrodynamic diameter of poly(MMA MAA) nanogel particles [Saunders et al., 1997].

Rodriguez and Wolfe studied the changes in the internal polymer segment density and particle swelling during the alkalization of internally cross-linked MAA-EA microgels using static and dynamic light scattering [Rodriquez and Wolfe, 1994]. Upon neutralization with a base, pronounced negative deviations of the ratio of the radius of gyration (R_g) to hydrodynamic radius (R_h) from the known value for homogenous spheres along with the curvature in Guinier plots of the angular dependent light scattering intensity indicating a non-uniform polymer segment distribution within the microgels [Wolfe and Scopazzi, 1989; Antonietti et al., 1990].

For polyelectrolytes [Guo, 1997; Kjoniksen et al., 1997; Kumacheva et al., 1997] where ionic charges are present, the polymer is very sensitive to the effect of salt in solution due to the coulombic repulsive forces between similar ionic charges and the attractive interactions between hydrophobic segments. The addition of inert electrolyte will lead to

deswelling of the particles. In Figure 2.4, the hydrodynamic radius of MAA-EA-DAP microgel is plotted against degree of neutralization [Tan et al., 2004]. The free ions distribute themselves inside and outside of the microgels therefore causing a net reduction in the osmotic pressure difference in the microgels. This is an additional screening of the electrostatic repulsion within the particles.

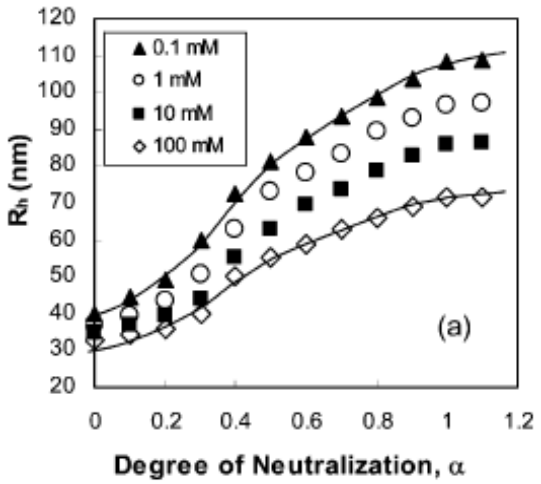

Figure 2.4 Results from dynamic light scattering illustrating the dependence of R_h on α for HASE 20-80-2 at different salt concentrations, [KCl] [Tan et al., 2004].

2.2.3 Particle swelling and deswelling theory

The equation for swelling of nanogels is due to the balance between the osmotic pressure inside the nanogels and the osmotic pressure outside [Cloitre et al., 2003]:

$$\Pi_{in} + \Pi_{el} = \Pi_{out} \tag{2.1}$$

where Π_{in} and Π_{out} are the osmotic pressure of the mobile ions inside the nanogels and in the solution respectively. Π_{el} is the elastic pressure of the polymeric network.

The elastic pressure (Π_{el}) of a polymeric network is the pressure needed to stretch the polymeric network from the collapsed state (reference state) to the swollen state:

$$\Pi_{el} = -\frac{RTc_o}{2N_x Q^{1/3}} \tag{2.2}$$

where $Q = \left(\frac{R_a}{R_{a=0}}\right)^3$ is the swelling ratio of the nanogels, N_x is the cross-link density and c_o is the polymer concentration when the particles are at the collapsed state. R_α represents the hydrodynamic radius of the particle at a particle α and $R_{\alpha=0}$ represents the hydrodynamic radius of the unneutralized ($\alpha = 0$) particle with both measured using the dynamic light scattering technique.

The terms Π_{in} and Π_{out} can be expressed as:

$$\Pi_{in} = RTC_{in}$$

$$\Pi_{out} = RTC_{out} \tag{2.3}$$

where C_{in} and C_{out} are the concentrations of ions inside and outside the nanogels respectively.

In the absence of salt, all the counter-ions associated with the ionised units are trapped inside the polymeric network by the electrostatic attraction exerted by fixed charges. Then, $C_{out} = 0$ and C_{in} is simply the concentration of ionised units inside the nanogels:

$$C_{in} = \frac{c_o x a}{Q} \tag{2.4}$$

where *x* is the molar fraction of acidic units and α is the degree of neutralization.

By combining Equations 2.1 to 2.4, the swelling ratio (Q) of the nanogels can be expressed as a function of the ionization degree and cross-linked density:

$$Q \propto \left(N_x a\right)^{3/2} \tag{2.5}$$

which assumes that all the counter-ions are trapped inside the nanogels.

Based on Figure 2.5a, Cloitre and co-workers found that the swelling ratio at maximum swelling (Q_m) is proportional to $N_x^{3/2}$. A plot of Q/Q_m as a function of $\alpha^{3/2}$ as shown in Figure 2.5b shows that when ionization degree is low, Q/Q_m is small indicating that the nanogels do not swell. When the ionization degree increases, the swelling ratio rises sharply.

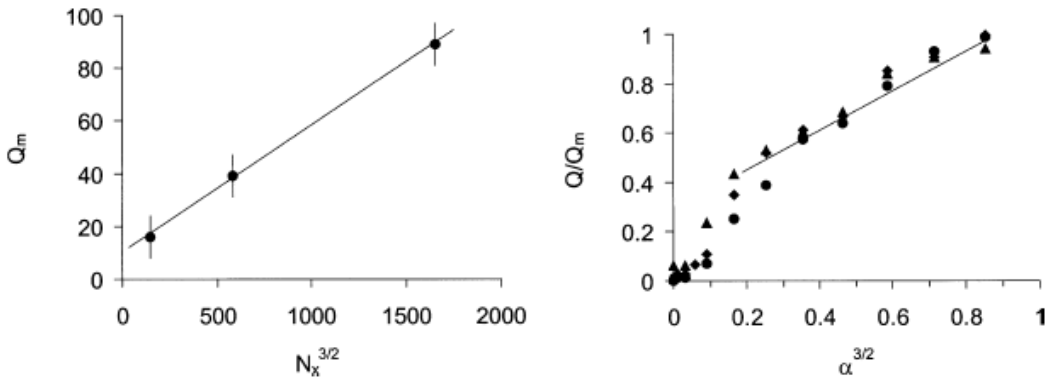

Figure 2.5 (a) Variation of the swelling ratio at maximum swelling versus the cross-link density. (b) Variation of the swelling ratio with the neutralization degree for N_x=140 (˜), N_x=70 (¿), N_x=28 (p) [Cloitre et al., 2003].

To test the previous hypothesis, Cloitre and co-workers compared the Debye length associated with the counter-ions at concentration C_{in} with the characteristic size of nanogels:

$$k_{in}^{-1} = \left(4p\mathbf{l}_B N_A C_{in}\right)^{-1/2} \tag{2.6}$$

where $\mathbf{l}_B$ is the Bjerrum length and N_A is the Avogadro number.

Only the counter-ions in the peripheral shell of thickness (κ^{-1}) can leave the nanogels and diffuse in the solution. The fraction of those counter-ions is:

$$\Gamma \cong \frac{3k_{in}^{-1}}{R_h} \tag{2.7}$$

Based on the findings by Cloitre and co-workers, a small fraction of counter-ions is not trapped and can diffuse freely in the solution. At high concentration, the concentration of free counter-ions in the solution can be large enough to induce an osmotic deswelling of the nanogels. This phenomenon can be quantified using Equations 2.1 to 2.3 where C_{in} and C_{out} can now take into account the existence of free counter-ions. The new expressions for C_{in} and C_{out} are given below [Borrega et al., 1999]:

$$C_{in} = \frac{a(1-\Gamma)zc_o}{\tilde{Q}}$$

$$C_{out} = \frac{a\Gamma yc_o f}{\tilde{Q}(1-f)} \tag{2.8}$$

where $\tilde{Q}$ is the swelling at finite concentration and ϕ is the volume fraction of nanogels in the solution.

Solving Equations 2.2, 2.3 and 2.8, the effect of osmotic deswelling can be estimated. The expression for the swelling ratio at finite concentration ($\tilde{Q}$) as a function of the swelling ratio at infinite dilution (Q):

$$\frac{\tilde{Q}}{Q} = \left(1 - \frac{\Gamma}{1-f}\right)^{3/2} \tag{2.9}$$

The volume of the nanogels can be reduced by one third near close packing ($\phi = 0.6$) and thus the osmotic deswelling of nanogels has important consequences for the flow behavior of nanogels suspensions at high concentration.

The mass concentration (c) of the dispersion and ϕ are related by:

$$f = \frac{\tilde{Q}}{V_m c_o} \frac{r_s}{r_p} c \tag{2.10}$$

where V_m is the molar volume of monomeric units and ρ_s and ρ_p are the specific mass of the suspension and polymer respectively. The volume fraction of nanogels can be easily computed using the values calculated for the swelling ratio. Cloitre and co-workers investigated nanogels with different cross-link density and showed that the data collapsed nicely on a single curve [Cloitre et al., 2003] which is very close to the analytical form for polydispersed hard sphere [Werff and Kruif, 1989]. By using the swelling ratio at infinite dilution (Q) would lead to an overestimation of the volume fraction by a large factor therefore it is crucial to use the swelling ratio at finite concentration ($\tilde{Q}$) to calculate the volume fraction of a nanogel.

2.3 Layer by layer coating

Layer by Layer (LBL) technique is a popular technique for preparing multilayered films due to its low cost, simplicity and versatility. This is not only a simple approach that would yield nanoarchitecture films with good positioning of individual layers but whose fabrication would be largely independent on the nature, size and topology of the substrate [Decher, 1997]. This technique makes use of electrostatic attractions between oppositely charged polyelectrolytes (PE) to construct layers with controllable thickness at nanometer length scale onto planar [Decher, 1997; Burke and Barrett, 2004] or curve [Caruso et al., 1998; De Geest et al., 2006; Hirsjärvi et al., 2006] surfaces. Beside the controllable thickness, different composition, morphology and chemical functionality of the surface could be achieved. The adsorption of molecules carrying more than one equal charge allows for charge reversal on the surface, which has two important consequences [Decher, 1997]: (i) repulsion of equally charged molecules and thus self-regulation of the adsorption and restriction to a single layer and (ii) the ability of an oppositely charged molecule to be adsorbed in a second step on top of the first one.

The formation forces of LBL films are not only limited to electrostatic interactions. Assemblies based on hydrogen bonding, charge transfer, covalent bonding, biological recognition and hydrophobic interactions could be carried out. Overall, the availability of a wide spectrum of fabricating components, variety of substrates and versatility of assembly methods dramatically enriches the biological applications of LBL films [Tang et al., 2006]. Moreover, multiple interactions in LBL films can potentially increase the stability of films while being exposed to physiological or even harsh conditions.

The coating process is extremely simple as depicted in Figure 2.6. When a negatively charged substrate is immersed in a solution of positively charged polyelectrolyte, such as poly(diallyldimethylammonium chloride) (PDDA), poly(allylamine hydrochloride) (PAH), or polyethyleneimine (PEI), and subsequently washed with distilled de-ionized water to remove excess or loosely bonded polyelectrolyte. There will be a charge reversal to overall positive because of the adsorption and overcompensation of polyelectrolyte (middle image in Figure 2.6B). Further immersion into a solution containing negatively charged polyelectrolyte, such as poly(styrene sulfonate) (PSS), poly(vinyl sulfate), or poly(acrylic acid) (PAA), leads to a reversal of net charge (right image in Figure 2.6B). As a result, a double layered multilayer coating is achieved. Under a cyclic coating process (Figure 2.6A), a multilayered coated substrate could be achieved with desirable structure and controllable thickness. In Figure 2.7, the effect of cyclic loading of different polyelectrolyte on the ζ-potential of negatively charged polystyrene is shown. The ζ-potential switches from negative to positive and back to negative again with different addition of polyelectrolyte layers.

In the work by Tjipto et al. [Tjipto et al., 2005], there is a systematic trend between the multilayer thickness and pH, with multilayer thickness decreasing with increasing pH. This is rationalized that at low pH, the polyelectrolyte chains have a reduced charged density and thereby adopting a more coiled conformation and able to absorb in greater amounts (as more polyelectrolyte is needed for charge overcompensation) [Tjipto et al., 2005]. The ionic strength of the deposition solutions was also found to have influenced the multilayer growth, with thinner, smoother and less regular growth of the multilayers resulted when no salt was present in the deposition solutions. Despite this, a similar trend between the multilayer thickness and pH was also observed. The ionic strength of the

solution can be seen to influence the ionization state within the multilayer film, resulting in different pH stability regimes. When salt was present in the deposition solutions, multilayers deposited at pH 2 and 5.8 were stable when placed in pH 11 while the one without salt became unstable. This is due to the complex interplay of polyelectrolyte conformation and ionization within the bulk multilayer films as the surrounding pH condition was varied [Tjipto et al., 2005].

The LBL technique may be extremely beneficial for preparing controllable shell layers of nanoparticles with varying permeabilities for drug release applications. This strategy may offer potential advantages over protein and nucleic acid encapsulation strategies: (1) the ability to control the order and location of multiple polymer layers with nano-scale precision and (2) the ability to define the concentrations of incorporated materials simply by varying the number of polyelectrolyte layers [Tang et al., 2006]. Coating created by PSS and PAH has semi permeable properties and this could be used to alter the release process or extend the therapeutic range of the controlled release device. Each polyelectrolyte pair that can be employed as layer component has unique properties that depend on the properties of each individual component and complex. The LBL assembly buildup leads to the formation of a stoichiometric inter-polyelectrolyte complex, however this stoichiometry can be violated upon any shift from the adsorption conditions [Antipov and Sukhorukov, 2004]. The most important parameters that may lead to this shift are pH and ionic strength. The change of the stoichiometry would necessarily lead to the occurrence of surplus charge and as a consequence to the change of physico-chemical properties of multilayers [Antipov and Sukhorukov, 2004].

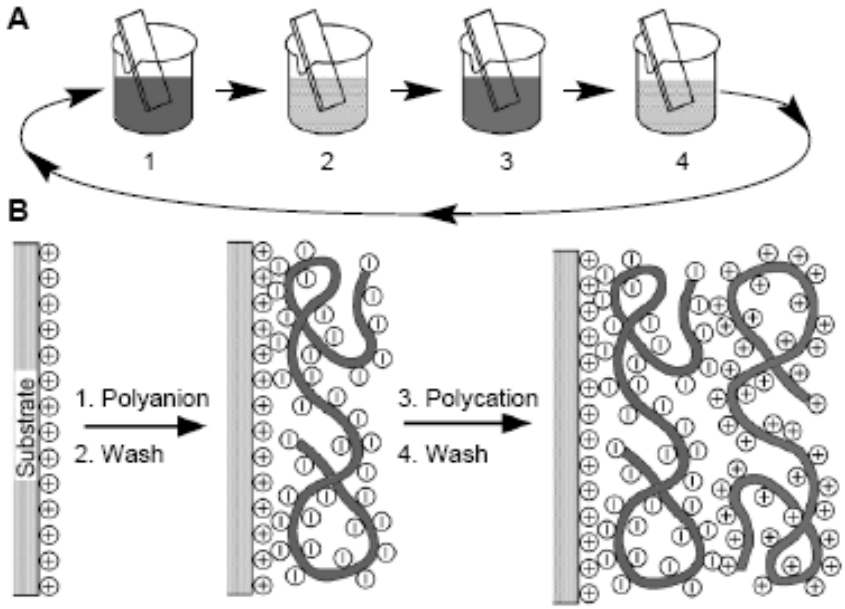

Figure 2.6 (A) Schematic of the film deposition process using slides and beakers. Steps 1 and 3 represent the adsorption of a polyanion and polycation, respectively, and steps 2 and 4 are washing steps. The four steps are the basic buildup sequence for the simplest film architecture, (A/B)*n*. The construction of more complex film architectures requires only additional beakers and a different deposition sequence. (B) Simplified molecular picture of the first two adsorption steps, depicting film deposition starting with a positively charged substrate. Counterions are omitted for clarity. The polyion conformation and layer interpenetration are an idealization of the surface charge reversal with each adsorption step [Decher, 1997].

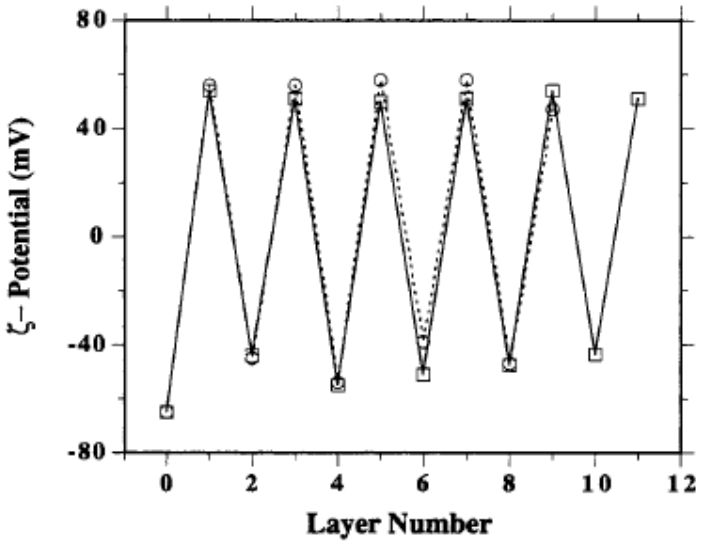

Figure 2.7 ζ-potential as a function of polyelectrolyte layer number for (circles) PAH/PSS and (squares) PDADMAC/PSS coated negatively charged PS latex particles. The odd layer numbers correspond to PAH or PDADMAC deposition and the even layer numbers to PSS deposition [Caruso et al., 1999].

2.4 Controlled drug release

2.4.1 Theoretical background of controlled drug release

Polymeric drug delivery systems have attracted increasing interest during the last two decades [Kositaz et al., 1999]. An idealized drug delivery system is one which the required amount of drug is made available at a desired time and at a specific site of action in the body [Lopez et al., 2005]. The drug delivery systems can be in various types of formulated products or dosage form (tablets, implants, injectables and transdermal patch). Through the use of such delivery systems, the efficiency of drug therapy will be greatly improved as compared to conventional dosage forms.

Polymer-based controlled release systems are normally classified into either reservoir (membrane) or matrix (monolithic) devices. In the former type, release is controlled by a polymeric membrane that surrounds the drug. For the latter, the drug is either dissolved or dispersed homogenously as solid particles throughout the polymer matrix. The released mechanisms by which the drugs can be released from the drug delivery system are diffusion, degradation and swelling followed by diffusion.

A continuous input of drug into the body can ensure that the concentration of drug remains above the lowest effective limit (ineffective range) that is required to provide the required response but does not exceed a higher value (toxic range) that will produce an excessive and possibly a dangerous response as shown in Figure 2.8. These situations are difficult to achieve with conventional dosage forms that must be administrated repeatedly at regular intervals as such administration provides a pulsed input.

Conventional dosage system has limitations like minimal synchronization between the time required for therapeutically effective drug concentrations.

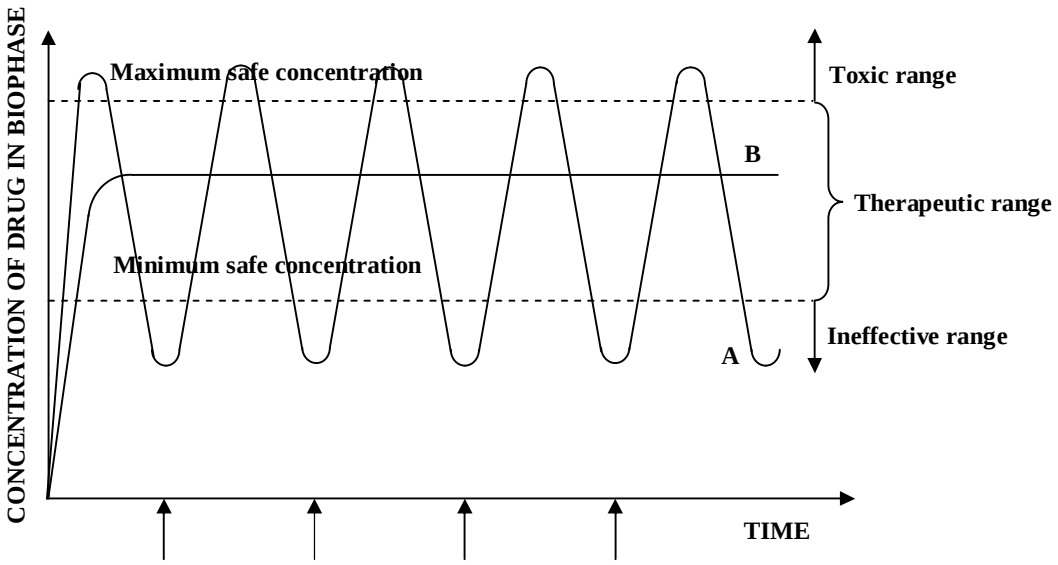

Figure 2.8 Drug concentration versus time profile of a drug following (A) administration of successive doses in a conventional dosage form (arrows indicate the time of administration and (B) a single administration of a controlled release dosage form.

The ability for a drug delivery system to maintain a desired concentration of drug in the biophase in the limits imposed by the ineffective and toxic range for an appropriate period is the most readily achievable of the two main aims of controlled release therapy. The second aim is to ensure that at least a substantial proportion of the active drug is released in the correct biophase at a controlled and satisfactory rate or is transported only to that biophase at some distant from the site of administration. The positioning of the delivery system near or adjacent to the appropriate biophase has received reasonable success. However, applications where the drug have to travel a long distance via the

blood or lymphatic site before reaching the final destination are still in their infancy [Richards, 1985].

2.4.2 pH responsive nanogels as drug delivery vehicles

The design of a drug delivery system is usually based on the drug's physicochemical and pharmacokinetic properties. Currently, investigations are ongoing to develop controlled release devices that can control the release of rapidly metabolized drugs and/or have the ability to protect sensitive drugs [Lopez et al., 2005]. Release systems based on the swelling controlled of nanoparticles (like nanogels) seem to fit the above requirements. As a result, the development of nanogels that are responsive to pH [Pillay and Fassihi, 1999; Kim and Peppas, 2003; Kurkuri and Aminabhavi, 2004] or ionic strength [Sutani et al., 2002] is an interesting area of research for the development of specific drug carriers, mainly for oral delivery. Oral delivery of drugs can be significantly improved with the use of nanoparticles as carriers since the major pathway for uptake of these particles is via the M-cells and payer's patches [Sahoo at al., 1998]. The uptake will increase with increasing hydrophobicity and decreasing particle sizes [Sahoo et al., 1998]. It has been widely reported that nanoparticles are ideal systems for such site specific delivery applications [Roman et al., 2004]. Histological studies showed that particles at 100 nm could diffuse through the submucosal layers, while larger particles (500 nm–10 μm) were found to concentrate within the epithelial tissue linings [Arifin at al., 2006].

The rate of release of drugs can be controlled by changing the pH as shown in Figure 2.9 [Sahoo et al., 1998 and Kim and Peppas, 2003]. By increasing the pH, the amount of

drug released can be increased. This is due to the swelling of the particles at high pH and the insulin or drug will be released rapidly. By changing the ionic strength in the release medium, the release profile could be modified as shown in Figure 2.10 [Sutani et al., 2002], where the drug was displaced from the polymeric network by the Na^+ ions.

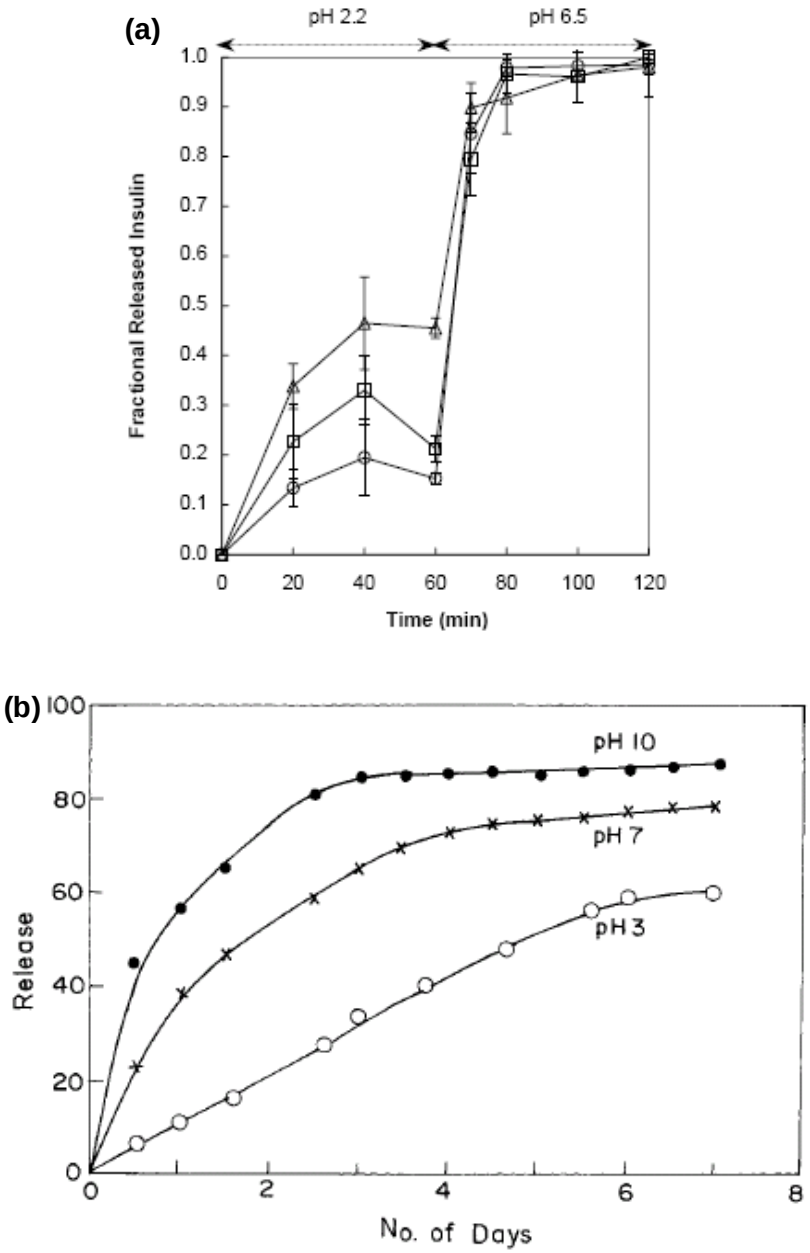

Figure 2.9 (a) Effect of the environmental pH change on the release of insulin from the insulin-incorporated P(MAA-g-EG) microparticles containing different grafted PEG chain molecular weight; PEGMA200 (○), PEGMA400 (□), and PEGMA1000 (△) (average ± S.D., n=3) [Kim and Peppas, 2003] and (b) Time dependent release of FITC-dextran from copoly[VP-AA20] nanoparticles in various pH solution at 22°C [Sahoo et al., 1998].

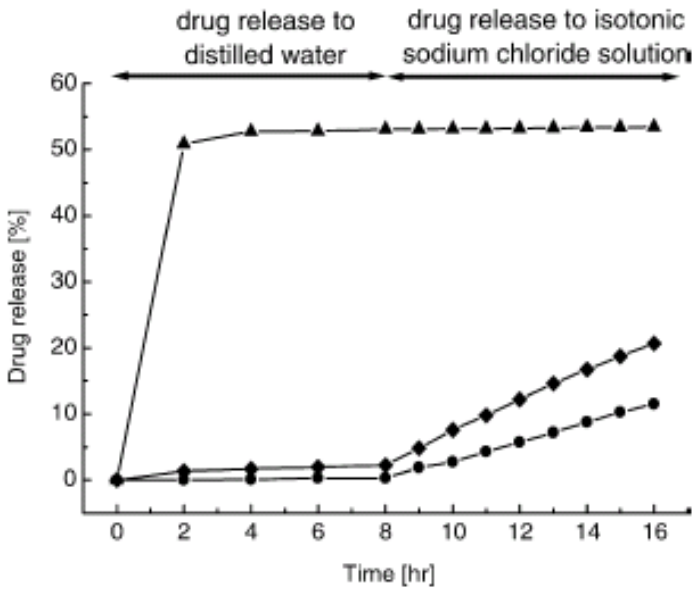

Figure 2.10 Differences in drug releases from ionic polymer gel based on 2-hydroxyethyl methacrylate (HEMA), pH sensitive monomers and cross-linker polyethyleneglycol #400 demethylacrylate (9G), in distilled water and in isotonic sodium chloride solution. Monomer composition: HEMA 100 mol, pH sensitive monomer (methylacryloyloxyethyltrimethylammonium chloride (MADQUAT), acrylic acid (AAc), 2-(dimethylammino)ethyl methacrylate (DMMA)) 10 mol, 9G 1 mol: pH sensitive monomer: (●) MADQUAT, (▲) AAc, (◆) DMMA; Ionic drug: metanil yellow (acidic drug) [Sutani et al., 2002].

2.5 Laser Light Scattering (LLS) of dilute polymer solutions

2.5.1 Theoretical background of Laser Light Scattering

Light scattering is a phenomenon of absorption and re-emission of electromagnetic radiation. When light waves fall on a molecule, the oscillating electric field associated with the light waves polarizes the electron clouds of the atoms in the molecules. These oscillating electron clouds serve as a secondary light source and emit light in different directions. This important idea suggested by Lord Rayleigh [Flory, 1953] paved the way for the development of Laser Light Scattering (LLS). Since the introduction of the idea, LLS has been widely used in determining the molecular dynamics of polymer chains.

During the early days of light scattering, only conventional chaotic lights are available thus allowing only time averaged scattered intensities to be measured. As only time averaged properties of the system are obtained, this is commonly known as Static Light Scattering (SLS) or Rayleigh scattering. The intensity of scattered light depends on the polarizability of the particles compared with that of the medium, in which, the particles are suspended, size of the particles and concentration of the particles [Flory, 1953]. The method is often used to determine microscopic properties of particles such as the z-average radius of gyration (R_g), weight average molecular weight (M_w) and second virial coefficient (A_2).

With the introduction of coherent laser sources, temporal variations of scattered light could be recorded and then subjected to spectral analyses based on the Photon Correlation Spectroscopy (PCS). Temporal variations of scattered radiation due to the random motion of the particles yield the familiar Doppler shift and the broadening of the

central Rayleigh line can be used to determine the dynamic properties of the system. This technique is often called Dynamics Light Scattering (DLS). DLS measures the intensity fluctuations with time and correlates the fluctuations to the properties of the scattering objects [Chu, 1991; Brown, 1993]. This method is often used to determine the hydrodynamic radius (R_h), polydispersity and shape of macromolecules.

In a typical experiment, a dispersion of particles is illuminated by an incident beam. The direction of propagation of this beam is defined by an incident wave vector ($\vec{k}$) with magnitude:

$$k = \frac{2pn}{l} = nw_0 c \tag{2.11}$$

where n is the medium refractive index and ω_0 is the circular frequency in vacuum. The radiation scattered by an angle (θ) with respect to the incident beam is characterized by a scattering wave vector ($\vec{q} = \vec{k}_i - \vec{k}_s$). By taking into account $\left|\vec{k}_i\right| = \left|\vec{k}_s\right|$, the magnitude of $\vec{q}$ can be represented by the following equation:

$$q = \frac{4pn}{l}\sin\left(\frac{q}{2}\right) \tag{2.12}$$

2.5.2 Static Light Scattering (SLS)

For Rayleigh scattering, the intensity of scattered light for a small particle can be described as follows:

$$\frac{I_s}{I_i} = \frac{p^2 a^2 \sin^2 q}{l^4 e_0^2 r^2} \tag{2.13}$$

where α is the polarizability of the particle and ε_0 the electric permittivity of vacuum. However, when the particle size is greater than $\lambda/20$ (e.g. high molecular weight polymer chain), the scattering intensity cannot be described by Rayleigh scattering method. Under this condition, the light scattered from different points of the particles will reach the detector with different phases. If the beams scattered from different points are coherent, this will lead to the phenomenon called intra-particle interference. Then the scattering intensity can be described by:

$$\frac{I_s}{I_i} = \frac{p^2 a^2 \sin^2 q}{l^4 e_0^2 r^2} \sum_{i,j=1}^{N} \exp\left[\mathbf{i} q.(r_i - r_j)\right] \tag{2.14}$$

When the scattering volume contains several polymer chains, the inter-particle interference also contributes to the scattered intensity. However, at low concentrations, polymer chains are sufficiently far apart and the scattering intensity for dilute polymer solution is as follows:

$$\frac{I_s}{I_i} = \frac{p^2 a^2 \sin^2 q}{l^4 e_0^2 r^2} n_p \sum_{i,j=1}^{N} < \exp\left[\mathbf{i} q.(r_i - r_j)\right] > \tag{2.15}$$

where n_p is the number of polymer chains in the scattering volume and the static structure factor (S(q,c)) is defined as the summation factor divided by N, monomer number of polymer chain:

$$S(q,c) = \frac{1}{N^2} \sum_{i,j=1}^{N} < \exp\left[\mathbf{i} q.(r_{ij})\right] > \tag{2.16}$$

The local segment density, which corresponds to the number of monomers per unit volume is defined as:

$$r(\mathbf{r}) = \sum_{m,i} d(\mathbf{r} - \mathbf{r}_{mi})$$

$$r = \langle r(\mathbf{r}) \rangle = n_p \frac{N}{V} \tag{2.17}$$

where the pair distribution function $<\rho(\mathbf{r})\rho(0)>$ is called the autocorrelation function of the segment density. The static structure factor is related to the density autocorrelation function by:

$$S(q,c) = \frac{4p}{r} \int_0^\infty \langle r(\mathbf{r}) r(0) \rangle \frac{\sin qr}{qr} r^2 dr = \frac{N_A N}{CM} \int_V \langle c(\mathbf{r}) c(0) \rangle \exp(\mathbf{i}\mathbf{q}.\mathbf{r}) dr \tag{2.18}$$

For a polymer chain with any conformation at low angle where $qR_g < 1$ (R_g is the z-average radius of gyration), the static structure can be approximated as:

$$S(q,c) = \frac{N}{1 + q^2 R_g^2 / 3} \tag{2.19}$$

In addition, the S(q,c) for a Gaussian chain at any scattering angles can be determined from the Debye function ($f_D(x)$) as follows:

$$f_D(x) = 2x^{-2}\left[1 - x^{-2}\left(1 - \exp\left(-x^2\right)\right)\right] \tag{2.20}$$

$$S(q,c) = N f_D(qR_g) \tag{2.21}$$

A plot of S(q,c) as a function of q^2 at small q gives the radius of gyration for any conformation but beyond the range, S(q,c) depends on the conformation. The form factor or internal structure factor (P(q)) is defined as the ratio of S(q,c) to S(q,0).

For Gaussian chain:

$$R_g^2 = \frac{Nb^2}{6} \tag{2.22}$$

$$P(q) = \frac{S(q,c)}{S(q,0)} = \frac{S(q)}{N} = f_D(qR_g) \tag{2.23}$$

For a hard sphere with radius (R_s):

$$R_g^2 = 0.6R_s^2 \tag{2.24}$$

$$P(q) = \left\{3(qR_s)^{-3}\left[\sin(qR_s) - (qR_s\cos(qR_s))\right]\right\}^2 \tag{2.25}$$

For a rod with rod length (L):

$$R_g^2 = \frac{L^2}{12} \tag{2.26}$$

$$P(q) = \frac{2}{qL}\int_o^{qL}\frac{\sin z}{z}dz - \left[\frac{2\sin(qL/2)}{qL}\right]^2 \tag{2.27}$$

For static light scattering on polymer solutions, the microscopic properties of particles can be determined from Zimm Plot as shown in Equation 2.28 and Figure 2.11.

$$\frac{Kc}{R_q} = \frac{1}{M_w}\left(1 + \frac{16p^2n^2R_g^2\sin^2\left(\frac{q}{2}\right)}{3l^2}\right) + 2A_2c \tag{2.28}$$

where K ($= 4p^2n^2(dn/dc)^2/N_A l^4$) is an optical constant, R ($= I_s r^2/I_t \sin q$) is the Rayleigh ratio, c is the concentration of the polymer solution in gram per milliliter, n is the refractive index of the solvent, θ is the angle of measurement, λ is the wavelength of the laser in vacuum and N_A is the Avogadro's constant. The refractive index increment of the polymer solution (dn/dc), can be measured using a differential refractometer where the values obtained was ~0.1 ml/g for all the nanogel solutions. A plot of (Kc/R_θ) against ($\sin^2(\theta/2)$ + kc) (where k is a plotting constant) and extrapolating the data to zero angles

and concentrations, R_g and A_2 can be obtained from the slopes respectively. A simultaneous extrapolation to zero angle and concentration yields an intercept which is the inverse of M_w.

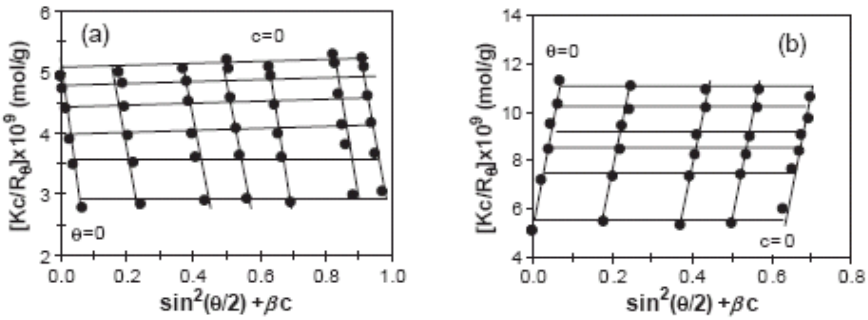

Figure 2.11 Zimm plot of HASE 20-80-2 microgel at (a) α = 0 and (b) a = 1 in aqueous solution at room temperature where the polymer concentration range was from 0.001 to 0.01 mg/ml [Tan et al., 2005]. HASE 20-80-4 refers to the microgel with 20 mole% MAA and 80 mole% EA cross-linked with 2 wt% DAP.

2.5.3 Dynamic Light Scattering (DLS)

Dynamic Light Scattering (DLS) takes into account the frequency broadening of the scattered light due to the transfer of a small amount of kinetic energy from the incident light. Therefore, DLS examines the intensity fluctuations with time and correlates these fluctuations to the properties of the scattering objects. The intensity fluctuations can either be caused by translational diffusion of particles, as they move in or out of the scattering volume, or rotational motion of non-spherical particles in the scattering volume. In general, the terms of correlation functions of dynamic variables are commonly used to describe the response of the scattering molecules to the incident light.

Due to the thermal motion, the molecules are constantly moving around and their positions and moment are changing with time. The average intensities (<I>) over long observation time (T) can be expressed by [Brown, 1993]:

$$\langle I(q)\rangle = \frac{1}{T}\lim_{T\to 0}\left(\int_0^T I(q,t)dt\right) \tag{2.29}$$

At time (t) and a time difference (τ) the intensity-intensity autocorrelation function is the average <I(t)I(t+τ)> which is a function of τ. Under the ergodicity assumption of the intensity, the autocorrelation function can be expressed by:

$$\langle I(t)I(t+t)\rangle = \lim_{T\to 0}\frac{1}{T}\int_0^T I(t)I(t+t)dt \tag{2.30}$$

In order to study the dynamic properties of the scattering system, correlation functions need to be obtained from the time dependent measurements. These functions can then be transformed using Fourier transformation techniques to yield appropriate scattering spectra that contain molecular information on the dynamics of the molecules. The autocorrelation function of scattered intensity is described below [Brown, 1993]:

$$G_2(t) = \langle I(t)I(t+t)\rangle \tag{2.31}$$

The normalized form of Equation 2.31 is shown below:

$$g_2(t) = \frac{\langle I(t)I(t+t)\rangle}{\langle I(t)^2\rangle} \tag{2.32}$$

where I(t) is an average value of the product of the scattered intensity at an arbitrary observation time (t) and I(t+τ) is the intensity at decay time (τ). The above expression can be simplified using Siegert relations [Brown, 1993]:

$$G_2(t) = B\left(1 + b\left|g_1(t)\right|^2\right) \tag{2.33}$$

$$g_2(t) = 1 + b\left|g_1(t)\right|^2 \tag{2.34}$$

where B is the baseline and β is the coherence factor that is normally considered an adjustable parameter in the data analysis procedure.

The other two correlation functions: field autocorrelation function ($G_1(t)$), and normalized field autocorrelation function ($g_1(t)$) are shown below:

$$G_1(t) = \left(G_2(t) - B\right)^{1/2} \tag{2.35}$$

$$g_1(t) = \sqrt{\frac{G_2(t) - B}{Bb}} \tag{2.36}$$

The dynamics structure factor ($S(q,c,\tau)$) is defined as follows:

$$S(q,c,t) = \frac{1}{N^2}\sum_{i,j=1}^{N} < \exp\left[\mathbf{i}q.\left(r_i(t) - r_j(0)\right)\right] > \tag{2.37}$$

where $r_i(\tau)$ is the position of segment i at time difference (τ). The angular bracket denotes an average over the space-time distance distribution.

$g_1(t)$ is related to the relaxation function by:

$$g_1(t) = \frac{S(q,c,t)}{S(q,c,0)} \tag{2.38}$$

For a system consisting of non-interacting, homogenous, mono-disperse and spherical particles, the normalized field autocorrelation function can be represented by the expression:

$$g_1(t) = \exp(-\Gamma t) = \exp\left(-\frac{t}{t}\right) \tag{2.39}$$

where τ is the time difference of the process and $\Gamma = 1/t$ is the decay rate.

For polydispersed systems, more than one-decay processes may exist thus for multiple decay processes, the following expression will be obtained [Chu, 1991; Brown, 1993]:

$$g_1(t) = \int w(\Gamma)\exp(-\Gamma t)d\Gamma \tag{2.40}$$

where w(Γ) is a continuous distribution function of decay rate.

The decay rate is related to the translational diffusion coefficient (D) by:

$$\Gamma = Dq^2 \tag{2.41}$$

The hydrodynamic radius can be determined from the diffusion coefficient through the Stokes-Einstein equation:

$$D = \frac{kT}{6phR_h} \tag{2.42}$$

where k is the Boltzmann constant, T is the absolute temperature, η is the solvent viscosity and R_h is the polymer particle hydrodynamic radius [Noggle, 1996].

2.6 Drug ion selective membrane electrode

2.6.1 Theoretical background of Ion Selective Electrode (ISE)

Ion Selective Electrodes (ISE) are electrochemical sensors that allow potentiometric determination of the activity of a particular ion in the presence of other interference ions. For instance, pH electrode is based on recording the $[H^+]$ dependence of the electromotive force (EMF) values using a hydrogen ion (H^+) selective glass electrode with only the H^+ ions allowed to pass through a special glass membrane. When the electrode is immersed in a test solution containing H^+ ions, the external ions will diffuse through the membrane until equilibrium is reached between the external and internal concentrations. Thus, there is a build up of charge inside of the membrane, which is proportional to the number of hydrogen ions in the bulk solution. Major developments in the history of ISE have occurred over the past hundred years. Gibbs (in 1875), Arrhenius (in 1887), Nernst (in 1888-1889), Ostwald and Planck (in 1890) [Rong, 2001] have conducted studies on the properties of semi-permeable membranes, thermodynamic relationships for membrane equilibria and theory of electrolyte solutions. Thus, concepts like diffusion potential, potential difference and ion mobility have led to birth of membrane electrochemistry.

ISE can be classified according to the nature of the basic membrane material. The main requirement is that the membrane must be as immiscible as possible with respect to the bathing solutions and solid contacts. There are four main types of ion selective electrodes [Vytras, 1989]:

- Solid-state membrane electrodes
- Liquid (or plastic) ion selective electrodes

- Glass membrane electrodes
- Electrodes with suitable additional membranes

Cremer [Rong, 2001], in 1906, developed a glass membrane electrode which was selective to hydrogen ions. By varying the glass composition, the glass electrode could be made more sensitive to other cations. Eisenman and co-workers [Rong, 2001] developed and completed the theory of glass membrane electrode such as ion-exchange and formation of diffusion potential, where they pioneered the glass membrane electrode for ISE applications. The first successful membrane electrode (containing silver halide precipitate) that was not fabricated using glass was attributed to Pungor and Hallos-Rokosinyi in 1961[Rong, 2001]. However, the first liquid membrane electrode (selective to calcium ions) is only introduced in 1967 by Ross [Srinivasan and Rechnitz, 1969]. This forms the basis for the development of drug selective electrodes.

Initially when the ISE is immersed into a solution containing the primary ions, the potential difference across the membrane is zero as on both sides of the membrane; there are equal number of cations and anions. However, very soon after the immersion, the establishment of an electrode potential is caused by charge separation at the surface of the electrode. The interpretation is connected by chemisorption of primary ions from the solution phase to the surface of the membrane [Pungor, 1998]. This will create a build up of positive charges (cations) on the inside of the membrane and a corresponding increase in negative charges (anions) outside. When equilibrium is reached, a membrane potential is established. Inside the ISE, the build up of positive charges at the membrane surface causes silver ions in the internal reference system to lose the charges and be deposited onto the wire. Thus, electrons are drawn through the external wiring from the meter and

from the external reference electrode. Then chloride ions are attached to the silver chloride coated wire and electrons are released by combining with silver atoms in the wire and potassium ions flow out into the sample solution through the liquid junction (Figure 3.9) to compensate for the positive charge deficiency caused by the loss of calcium. At equilibrium, the electron flow ceases but there are residual voltage differences at each metal-liquid, solid-liquid, solid-solid and liquid-liquid junction. Together with the membrane potential and the reference electrode stable voltage, the measured potential difference will be the sum of all potentials.

ISE will respond selectively to the activity rather than the concentration of ions in solution. If the relationship between the activity and concentration can be fixed by adding a constant concentration of an inert electrolyte to the samples to swamp out minor variations in the sample concentration, then the electrode may be directly used for concentration measurements. The ISE should respond ideally according to the Nernst equation:

$$E_{cell} = \Delta E^{o} \pm \frac{RT}{nF} \ln a_i \qquad (2.43)$$

where ΔE^{o} is the standard potential of the cell containing an *i*-selective electrode and an ion *i*, a_i is the activity of ion *i*, R (=8.314) is the universal gas constant in $Jmol^{-1}K^{-1}$, T is temperature in K, n is the charge number of ion *i* and F (=96485C) is the Faraday constant. The sign $\pm$ should be taken as positive when *i* is a cation and negative when *i* is an anion.

2.6.2 Drug selective membrane electrode

For analytical control, most of the pharmacopoeias describe accurate methods but most of them are lengthy and difficult [Stefan et al., 1996]. The development and application of such electrodes continues to be of interest in pharmaceutical research in the past several decades because these sensors offer the advantage of simple operation, good selectivity, low cost, low detection limit, wide linear concentration range, fast response, good accuracy, applicability to colour, turbid solutions and possible interfacing with automated and computerized system [Takisawa et al., 1988; Watanabe et al., 1995; Fu et al., 1996; Stefan et al., 1996; Katsu et al., 1999; Aboul-Enein and Sun, 2000; Alizadeh and Mehdipour, 2002; Shahrokhian et al., 2002; Khalil et al., 2003]. In Figures 2.12a and 2.12b, the cocaine [Watanabe et al., 1995] and ketamine [Alizadeh and Mehdipour, 2002] drug selective electrodes have shown to have wide linear concentration range and good Nernstian behavior. Moreover, the electrodes can be easily manufactured in different shapes and sizes and are less affected by the response of biological substrates such as proteins, enzymes and antibodies [Alizadeh and Mehdipour, 2002].

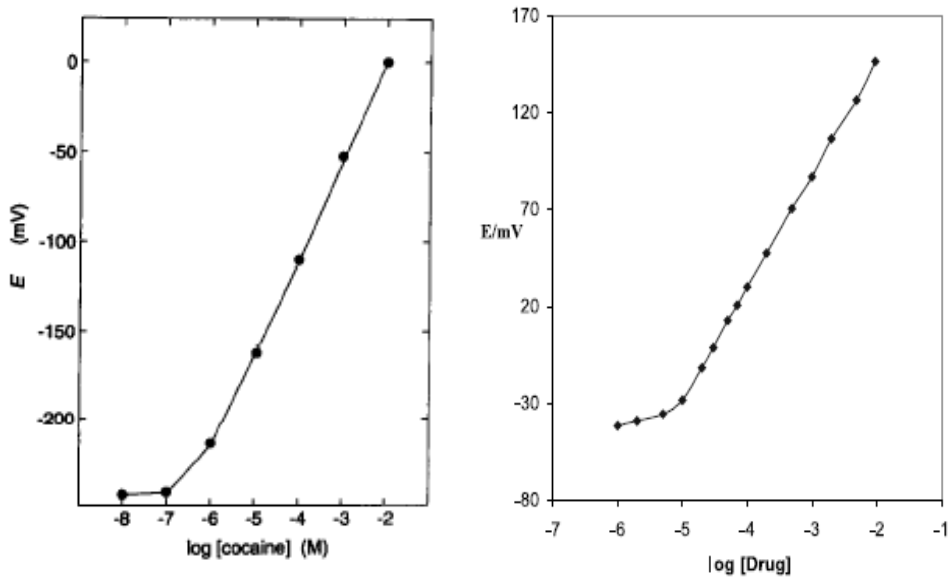

a **b**

Figure 2.12 (a) Calibration graph for the determination of cocaine [Watanabe et al., 1995]. (b) Calibration curve for ketamine hydrochloride electrode obtained in 0.01M NaCl [Alizadeh and Mehdipour, 2002].

Some problems encountered with the membranes are the need for extensive pre-conditioning treatment before use, care in storage, ionic strength of the solution sensitivity to some hydrophobic counter-ions and relatively short life-span [Takisawa et al., 1988; Alizadeh and Mehdipour, 2002]. The potentiometric performance of the electrode is dependent on the formation ability of the drug ions with the ion exchanger. Among the different kinds of amines, primary amines generally show the least tendency to form such ion-associates leading to poor response [Katsu et al., 1999].

The drug selective membrane is a liquid plasticized poly(vinyl-chloride) (PVC) and are based on a water insoluble ion-pair complex acting as an ion exchanger. In conjunctions with the study of surfactant electrodes and drug electrodes, many of the problems

encountered are slowly being resolved by using modified PVC having ionic end groups as ion exchange sites and by adding a plasticizer. The former inhibits the dissolution of the ion exchanger and the latter yields membrane, which have a longer life-span [Alizadeh and Medhipour, 2002]. Recently, ion exchangers like sodium tetrakis [3,5-bis(trifluoromethyl)phenyl]borate (NaTFPB), sodium tetraphenylborate (NaTPB) and potassium tetrakis(p-chlorophenyl)borate (KTpCIPB) and solvent mediator like dioctyl phthalate (DOP), tricresyl phosphate (TCP), tetrakis(2-ethylhexyl) pyromellitate (TEHPY), 2-fluoro-2'-nitrodiphenyl ether (FNDPE) and tris(2-ethylhexyl) trimellitate (TEHT) have been added to improve the sensitivity and selectivity of the membrane especially to sodium and chloride ions [Watanabe et al., 1995; Katsu et al., 1999; Alizadeh and Mehdipour, 2002].

To date, there are few clinical applications of drug sensitive electrodes (DSE) being published [Katsu et al., 1999] and the application of such electrodes has been limited to the determination of specific drug contained in a tablet [Bouklouze et al., 1992; Aboul-Enein and Sun, 2000] or dissolution test measuring the rate of dissolution of drug under defined conditions [Stefan et al., 1996] or as a sensor for determining the amount of drugs in body fluids [Katsu et al., 1999] or determining the drug binding to proteins or cyclodextrins [Takisawa et al., 1988; Alizadeh and Mehdipour, 2002].

The procaine (PrHy) and imipramine (IMI) selective electrode will be applied to measure the drug release from different nanogels. This is a novel method as normally drug release are either being conducted using the high performance liquid chromatography (HPLC) [Madeline and Peppas, 1999; Foss et al., 2004] or UV-spectrophotometer [Soppimath et al., 2001; Yang et al., 2004]. All these techniques would require the use of a dialysis

membrane or centrifugal machine to isolate the nanoparticles from free drugs before measurements could be made. Such techniques will affect the measurements as drugs can be absorbed onto the dialysis membrane and be inhibited by the diffusional barrier of the membrane or the high centrifugal forces may also force additional drugs to be released from the delivery vehicle. The UV-spectrophotometer and HPLC techniques are tedious and cannot be automated as compared to the drug electrode which makes it a simpler and more efficient method for determining the drug release profile.

2.6.3 Potential measurement of the Ion Selective Electrode

The measurement of the EMF of a cell is required for potentiometric studies using ion selective membrane electrodes. The cell consists of two solutions separated by the membrane and the reference electrode in the following order:

Inner Ag/AgBr reference electrode (2)	**Internal solution (II)**	**Drug selective membrane**	**Test solution (I)**	**Ag/AgCl reference electrode (1)**

The EMF of the cell is as shown below:

$$EMF_{cell} = E_2 + \Delta\Phi_M - E_1 \qquad (2.44)$$

where $\Delta\Phi_M$ is the membrane potential and E_1 and E_2 are the potential response of reference electrode 1 and 2 respectively. The membrane potential is of importance for the analytical use of ion selective electrode.

The sum of the potential of the internal reference electrode and the membrane potential will be the potential of the ion selective electrode (E_{ISE}):

$$E_{ISE} = E_2 + \Delta\Phi_M \tag{2.45}$$

For a membrane of an ISE, which is in contact on both sides with the solutions of the same ion *i*, whose activity is to be measured in the test solution and neither the test solution nor the internal solution contains another ion that will influence the membrane potential (interference ion *j*), the membrane potential is given by:

$$\Delta\Phi_M = \left(\frac{RT}{nF}\right)\ln\left[\frac{a_i(I)}{a_i(II)}\right] \tag{2.46}$$

where $a_i(I)$ and $a_i(II)$ are the ion activity in test solution (I) and internal solution (II) respectively.

Equation 2.45 will be identical to Nernst equation in Equation 2.43 for the potential of a concentration cell without transfer. For the statement to be true, the internal solution should have a constant activity and E_2 in Equation 2.45 must be a constant. Therefore, Equation 2.43 can be re-written as follow:

$$\begin{aligned} E_{ISE} &= \left(\frac{RT}{nF}\right)\ln a_i(I) + C \\ &= \left(\frac{2.303RT}{nF}\right)\log a_i(I) + C \end{aligned} \tag{2.47}$$

where $C = \left(\frac{RT}{nF}\right)\ln a_i(II)$ which is determined by quantities that are independent of the activity of the determinable ion in the test solution. Therefore a plot of E_{ISE} against log $a_i(I)$ will give a Nernstian slope of $\left(\frac{2.303RT}{nF}\right)$.

2.6.4 Drug concentration measured by drug ion selective electrode

If the DSE is immersed in a test solution containing the drug in a fixed concentration of an added salt, the potential of the cell in terms of Nernst equation is as shown:

$$E_{cell} = E^o \pm \frac{RT}{nF} \ln \frac{a_{drug}}{a_{salt}} \tag{2.48}$$

where a_{drug} and a_{salt} are the activity of drug and salt respectively.

The activities of the drug and salt can be expressed in terms of concentration as follow:

$$E_{cell} = E^o \pm \frac{RT}{nF} \ln \frac{C_{drug} g_{drug}}{C_{salt} g_{salt}} \tag{2.49}$$

where C_{drug} and C_{salt} are the concentration of drug and salt present in the test sample respectively and γ_{drug} and γ_{salt} are the activity coefficient of the drug and salt respectively.

For mono-valent ions with the same charge, the activity coefficients are approximately equal. Then Equation 2.49 can be re-written as follows:

$$E_{cell} = E^o \pm \frac{RT}{nF} \ln \frac{C_{drug}}{C_{salt}}$$

$$= E^o \pm \frac{RT}{nF} \ln C_{drug} \mp \frac{RT}{nF} \ln C_{salt} \tag{2.50}$$

Since the concentration of salt in the internal solution (I) and test solution (II) is kept constant, $E^o_{cell} = E^o \mp \frac{RT}{nF} \ln C_{salt}$ can be defined and Equation 2.50 will become:

$$E_{cell} = E^o_{cell} \pm \frac{RT}{nF} \ln C_{drug}$$

$$= E^{o}_{cell} \pm \frac{2.303RT}{nF} \log C_{drug} \tag{2.51}$$

By plotting E_{cell} against log C_{drug}, Equation 2.51 can be rewritten as follows:

$$E_{cell} = Intercept \pm (slope)(\log C_{drug}) \tag{2.52}$$

From Equation 2.52, the concentration of drug present in the test solution can be found:

$$\log C_{drug} = \frac{E_{cell} - Intercept}{\pm slope}$$

$$C_{drug} = 10^{\frac{E_{cell} - Intercept}{\pm slope}} \tag{2.53}$$

2.6.5 Selectivity determination for drug ion selective electrode

The DSE may respond to certain other ions (interference(*j*) ions) present in the sample, in addition, to the selected (*i*) drug ions. The drug ion selective electrode potential is given by Nikolskii equation [Vytras, 1989]:

$$E_{cell} = E^{o} \pm \frac{2.303RT}{nF} \log\left(a_i + \sum_j K_j a_j\right) \tag{2.54}$$

where a_i and a_j are the activities of drug ion *i* and interference ion *j* respectively and K being the selectivity ratio of interference ion *j*.

For the full utility of the electrodes to be realized, reliable methods for establishing the selective characteristics and accurate numerical data on selectivities must be available. The selectivity ratio can be evaluated using Nikolshii equation with potentiometric measurement in solutions containing mixtures of the drug ion of interest or by utilizing a

series of solutions each containing only a single salt. There are three methods to determine the selectivity ratio [Srinivasan and Rechnitz, 1969]; the first two methods will involve measurements in solutions containing either ions *i* or *j* in any test solution and the last method will involve measurements in a solution containing both ion *i* and interference ion *j*.

Method 1:

The potential of a drug ion selective electrode in a solution containing only the univalent ion of interest (ion *i*) is given by:

$$E_i = E_o \pm \frac{2.303RT}{F} \log a_i \qquad (2.55)$$

If the solution does not contain the univalent ion of interest but any other univalent interference ion (ion *j*) with selectivity ratio (K) the potential of the drug electrode is as shown below:

$$E_j = E_o \pm \frac{2.303RT}{F} \log\left(Ka_j\right) \qquad (2.56)$$

The selectivity ratio (K) can be measured at any concentration as long as the activities of the two ions are the same in their respective solutions. Given $a_i = a_j$ and by combining Equation 2.55 and 2.56:

$$\log K = \frac{E_i - E_j}{2.303 RT/F} \qquad \text{(For anion)}$$

$$\log K = \frac{E_i - E_j}{-2.303 RT/F} \qquad \text{(For cation)} \qquad (2.57)$$

Method 2:

If the activities of ion *i* and interference ion *j* produces the same potential when present separately, the selectivity ratio (K) can be found by equating $E_i = E_j$:

$$K = \frac{a_i}{a_j} \qquad \text{(For both anion and cation)} \tag{2.58}$$

Method 3:

The potential of the electrode in a solution containing both the ions can be expressed by combining Equation 2.54 and 2.55:

$$E_i - E_{cell} = \pm \frac{2.303RT}{F} \log\left(\frac{a_i + Ka_j}{a_i}\right) \tag{2.59}$$

From Equation 2.59, an explicit expression for K can be obtained:

$$K = \frac{\left[\exp\left(\frac{E_i - E_{cell}}{RT/F}\right)\right] a_i - a_i}{a_j} \qquad \text{(For anion)}$$

$$K = \frac{\frac{a_i}{\exp\left(\frac{E_i - E_{cell}}{RT/F}\right)} - a_i}{a_j} \qquad \text{(For cation)} \tag{2.60}$$

Instead of using Equation 2.60 to calculate the selectivity ratio from only two potential measurements; one in a pure solution of ion *i* and the other in a mixture of ions *i* and *j*, a graphical procedure involving a series of measurements can be adopted. The potential (E_i) is first measured in a known volume of solution containing ion *i* at an activity (a_i) and known volume of solution containing ion *j* are added successively and the potential

E' being measured after each addition. Alternatively, E' can be measured in a series of separately prepared solutions containing varying activities of the two ions. The potential E' measured in any one of the series of solutions can be measured:

$$E' = E_o \pm \frac{2.303RT}{F} \log\left(a'_i + Ka'_j\right) \tag{2.61}$$

Combining Equation 2.61 and 2.55:

$$\left[\exp\left(\frac{E_i - E'}{RT/F}\right)\right] a_i - a'_i = Ka'_j \qquad \text{(For anion)}$$

$$\frac{a_i}{\exp\left(\frac{E_i - E'}{RT/F}\right)} - a'_i = Ka'_j \qquad \text{(For cation)} \tag{2.62}$$

By plotting the left hand side of Equation 2.62 against a'_j, the graph as shown in Figure 2.13 should be a straight line passing through the origin and the slope will give the value of selectivity ratio (K).

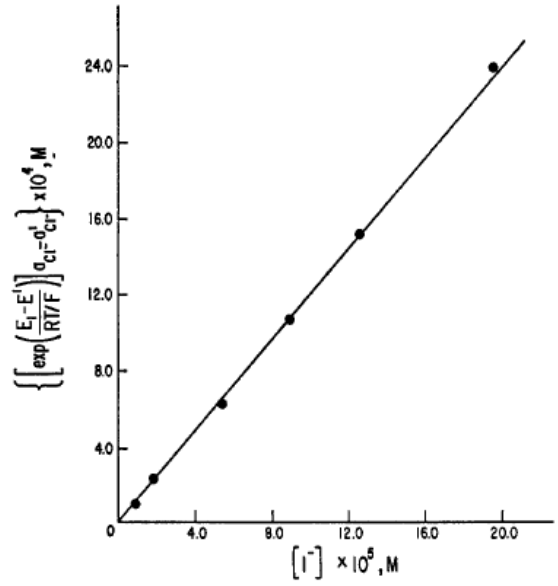

Figure 2.13 Selectivity plot for iodide with chloride ion selectivity electrode [Srinivasan and Rechnitz, 1969]. (Test for Equation 2.62)

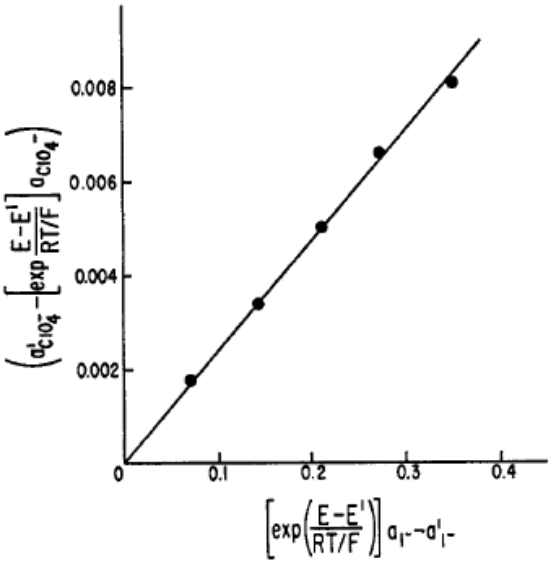

Figure 2.14 Selectivity plot for iodide with perchlorate ion selective electrode [Srinivasan and Rechnitz, 1969]. (Test for Equation 2.63)

For low values of K, a different approach will be taken. In such cases, the potential will not be sensitive to small increments of concentrations of ion *j*. A series of values of E' will be measured varying the concentration of the ion *i* while keeping the concentration of ion *j* at a fairly high value. By combining Equation 2.54 and 2.61:

$$a'_i - \left[\exp\left(\frac{E_{cell} - E'}{RT/F}\right)\right] a_i = K\left\{\left[\exp\left(\frac{E_{cell} - E'}{RT/F}\right)\right] a_j - a'_j\right\} \quad \text{(For anion)}$$

$$a_i - \left[\exp\left(\frac{E_{cell} - E'}{RT/F}\right)\right] a'_i = K\left\{\left[\exp\left(\frac{E_{cell} - E'}{RT/F}\right)\right] a'_j - a_j\right\} \quad \text{(For cation)} \quad (2.63)$$

A plot of the left hand side of Equation 2.63 against the functions within the brackets on the right hand side, the graph as shown in Figure 2.14 will be a straight line passing through the origin and the slope will give the value of selectivity ratio (K).

2.7 Summary

The literature review demonstrates that significant progress has been made in the field of drug delivery using nanogels as drug vehicles. Majority of the drug release profiles are measured using the UV-spectrophotometer or HPLC. Each of the mentioned methods has their own disadvantages. For example, the UV-spectrophotometer or HPLC will need a dialysis membrane for carriers below the sub-microns sizes. The drug release profile measured will not be diffusion of drugs from the drug carrier but rather diffusion of drugs from the dialysis membrane. Therefore a novel technique using the drug selective membrane electrode will be introduced to eliminate any disadvantages of traditional techniques.

The PrHy and IMI selective electrode will be carefully characterized to ensure the stability and reproducibility. This will be essential before the drug electrode is being applied to measure the drug release profile from nanogels.

In the result section, the problem associated with diffusion barriers created by the dialysis membrane will be solved by the using the DSE, where the contributions of chain relaxation and diffusion during drug release could be distinguished. Understanding the drug-polymer interaction is key to designing an efficient drug carrier, where drugs can be effectively released by manipulating the external environments. By making use of the LBL approach in coating the drug loaded nanogels, high burst associated with nanoparticles could be controlled.

3.0 MATERIALS AND EXPERIMENTAL TECHNIQUES

3.1 Synthesis of polymeric samples

3.1.1 Cross-linked MAA-EA nanogels

Hydrophobically modified Alkali-Swellable Emulsions (HASE) polymers were prepared by conventional semi-continuous emulsion polymerization of methacrylic acid (MAA) and ethyl acrylate (EA) cross-linked with di-allyl phthalate (DAP). A monomer mixture with a total weight of 620 g corresponding to a desired molar ratios was prepared by charging ethyl acrylate, methacrylic acid and di-allyl phthalate (all from Aldrich Chemical Co.), together with 26 g of a 75 % solution of Aerosol OT surfactant (American Cyanamid, Stamford, Connecticut) and 60 g of distilled de-ionized water to a bottle and the contents dispersed with vigorous shaking. This monomer mixture was then charged to a 1-litre graduated monomer-feed cylinder. An initiator feed mixture comprising 8 g of sodium persulfate (Aldrich Chemical Co.), 2 g of sodium bicarbonate (Aldrich Chemical Co.) and 45 g of distilled de-ionized water was prepared in another container and was charged to a 100-millilitre syringe pump. In a third container, 16 g of sodium persulfate was dissolved in 40 g of distilled de-ionized water to form the initial catalyst solution. 1377 g of distilled de-ionized water, 5.3 g of 2-sulfoethyl methacrylate (Hampshire Chemical Co.) and 5.3 g of 75 % solution of Aerosol OT surfactant were charged into the reaction vessel (a 3-litre resin flask). Under nitrogen purge, the reactor was heated to 80 ^{o}C, whereupon, 68 g of monomer mixture was added.

When the reactor temperature reached 80 ^{o}C, the catalyst solution was added to the reactor to initiate polymerization. After the initial monomers had reacted for 30 minutes

to form an in-situ seed product, the remaining monomer and initiator feed mixtures were conveyed to the reaction vessel over a two hour and two and a half hour period respectively while the reaction mixture was under continuous stirring at a reaction temperature of 80 ^{o}C. The reaction was left to proceed for another hour to react residual monomer after which the solid product was cooled and filtered through a 200-mesh nylon cloth. The final solid content of the nanogels is approximately 10 wt%.

The polymer latex, with pH of between 1.8 and 2.3, was dialyzed in distilled de-ionized water using regenerated cellulose tubular membrane (retaining molecular weight above 12000-14000 Da). This dialysis process removes all the impurities and unreacted chemicals. The cleaning was carried out for a month where the water was replaced every 2 to 3 days. At the end of the month, the concentration of the polymer latex was measured. Varying concentrations of nanogel samples were prepared from the stock solution.

The chemical structure of the cross-linked MAA-EA nanogel is depicted in Figure 3.1 and the properties are tabulated in Table 3.1. Two series of MAA-EA nanogels were examined in this study. The first series is cross-linked nanogels with constant MAA-EA molar ratio (20:80) but varying cross-linked density (1 to 4 wt%). The second series is cross-linked nanogels with constant cross-linked density (4 wt%) but varying MAA-EA molar ratio (20:80 to 50:50). These nanogels were designated as HASE x-y-z, where x and y correspond to the molar fractions of MAA and EA respectively and z denotes the weight percentage of cross-linker. For example, HASE 20-80-4 refers to a nanogel with MAA-EA molar ratio of 20:80 and cross-linked density of 4 wt%.

Table 3.1 Characteristics of cross-linked MAA-EA nanogels with DAP.

Name of nanogel	MAA/EA Molar Ratio (%)	DAP (wt%)	pH	R_h (a=0) (nm)	Polydispersity Index M_w/M_n	Solid Content (wt%)
HASE 20-80-1	20:80	1.0	1.84	36.5	1.27	9.91
HASE 20-80-2	20:80	2.0	2.24	39.8	1.25	9.90
HASE 20-80-4	20:80	4.0	1.80	41.1	1.21	9.88
HASE 30-70-4	30:70	4.0	1.99	45.8	1.30	9.95
HASE 40-60-4	40:60	4.0	1.96	49.3	1.33	9.99
HASE 50-50-4	50:50	4.0	1.85	52.5	1.36	9.96

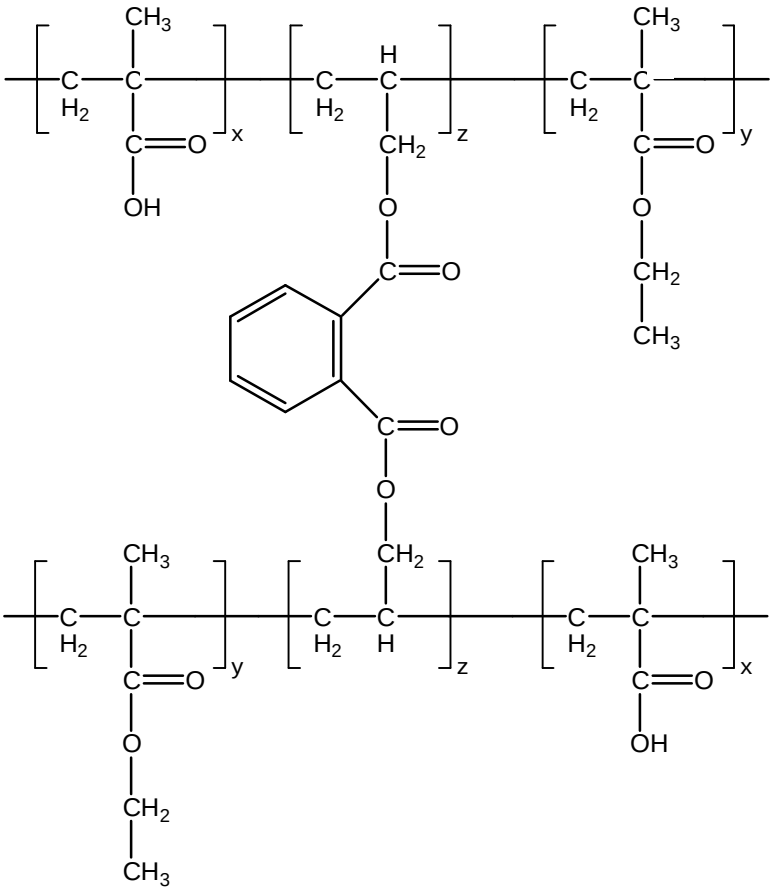

Figure 3.1 Chemical structure of cross-linked MAA-EA nanogels with DAP.

3.1.2 Cross-linked MAA-EA grafted with PEGMA nanogels

The polymeric nanogels were prepared by conventional semi-continuous emulsion polymerization of 50 mol% methacrylic acid (MAA) and 50 mol% ethyl acrylate (EA) cross-linked with 4 wt% di-allyl phthalate (DAP) and sterically stabilized by poly(ethylene glycol)methacrylate (PEGMA). A monomer mixture consisting of 5 g MAA (Aldrich Chemical Co.), 5.7 g EA (Aldrich Chemical Co.) and 0.6 g DAP (Aldrich Chemical Co.), together with 1.2 g of a 75 % solution of Aerosol OT surfactant (American Cyanamid, Stamford, Connecticut) and 4 g of distilled de-ionized water (resistivity of 18.2 μΩ.cm, obtained from Millipore Alpha-Q water purification system) was used. An initiator feed mixture comprising 0.2 g of sodium persulfate (Aldrich Chemical Co.), 0.05 g of sodium bicarbonate (Aldrich Chemical Co.) and 2 g of distilled de-ionized water was prepared in another container and was charged into a 10-millitre syringe pump. In a third container, 0.3 g of sodium persulfate was dissolved in 1.25 g of distilled de-ionized water to form the initial catalyst solution. Into the reaction vessel (a 500-millitre 4-neck flask) equipped with a condenser, 180 g of distilled de-ionized water, 0.3 g of 2-sulfoethyl methacrylate (Hampshire Chemical Co.) and 1 g of 75 % solution of Aerosol OT surfactant were charged. Under a nitrogen purge, the reactor was heated to 80 ^{o}C, and 10 wt% of the monomer mixture (i.e., 1.2 g) was added.

When the reactor temperature reached 80 ^{o}C, the catalyst solution was added to the reactor to initiate polymerization. After the initial monomers had reacted for 30 minutes to form an in-situ seed product, the remaining monomer and initiator feed mixtures were conveyed to the reaction vessel over a 2 and a 2.5 hours period respectively, while the reaction mixture was under continuous stirring at a reaction temperature of 80 ^{o}C. Fifteen

minutes before the addition of the monomer feed was completed, 1.2 g of PEGMA (Aldrich Chemical Co.), equivalent to 10 wt% of the total feed monomer, was added to the 500 ml monomer-feed cylinder. The PEGMA was added in the final 15 minutes to ensure that the stabilizer was grafted onto the particle surface. The PEGMA would prevent the nanogels from aggregating during the layer by layer (LBL) coating process. Finally, the reaction was left to proceed for another hour to react residual monomers after which the reaction mixture was cooled. After cooling the product, filtering through a 200-mesh nylon cloth was carried out to get rid of any scrape. The final solid content of the nanogels is approximately 10% by weight.

The polymer latex, with pH between 1.8 and 2.3, was dialyzed in distilled de-ionized water using regenerated cellulose tubular membrane (retaining molecular weight above 12,000-14,000 Da). This dialysis process removed all unreacted chemicals and monomers. The cleaning was carried out for a month where the water was replaced every 2 to 3 days. At the end of the month, the concentration of the polymer latex was measured.

3.1.3 Cross-linked MAA-BMA and MAA-MMA nanogels

Methacrylic acid (MAA)-butyl methacrylate (BMA) and methacrylic acid (MAA)-methyl methacrylate (MMA) cross-linked with di-allyl phthalate (DAP) were prepared by conventional semi-continuous emulsion polymerization. For the synthesis of MAA-BMA or MAA-MMA nanogels, a monomer mixture consisting of 9.6 g of MAA (Aldrich Chemical Co.), 15.8 g of BMA (Lancaster Synthesis Inc.) or 11.1 g of MMA (Lancaster Synthesis Inc.) and 0.83 g of DAP (Aldrich Chemical Co.), together with

0.14 g of a 75 % solution of Aerosol OT surfactant (American Cyanamid, Stamford, Connecticut) and 3.1 g of distilled de-ionized water were added to a bottle and the contents dispersed with vigorous shaking. An initiator feed mixture comprising 0.5 g of sodium persulfate (Aldrich Chemical Co.), 0.12 g of sodium bicarbonate (Aldrich Chemical Co.) and 5 g of distilled de-ionized water was prepared in another container and was charged to a 100-millilitre syringe pump. In a third container, 0.9 g of sodium persulfate was dissolved in 3.7 g of distilled de-ionized water to form the initial catalyst solution. Into the reaction vessel (a 500-millilitre 4-neck flask) equipped with a condenser, 350 g of distilled de-ionized water, 0.62 g of 2-sulfoethyl methacrylate (Hampshire Chemical Co.) and 0.56 g of 75 % solution of Aerosol OT surfactant were charged. Under nitrogen purge, the reactor was heated to 80 ^{o}C, 10 wt% of monomer mixture (2.9 g for MAA-BMA or 2.5 g for MAA-MMA) was added.

When the reactor temperature reached 80 ^{o}C, the catalyst solution was added to the reactor to initiate polymerization. After the initial monomers had reacted for 30 minutes to form an in-situ seed product, the remaining monomer and initiator feed mixtures were conveyed to the reaction vessel over a 2 and a 2.5 hours period respectively, while the reaction mixture was under continuous stirring at a reaction temperature of 80 ^{o}C. The reaction was left to proceed for another hour to react residual monomer after which the solid product was cooled and filtered through a 200-mesh nylon cloth. The final solid content of the nanogels is approximately 10 wt%.

The chemical structure of the cross-linked MAA-BMA and MAA-MMA nanogels are depicted in Figure 3.2 and the properties are tabulated in Table 3.2. These nanogels were

designated as 50MAA-50BMA and 50MAA-50MMA. The MAA-EA nanogels used for elucidating the effect of polymeric T_g on drug release are designated as 50MAA-50EA.

The polymer latex was dialyzed in distilled de-ionized water using regenerated cellulose tubular membrane (retaining molecular weight above 12000-14000 Da). This dialysis process removes all the impurities and unreacted chemicals. The cleaning was carried out for a month, where the water was replaced every 2 to 3 days. At the end of the month, the concentration of the polymer latex was measured. Varying concentrations of nanogel samples were prepared from the stock solution.

Table 3.2 Characteristics of cross-linked MAA-EA, MAA-BMA and MAA-MMA nanogels with DAP.

Name of nanogel	**Molar Ratio (%)**	**DAP (wt%)**	**pH**	**R_h (a=0) (nm)**	**Polydispersity Index M_w/M_n**	**Solid Content (wt%)**
50MAA-50EA	50:50	4.0	1.85	52.5	1.36	9.96
50MAA-50BMA	50:50	4.0	1.77	62.3	1.21	9.89
50MAA-50MMA	50:50	4.0	1.82	78.8	1.27	9.91

(a)

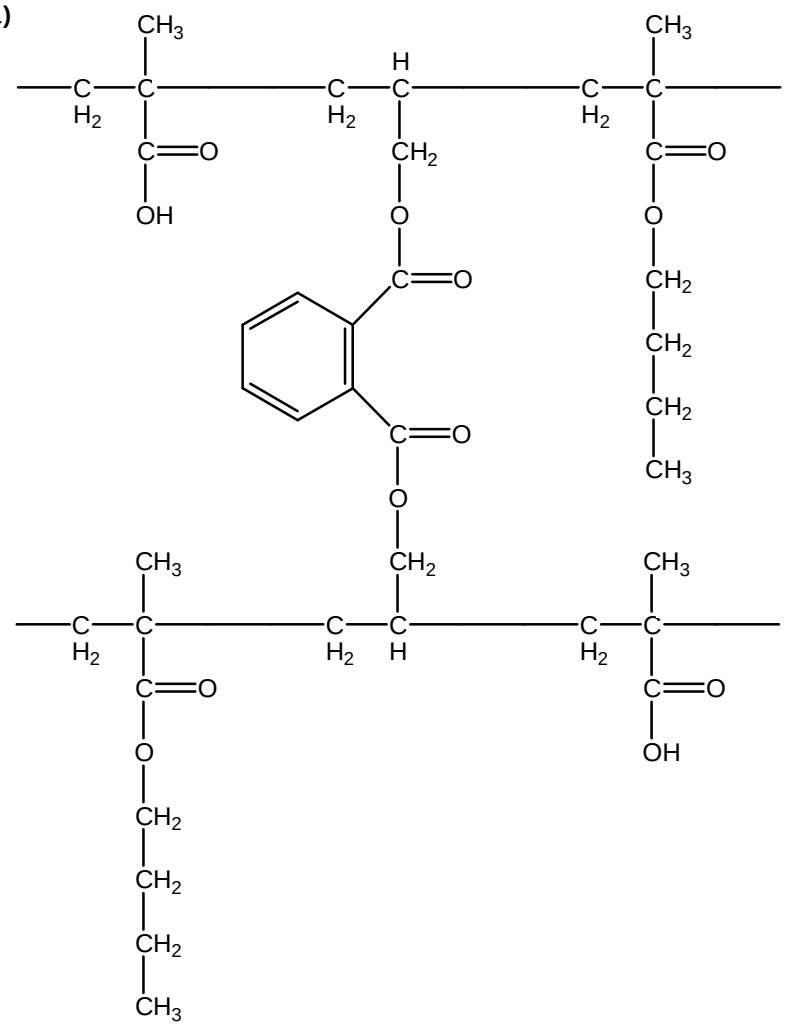

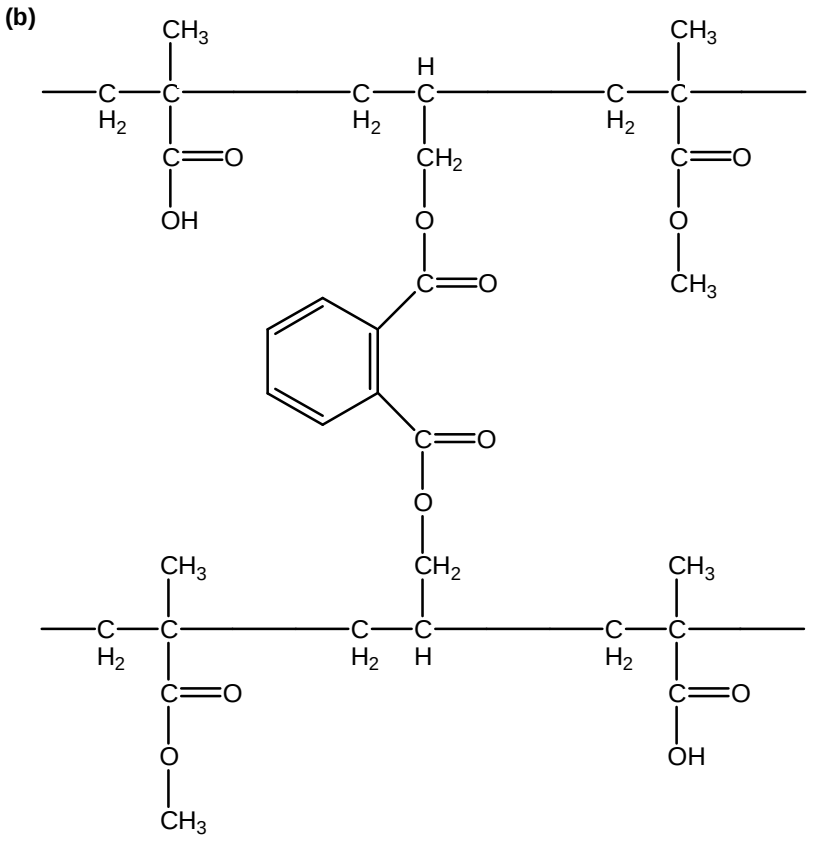

Figure 3.2 Chemical structure of cross-linked (a) MAA-BMA and (b) MAA-MMA nanogels with DAP.

3.2 Polymeric samples preparation and drug loading

Dust is a major problem affecting the laser light scattering measurements, thus samples used for laser light scattering measurements must be rid off any dust particles (with radius > 1000 nm). Dust is a generic term assigned to any object that acts as a large scatterer and hence contributes to the output signals. These undesirable signals will affect the quality of the correlation functions and limit the reproducibility of the results. Dust will be more of a problem when using a polar solvent like water and is usually detected by a sudden jump in scattering intensity. Filtration and centrifugation are commonly used to remove dust particles from the samples. First, the samples were centrifuged and large dust particles will be driven to the bottom of the test tubes. The samples were centrifuged at 3000 rpm for more than 5 hours to remove and dust that may be present in the samples. Next, the centrifuged samples were passed through a BI-SFS filtration system with a 0.8 μm filter to remove the dust. The samples were pumped through the filter at 300 strokes/minute for 20 minutes. All glassware used were previously cleaned with a small brush with soft detergent such as sodium dodecyl sulfate and rinsed thoroughly in tap water followed by distilled de-ionized water.

To 0.1 wt% nanogel solution, various amount of PrHy or IMI solution was added. By varying the amount of drug, a variety of nanogels to drug weight ratios were prepared. After the addition of drug, the drug-polymer solutions were left to equilibrate for 24 hours at 25 ^{o}C. The temperature was controlled by a PolyScience water bath and the temperature fluctuation is within ± 0.1 ^{o}C. The free drugs were filtered using a membrane with pore size of 20 nm, and the resulting solution was measured using the UV-Visible Spectrophotometer. No loss of drug was found when pure PrHy or IMI

solution was passed through the filter and the concentration before and after filtration was identical. Appropriate dilutions were made to obtain absorbance readings in the linear range of Beer's law. The calibration curve for the UV-Visible Spectrophotometer for PrHy and IMI is shown in Figure 3.3 and 3.4 respectively. Similar results were obtained with the drug selective membrane electrode. The uptake of PrHy or IMI by the nanogels (g of drug/g of polymer) was calculated using Equation 3.1:

$$Uptake = \left(\frac{A_c - A_s}{A_c} \right) V_{sys} m_{microgel}^{-1} C_{stock} \qquad (3.1)$$

where A_c and A_s are the absorbance of the control (contained only drug solution) and sample (contained drug-polymer solution) solution respectively, V_{sys} is the volume of the system, m_{gel} is the mass of nanogels in the system and C_{stock} is the concentration at which the drug stock solution was prepared.

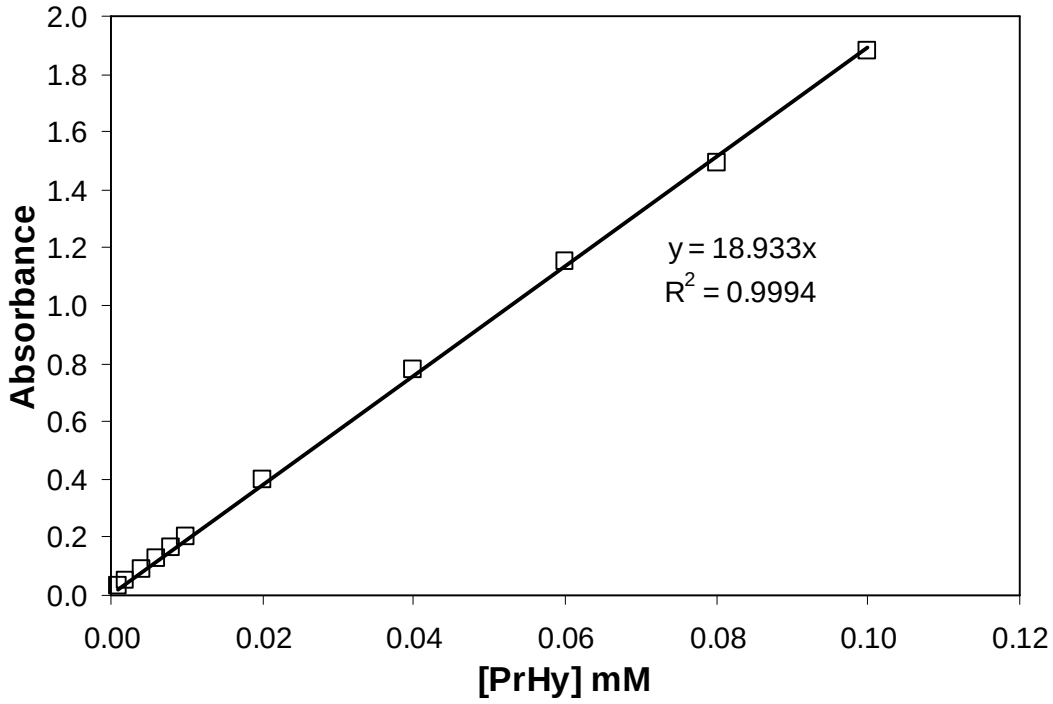

Figure 3.3 UV-Visible Spectrophotometer absorbance calibration curve for PrHy in 10 mM NaCl solution as a function of concentration.

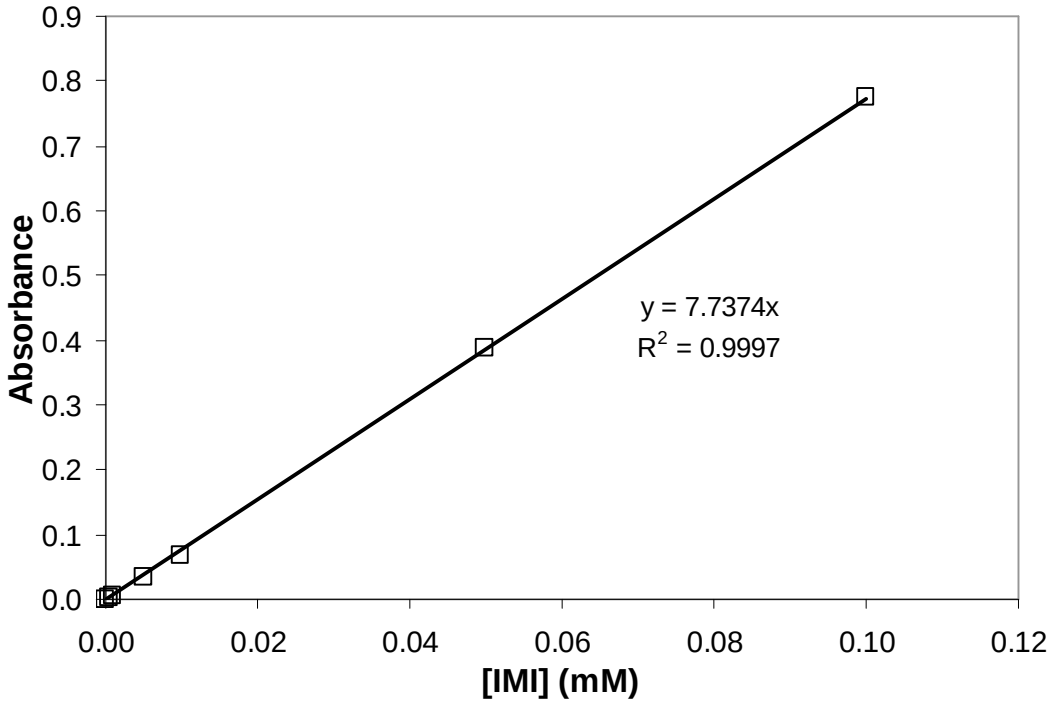

Figure 3.4 UV-Visible Spectrophotometer absorbance calibration curve for IMI in 10 mM PB solution as a function of concentration.

3.3 Neutralization of nanogel samples

The nanogel samples are either partially or fully neutralized with sodium hydroxide (NaOH). The degree of ionization can be characterized by the degree of neutralization (α). The degree of neutralization (α) is defined as the molar ratio of added base to acid groups on the nanogels and can be expressed in the following expression:

$$a = \frac{[BASE] + [H^+] - [OH^-]}{C_{COOH}} \tag{3.2}$$

where [BASE], $[H^+]$ and $[OH^-]$ are the molarities of added base, free hydrogen ions and hydroxide ions respectively and C_{COOH} is the total concentration of methacrylic acid groups expressed in moles per liter. The hydrogen and hydroxide ion concentration terms were calculated from the pH where the activity coefficient in dilute solution is assumed to be unity. With this definition, α = 1 at complete neutralization.

The concentration of C_{COOH} was determined by the following expression:

$$C_{COOH} = \frac{10vxc}{86x + 100y + 248z} \tag{3.3}$$

where x, y and z are the molar fractions of MAA, EA or BMA or MMA or DEA and cross-linker DAP respectively, c is the concentration of the nanogel expressed in weight percent and v is the total volume of nanogel sample prepared expressed in millimeter.

The densities of the nanogel samples ($\rho_{nanogel} \approx 1$ g/ml) was checked and found to be very similar to the density of water for all the range of nanogel concentration studied. There is a slight deviation but is within the permissible range for experimental errors.

3.4 Reagents and drugs

The titrant used in the potentiometric and conductiometric titrations is standard 1 M sodium hydroxide (NaOH) or hydrochloric acid solution (HCl) (all from Merck). The cationic drugs used in the drug release studies are procaine hydrochloride (PrHy, from Sigma) and imipramine hydrochloride (IMI, from Sigma) and were used without further purification. The chemical structure of the drugs is shown in Figure 3.5. PrHy is the first chemically synthesized, non-addictive and injectable local anesthetic used in dental surgery. However, due to the short anesthetic duration and highly allergenic properties, PrHy is no longer used in dental surgery. IMI is primarily used as anti-depressant. Distilled de-ionized water was obtained from the Millipore Alpha-Q water purification system which has a resistivity of 18.2 μΩ.cm. The system removes ions and other traces of organic materials and particles that are larger than 0.45 μm.

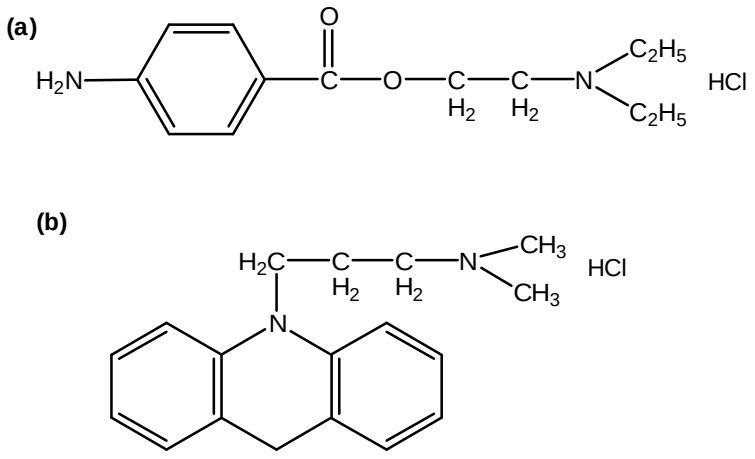

Figure 3.5 Chemical structure of (a) procaine hydrochloride (PrHy) and (b) imipramine hydrochloride (IMI).

3.5 Drug ion selective membrane electrode

3.5.1 Preparation of drug selective membrane

3.5.1.1 Preparation of drug poly (vinyl chloride) complex

Poly(vinyl chloride-co-acrylic acid) (PVC) (from Aldrich Chemical Co.) weighing 0.5 g was dissolved in 30-millilitre of tetrahydrofuran (THF) (from Merck). 0.955 g of procaine hydrochloride (for PrHy membrane) or 1.109 g of imipramine hydrochloride (for IMI membrane) was dissolved separately in distilled de-ionized water and tetrahydrofuran (THF) mixture of ratio 1:9. The total volume of the distilled de-ionized water and THF is 100-millilitre. The PVC-PrHy or PVC-IMI complex after stirring for 48 hours was precipitated in 1 liter of distilled de-ionized water. The precipitate was filtered using a 20-25 μm filter paper and washed repeatedly with distilled de-ionized water and dried at room temperature.

3.5.1.2 Preparation of drug selective membrane

The drug selective membrane was prepared using the following procedure. An optimum relative amount (weight percent) of drug PVC complex, polymeric plasticizer (poly (ethylene-co-vinyl acetate-co-carbon monoxide) (PE-co-PVA-co-CO) (from Aldrich Chemical Co.) and additive (sodium tetraphenylborate (NaTPB)) (from Fulka), totaling 0.3 g, was dissolved in 30-millilitre of THF. The different combinations of the mixture are tabulated in Table 3.3. When the dissolution was completed, the mixture was poured into a petric dish of 55 mm in diameter and the solvent was evaporated at room temperature for 2-3 days. Finally, a membrane disk of 12 mm in diameter and ~0.3 nm in thickness was cut and fixed onto the Teflon tubing.

Table 3.3 Different composition ratios of drug selective membrane electrode.

Membrane	Membrane Composition (wt%)		
	Drug PVC complex	PE-co-PVA-co-CO	NaTPB
1	40	60	0
2	38	60	2
3	35	63	2
4	32	63	5
5	35	60	5

3.5.2 Fabrication of drug ion selective electrode

The drug ion-selective electrode body was constructed in the laboratory at Salford University based on the design of a commercially available EDT calcium selective electrode. A schematic diagram of the electrode is illustrated in Figure 3.6.

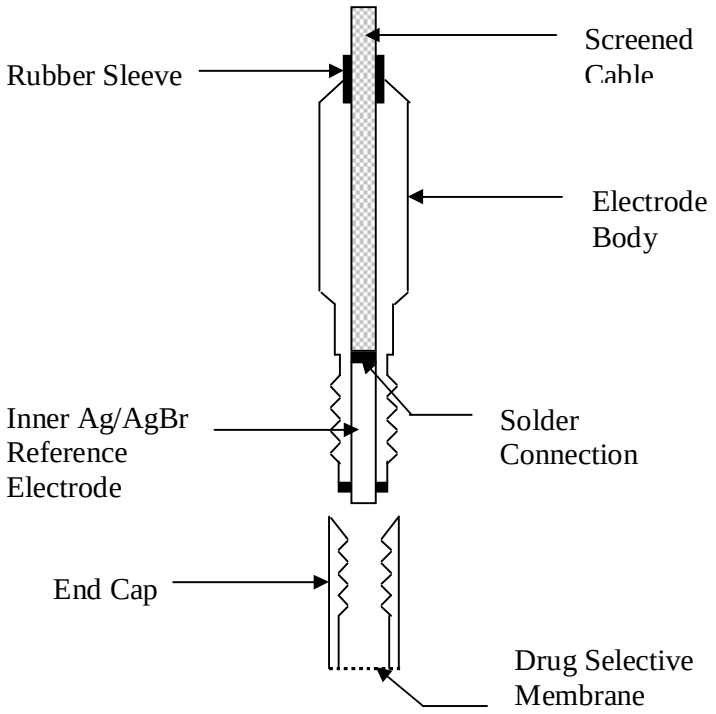

Figure 3.6 Schematic diagram of all the components of a drug ion selective electrode.

The drug ion selective electrode consists of four parts: electrode body; inner Ag/AgBr reference electrode; end cap and drug membrane. The inner Ag/AgBr reference electrode is made by coating the silver rod with silver bromide through electrolysis in a 100-millilitre of 1 M NaBr for 20 minutes with silver rod as anode and platinum electrode as cathode.

The drug membrane was cut-out using a number 7 cork borer and the membrane disc was adhered onto the end cap tip using THF which is placed on the contact end area of the tip. Leakages of the tip with drug membrane were tested by filling the tip with distilled de-ionized water after the THF had been evaporated. After checking for leakages, the end cap with drug membrane was dried and stored in a desiccator and kept away from light. Prior to use, the membrane was soaked in a 0.01 M PrHy solution (PrHy membrane) or 0.01 M IMI solution (IMI membrane) for half an hour.

3.6 Layer by layer coating

The procedure for LBL is described below:

0.3-millilitre of a 1 wt% poly(allylamine hydrochloride) (PAH) (Sigma Aldrich, M_w = 70000 g/mol) containing 100 mM NaCl (pH 6) was added to 30-millilitre of 0.01 wt% MAA-EA nanogel grafted with PEGMA loaded with 1.42 g of PrHy/g of nanogel (pH 6). The mixture was continuously stirred for 30 minutes to allow for the adsorption of PAH onto the negatively charged nanogels. Excess PAH was removed by four repeat filtration using the ultrafiltration cell [Funasaki and Hada, 1980; Warr et al., 1983; Huang and Somasundaran, 1993; Makayssi et al., 1993] with cut-off size filters of 20 nm at pH of 6.

0.9-millilitre of a 1 wt% poly(sodium 4-styrenesulfonate) (PSS) (Sigma Aldrich, M_w = 70000 g/mol) containing 100 mM NaCl (pH 6) was added to 30-millilitre of 0.01 wt% PAH coated nanogels (pH 6). The mixture was continuously stirred for 30 minutes to allow the adsorption of PSS onto the positively charged PAH coated nanogel. The excess PSS was removed by ultrafiltration cell, similar to that described for PAH. This procedure was repeated for the subsequent coating of PAH and PSS. The chemical structure for PAH and PSS is shown in Figure 3.7.

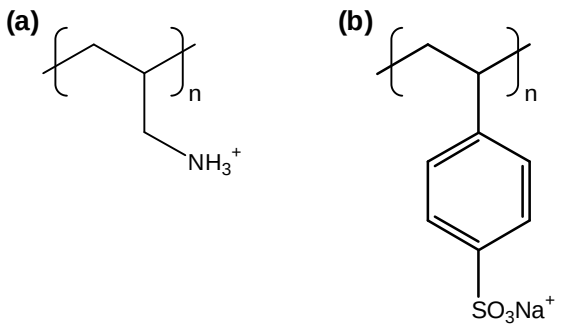

Figure 3.7 Chemical structure of (a) PAH and (b) PSS.

3.7 Equipment and experimental techniques

3.7.1 Potentiometric and conductiometric titration

All potentiometric titrations were conducted using the Radiometer ABU93 Tri-Burette Titration System and conductiometric measurements were conducted using the CDM83 Conductivity Meter. A standard RS232C interface is integrated with the instrument and all titrations are fully controlled by the computer using the ALIQUOT titration software. The software works in the Microsoft Excel environment which allows the user to input adjustable experimental parameters. The electrodes used are the Radiometer pHG201 pH glass, Radiometer REF201 reference electrode and Radiometer CDC741T.

All titrations were conducted at 25 ^{o}C in a titration vessel containing desired amount of polymer solution and with constant stirring. The temperature is controlled by a PolyScience water bath and the temperature fluctuation is within ± 0.1 ^{o}C. A minute of lag time was allowed between each titration to ensure that the reaction had reached equilibrium. The electrodes are not affected by the polymer latexes as the electrodes yielded identical reading before and after the titrations.

3.7.2 Electromotive force (EMF) measurements

Drug membrane electrode selective to PrHy or IMI was used to determine the PrHy and IMI concentration respectively by measuring the EMF relative to a Metrohm Ag/AgCl reference electrode as shown in Figure 3.8. The Radiometer ABU93 Tri-Burette Titrator with a build in micro voltage meter integrated with the modified ALIQUOT titration software was used to record all the EMF values. A CDM83 conductivity meter was used

to monitor the shift in the conductivity during the calibration and drug release measurements. A constant ionic strength of 10 mM NaCl solution was used for all the EMF measurements.

All the EMF measurements were conducted at 37 ± 0.1 ^{o}C which is controlled by a PolyScience water bath. For the calibration of the PrHy or IMI selective membrane, a 0.3 M PrHy or IMI solution in 10 mM NaCl solution was titrated into a constantly stirred 30 ml, 10 mM NaCl solution. A minute lag time was allowed between each titration to ensure that the reaction had reached equilibrium before the EMF value was measured.

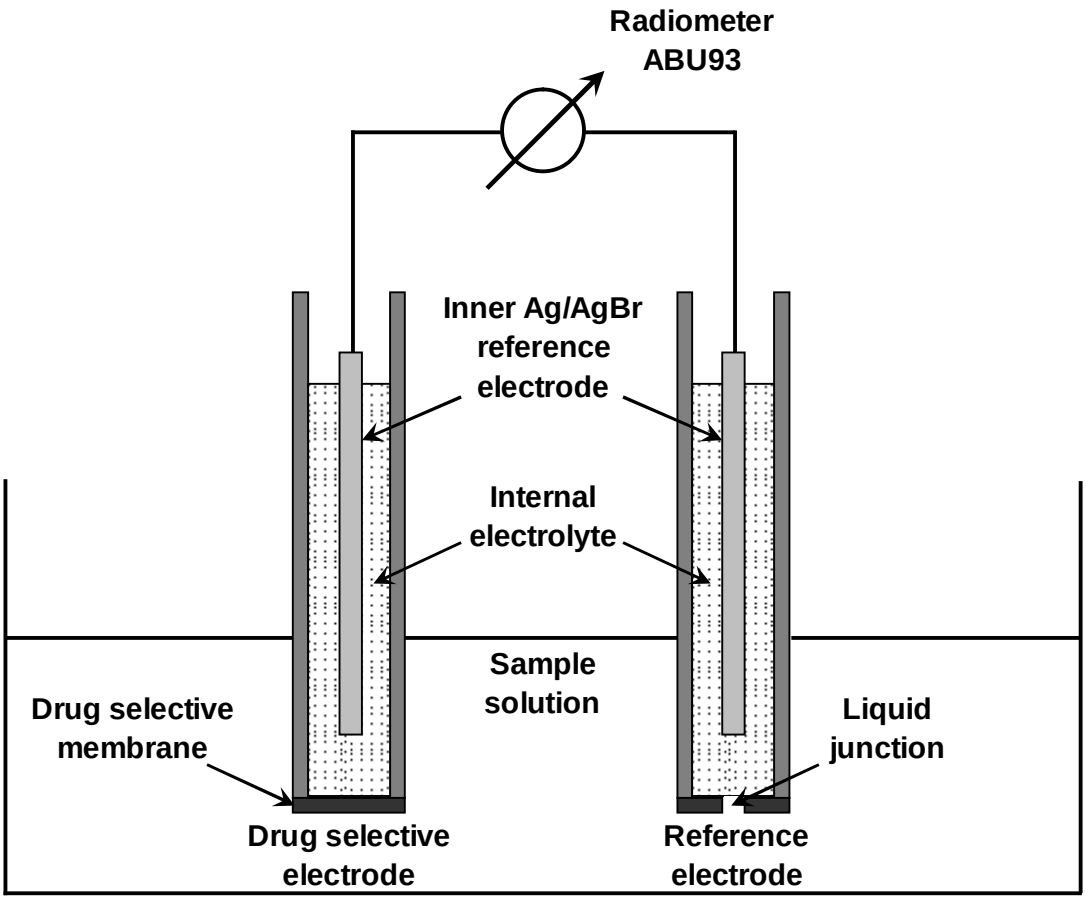

Figure 3.8 Experimental setup for the use of Drug Selective Electrode (DSE).

3.7.3 Isothermal Titration Microcalorimetric measurements

Calorimetric analysis measures the amount of energy exchanged in the form of heat flow between two systems within a short period of time. This technique represents a useful method for studying the thermodynamic properties, such as the enthalpy (ΔH), entropy (ΔS), Gibbs free energy (ΔG) and heat capacity (C_p). A detailed classification of calorimetric methods can be found in a monograph by Hemminger [Hemminger, 1994]. The "micro" prefix in microcalorimetry refers to a calorimetric measurement that is able to measure heat changes as low as 1 μW.

Isothermal Titration Calorimetry (ITC) is a technique that combines thermochemical and analytical applications where the enthalpy change of a chemical reaction as a function of the amount of titrant is quantified. The measuring principle of the Microcal ITC is the detection of heat flow using the power consumption technique. The quasi-isothermal condition during measurement ensures that heat loss does not contribute to large errors therefore a more precision measurement of heat is possible.

All calorimetric measurements were obtained using the Microcal ITC (Microcal Inc., MA). The schematic diagram of the ITC is shown in Figure 3.9. The power compensated and differential instruments are previously described in details by Wiseman et al [Wiseman et al, 1989]. The machine has a reference cell and a 1.35-millilitre sample cell which are both insulated by an adiabatic shield. All titrations are carried out at 25 ± 0.1 ^{o}C by a step by step injection of titrant from a 250 μl injection syringe into the sample cell. The syringe is tailored made such that the tip acts as a blade-type stirrer to ensure continuous mixing efficiency of 400 rpm. All the titration parameters like

injection volume and lag time between each injection are controlled by an interactive software.

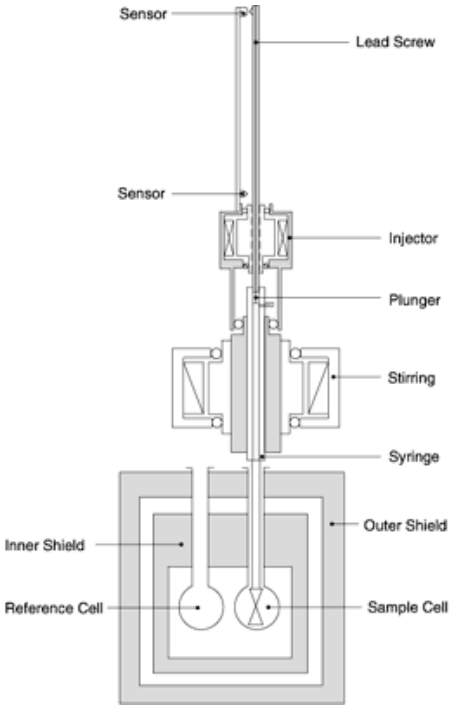

Figure 3.9 Schematic diagram of Isothermal Titration Calorimeter (ITC).

3.7.4 Ultraviolet (UV) spectrophotometric measurements

Many compounds absorb ultraviolet or visible light thus the amount of radiation absorbed can be measured. The transmittance (T) is given by:

$$T = \frac{P}{P_o} \tag{3.4}$$

where P is the radiant power leaving the sample and P_o is the radiant power directed at the sample. Thus absorbance (A) can be measured based of the following equation:

$$A = \log_{10} \frac{1}{T} \tag{3.5}$$

Based on the Beer-Lambert Law, the concentration of drugs present can be determined from Equation 3.6:

$$A = ebc \tag{3.6}$$

where ε is the molar absorbtivity in liters per moles per centimeter, b is the path length in centimeter and c is the concentration of the compound in solution in moles per liter. The calibration curves for PrHy and IMI is shown in Figure 3.3 and Figure 3.4 respectively. These values are taken at the peak wavelength of 290 and 251 nm respectively.

The Hewlett Packard UV-Visible Spectrophotometer (Agilent Technology, Germany) with a path length of 1 cm was used to measure the concentration of drugs released. The Hewlett Packard-89090A temperature control system is used to keep the temperature constant at 25 ^{o}C.

3.7.5 Laser light scattering

The Brookhaven laser scattering system (Brookhaven Instruments Corporation, NY) which consists of a BI200SM goniometer (Version 2.0), BI-9000AT digital correlator and other supporting data acquisition, analysis software and accessories. The schematic diagram of the system is shown in Figure 3.10. The goniometer system includes the focusing optics, rotating arm, detector optics, photon detector, neutral density filter, beam focus, sample cell assembly, cells and high voltage power supply for the detector. The accessories include a 350 mW, 488 nm power adjustable argon-ion laser use as the light source, digital temperature controller water bath and matching liquid filter. In order to improve the accuracy of the measurement, the matching fluid (decahydronaphthalene) was filtered by pumping the fluid through a 200 nm filter for about 10 minutes. The

temperature of the vat and cell was kept constant at the desired temperature using an external water bath.

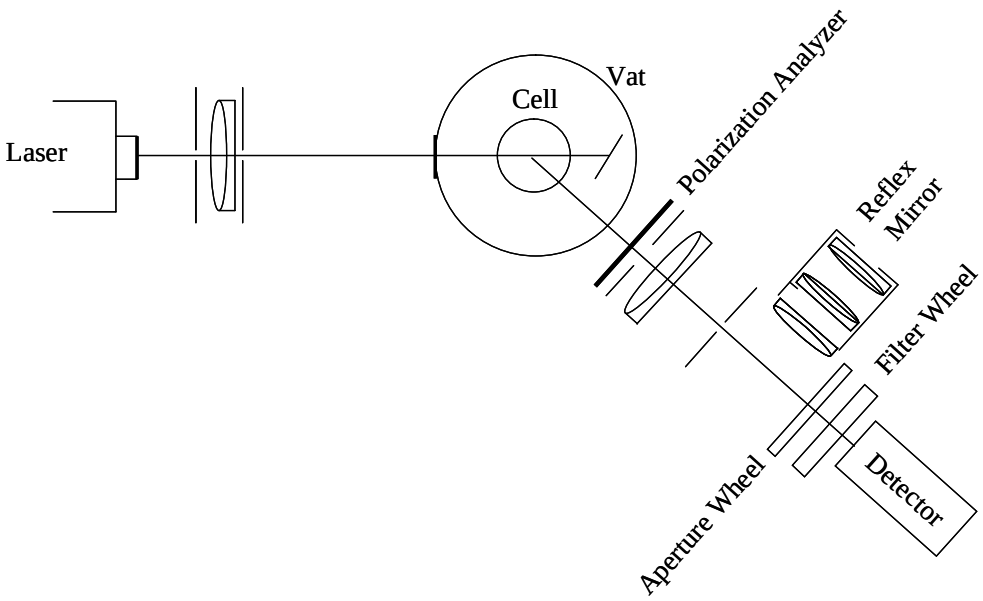

Figure 3.10 Schematic diagram of Brookhaven Laser Light Scattering system.

In light scattering measurements, stray light and dusts are the two major problems that have to be eliminated. Brookhaven's cell sample cavity is specially designed to minimize stray light by using matching liquid in the matching vat. When the laser, index matching vat and sample cell are properly maintained and aligned, stray light does not pose a significant problem. As the equipment is an optical instrument, the laser has to be aligned to reduce measurement errors and the stability of the laser over the measurement period has to be routinely checked. The stability test, alignment and adjustment of the equipment are explained in details in the equipment manual (Brookhaven Corporation, 1993). The alignment of the laser optics and detectors is checked by measuring the intensities of toluene between 15 and 155 degrees. The averaged intensity at each angle

is corrected and compared with that at 90 degrees and deviations are calculated. Good alignment is obtained when the deviation is less than 2%.

During the dynamic light scattering (DLS) or static light scattering (SLS) measurements, the count rates are controlled by adjusting the pinhole size and the laser power in order to achieve count rates of between 10^5 to 10^6 counts per seconds. Under such condition, good signal to noise ratio is obtained. The laser is allowed to warm up for at least 30 minutes at the beginning of each day before any experiment is performed. The laser power is adjusted to approximately 100 to 150 mW. Both the SLS and DLS are absolute techniques to measure M_w and R_h respectively, therefore, no additional calibrations are needed.

The data obtained from the DLS measurements are the correlation functions represented by either the field autocorrelation function ($g_1(t)$), or the intensity auto correlation function ($g_2(t)$). These functions can be analysed using the Inverse Laplace Transform technique to obtain the distribution of decay time. The Inverse Laplace Transform technique used is Regularized Positive Exponential Sum (REPES) supplied with the GENDIST software package with the probability to reject set as 0.5 and grid density set as 12. The GENDIST program is used in the analysis of Photon Correlation Spectroscopy (PCS) experiments in the homodyne mode. This routine performs an Inverse Laplace Transformation with variable degree of regularization. The fitting is performed directly on $g_2(t)$ rather than on $g_1(t)$. The results are presented in graphical form and in tabular form (moments of the distribution).

The $g_1(t)$ data can be analyzed using the cumulants method, which is a non-Laplace Transform technique introduced by Koppel [Koppel, 1972]. In practice, log $g_1(t)$ is fitted to a polynomial of second order, which yields the first cumulant ($\bar{\Gamma}$) and the second cumulant (μ_2). $\bar{\Gamma}$ is an important quantity as it can be calculated for many physical systems and situations. μ_2 is a measure of the width of the distribution (w(T)) and hence the effective polydispersity of the sample. For unimodal distributions of moderately polydispersed spherical particles in solution, the second cumulant is given by Equation 3.7 [Brown, 1993]:

$$\frac{m_2}{\bar{\Gamma}^2} \approx \left(\frac{M_w}{M_n} - 1 \right) \Big/ 4 \qquad (3.7)$$

where M_n is the number averaged molecular weight and M_w is the weight averaged molecular weight. The ratio M_w/M_n is known as the polydispersity index. This provides information on the sample polydispersity, and $M_w/M_n = 1$ represents very uniform particle sizes. As the polydispersity of the sample increases, the ratio M_w/M_n becomes greater than 1. The method of cumulants is very sensitive to the distribution of particle sizes thus providing a quantitative measure of the dispersity of particle sizes in the sample. The information on the polydispersity of the nanogels particles obtained in Equation 3.6 is included in Table 3.1 and 3.2.

Since the pH responsive nanogels are polyelectrolytes with potentially strong inter-particle interactions, the concentration of the nanogels must be sufficiently low such that inter-particle interactions do not affect the light scattering results. At low pH, the nanogel yields extremely high scattering intensity which may damage the detector of the light scattering device. Therefore dilution of the nanogel samples is a necessity. For

systems, which form precipitates or insoluble particles, neutral density filters of various filtering capacity are placed at the incident laser to reduce the intensity of the laser beam.

3.7.6 Electrophoretic mobility (m_e) and zeta potential (z)

Electrophoresis refers to the movement of charged colloidal particle when under the influence of an electric field. Random movement of charged colloidal particle is known as microelectrophoresis. When the applied electric field is small enough, the velocity of the charged particle will be proportional to the electric field and can be expressed as:

$$n = m_e E \tag{3.8}$$

where n is the particle movement velocity (ms^{-1}), m_e is the electrophoretic mobility ($m^2V^{-1}s^{-1}$) and E is the electric field strength (Vm^{-1}).

When an electric field is applied, the electrical force will cause the charged particle to move. However, friction will try to prevent the charged particle from moving. The effect of these forces acting on each charged particle and the ions on the surface is known as electrophoretic mobility. A positive mobility indicates that the particle is positively charged while a negative mobility shows that the particle is negatively charged. The equation for calculating electrophoretic mobility is as follows:

$$m_e = \frac{q}{6phr} \tag{3.9}$$

where q is the charge on the charged particle, h is the solution viscosity and r is the particle radius. From Equation 3.9, a higher charge and a smaller size will lead to a higher electrophoretic mobility while a lower charge and larger size will lead to a lower electrophoretic mobility.

When a colloidal particle is suspended in liquid, counter ions will form an electric double layer around it as shown in Figure 3.11. The inner region of the liquid layer is called the Stern layer with the counter ions being strongly bonded to the particle. The outer layer is called the diffuse layer and consists of movable ions. As the distance from the particle increase, the potential of the particle decreases due to the building up of counter ions. This decrease can be either a linear or exponential function of distance depending on the distribution of ion. If the ions are regularly distributed, the decrease will be linear. An irregular distribution of ions will result in an exponential decrease and the number of counter ions decreased with distance. Thus, within the Stern layer, there will be a linear decrease whereas within the diffuse layer, it is an exponential decrease.

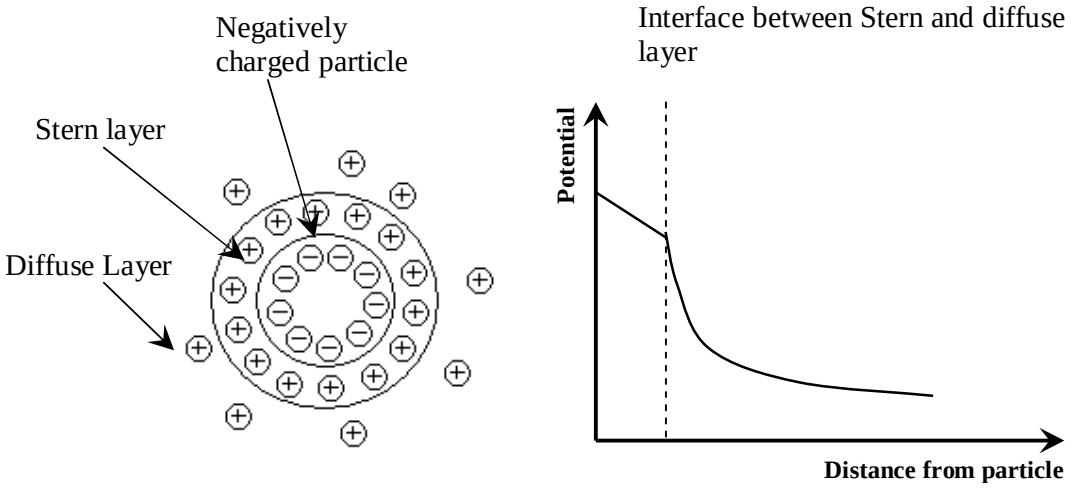

Figure 3.11 Particle Layers and Potential vs. Distance Graph.

Within the diffuse layer, there exists an imaginary layer called the slipping plane. When a voltage is applied to the particle and diffusion movement is induced, ions within the slipping plane act and move as a single entity. Any counter ions outside of the slipping plane are lost and as a result a charge forms at the sliding plane. The charge at the sliding

plane is referred to as the zeta potential. The zeta potential (ζ-potential) of a particle can be calculated:

$$z = \frac{3\eta m_e}{2\varepsilon f(ka)} \tag{3.10}$$

where ζ is the zeta potential (mV), η is the viscosity of solvent, m_e is the electrophoretic mobility, ε is the dielectric constant of sample and $f(ka)$ is the Henry's function.

The Henry's function is a function of k, the inverse of the Debye length (thickness of electric double layer) and the particle radius (a). Therefore, ka is the ratio of the particle radius to the electric double layer. When the electric double layer is thin (ka>1), Smoluchowski approximation is used and Henry's function taken as 1.5, thus simplifying the equation to $z = \frac{\eta m_e}{\varepsilon}$. The point where the zeta potential is zero is known as the isoelectric point (IEP) and is where the colloidal system is the most unstable. However, a zeta potential value of between –20 to 20 mV is generally considered unstable and will cause aggregation.

The zeta potential measurements were carried out using the Brookhaven Zeta PALS (phase analyzer light scattering). The zeta potential was calculated via the Smoluchowski model. Appropriate dilution will be required to make sure that the high intensity will not result in inaccurate or non-repeatable results.

3.7.7 Transmission Electron Microscopy (TEM)

A TEM model JEM 2010 was used for the present study. The typical magnification is between l000 to 1000000 times. The sample holder is copper grid with formvar, carbon

or formvar/carbon coating. The samples are stained with phosphotungstic acid before measurements are carried out.

4.0 CHARACTERIZATION OF DRUG SELECTIVE ELECTRODE

In Chapter 3, the method to construct the procaine hydrochloride (PrHy) and imipramine hydrochloride (IMI) membrane was introduced and in this chapter, the drug electrodes will be characterized, where the stability, reproducibility and limitations for potential use in quantifying the drug release profiles will be discussed. The EMF measurements were conducted over a concentration range of 1 x 10^{-6} to 1 x 10^{-1} M PrHy and IMI and the resulting data analyzed using the Nernst equation as described previously in Chapter 2.

4.1 Drug selective electrode response time and reproducibility

The overall PrHy electrode response characteristics were investigated on the basis of the calibration curves obtained by plotting the measured electromotive force (EMF) against the concentration of drug in 10 mM NaCl solution as shown in Figure 4.1. From the figure, the plot of EMF against log concentration of drug is shown to be reproducible. Both run 1 and 2 possess almost identical slopes of 44.0 and 44.5 mV/decade respectively and a y-intercept of 128.49 and 127.99 mV respectively in the linear concentration range (~1 x 10^{-3} to 1 x 10^{-1} M). This confirmed that the electrode responses are stable and repeatable.

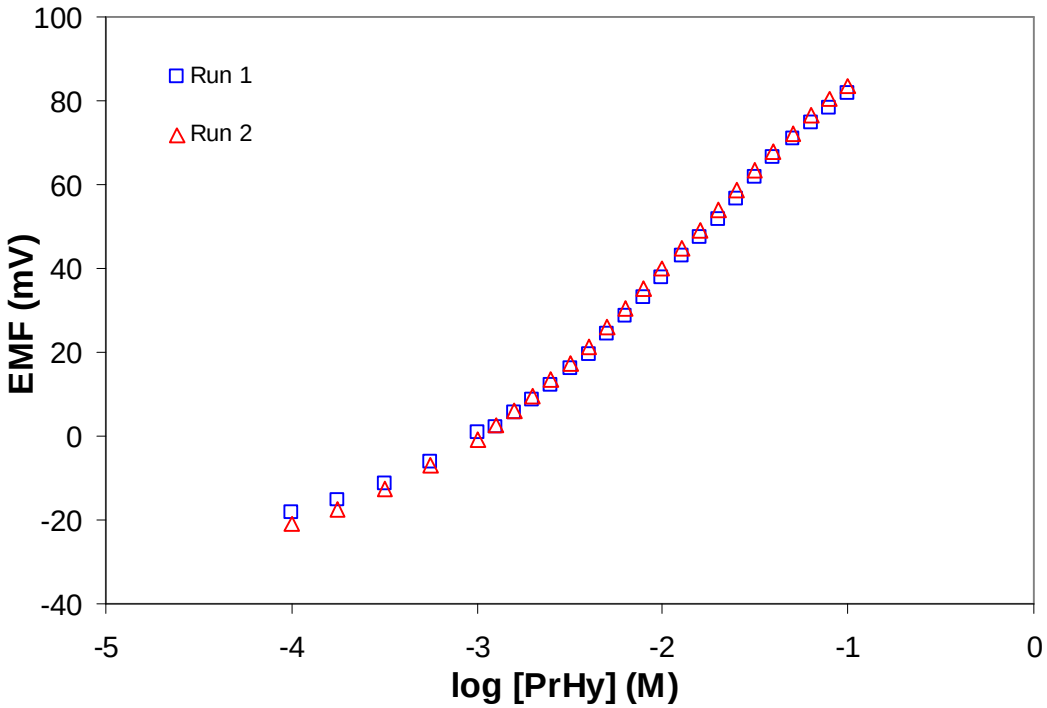

Figure 4.1 Calibration curve for procaine hydrochloride (PrHy) electrode obtained in 10 mM NaCl at 37 ^{o}C.

The stability of the PrHy electrode response was monitored continuously in 0.02 M PrHy solution at a temperature of 37 ^{o}C. Within the 24 hours period that the electrode was tested, the EMF values were stable as shown in Figure 4.2. The potential drift was shown to be < 0.1 mV/hr. The response time (time taken for the EMF measured by the electrode to reach a stable value) for the PrHy electrode was always less than 1 minute in the range of 1 x 10^{-5} to 1 x 10^{-1} M. In the range of 1 x 10^{-6} to 1 x 10^{-5} M, the response time ranges from 30 minute to 1 minute. However, the response time for the IMI electrode was less than 1 minute in the range of 5 x 10^{-4} to 4 x 10^{-2} M, and beyond this the response time ranges from 30 minute to 1 minute. The slower response time at the concentration below the detection limit is due to the inability of the electrode to sense the presence of the drug. The response time will decrease as the concentration of drug present reaches the detectable range.

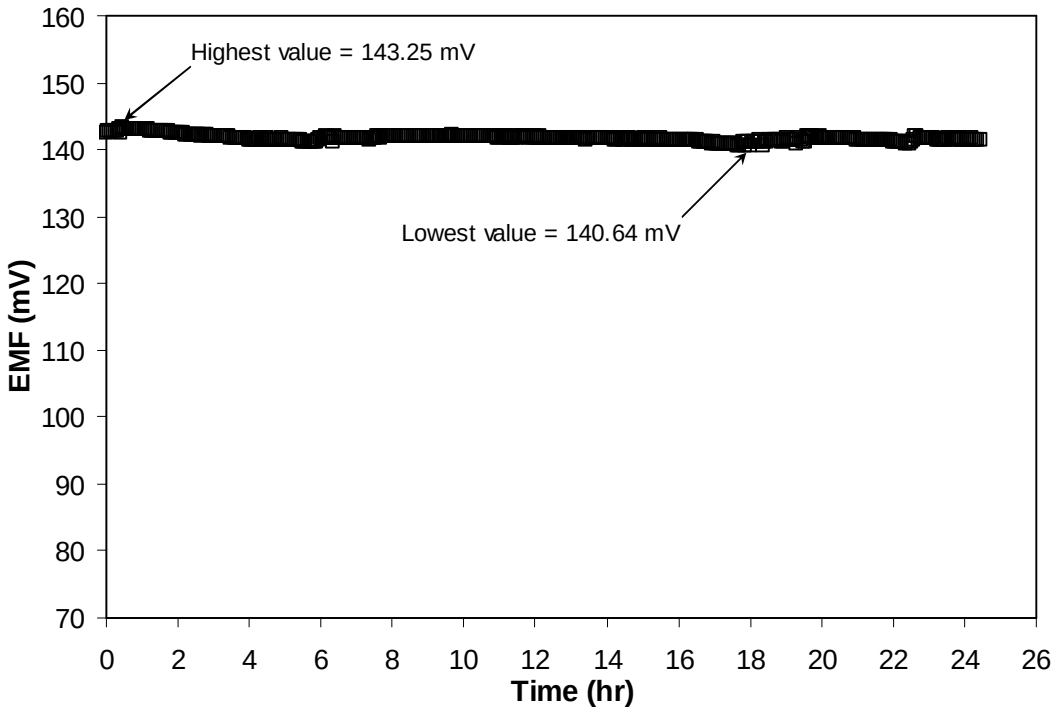

Figure 4.2 Stability of procaine hydrochloride (PrHy) electrode obtained in 10 mM NaCl at 37 ^{o}C over a period of 24 hours.

4.2 Drug electrode responses

Drug selective membranes are usually prepared by incorporating an appropriate ion-exchanger and solvent mediator into a poly(vinyl chloride) (PVC) membrane matrix [Watanabe et al., 1995]. The influence of the membrane composition on the potential response of PrHy ion-selective electrode was investigated. Optimum relative amounts of drug complex (drug electrostatic bonded to carboxlyated PVC), solvent mediator (PE-co-PVA-co-CO) and ion-exchanger (NaTPB) in the construction of the drug selective membrane were used. These membranes were designated as x-y-z, where x, y and z correspond to the weight percent drug complex, solvent mediator (or plasticizer) and ion-exchanger (or additives) respectively. The response and calibration graphs are summarized in Table 4.1 and Figure 4.3 respectively. All calibrations were conducted at 37 ^{o}C in the presence of 10 mM NaCl. For all the five membranes investigated, the calibration plots were repeated three times and were shown to be reproducible.

By comparing membrane 40-60-0 to the rest of the other membranes, the presence of ion-exchanger improves the Nernstian response and linearity range. There is an increase in slope from ~44.6 to ~55 mV/decade with the addition of ion-exchanger as indicated in Figure 4.3. The results obtained show good agreement to the work by Watanabe et al. [Watanabe et al., 1995], Alizadeh and Mehdipour [Alizadeh and Mehdipour, 2002] and Bouklouze et al. [Bouklouze et al., 1992], where the sensitivity and responses are greatly improved in the presence of ion-exchanger. This is due to the added stability of NaTPB as NaTPB has a highly lipophilic character and high stability [Watanabe et al., 1995]. In the presence of more NaTPB, more electroactive site carriers are present in the membrane to aid the transfer of ions. However, the two membranes with the 5 wt%

NaTPB showed a drop in the linearity range and this may be due to the low solubility of NaTPB in tetrahydrofuran (THF) solvent. From the results shown in Table 4.1, the ratio of drug complex to solvent mediator used will not affect the sensitivity of the electrode.

The slopes from the EMF plots show that there are deviations from the predicted Nernstian response and this could be due to the small amount of self-aggregation of the drug molecules or impurities presence in the samples [Takisawa et al., 1988]. Based on Figure 4.3, deviations from linear Nernstian behavior were observed at both low and high concentrations. The deviations at low concentration (< 1 x 10^{-5} M for 38-60-2 and 65-63-2 and < 1 x 10^{-3} M for 40-60, 35-60-5 and 32-63-5) are due to the sensors being insensitive in this region as the transport number of the drug in the membrane falls below unity [Alizadeh and Mehdipour, 2002], while deviations at higher concentrations are presumably due to the aggregation of the drugs. Similar deviations from linear Nernstian behavior were found for the IMI electrode as shown in Figure 4.4b. The two calibration plots that will be used throughout this thesis are shown in Figure 4.4.

Table 4.1 Characteristics of procaine hydrochloride (PrHy) membrane.

Membrane	Membrane Composition (% w/w)			Slope (mV/decade)	Linearity Range (M)
	Complex	PE-co-PVA-co-CO	NaTPB		
1	40	60	0	44.6	1 x 10^{-3} – 1 x 10^{-1}
2	38	60	2	55.6	1 x 10^{-5} – 1 x 10^{-1}
3	35	63	2	55.3	1 x 10^{-5} – 1 x 10^{-1}
4	32	63	5	58.8	1.26 x 10^{-3} – 1 x 10^{-1}
5	35	60	5	55.3	1.58 x 10^{-3} – 1 x 10^{-1}

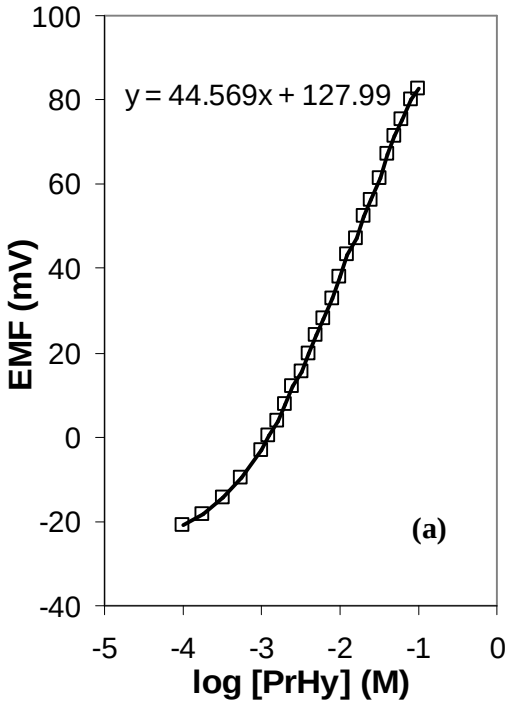

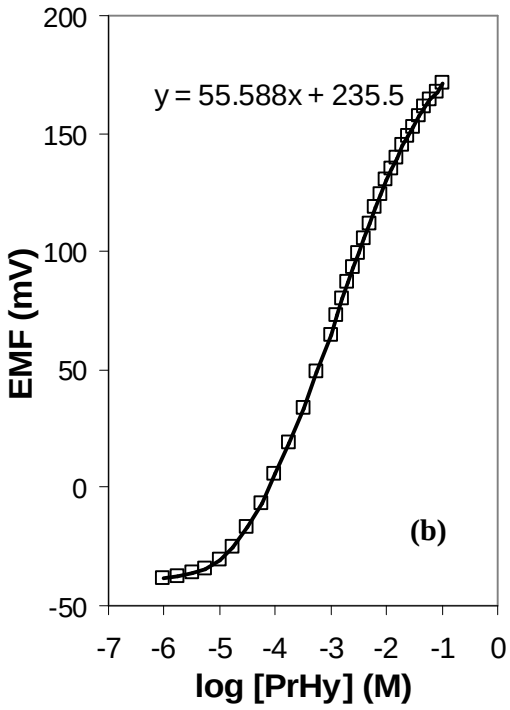

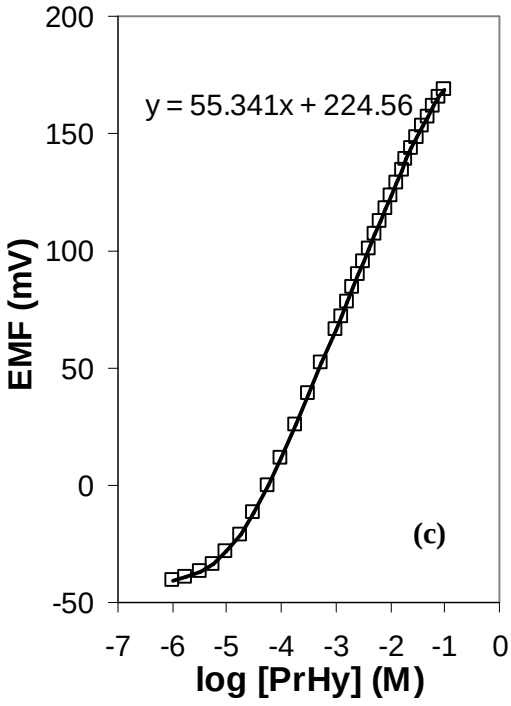

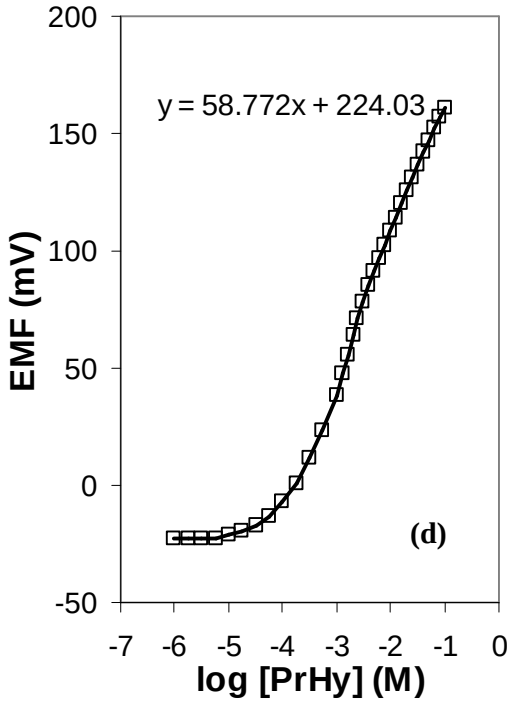

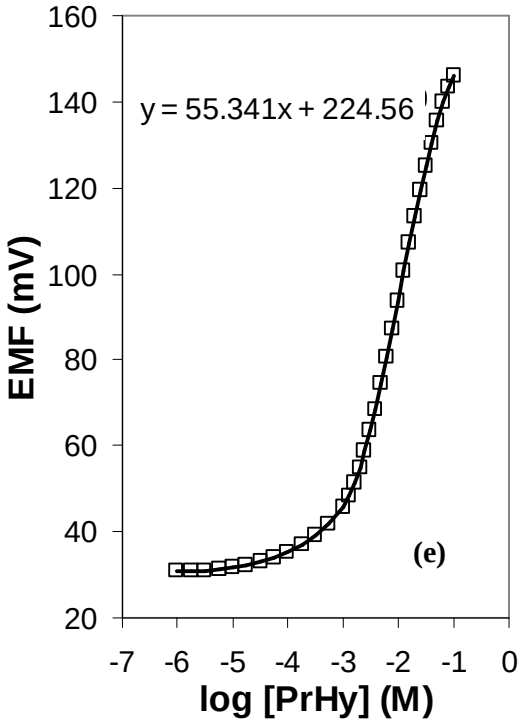

Figure 4.3 Calibration curve for a procaine hydrochloride (PrHy) electrode with membrane composition of (a) 40-60-0, (b) 38-60-2, (c) 35-63-2, (d) 32-63-5 and (e) 35-60-5 obtained in 10 mM NaCl at 37 ^{o}C.

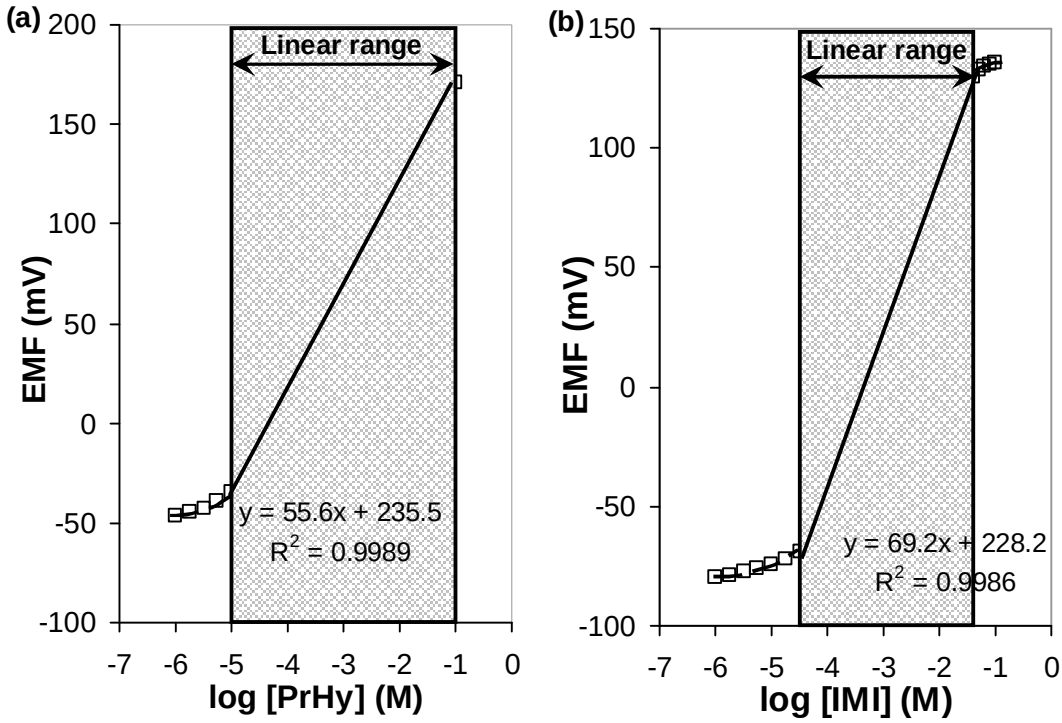

Figure 4.4 (a) Calibration curve for a procaine hydrochloride (PrHy) electrode with membrane composition of 38-60-2 and (b) calibration curve for an imipramine hydrochloride (IMI) electrode with membrane composition of 38-60-2 obtained in 10 mM NaCl at 37 ^{o}C. The linear Nernstian behavior is shaded in grey.

4.3 Effect of pH on the drug electrode response

The effect of pH on the electrode potential was examined by measuring the EMF values of PrHy selective electrode in PrHy solution and IMI selective electrode in IMI solution. Both the PrHy and IMI solutions contain 10 mM NaCl solution for the maintenance of the ionic environment. The pH of the solution was altered by titrating very small values of 1 M HCl and NaOH solution. The results were again reproducible within the allowed experimental error of ± 2%.

As shown in Figure 4.5, the EMF values remained constant over the pH range of 3 to 8.5, hence the PrHy electrode can be applied to determine the concentration of PrHy presence in a solution or being applied to obtain the drug release profile. This result is in agreement with ketamine hydrochloride electrode [Alizadeh and Mehdipour, 2002], amiodarone electrode [Stefan et al., 1996] and propranolol electrode [Aboul-Enein et al., 2000] but not in agreement with the results from cocaine electrode [Watanabe et al., 1995], prazosine electrode [Khalil et al., 2003] and the various drug electrode by Takisawa et al. [Takisawa et al., 1988]. This is probably due to the presence of large amount of H^+ ions creating significant ionic interference. The large decrease in EMF values observed at pH higher than 8.5 is attributed to the increase in the concentration of unprotonated PrHy. The decrease in EMF values at pH lower than 3 is presumably due to the electrode being insensitive to the PrHy ions and high interference created by H^+ ions. Similar explanation is applicable for the IMI electrode which has a stable EMF reading in the range from pH 4 to 8 as shown in Figure 4.6.

In principle, the pK_a value for the drug can be estimated using the data from Figure 4.5 and Figure 4.6 [Takisawa et al., 1988]. The pK_a is equal to the pH where the initial concentration of protonated drug is halved. However, this method is only possible if no precipitation of unprotonated drug occurs. The estimated pK_a value PrHy is around 9.6. Based on the literatures, the pK_a value of PrHy is 9.2. The estimated pK_a value for IMI from Figure 4.6 is around 9.2. Based on the literatures, the pK_a value of IMI is 9.4.

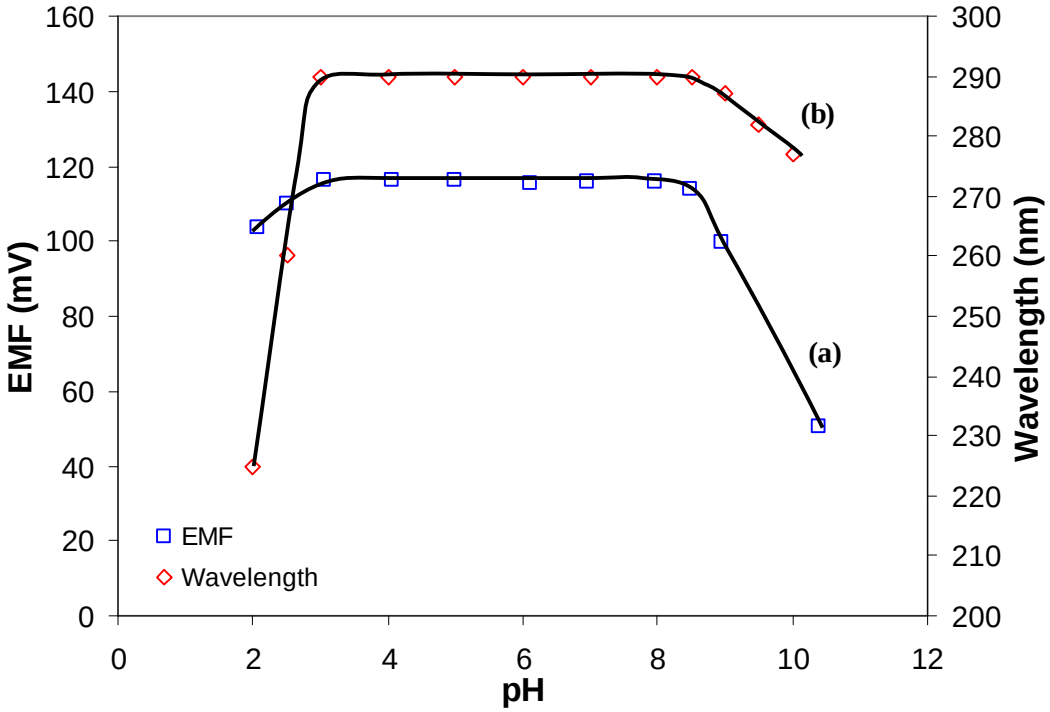

Figure 4.5 Effect of pH (a) on the EMF values measured by the procaine hydrochloride (PrHy) electrode (□) and (b) on the wavelength measured by the UV-Visible Spectrophotometer (◇).

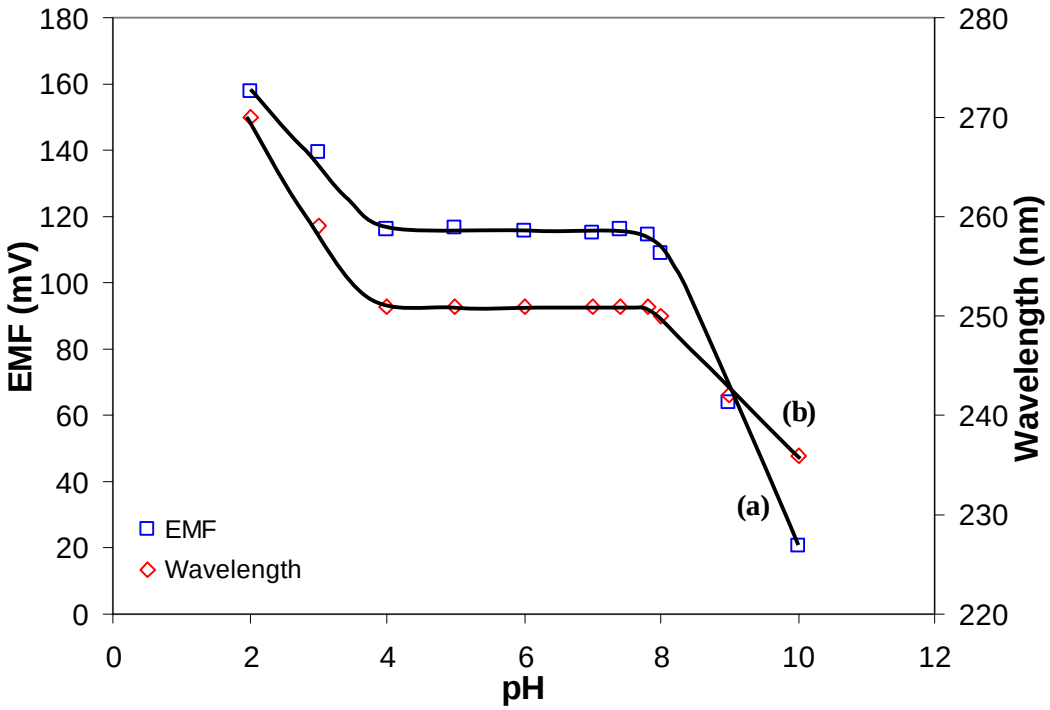

Figure 4.6 Effect of pH (a) on the EMF values measured by the imipramine hydrochloride (IMI) electrode (□) and (b) on the wavelength measured by the UV-Visible Spectrophotometer (◇).

A similar experiment was conducted using the UV-Visible Spectrophotometer to measure the effect of pH change on the peak wavelength of PrHy and IMI. The concentration used is 0.1 mM PrHy or IMI solution in 10 mM NaCl solution. Based on Figure 4.7, the peak wavelength for PrHy had shifted from 290 nm to a lower wavelength at pH greater than 8.5 and lower than 3.

From Figures 4.5 and 4.6, the peak wavelength remained constant at 290 nm at the pH range of 3 to 8.5 for PrHy while for IMI the peak wavelength remained constant at 251 nm from pH 4 to 8. The peak wavelength was noticed to decrease drastically at pH greater than 8.5 and pH lower than 3. This trend was similar to the PrHy selective electrode. The peak wavelength for IMI increased at pH lower than 4 and decreased at

pH higher than 8, which was similar to the trend measured by the IMI selective electrode. The change in peak wavelength at high pH was attributed to the higher concentration of unprotonated drug molecules and at low pH presumably due to the presence of large amount of H^+ ions. Similar trend was observed by Takisawa and co-workers using different drug electrodes [Takisawa et al., 1988].

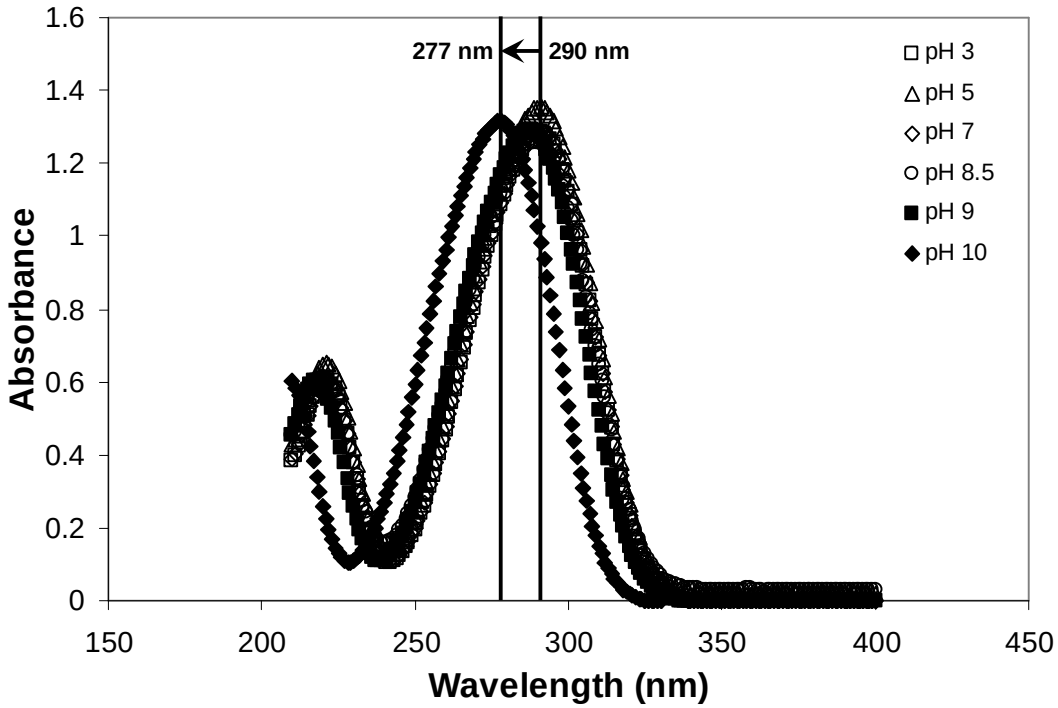

Figure 4.7 Wavelength shift due to changes in pH.

4.4 Selectivity

The most important characteristic of a membrane sensor is perhaps its relative response for the primary ion over other interfering ions present in the solution, which is expressed in terms of potentiometric selectivity coefficients (K_{ij}). The influences of interfering inorganic cations, Na^+, K^+, Ca^{2+}, Mg^{2+}, as well as organic cations, procaine, imipramine and desipramine, on the drug selective electrode were investigated. The selectivity coefficients (K_{ij}) were evaluated graphically by the Mixed Solution Method (MSM) based on Nikolsky equation:

$$K_{ij}C_j^{z_i/z_j} = \left[\exp\left(\frac{E_j - E_i}{RT/z_iF}\right)\right] - C_i \qquad (4.1)$$

where C_i and C_j are the concentration of the drug ion *i* and interfering ion *j* respectively.

A graph of $\left[\exp\left(\frac{E_j - E_i}{RT/z_iF}\right)\right] - C_i$ against $C_j^{z_i/z_j}$ with the curve passing through the origin will be plotted and the slope obtained will be the selectivity coefficient (K_{ij}). These values of selectivity coefficients are obtained by measuring the EMF values of PrHy solution or IMI solution in varying concentration of interfering ions. The resulting curves for the interfering ions and drugs for PrHy were plotted in Figure 4.8 and 4.9 respectively while those for IMI were plotted in Figure 4.10 and 4.11 respectively. A typical potentiometric selectivity patterns for PrHy selective membrane electrode is as follows:

imipramine > desipramine > Na^+ > K^+ > Ca^{2+} > Mg^{2+}

A typical potentiometric selectivity patterns for IMI selective membrane electrode is as follows:

$$\text{procaine} > \text{desipramine} > Na^{+} > K^{+} > Ca^{2+} > Mg^{2+}$$

Table 4.2 Selectivity coefficients (K_{ij}) for PrHy electrode's interfering ions and drugs.

Interfering ions	**Selectivity coefficient, K_{ij}**
Na^{+}	0.00604
K^{+}	0.00470
Mg^{2+}	0.000714
Ca^{2+}	0.000973

Interfering drugs	**Selectivity coefficient, K_{ij}**
Imipramine	0.75064
Desipramine	0.72261

Table 4.3 Selectivity coefficients (K_{ij}) for IMI electrode's interfering ions and drugs.

Interfering ions	**Selectivity coefficient, K_{ij}**
Na^{+}	0.00658
K^{+}	0.00526
Mg^{2+}	0.000867
Ca^{2+}	0.000924

Interfering drugs	**Selectivity coefficient, K_{ij}**
Procaine	0.69654
Desipramine	0.63932

Straight lines graphs were obtained for all interfering ions and drugs which are in conformity to the results obtained from Equation 4.1. The high R^2 values showed that the results obtained were reliable and accurate. The selectivity coefficients for the interfering

ions and drugs were recorded in Table 4.2 for PrHy selective electrode and in Table 4.3 for IMI selective electrode.

From Table 4.2 and 4.3, the selectivity coefficients for monovalent cations were in the range of 10^{-3} and divalent cations were in the range of 10^{-4}. Thus, the effectiveness of the drug selective electrode will not be affected by the presence of such common cations owing to the differences in ionic size and consequently their mobilities and permeability. This is similar to the trends reported by Aboul-Enein et al. [Aboul-Enein et al., 2000], Alizadeh and Mehdipour [Alizadeh and Mehdipour, 2002] and Watanabe et al. [Watanabe et al., 1995]. However, the selectivity coefficient for organic substances like cationic drugs is in the range of 10^{-1}. The interference by lipophilic amines is a characteristic of an ion selective electrode prepared with an ion exchanger [Katsu et al., 1999]. Although the effectiveness of the drug selective electrode will be greatly hampered by these both cationic drugs but these drugs are never associated with PrHy and IMI in pharmaceutical formulations and are usually not present in normal biological fluids. On the other hand, these interfering compounds do not affect the electrode behavior as the initial potential is immediately restored after rinsing without any regeneration procedure. Similar observations are obtained by Bouklouze et al. [Bouklouze et al., 1992], Katsu et al. [Katsu et al., 1999] and Takisawa et al. [Takisawa et al., 1988].

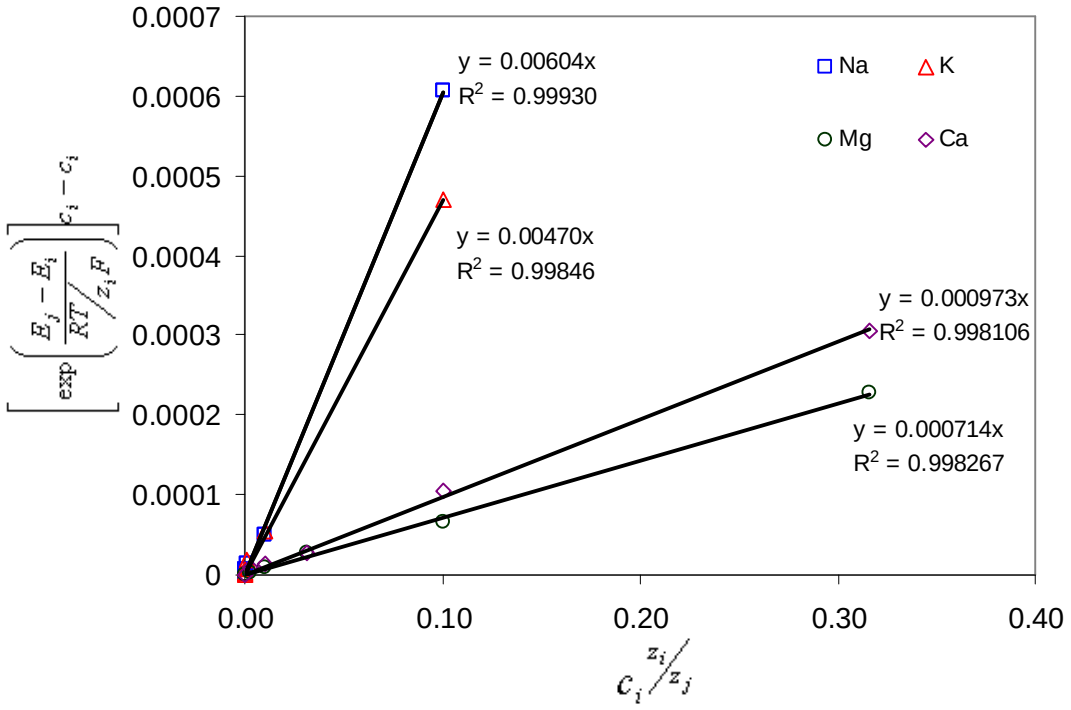

Figure 4.8 Selectivity plot for interfering ions, sodium, potassium, magnesium and calcium for procaine (PrHy) selective electrode.

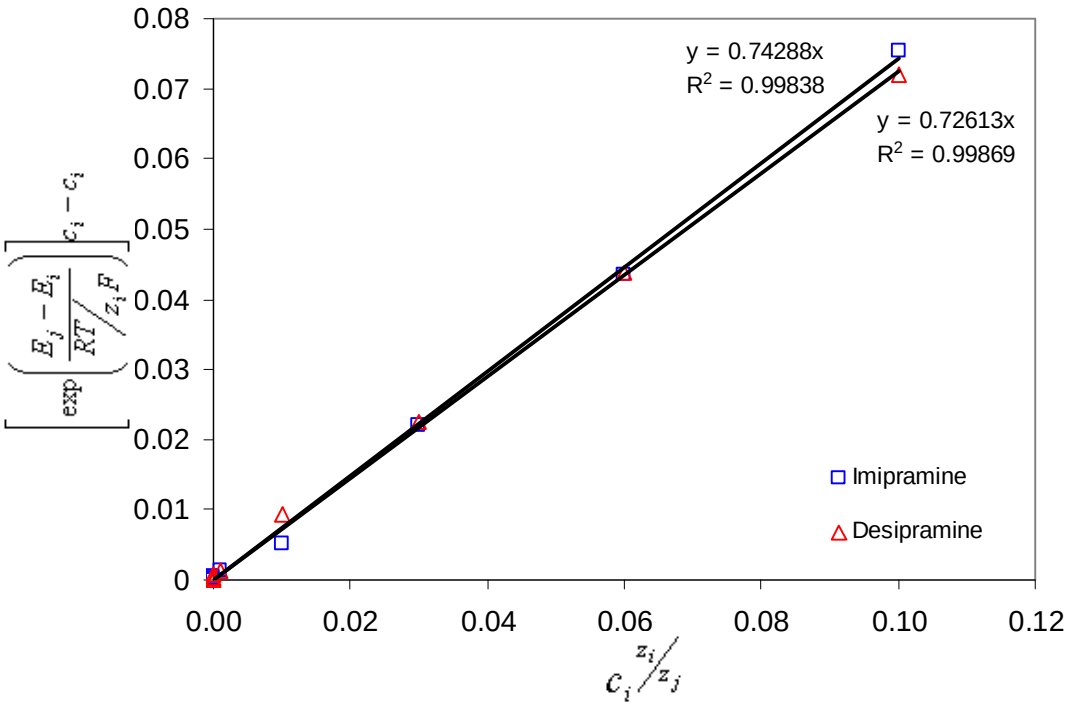

Figure 4.9 Selectivity plot for interfering drugs, imipramine and desipramine for procaine (PrHy) selective electrode.

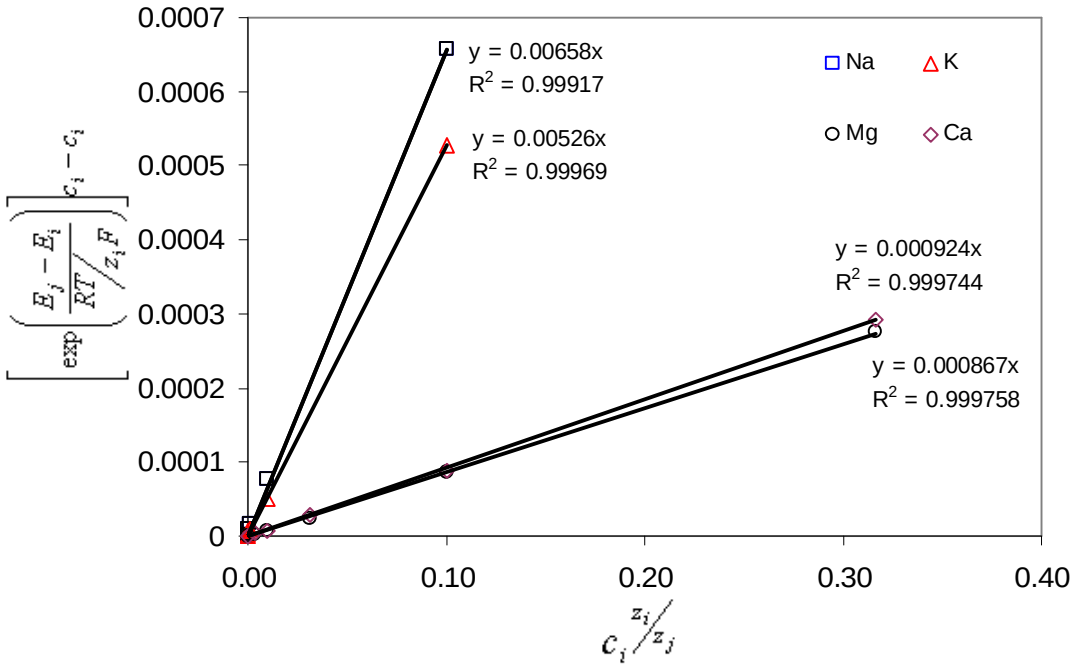

Figure 4.10 Selectivity plot for interfering ions, sodium, potassium, magnesium and calcium for imipramine (IMI) selective electrode.

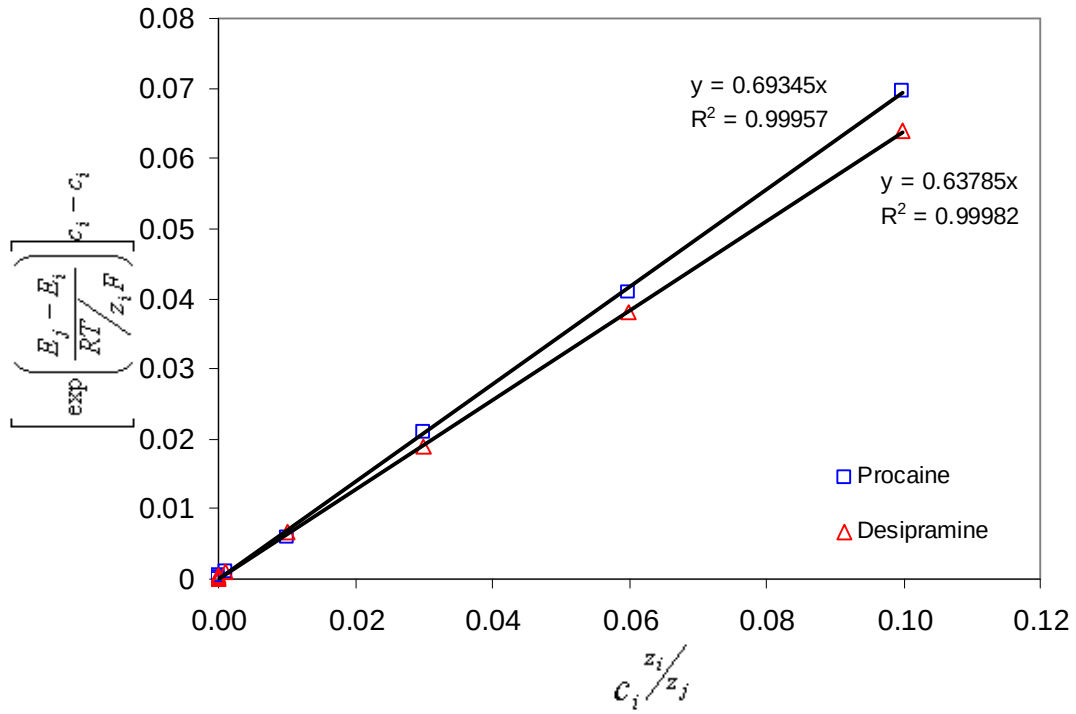

Figure 4.11 Selectivity plot for interfering drugs, procaine and desipramine for imipramine (IMI) selective electrode.

4.5 Summary

The PrHy and IMI selective electrodes showed excellent reproducibility and stability. However, all the membranes showed deviation from the ideal Nernstian response and this could be due to the slight self-aggregation of the drug molecules. Deviations at higher and lower concentrations of both drug solutions were noticed and this might be related to aggregation of drug molecules and the insensitivity of the sensor respectively.

Through the incorporation of ion-exchanger, the sensitivity of the membrane could be improved as the ion-exchanger would impart added stability and more electroactive sites carriers would be present for the transfer of ions. However, there was a maximum amount of ion-exchangers that could be added. The changes in ratio of solvent mediator to drug complex would not have any effect on the sensitivity of the membrane.

The PrHy selective electrode was only stable over pH of 3 to 8.5, while IMI selective electrode was only stable in the pH range of 4 to 8. This was due to the increase in number of deprotonated PrHy or IMI molecules at pH > 8.5 or pH > 8 respectively. At low pH, the presence of large amount of H^+ ions created significant interference on the outputs. pK_a of PrHy was found using the drug electrode to be 9.6 while the pK_a of IMI was found to be 9.2, which were quite similar to those reported in the literature. The response of the electrode would not be affected by the common cations like Na^+, K^+, Mg^{2+} and Ca^{2+} found in the body fluids but marked interference from lipophilic antiarrhythmic drugs like procaine, imipramine and desipramine could be observed.

5.0 MAA-EA NANOGELS AND PrHy INTERACTIONS, RELEASE AND MODELING

Two series of pH-responsive nanogels, prepared with varying cross-linking (DAP) density and molar ratio of acidic groups (MAA) will be examined as a function of neutralization degree (α) of the acidic groups. The swelling behavior (microscopic) of the pH-responsive nanogel will be studied by varying the ionic strength. The pH and conductivity curves as a function of α exhibit a well-defined equivalence point corresponding to complete neutralization of MAA groups at $\alpha = 1$. Therefore, the actual molar ratio of MAA and EA in the nanogels is very close to the targeted value and the slight deviation is within experimental error of 2%. The nanogel and drug solutions of desired concentrations were prepared from stock solutions for isothermal titration calorimetric, ζ-potential and laser light scattering studies. Through these characterizations, the drug binding mechanism of PrHy to MAA-EA nanogels will be studied and changes in particle sizes at different drug loading ratios will be investigated. The binding mechanism will provide insights on the release behavior.

From the literature [Ritger and Peppas, 1987; Xiong et al., 2001], it was reported that the fraction (M_t/M_∞) of the amount of drug released at time t is widely used to interpret the drug release behaviors. Here, M_t is the amount of drugs released at time t and M_∞ is the amount of drugs released at infinite time or the total amount of drugs incorporated in the carrier. Assuming that the swelling occurred first at the surface and the drug was uniformly distributed in the nanogels, the drug on the surface layer will contribute to a higher release rate. The delayed release of the drug may be a consequence of extraction

of drug from inside the nanogel. Drug release was carried out with varying parameters, such as concentration gradient, pH, drug loading ratio, cross-linking density and MAA-EA molar ratio, using the novel drug selective electrode (DSE) method. Modeling with an existing Berens and Hopfenberg model was carried out to gain insights into the diffusion and chain relaxation behavior during the release process.

5.1 Characterization of MAA-EA nanogels

5.1.1 Effect of cross-linking density

5.1.1.1 Potentiometric titration studies

The pH and conductivity curves obtained from titrating 1 M NaOH into 0.1 wt% MAA-EA nanogels containing 20 mole percent MAA at varying cross-linking density in 10 mM NaCl solution are shown in Figure 5.1. In Figure 5.1, the pH and conductivity were plotted against α.

There is a sharp increase in pH values from approximately 4.2 to 6 in the range of $\alpha = 0$ to $\alpha \sim 0.1$ for all the three different nanogel samples. Thereafter, the pH curves increased progressively until the neutralization process was complete at $\alpha = 1$. This may indicate that the nanogels do not undergo conformational transition throughout the neutralization process, which is unlike the HASE polymer containing hydrophobic pendant side groups where a plateau was observed [Wang et al., 2000]. The sharp increase in pH at low α is due to strong acid-base interaction caused by neutralization of small amounts of sulfate ($\sim SO_3H$) groups introduced from the initiator during synthesis. This is a typical phenomenon for synthetic polyacid and was observed in many studies on surface charges of colloidal particles [Wang, 2004].

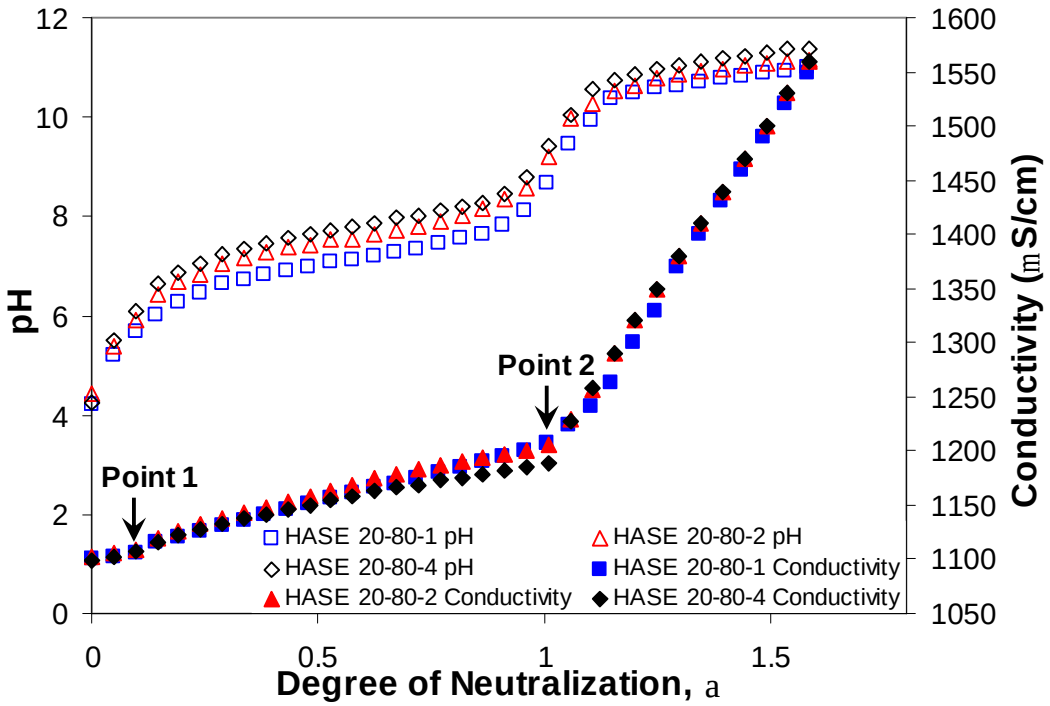

Figure 5.1 pH and conductivity curves obtained from titrating 1 M NaOH into 0.1 wt% MAA-EA nanogels containing 20 mole percent MAA with varying cross-linking density in 10 mM NaCl solution.

On the conductivity curves, two distinct equivalence points (Points 1 and 2) as indicated by the arrows were observed. The first equivalence point (Point 1) corresponded to a sharp increase in pH at $\alpha \sim 0.1$, which is due to the strong acid-base neutralization of small amounts of sulfate ($\sim SO_3H$) groups introduced by the initiator. The second equivalence point (Point 2) at $\alpha = 1$, is due to the complete neutralization of MAA groups and beyond this point conductivity increased progressively with the addition of excess NaOH. The conductivity curves leveled off with an increase in cross-linking density, which is due to the reduction in particle mobility when the polymer chains were increasingly cross-linked. The values of the conductivity over the course of neutralization were fairly identical showing that the H^+ ions from COOH in the nanogels

have analogous diffusion velocity that is independent of cross-linked density indicating nanogels have comparable size and molecular weight. The three nanogels (HASE 20-80-1, HASE 20-80-2 and HASE 20-80-4) with feed monomer mole percent of 20% MAA-80% EA has an actual composition of 22:78, 23:77 and 21:79 respectively.

5.1.1.2 Particle size characterization

The particle sizing of 0.1 wt% pH-responsive MAA-EA nanogels containing 20 mole percent MAA at varying cross-linking density in 10 mM NaCl solution were obtained using the Brookhaven Dynamic Light Scattering (DLS) system for α ranging from 0 to 1. In the unneutralized state, all the different nanogels have a hydrodynamic radius (R_h) of ~33 nm. The R_h increased continuously with α (or pH) from 0 to 1 as can be seen in Figure 5.3. As dissociation of MAA groups occurred, increasing charges within the nanogels caused electrostatic repulsions between the chains, which swelled the particles. The enhanced osmotic pressure exerted by counter-ions trap inside the nanogels by electrostatic attraction with the ionized carboxylate groups, as depicted in Figure 5.2, an increase in α also produced an increase in R_h.

The swelling characteristics at $\alpha \leq 0.3$ is roughly similar for all the three MAA-EA nanogels containing 20 mole percent MAA at varying cross-linking density. The R_h values deviated more when α exceeded 0.3. The hydrophobic attraction between the EA blocks will limit the increase of R_h at $\alpha \leq 0.3$, whereas the osmotic pressure caused by counter-ions attracted to the carboxylate groups will produce a sudden increase in R_h after $\alpha = 0.3$. Therefore, a transition region of nanogels caused by the competition of these two types of interactions was observed at $\alpha = 0.3$.

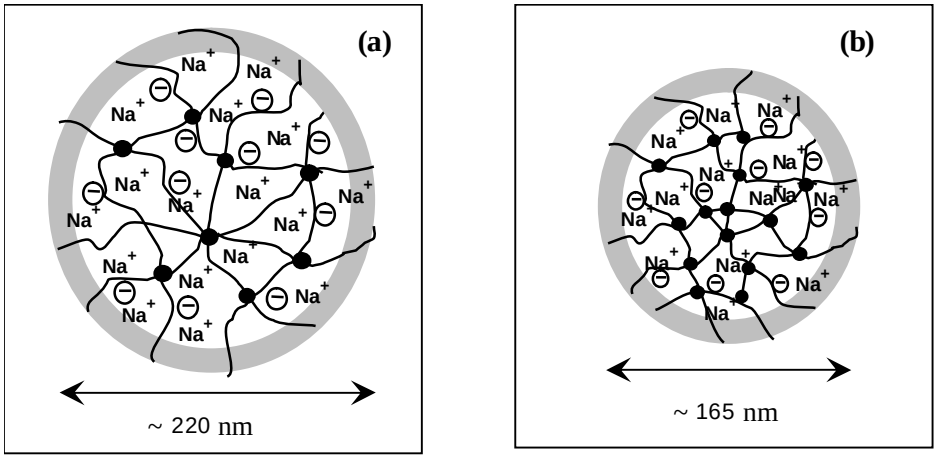

Figure 5.2 Schematic representation of nanogels in the swollen state, cross-linked at different density; (a) low cross-linked density (HASE 20-80-1) and (b) high cross-linked density (HASE 20-80-4). The full dots between chain segments represent the cross-linker. The counter-ions from the base (NaOH) used to neutralize the nanogels are represented by the symbol Na^+ and the symbol y represents the neutralized carboxylic groups, COO^-. The outer shell represents the region where electro-neutrality is not satisfied locally.

At $\alpha \leq 0.3$, the increment in R_h was smaller due to the osmotic pressure exerted by the counter-ions and the electrostatic repulsion between the carboxylate groups that are insufficient to overcome the strong hydrophobic attraction between EA blocks. When α was increased beyond 0.3, the osmotic pressure overcame the hydrophobic attraction, which caused the R_h to increase rapidly. The swelling behavior for nanogels with lower cross-linking density was higher than nanogels with higher cross-linking density as observed in Figure 5.2 and 5.3. The maximum R_h for HASE 20-80-1 was ~110 nm as compared to ~82 nm for HASE 20-80-4.

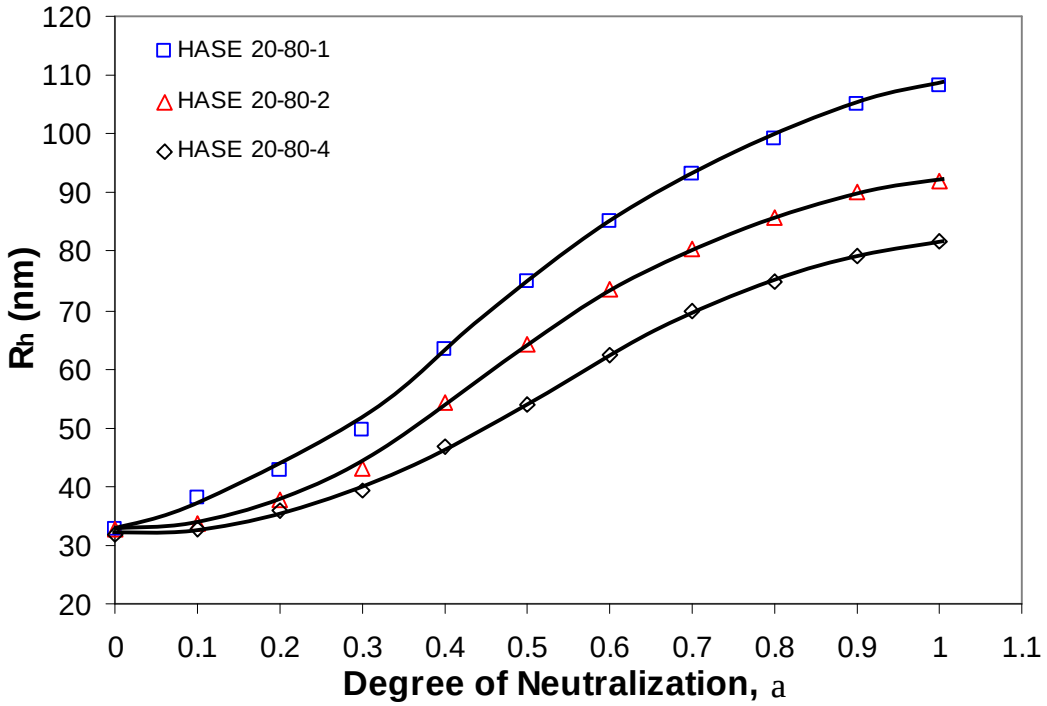

Figure 5.3 Dependence of hydrodynamic radius (R_h) on degree of neutralization (α) for 0.1 wt% MAA-EA nanogels containing 20 mole percent MAA with varying cross-linking density in 10 mM NaCl solution.

5.1.1.3 ζ-potential studies

The ζ-potential of 0.1 wt% pH-responsive MAA-EA nanogels containing 20 mole percent MAA at varying cross-linking density in 10 mM NaCl solution is shown in Figure 5.4. The ζ-potential generally became more negative with increasing α, and it became less negative after $\alpha = 0.3$. This trend was similar to the particle size shown in Figure 5.3. The trend before $\alpha = 0.3$ was due to an increase in the amounts of COO^- groups without a significant increase in size resulting in the ζ-potential becoming more negative. After the critical point of $\alpha = 0.3$, the osmotic pressure was able to overcome the hydrophobic forces between EA segments, which produced enhanced swelling of the

nanogels. The large increase in size will reduce the mobility of nanogels, hence the ζ-potential became less negative. The ζ-potential for HASE 20-80-1 (at α = 1, ~-24.2 mV) was less negative than HASE 20-80-2 (at α = 1, ~-25.7 mV) and HASE 20-80-4 (at α = 1, ~-27.2 mV) after α = 0.3 as the size was larger and mobility was reduced. At α < 0.3, the increase in ζ-potential was identical for the 3 nanogels.

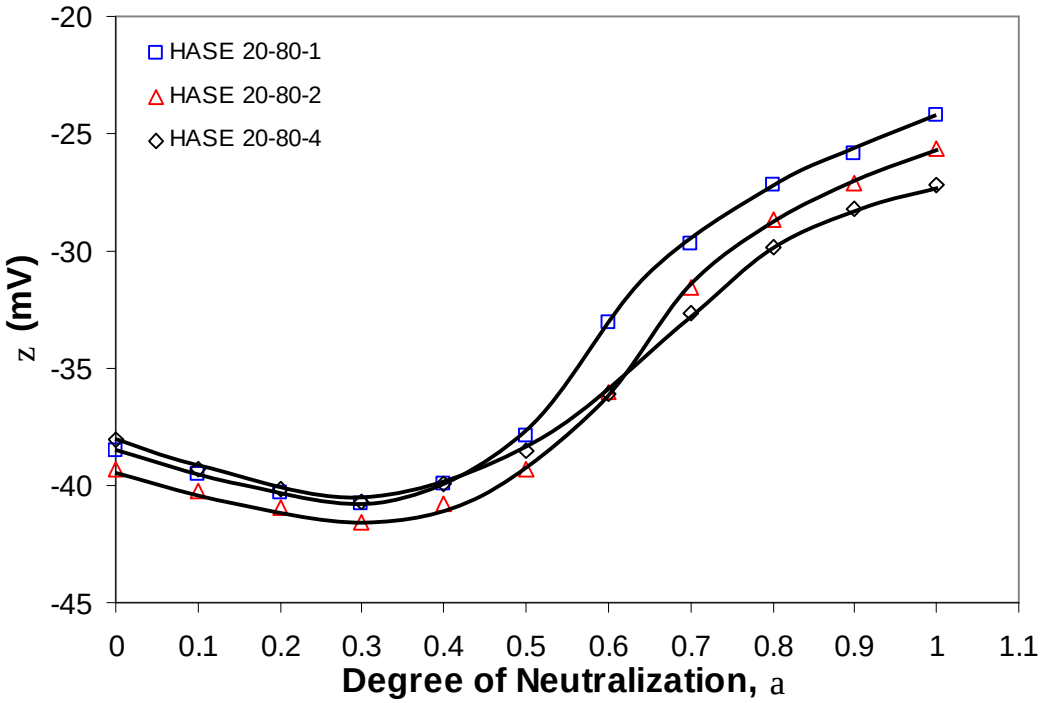

Figure 5.4 Dependence of ζ-potential on degree of neutralization (α) for 0.1 wt% MAA-EA nanogels containing 20 mole percent MAA with varying cross-linking density in 10 mM NaCl solution.

5.1.2 Effect of MAA-EA molar ratio

5.1.2.1 Potentiometric titration studies

The pH and conductivity curves obtained from titrating 1 M NaOH into 0.1 wt% MAA-EA nanogels cross-linked with 4 wt% DAP in 10 mM NaCl solution are shown in Figure 5.5. There was a sharp increase in pH values from approximately 4 to 6 in the range of $\alpha = 0$ to $\alpha \sim 0.1$ for all the four different nanogels. Thereafter, the pH curve increased progressively until the neutralization process was completed at $\alpha = 1$. This may indicate that the nanogels did not undergo conformational transition throughout the neutralization process. The sharp increase in pH at low α was due to the strong acid-base interaction caused by the neutralization of a small amount of sulfate ($\sim SO_3H$) groups introduced from the initiator during synthesis.

The conductivity curves possessed two transition points as indicated by the arrows in Figure 5.5. The first transition was due to the strong acid-base neutralization of ($\sim SO_3H$) groups and the second transition was due to the complete neutralization of MAA groups. Based on the work of Wang [Wang, 2004] on linear MAA-b-EA copolymers, the slopes of the nanogels conductivity curves were gentler than those of the block copolymers. The cross-linked nanogels have polymer chains that were chemically bonded and cannot diffuse freely as compared to block copolymers. As a result, the mobility of the poly-ions was reduced leading to a gentler slope on the conductivity curves. The values of the conductivity over the course of neutralization were fairly identical as the H^+ ions from COOH in the nanogels have analogous diffusion velocity that was independent of MAA-EA molar ratio indicating nanogels have comparable size. The four nanogels (HASE 20-80-4, HASE 30-70-4, HASE 40-60-4 and HASE 50-50-4) with feed monomer

mole percent of 20% MAA-80% EA, 30% MAA-70% EA, 40% MAA-60% EA and 50% MAA-50% EA has an actual composition of 21:79, 31:69, 39:61 and 53:47 respectively.

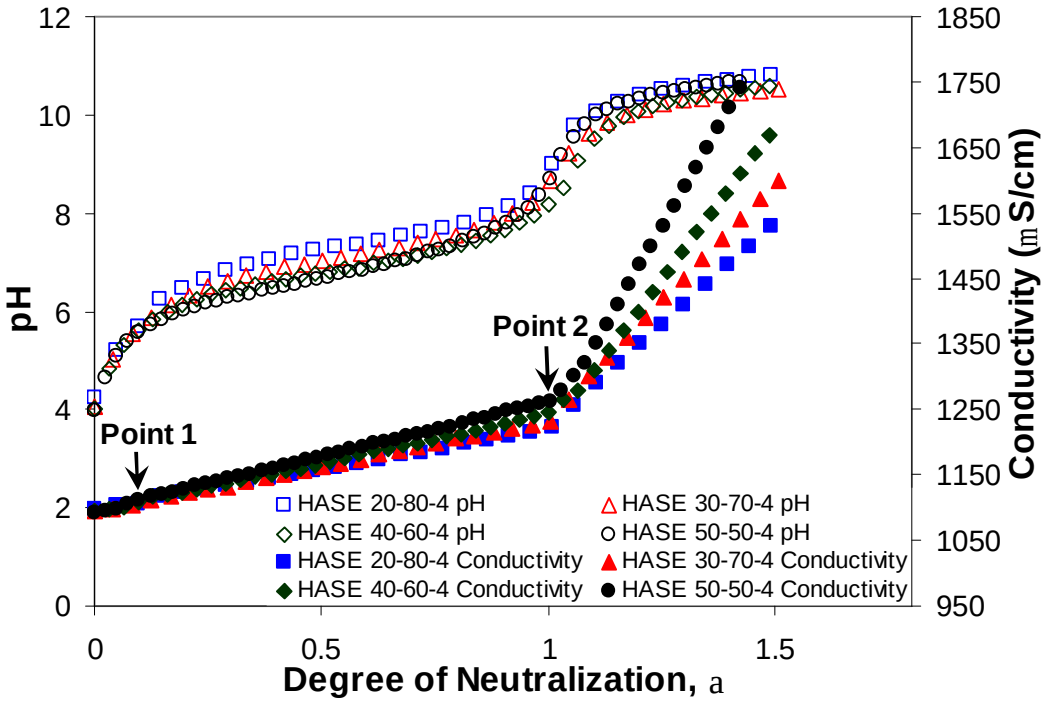

Figure 5.5 pH and conductivity curves obtained from titrating 1 M NaOH into 0.1 wt% MAA-EA nanogels cross-linked with 4wt% DAP with varying MAA-EA molar ratio in 10 mM NaCl solution.

5.1.2.2 Particle size characterization

Particle sizing of 0.1 wt% MAA-EA nanogels with fixed cross-linking density (4 wt% DAP) but varying MAA-EA ratio (HASE 20-80-4, HASE 30-70-4, HASE 40-60-4 and HASE 50-50-4) were characterized in 10 mM NaCl solution by the DLS for α ranging from 0 to 1. The change in R_h as a function of α is shown in Figure 5.6. The pH responsive R_h shows a continuous increase as α increased from 0 to 1. This is due to the

enhanced osmotic pressure exerted by the counter-ions trapped inside the nanogels by electrostatic attraction with the ionized carboxylate groups. The nanogels with lower MAA-EA molar ratio were less swellable as a lower osmotic pressure will be generated by a lower MAA content. The R_h for HASE 50-50-4 at $\alpha = 1$ was ~148 nm and R_h for HASE 20-80-4 at $\alpha = 1$ was ~82 nm.

From Figure 5.6, at $\alpha = 0$, the R_h for nanogels with a larger content of MAA was larger, whereas the R_h for HASE 20-80-4 and HASE 50-50-4 was ~32 and ~42 nm respectively. During the seeded emulsion polymerization, EA will reside in the core of the particle due to the hydrophobicity while MAA, being more hydrophilic will remain on the surface of the particle and the particle became larger as the content of MAA was increased during polymerization.

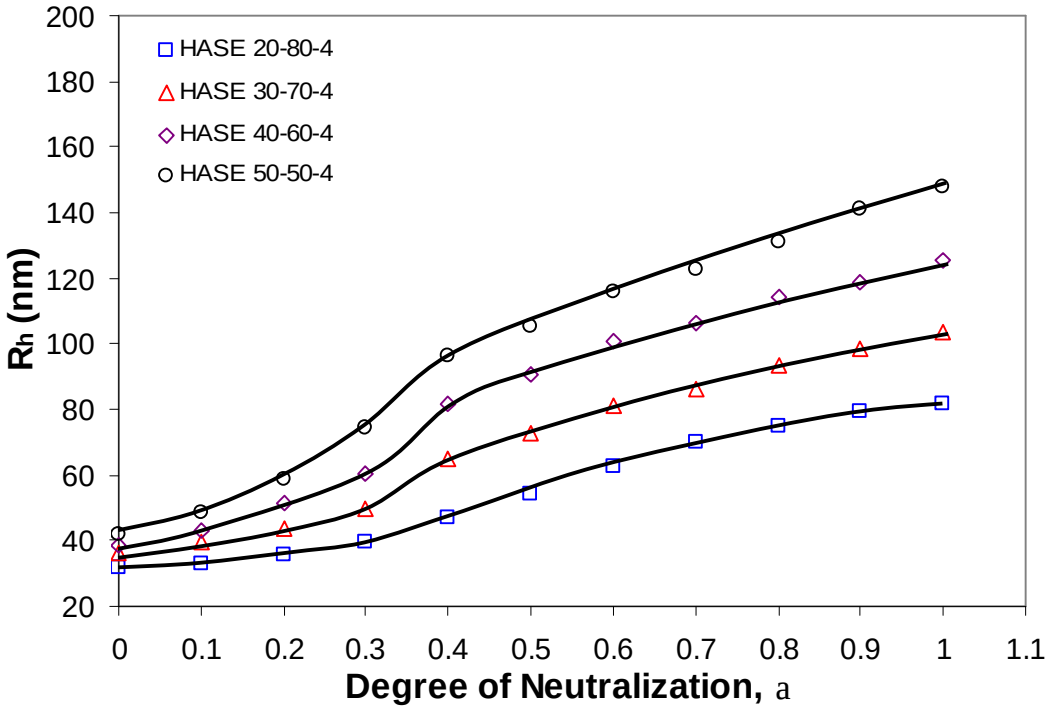

Figure 5.6 Dependence of hydrodynamic radius (R_h) on degree of neutralization (α) for 0.1 wt% MAA-EA nanogels cross-linked with 4 wt% DAP with varying MAA-EA molar ratio in 10 mM NaCl solution.

Based on Figure 5.6, particle sizes began to increase at a higher rate as reflected by a sharp increase at $\alpha > 0.3$. This is caused by the competition between hydrophobic attraction and osmotic pressure. At $\alpha \leq 0.3$, the strong hydrophobic attraction between the EA blocks will be larger than the osmotic pressure created by counter-ions attracted to the ionized carboxylate groups, thus limiting the increase in particle size. After the transition point ($\alpha = 0.3$), the osmotic pressure was able to overcome the hydrophobic attraction resulting in a sharp increase in the particle size.

5.1.2.3 ζ-potential studies

The ζ-potential of 0.1 wt% pH-responsive MAA-EA nanogels with fixed cross-linking density (4 wt% DAP) but varying MAA-EA ratio in 10 mM NaCl solution is shown in Figure 5.7. The ζ-potential generally became more negative with increasing α before becoming less negative after $\alpha = 0.3$. This trend is similar to the trend in the particle size as shown in Figure 5.6. After $\alpha = 0.3$, due to the increase in osmotic pressure exceeding the hydrophobic attractions, HASE 50-50-4 will swell the most therefore having a less negative ζ-potential (at α = 1, ~-24.0 mV) as compared to HASE 20-80-4 (at α = 1, ~-27.2 mV), HASE 30-70-4 (at α = 1, ~-26.1 mV) and HASE 40-60-4 (at α = 1, ~-24.5 mV). Before $\alpha = 0.3$, HASE 50-50-4 has the largest increase in ζ-potential as there are more MAA groups within the nanogels, which will result in a more negative ζ-potential.

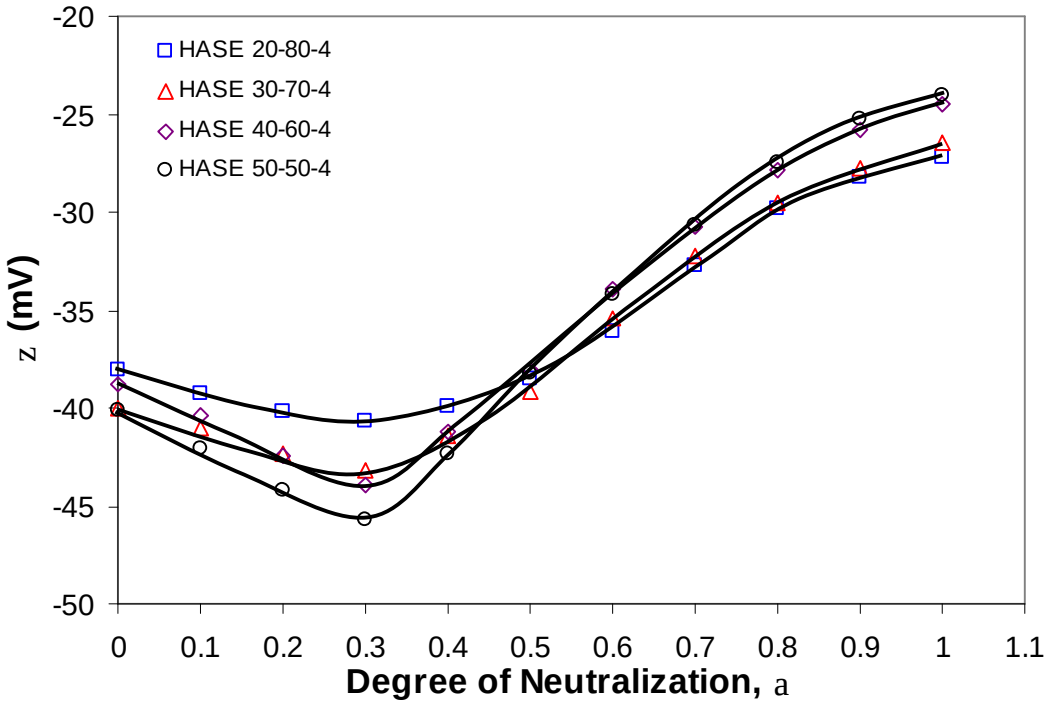

Figure 5.7 Dependence of ζ-potential on degree of neutralization (α) for 0.1 wt% MAA-EA nanogels cross-linked with 4 wt% DAP with varying MAA-EA molar ratio in 10 mM NaCl solution.

5.1.3 Effect of ionic strength on particle size

The dependence of R_h on varying α for 0.1 wt% HASE 20-8-2 were characterized by DLS in salt concentration ranging from 0.1 to 100 mM NaCl.

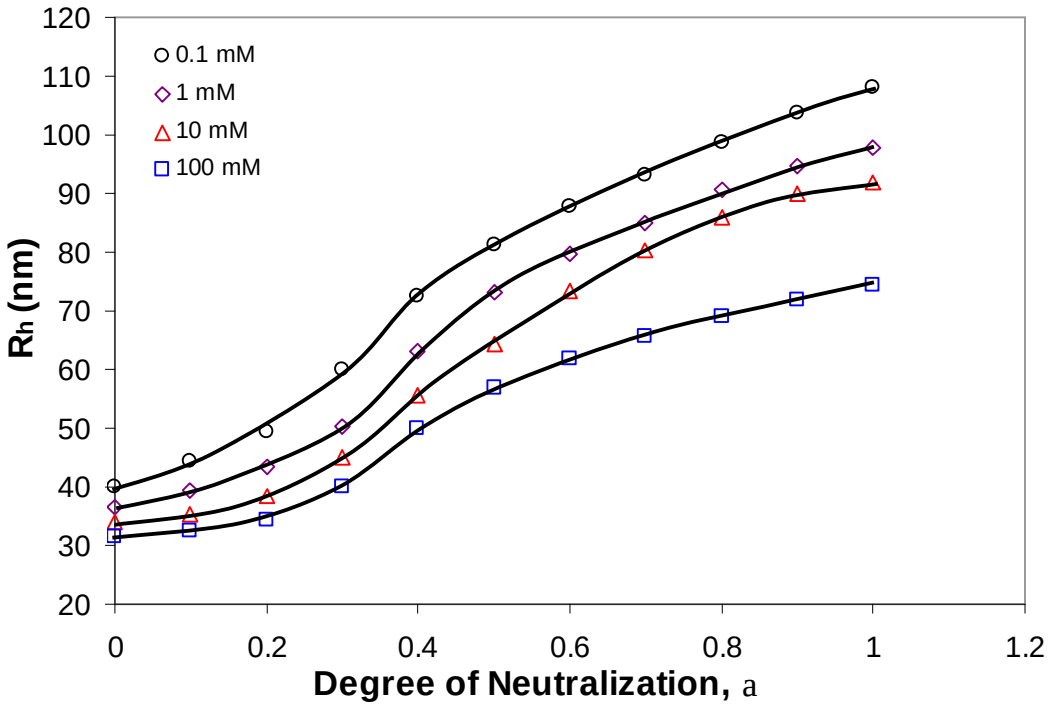

Figure 5.8 Dependence of R_h on α for 0.1wt% HASE 20-80-2 in different salt concentrations, [NaCl].

Based on the work of Cloitre [Cloitre et al., 2003] and Tan [Tan et al., 2004], in the presence of salt, there are two sources of counter-ions: Na^+ from the NaCl solution and Na^+ from NaOH added to neutralized the nanogels. The particle sizes of the nanogels decreased with the addition of salt due to charge shielding effect from NaCl. The assumption that all the counter-ions associated with ionized units will not be trapped inside the nanogel as in the case of salt free solution is not valid.

From the work of Tan et al. (Figure 5.9) [Tan et al., 2004], the concentration of K^+ ions (C_{K^+}) in the bulk solution, measured using the potassium ion selective electrode, undergoes a slight decrease in concentration with increasing α while the concentration of mobile Na^+ ions (C_{Na^+}) in the bulk increases with α. The slight decrease in C_{K^+} with

increasing α shows that some of the K^+ ions will penetrate into the nanogels and shield the carboxylate groups. The increase in C_{Na^+} with increasing α shows that with the penetration of K^+ ions some of the Na^+ ions will be expelled.

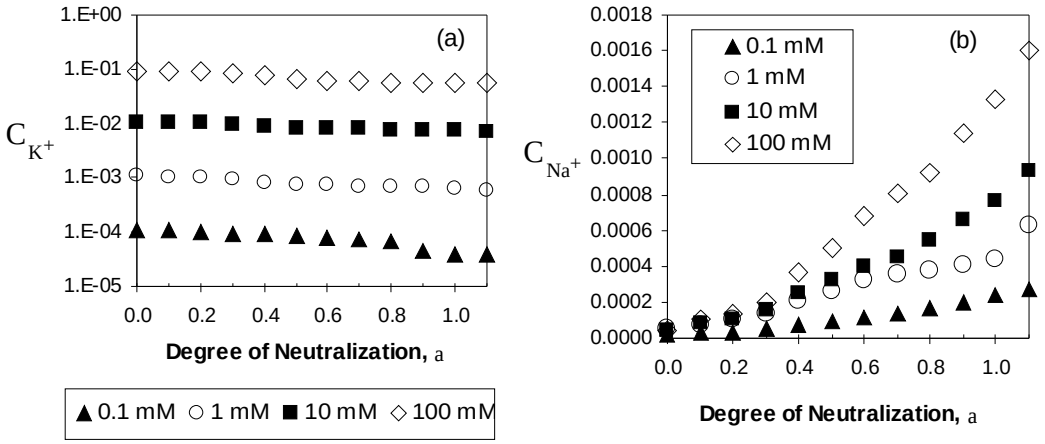

Figure 5.9 Concentration of mobile counter-ions (a) potassium, C_{K^+} and (b) sodium, C_{Na^+}, for HASE-20-80-2 at varying α and four different salt concentrations, [KCl] [Tan et al., 2004].

With the addition of NaCl, some of the counter-ions from NaCl (Na^+) will remain mobile in the bulk solvent while the rest will penetrate the porous nanogels to shield the negatively charged carboxylate groups. As a result, some of the Na^+ counter-ions from NaOH will be expelled and thereby regaining translational entropy to become mobile sodium ions. Figure 5.10 illustrates the effect of addition of salt on the counter-ions inside the nanogel and bulk solution at low and high salt concentration. With the increase in salt concentration, the charge shielding effect will become stronger. As a result, the osmotic pressure as well as the particle size will decrease and more Na^+ ions will be expelled from the nanogels to the bulk solution as illustrated in Figure 5.10 where more Na^+ ions can be seen in the nanogel.

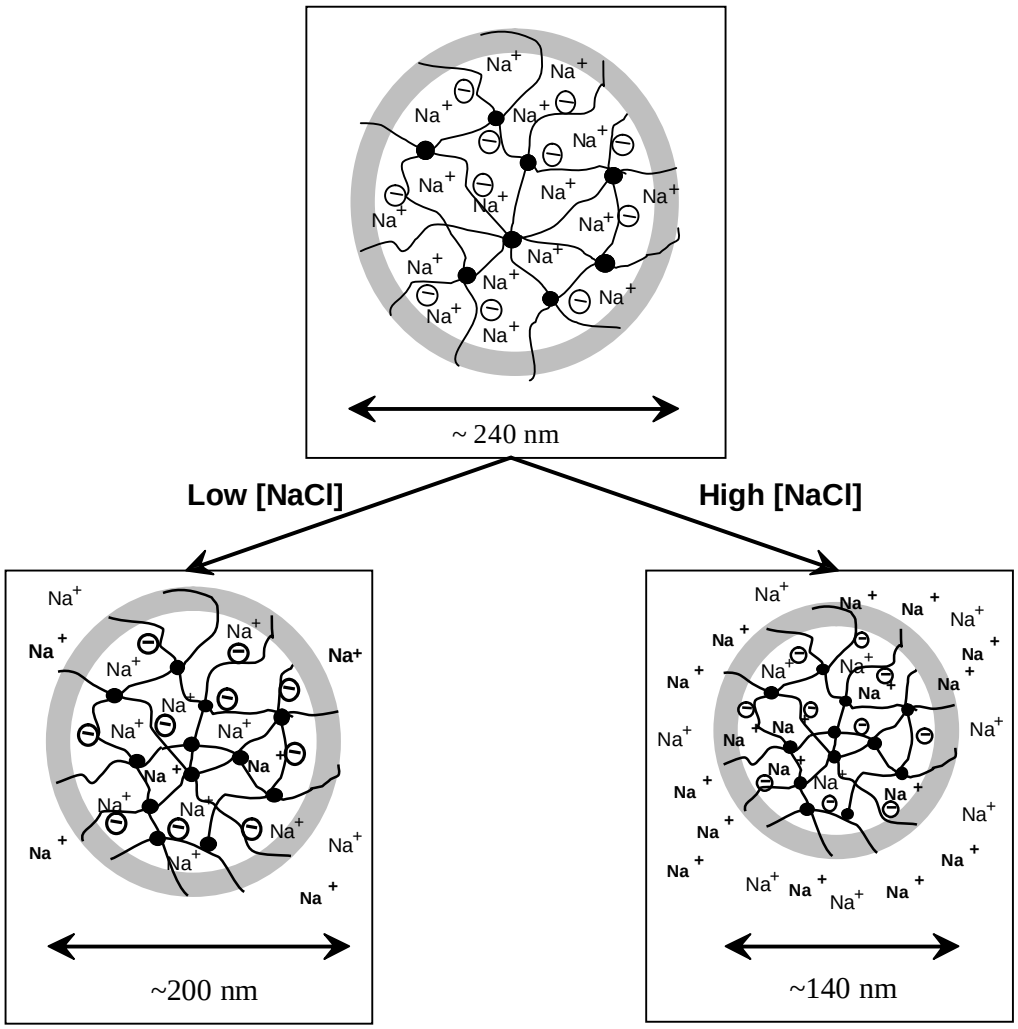

Figure 5.10 A pictorial representation of the effect of salt (NaCl) (**Na^+**) on the counter-ions (Na^+) inside the nanogels and bulk solution at different salt concentrations.

5.2 Drug interactions with MAA-EA nanogels

Polyelectrolytes are widely used as drug release vehicles [Eichenbaum et al., 1999; Madeline and Peppas, 1999; Kim and Peppas, 2003; Foss et al., 2004; Yang at al., 2004] due to the ability to swell or deswell at different pHs, which enables the release of drugs at different rates. The binding between cationic drugs and anionic polyelectrolytes is generally considered an ion-exchange process through the electrostatic binding, where condensed counter-ions on the polymer chains are replaced by bounded drugs [Eichenbaum et al., 1999; Madeline and Peppas, 1999; Kiser at al., 2000]. Cationic drugs will exhibit a molecular structural shift between two forms, depending on the pH of the solution; an uncharged base molecule (RN), and a positively charged cation (RNH^+):

$$RNH^+ \leftrightarrow RN + H^+ \tag{5.1}$$

When the solution becomes more acidic, the concentration of hydrogen ions (H^+) increases and combines with the uncharged basic molecule, which shifts the equilibrium to the left. As the pH increases, there will be less positively charged hydrogen ions thus shifting the equilibrium to the right.

The differential enthalpy curves for titrating 0.6 M PrHy solution into fully neutralized (α = 1) 0.1 wt% MAA-EA nanogels containing 20 mole percent MAA with varying cross-linking density in 10 mM NaCl solution and fully neutralized 0.1 wt% MAA-EA nanogel cross-linked with 4 wt% DAP with varying MAA-EA molar ratio in 10 mM NaCl solution are shown in Figures 5.11 and 5.12 respectively. In both figures, the enthalpy was plotted against the concentration of PrHy. A titration of the drug into 10 mM NaCl, named as dilution, was included in Figures 5.11 and 5.12.

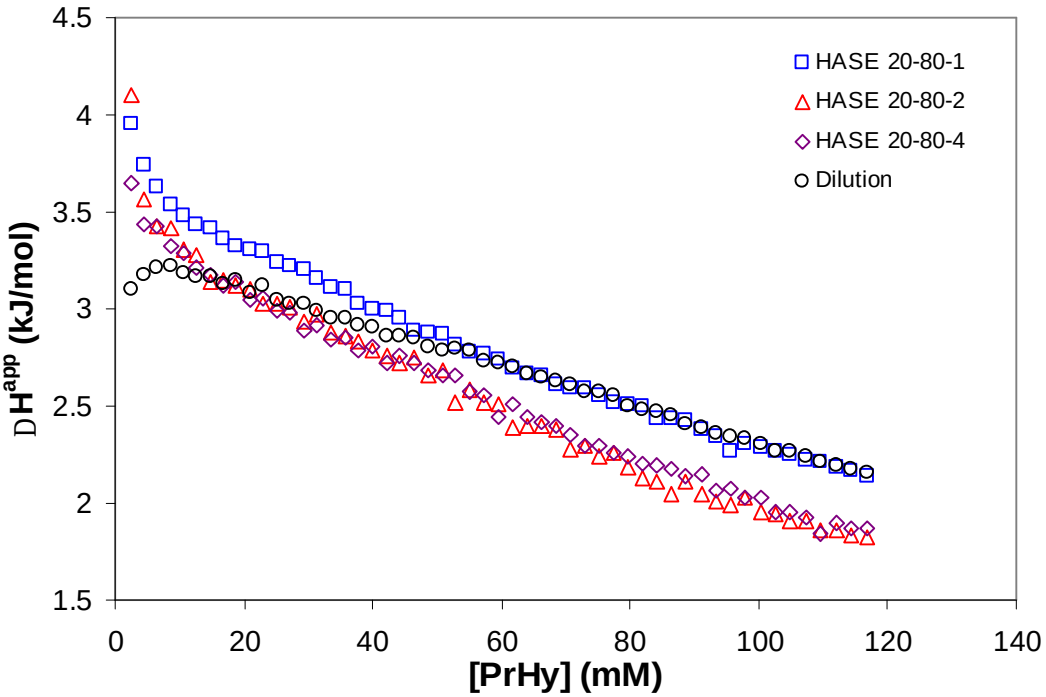

Figure 5.11 Differential enthalpy curves for titrating 0.6 M PrHy into 0.1 wt% MAA-EA nanogels containing 20 mole percent MAA with varying cross-linking density in 10 mM NaCl solution at 25 ^{o}C.

From Figure 5.11, the enthalpy profiles for titrating PrHy into different nanogels with varying cross-linking density showed no change in shape from the titration of PrHy into 10 mM NaCl solution. The enthalpies of dilution for all the curves were similar to each other, suggesting that PrHy did not bind electrostatically to MAA-EA nanogels. The drug molecules would diffuse into the nanogel and be bound hydrophobically. The pH for fully neutralized MAA-EA nanogels was ~8.5 which was also the pH where most of the amine type of drugs was deprotonated. In Chapter 4.3, the procaine drug electrode has also shown that there is a considerable reduction in EMF values at pH greater than 8.5. This is attributed to the large number of unprotonated PrHy as shown in Equation 5.1.

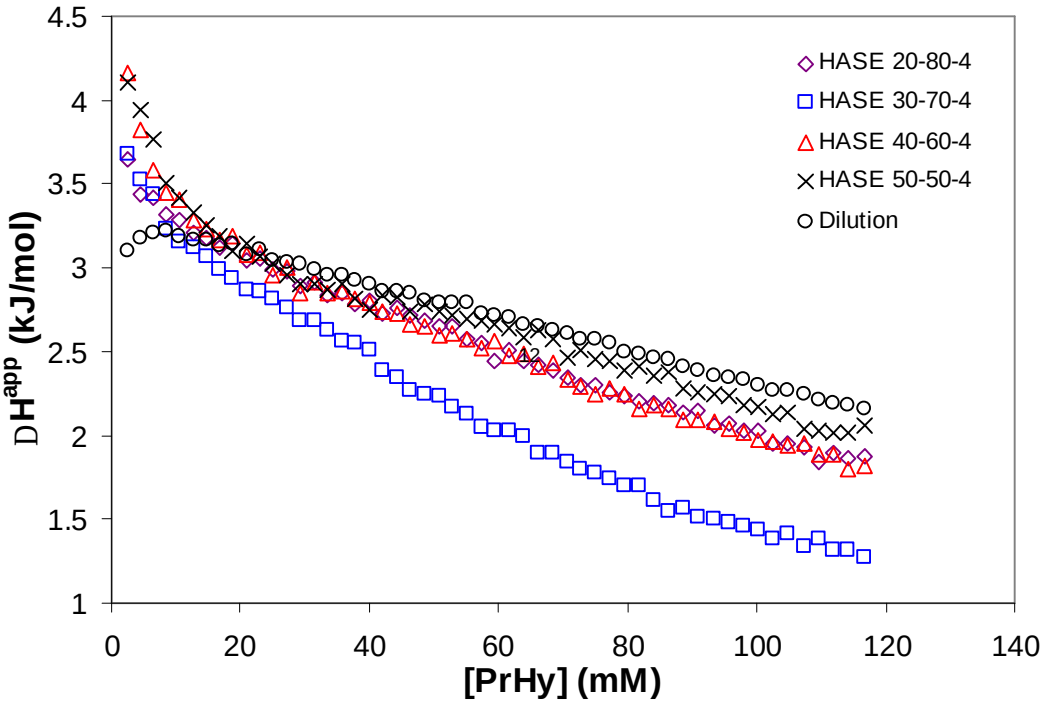

Figure 5.12 Differential enthalpy curves for titrating 0.6 M PrHy into 0.1 wt% MAA-EA nanogel cross-linked with 4 wt% DAP with varying MAA-EA molar ratio in 10 mM NaCl solution at 25 ^{o}C.

Similar trends were observed for the titration of PrHy into MAA-EA nanogels with varying MAA-EA content as shown in Figure 5.12. The pH for all the fully neutralized nanogels was ~8.5. Due to the presence of large number of unprotonated PrHy, the drug molecules will be loaded into the nanogel via diffusion and hydrophobic interaction, and not by electrostatic interactions.

The differential enthalpy curves for titrating 0.6 M PrHy into partially neutralized (α = 0.3, α = 0.5 and α = 1) 0.1 wt% HASE 50-50-4 in 10 mM NaCl is shown in Figure 5.13. Based on Figure 5.13, the titration results showed no electrostatic binding between the negatively charged COO^- groups and positively charged PrHy even when the pH was lowered from pH 9 (α = 1) down to pH 6.9 (α = 0.5) or pH 6.3 (α = 0.3), which

significantly lowered the concentration of unprotonated PrHy. This is probably due to the steric hindrance created by the two ethyl groups around N^+ as shown in Figure 5.14a. The two ethyl groups restrict the accessibility of the positively charged N^+, to the negatively charged COO^- ions. A similar titration was conducted using doxorubicin (DOX), under similar conditions as shown in Figure 5.15 to verify this hypothesis. DOX has no steric hindrance around the N^+ as shown in Figure 5.14b and the hydrogen ions around the N^+ do not shield the positive charge from the negatively charged COO^- groups. The differential enthalpy curves revealed an electrostatic interaction between the negatively charged COO^- groups and positively charged DOX. A higher concentration of DOX is required to achieve equilibrium for MAA-EA nanogels at $\alpha = 0.5$ as compared to $\alpha = 0.3$ as more COOH groups are ionized at $\alpha = 0.5$. However, $\alpha = 0.3$ has a steeper gradient in the initial stage as less of the DOX is deprotonated.

The concentration at which the enthalpy tended to zero (~20 mM) (in Figure 5.13) was almost the same for at all α which showed that the binding of PrHy onto the nanogels was not through electrostatic attraction. When the interaction is electrostatic, the concentration at which enthalpy becomes zero will be different due to the differences in number of binding sites on negatively charged MAA segments. No hydrogen bonding was believed to occur between PrHy and the nanogels as the enthalpy found in Figure 5.13 did not change much when the α changed from 1 to 0.3. Through the decrease in degree of neutralization, more COOH groups will be present and hydrogen bonding should be stronger but the result in Figure 5.13 showed otherwise. The ethyl groups surrounding the N^+ should create a steric hindrance to prevent the formation of hydrogen bonding.

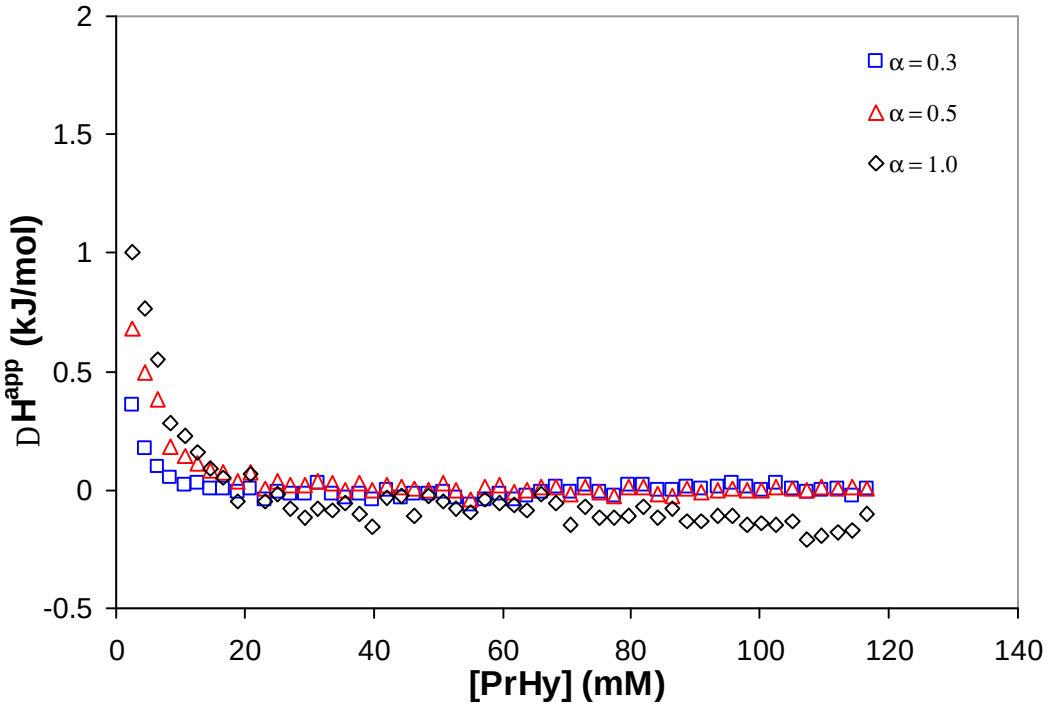

Figure 5.13 Differential enthalpy curves for titrating 0.6 M PrHy to HASE 50-50-4 at varying α in 10 mM NaCl solution at 25 °C.

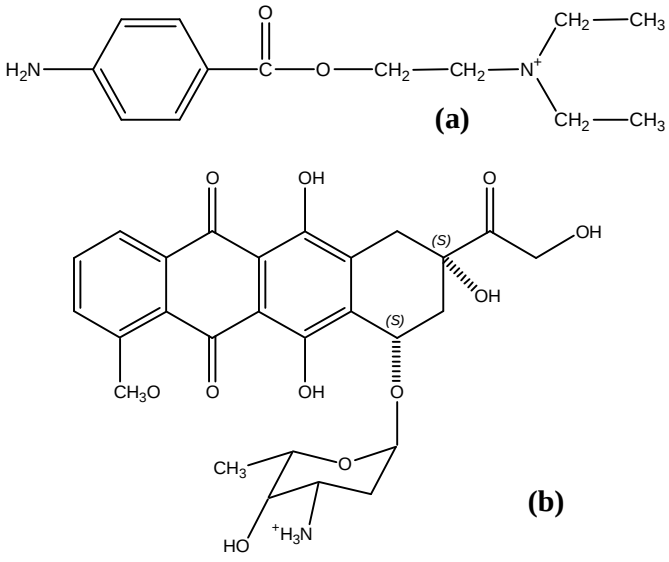

Figure 5.14 (a) Chemical structure of procaine (PrHy) and (b) chemical structure of doxorubicin (DOX).

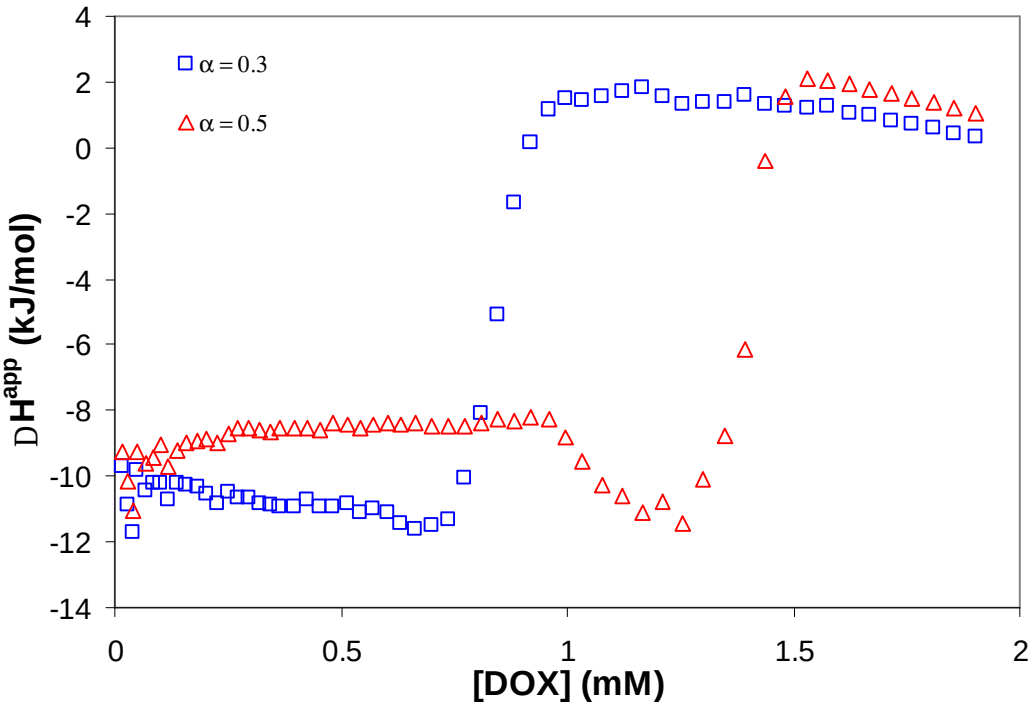

Figure 5.15 Differential enthalpy curves for titrating 7.5 mM DOX to HASE 50-50-4 at varying α in 10 mM NaCl solution at 25 ^{o}C.

The differential enthalpy curves for titrating 0.6 M PrHy solution into fully neutralized (α = 1) 0.1 wt% HASE 50-50-4 in 10 mM NaCl solution at varying temperature is shown in Figure 5.16. As the temperature was increased from 25 to 50 ^{o}C, ΔH showed a correspondingly higher value. This can be attributed to the enthalpy changes associated with an increase in the hydrophobic environment resulting in a stronger hydrophobic interaction between PrHy and MAA-EA nanogels. Therefore, PrHy was loaded onto the nanogels through hydrophobic interactions rather than electrostatic binding.

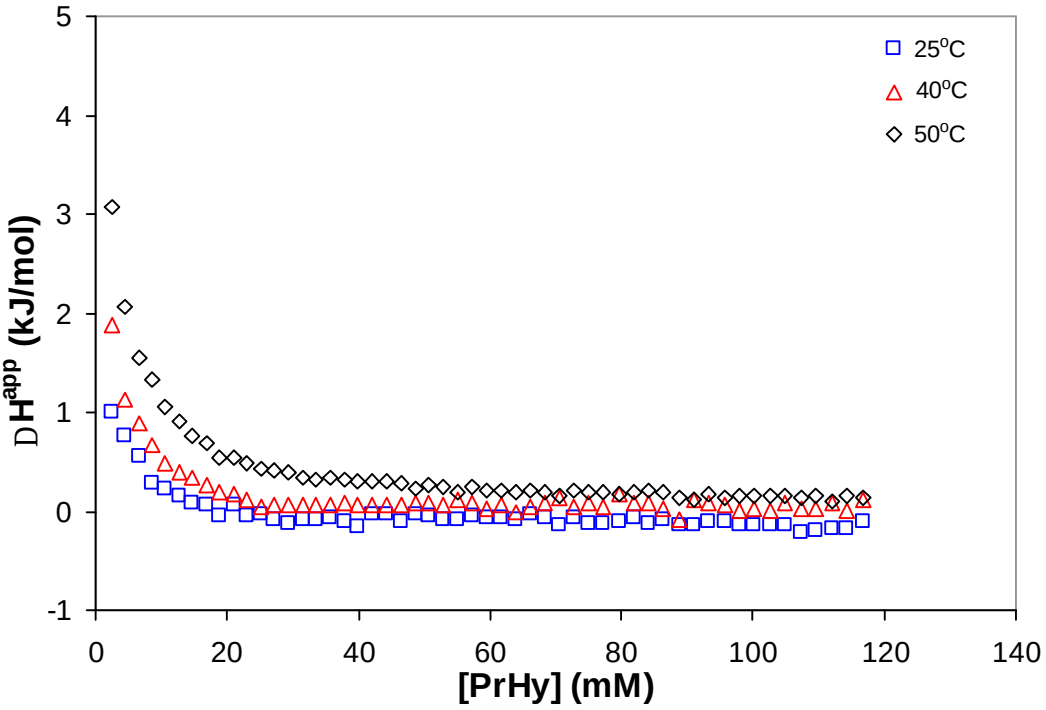

Figure 5.16 Differential enthalpy curves for titrating 0.6 M PrHy into 0.1 wt% HASE 50-50-4 in 10 mM NaCl solution at varying temperature.

Since the nanogel had been neutralized with NaOH, sodium ions (Na^+) are present in the solution, and if there is no increase in the concentration of Na^+, the results shown in Figure 5.13 can be further confirmed. Sodium ion-selective electrode was used to measure the concentration of mobile Na^+ ions as a function of time. Figure 5.17 displays the concentrations of mobile Na^+ ions as determined from Equation 5.2:

$$EMF = 241.165 + 49.256 \log C_{Na^+} \quad (5.2)$$

Figure 5.17 shows that the concentration of mobile Na^+ ions remained constant after the addition of 0.018 M PrHy into HASE 20-80-1 nanogel at $\alpha \sim 0.5$. This showed that the drug was not electrostatically attracted to the nanogel but diffused into the nanogel and

be hydrophobically bound. Thus, the drug did not displace the sodium ions from the negatively charged carboxylate groups.

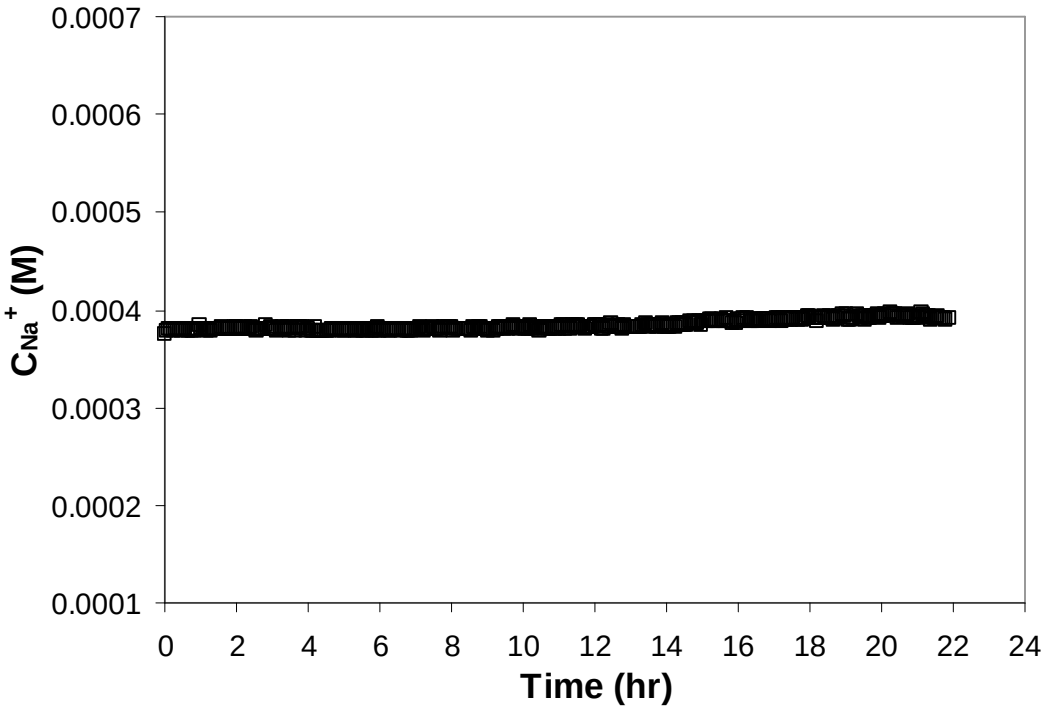

Figure 5.17 Concentration of mobile counter-ions (sodium), C_{Na}^{+}, calculated using the Nernst equation, Equation 5.2 for HASE 20-80-1 at α = 0.5 and using 0.018 M PrHy in 10 mM NaCl.

A change in transmittance of light is an indication of aggregation of particles resulting from the instability of the particles. Hydrophobicity is usually the main cause that induces instability in the particles. Transmittance for 0.5 M PrHy solution at varying pH was measured using the UV-Visible Spectrophotometer and the result was plotted as shown in Figure 5.18.

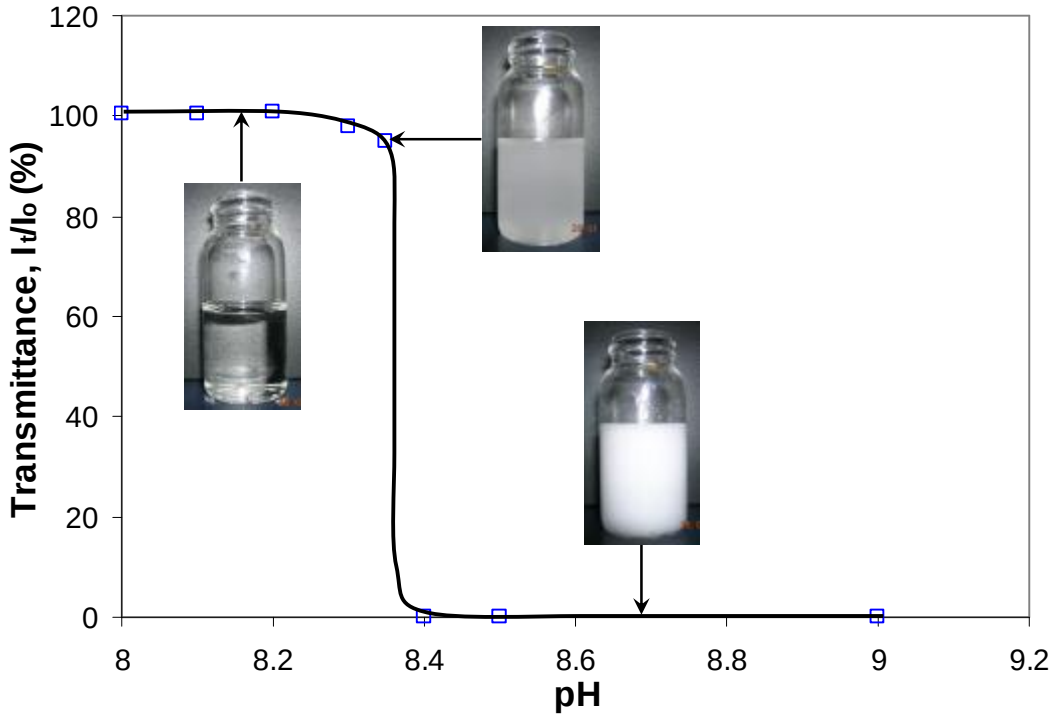

Figure 5.18 Transmittance of 0.5 M PrHy at varying pH.

The transmittance of 0.5 M PrHy solution was at 100% (clear solution) for all pH except at pH greater than 8.2. Above pH 8.2, the transmittance experienced a drop and fell abruptly to 0% (cloudy solution) at around pH of 8.4. This reduction in transmittance was the result of aggregation of hydrophobic PrHy molecules, which further proved that the loading mechanism of PrHy into nanogels is through a diffusion process driven by a concentration gradient difference between the internal and external environment of the nanogels. Once the drug molecules are in the interior of the nanogels, hydrophobic interaction induced the binding of drug and nanogels.

5.3 Variation in particle sizes and z-potential with drug concentration

The effect of drug concentration on particle sizes for the two different series of nanogels, i.e. nanogels with 20 mole percent MAA cross-linked with varying cross-linking density and nanogels with 4 wt% DAP and varying MAA-EA molar ratio is shown in Figures 5.21 and 5.23 respectively. The hydrodynamic radius (R_h) at varying drug concentration was normalized against the hydrodynamic radius of nanogel in the absence of drugs at $\alpha = 1$ ($R_{h\,(c=0)}$).

The relaxation time distribution functions measured at 90^o for 0.1 wt% HASE 20-80-1 in 10 mM NaCl solution with varying PrHy concentration is shown in Figure 5.19. The features of the distribution functions obtained for other nanogel series were identical to Figure 5.19 and will not be shown. Before the addition of PrHy, nanogels were in the fully neutralized state and the distribution function possessed a broad range of relaxation times. When PrHy was added to the polymer solution, the relaxation time shifted to a lower value with narrow range of relaxation time. As more PrHy was added to the nanogels, the solution changed from clear to cloudy.

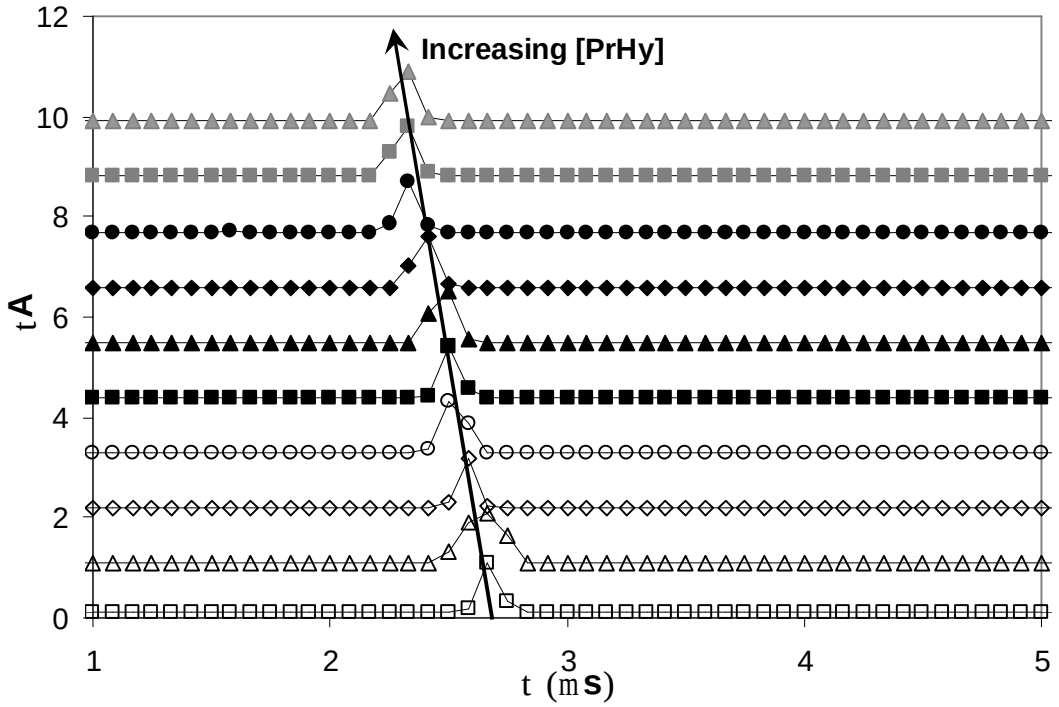

Figure 5.19 Relaxation time distribution functions for 0.1 wt% HASE 20-80-1 in 10 mM NaCl solution with varying PrHy concentration (0 to 0.054 M). Only selected PrHy concentrations are shown in the Figure.

The relationship between the relaxation rates of Γ and q^2 for 0.1 wt% HASE 20-80-1, HASE 20-80-2, HASE 20-80-4, HASE 30-70-4, HASE 40-60-4 and HASE 50-50-4 in 10 mM NaCl and 0.018 M PrHy solution are shown in Figures 5.20a to 5.20f respectively. All the decay functions decreased with increasing scattering angles. The relaxation rates exhibited q^2 dependence confirming that the scattering corresponded to translational diffusion. The translational diffusion coefficients were obtained from the slope of Figures 5.20a to 5.20f and based on Stokes-Einstein relationship, R_h of the particle was calculated. R_h for HASE 20-80-1, HASE 20-80-2, HASE 20-80-4, HASE 30-70-4, HASE 40-60-4 and HASE 50-50-4 was found to be 29.9, 35.5, 36.0, 53.2, 57.1 and 81.1 nm respectively.

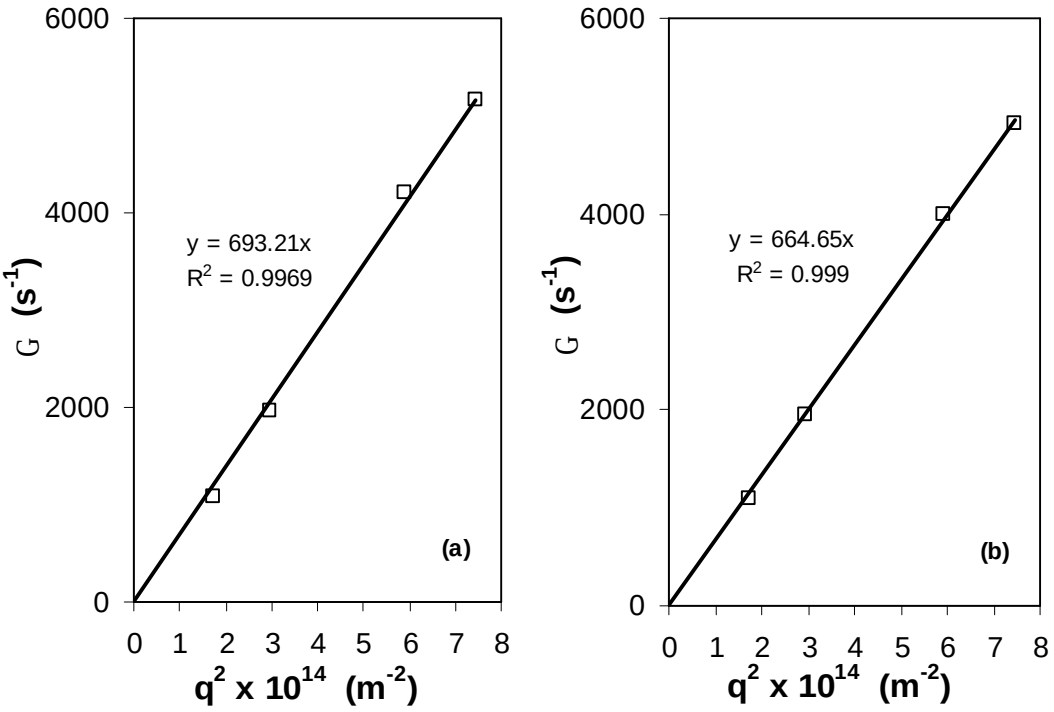

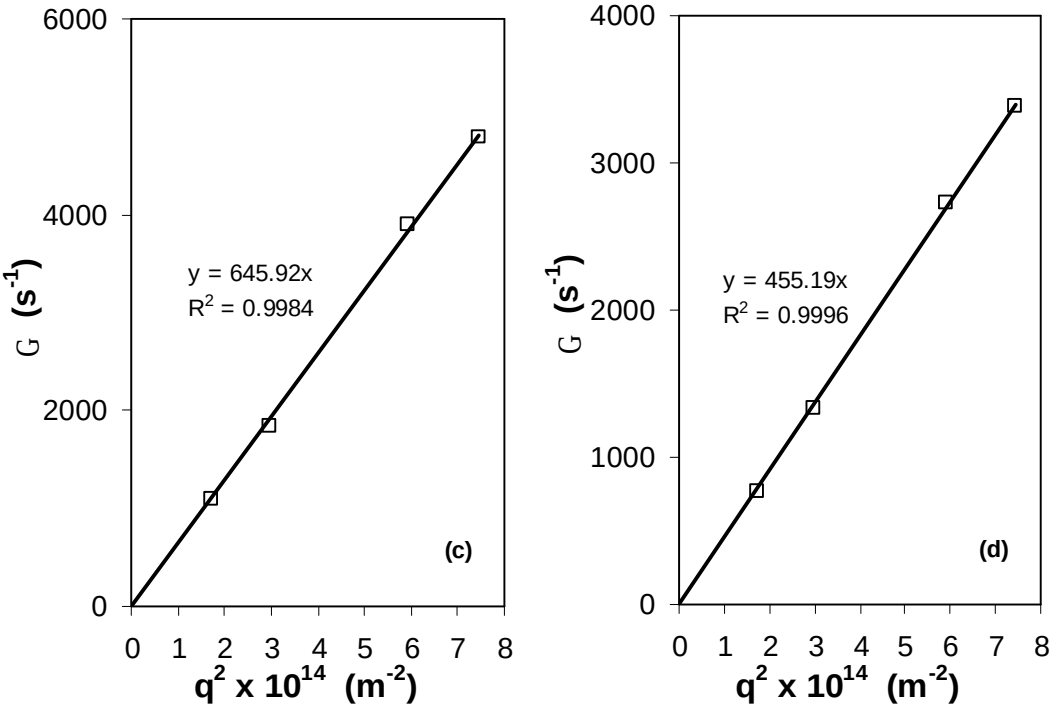

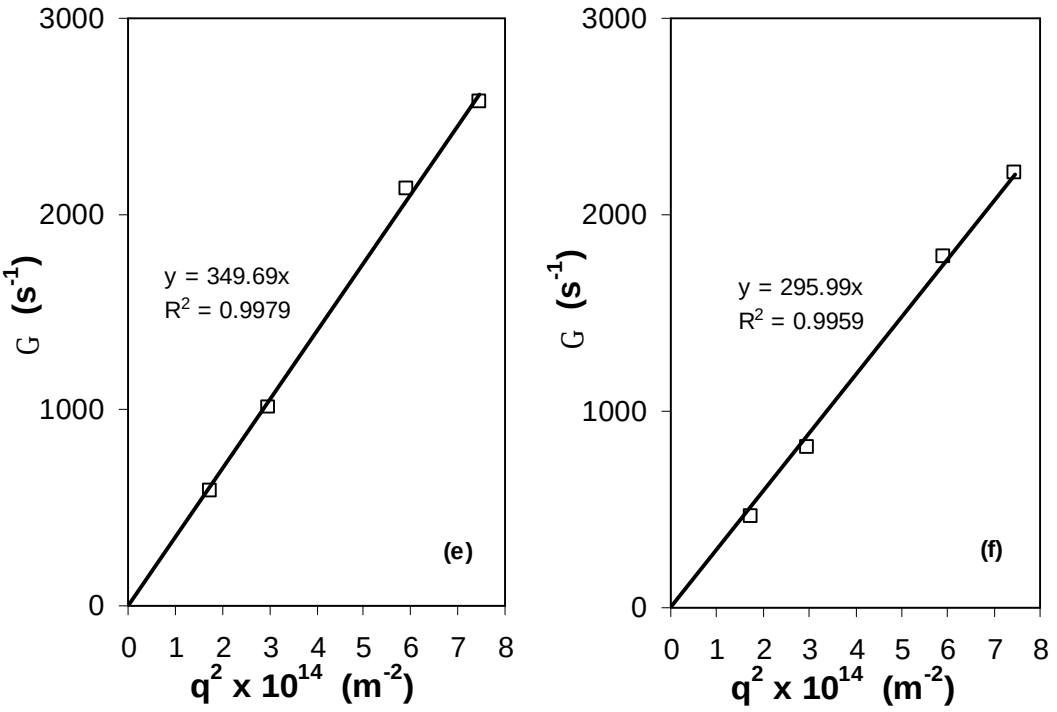

Figure 5.20 The relationship of Γ and q^2 for 0.1 wt% (a) HASE 20-80-1, (b) HASE 20-80-2, (c) HASE 20-80-4, (d) HASE 30-70-4, (e) HASE 40-60-4 and (f) HASE 50-50-4 in 10 mM NaCl and 0.018 M PrHy solution.

Based on Figures 5.21 and 5.23, the particle sizes decreased with increasing drug concentration. As more drugs are incorporated into the nanogels, the resultant shielding effect on the charged groups present in the nanogels will increase. This shielding will result in a reduction in the internal charge repulsion between ionized MAA groups. There will also be a concomitant reduction in the polymer-solvent interactions as the overall effect of drug loading produced a lower polar environment within the nanogels due to the hydrophobicity of PrHy, which produced a more compact nanogel structure. Similar trends have also been observed by Lopez et al. [Lopez et al., 2005] and Bromberg [Bromberg, 1998]. As shown in Figure 5.21, HASE 20-80-1 possessed the lowest ratio

($R_h/R_{h\,(c\,=\,0)}$) as the particle size at $R_{h\,(c\,=\,0)}$ for HASE 20-80-1 was the largest due to the lowest amount of cross-linking density. HASE 20-80-1 was also the most flexible, resulting in the largest deswelling in the presence of drug (open squares). The $R_h/R_{h\,(c\,=\,0)}$ ratio increased with increasing cross-linking density due to the reduction in the particle size at $R_{h(c\,=\,0)}$ with increasing cross-linking density. The slope for HASE 20-80-1, indicated by (a), was the steepest as compared to HASE 20-80-2, indicated by (b), and HASE 20-80-4, indicated by (c), as a larger amount of cross-linking density will make the nanogels more rigid thus gentler the slope.

The ζ-potential became more negative with increasing concentration of PrHy loaded as shown in Figure 5.22. As the particle size decreased, the mobility of the nanogels will increase. Since ζ-potential is directly proportional to mobility of the nanogels, the ζ-potential will become more negative. The concentrations that the ζ-potential and particle size became constant were the same for HASE 20-80-1 to HASE 20-80-4 (Figure 5.21 and 5.22).

The drug loading capability for nanogels with 20 mole percent MAA of varying cross-linking density was compared at an added drug content of 0.018 M. The loading capacity of drugs exhibited a decreasing trend with increasing cross-linking density as shown in Table 5.1. Similar trend was observed by Kurkuri and Aminabhavi using poly(acrylic acid) and poly(vinyl alcohol) cross-linked with glutaraldehyde pH-sensitive microspheres [Kurkuri and Aminabhavi, 2004]. The increase in cross-linking density will cause the nanogels to become more rigid thus decreasing the free volume space within the polymer matrix. This reduction in free volume space will reduce the drug loading capability. For future drug release studies, the same drug loading ratio will be used.

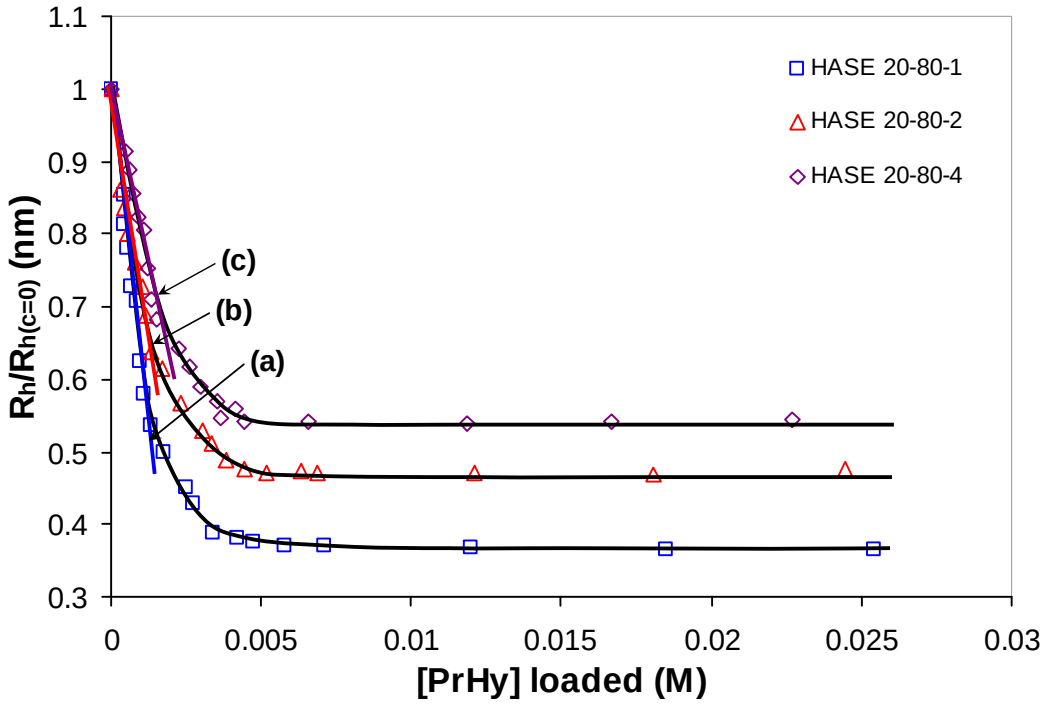

Figure 5.21 Dependence of the ratio of hydrodynamic radius with drugs (R_h) normalized with hydrodynamics radius without drug at $\alpha = 1$ ($R_{h\,(c=0)}$) on [PrHy] loaded for nanogels with 20 mole percent MAA with varying cross-linking density in 10 mM NaCl solution.

Table 5.1 Results of drug loading capability and particle size for nanogels with 20 mole percent MAA with varying cross-linking density.

Name of nanogel	Loading (g of drug/g of polymer)	Particle size, R_h (nm)
HASE 20-80-1	1.95	29.9
HASE 20-80-2	1.88	35.5
HASE 20-80-4	1.80	36.0

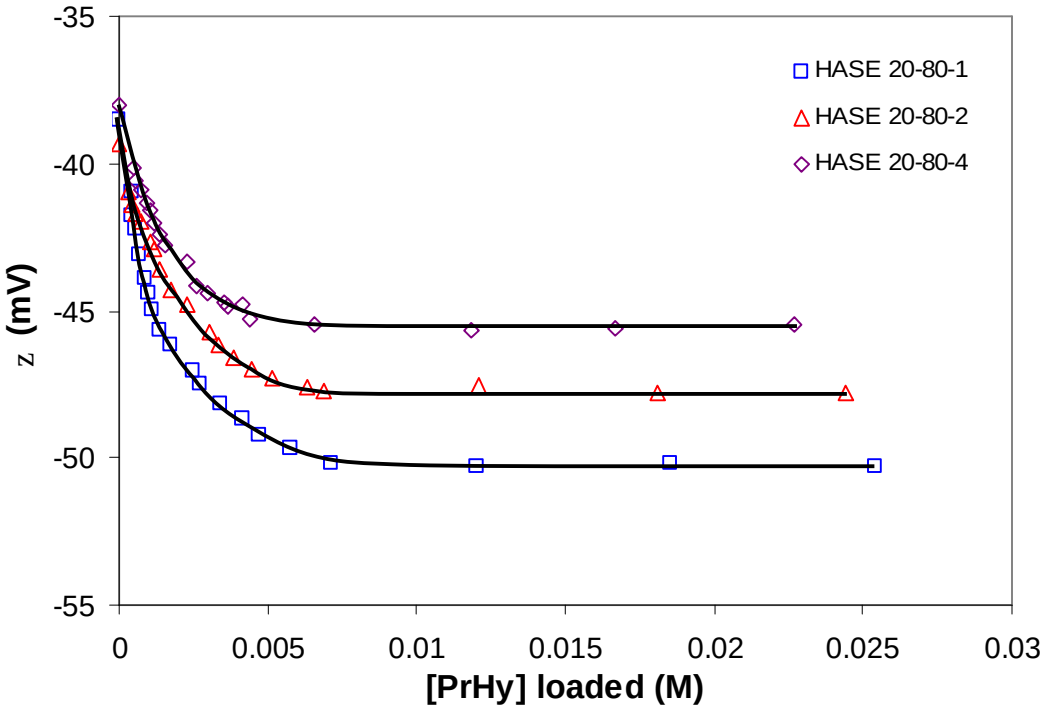

Figure 5.22 Dependence on the ζ-potential on [PrHy] loaded for nanogels with 20 mole percent MAA with varying cross-linking density in 10 mM NaCl solution.

As shown in Figure 5.23, HASE 20-80-4 possessed the steepest slope, indicated by (a), as compared to the rest of the nanogels, indicated by (b), (c) and (d). Since HASE 20-80-4 has the lowest MAA content, the impact of hydrophobic force from the drug and EA segments brought about the largest reduction in the particle size at any drug concentration as compared to the other nanogels with higher MAA content at similar drug concentration. HASE 20-80-4 began to precipitate first as compared to HASE 30-70-4, HASE 40-60-4 and HASE 50-50-4. HASE 20-80-4 has the least amount of charged groups thus the least stable in a hydrophobic environment while HASE 50-50-4 has the most charged groups thus the most stable in a hydrophobic environment.

The ζ-potential became more negative with increasing concentration of PrHy loaded as shown in Figure 5.24. As the particle size reduced, the mobility of the nanogels increased. Since ζ-potential is directly proportional to mobility of the nanogels, the ζ-potential will become more negative. The ζ-potential for HASE 50-50-4 was less than HASE 20-80-4 as the particle size for HASE 50-50-4 was larger than HASE 20-80-4. The concentrations that the ζ-potential and particle size became constant were the same for HASE 20-80-4 to HASE 50-50-4 (Figures 5.23 and 5.24).

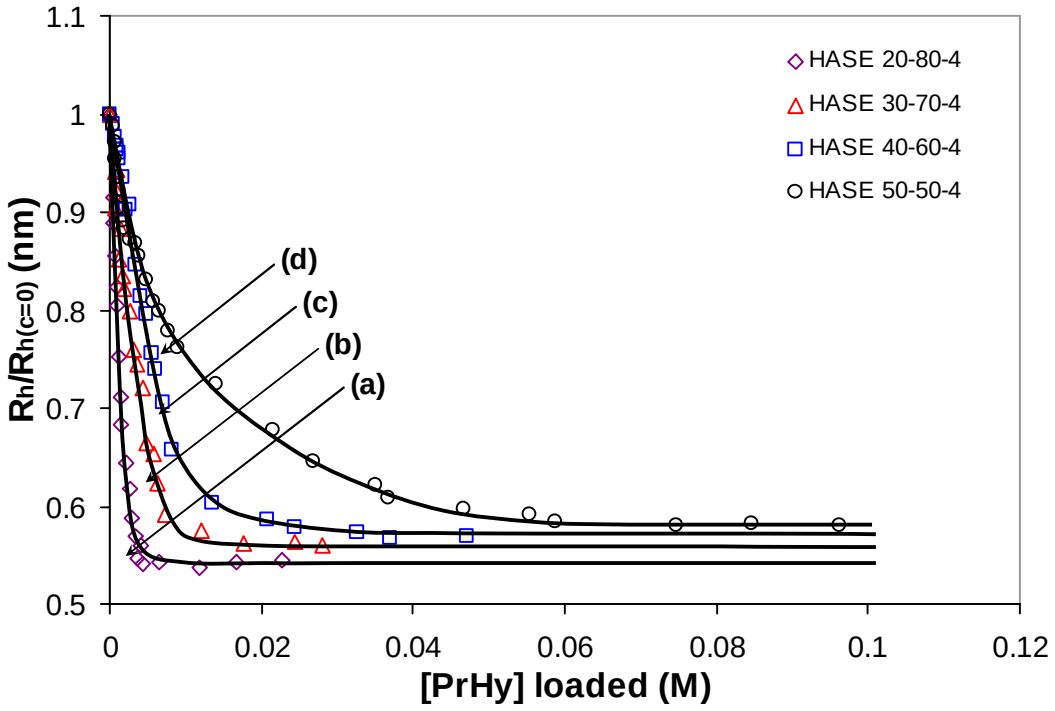

Figure 5.23 Dependence of the ratio of hydrodynamics radius with drugs (R_h) normalized with hydrodynamics radius without drug at $\alpha = 1$ ($R_{h\,(c=0)}$) on [PrHy] loaded for nanogels with 4 wt% DAP with varying MAA-EA molar ratio in 10 mM NaCl solution.

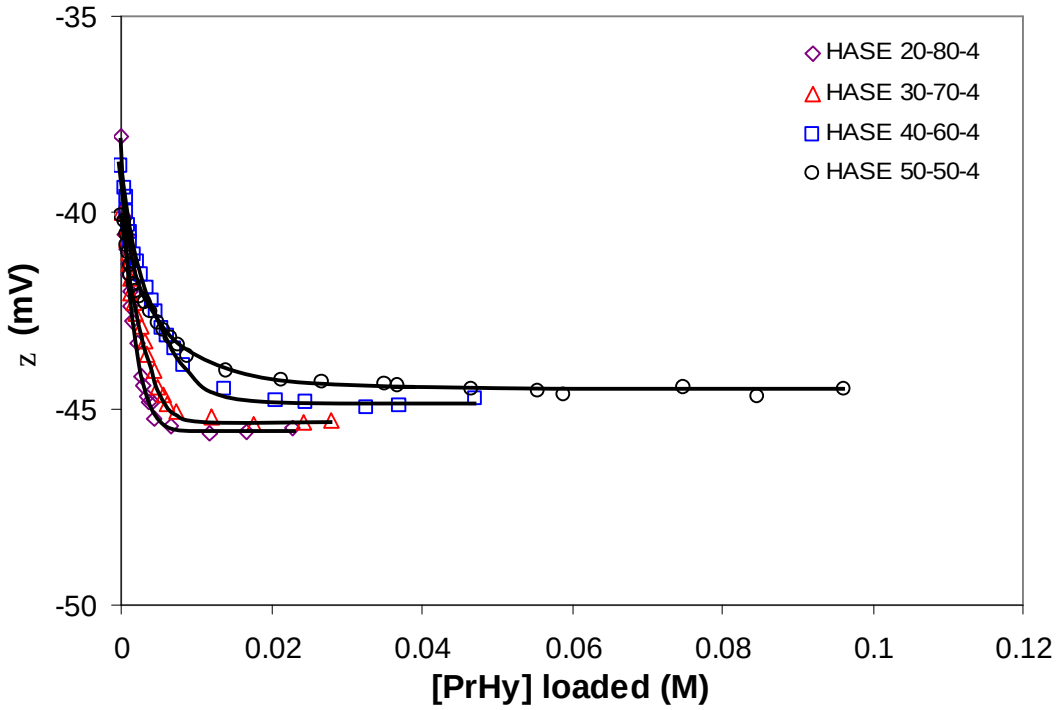

Figure 5.24 Dependence on the ζ-potential on [PrHy] loaded for nanogels with 4 wt% DAP with varying MAA-EA molar ratio in 10 mM NaCl solution.

Table 5.2 Results of drug loading capability and particle size for nanogels with 4 wt% DAP with varying MAA-EA molar ratio at an added drug concentration of 0.018 M.

Name of nanogel	Loading (g of drug/g of polymer)	Particle size, R_h (nm)
HASE 20-80-4	1.80	36.0
HASE 30-70-4	2.00	53.2
HASE 40-60-4	2.27	57.1
HASE 50-50-4	2.44	81.1

The drug loading capability for nanogels with 4 wt% DAP with varying MAA-EA molar ratio was compared at an added drug concentration of 0.018 M. The loading capacity of drugs showed an increasing trend with increasing MAA content as shown in Table 5.2.

Similar trend was observed by Kurkuri and Aminabhavi using poly(acrylic acid) and poly(vinyl alcohol) cross-linked with glutaraldehyde pH sensitive microspheres [Kurkuri and Aminabhavi, 2004]. The increase in MAA content will allow the nanogel to swell to a larger size due to enhanced osmotic pressure thus allowing more drugs to diffuse into the nanogel.

5.4 Effect of varying parameters on PrHy release

5.4.1 Varying concentration gradient

Release of drugs from nanogels was studied at intestinal pH condition of 7.4 and measured using the DSE. The drug release was conducted twice to ensure the stability and repeatability of the electrode in the presence of nanogels. Figure 5.25 shows the release characteristics of PrHy from 0.1 wt% HASE 20-80-1 in the presence of 10 mM NaCl at pH 7.4.

Based on Figure 5.25, the two drug release profiles, conducted twice under similar conditions, were found to be identical. Nanogels did not stick to the surface of the membrane as proven by the plateau in Figure 5.25, which further enhanced the suitability of the DSE in obtaining the drug release profile.

Drug release profiles for 0.1 wt% HASE 20-80-1 was conducted at varying concentration gradients, 2 times, 5 times, 7 times, 10 times and 20 times, at pH 7.4 in 10 mM NaCl solution at 37 ^{o}C. The concentration of drug in the bulk solution is dictated by the volume of release medium and it has an impact on the amount of drugs released from the nanogels. The amount of drug loaded used in the release was 1.95 g drug/g polymer. For example, 5 times means the volume of 10 mM NaCl at pH 7.4 used is 5 times the volume of polymer and drug solution, which is illustrated by Figure 5.26. The drug release profile for varying concentration gradient difference is displayed in Figure 5.27.

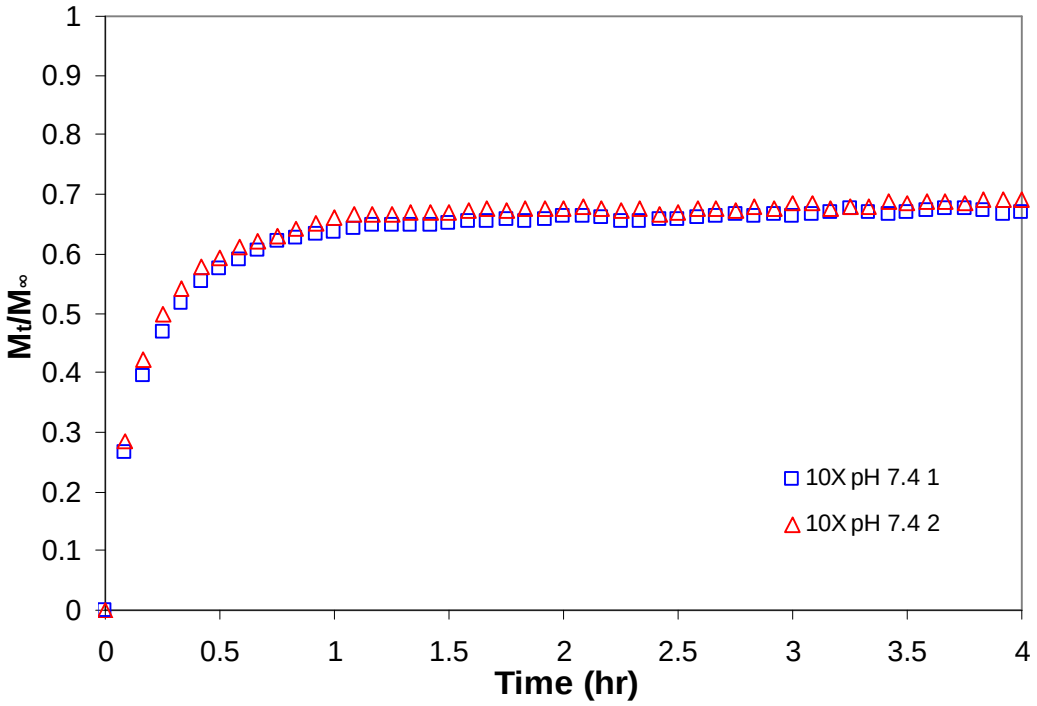

Figure 5.25 Fraction of PrHy released from 0.1 wt% HASE 20-80-1 nanogels loaded with 1.95 g drug/g polymer in 10 mM NaCl solution at pH 7.4.

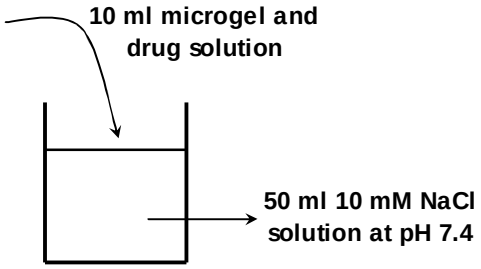

Figure 5.26 Schematic diagram illustrating the concentration gradient difference of 5 times.

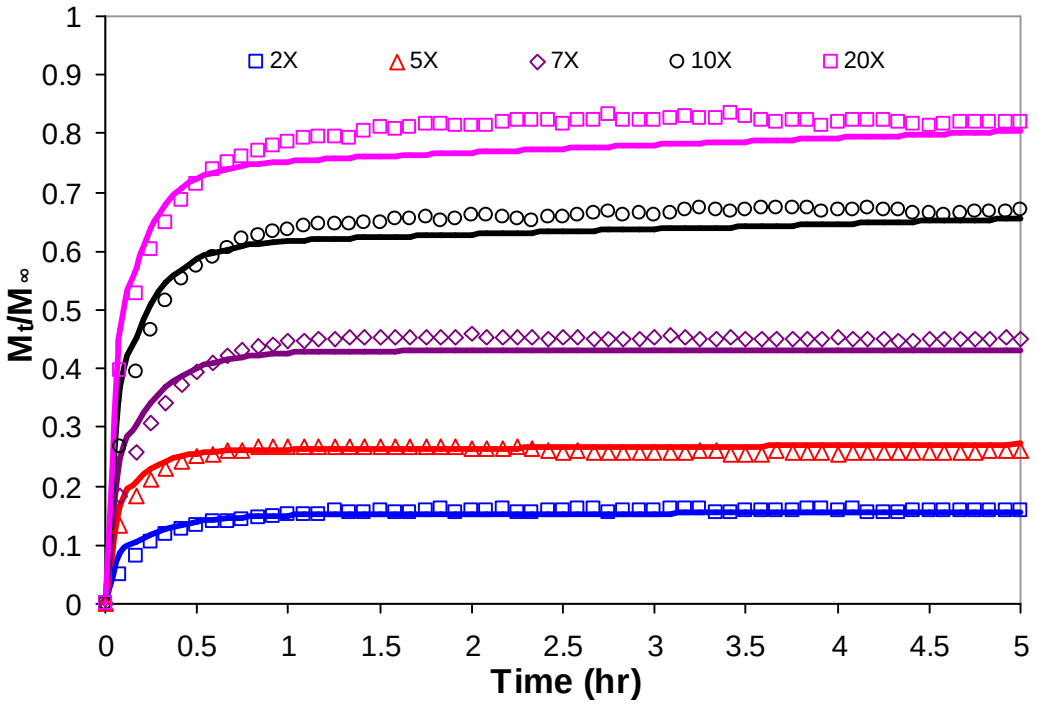

Figure 5.27 Release profile for 0.1 wt% HASE 20-80-1 in 10 mM NaCl solution at pH 7.4 with varying concentration gradient difference (a) 2X (□), (b) 5X (△), (c) 7X (◇), (d) 10X (○) and (e) 20X (□) and theoretical fit of the Berens and Hopfenberg mathematical model taking into account drug diffusion and chain relaxation (solid lines).

All the profiles showed a fast release of drugs within the first 15 minutes after which the release slowed down and leveled off after about 1.5 hours. The drug release from nanogels appeared to possess two components comprising of a burst release in the first 15 minutes that was related to the release of drug from the nanogel surface and a slow exponential release of drugs embedded within the nanogel matrix. This delayed exponential release may be attributed to the diffusion of drug within the core of the nanogels to the bulk solution. After loading with drugs, the nanogels possessed a diameter of about 60 nm. When the nanogels loaded with drugs was placed in the pH 7.4 solution, the nanogels swelled thus promoting the release of drugs due to a concentration

gradient difference between the internal and external nanogel environment. From Figure 5.27, the release of PrHy increased with increasing concentration gradient difference. As PrHy was loaded to the nanogels via diffusion and hydrophobic interaction, the increase in concentration gradient promoted a faster release of drugs from the nanogels due to a larger driving force.

Table 5.3 Release characteristics for PrHy from HASE 20-80-1 at various concentration gradient difference.

Sample	Ratio	Ratio of drug loaded polymer to release medium	0.5h%	$t_{fully\ release}$
(a)	2X	10:20	13.3	0.8 hour
(b)	5X	10:50	25.0	1 hour
(c)	7X	10:70	39.5	1.25 hours
(d)	10X	10:100	57.4	1.5 hours
(e)	20X	10:200	71.4	2 hours

The characteristic parameters for the release of PrHy from HASE 20-80-1 were obtained from individual experimental curves and summarized in Table 5.3, where 0.5 h% and $t_{fully\ release}$ represent the percentage release after 30 minutes and time taken to achieve an equilibrium release respectively. From Table 5.3, the concentration gradient difference effect on the release behavior can be clearly observed. The percentage release at 30 minutes increased with increasing concentration gradient difference. The time taken to achieve fully release was greater for higher concentration gradient difference due to a higher percentage of drugs being released.

5.4.2 Varying pH

In-vitro release studies were performed at varying pHs, namely at pH of 5, 6, 7.4 and 8 as shown in Figure 5.28. The drug release was conducted with 0.1 wt% HASE 50-50-4 loaded with 2.44 g drug/g polymer in 100-millilitre 10 mM NaCl solution.

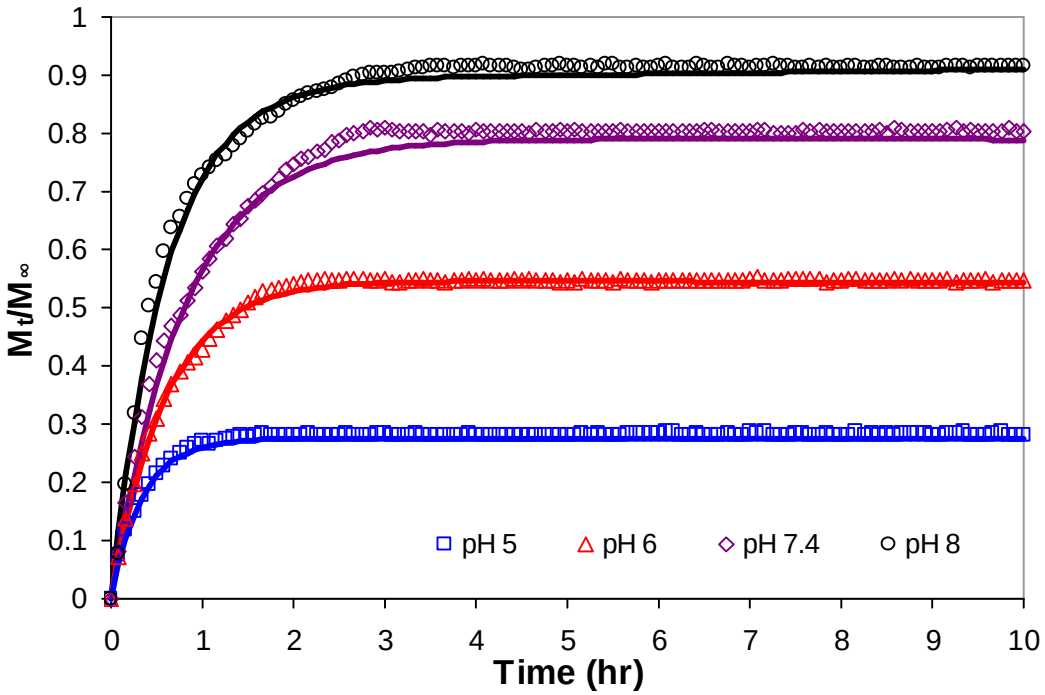

Figure 5.28 Release profile for 0.1 wt% HASE 50-50-4 in 100-millilitre 10 mM NaCl solution at varying pH (a) pH 5 (□), (b) pH 6 (△), (c) pH 7.4 (◇) and (d) pH 8 (○) and theoretical fit of the Berens and Hopfenberg mathematical model taking into account drug diffusion and chain relaxation (solid lines).

The fraction of PrHy released at pH 8 was ~90% compared to ~30% at pH 5. The degree of neutralization (α) was 0.9 at pH 8 and 0.0 at pH 5, and the difference in the amounts of PrHy released was due to the different degree of neutralization of COOH groups. At

low pH, the nanogels possessed a compact structure and a lower porosity, which resulted in a lower release of drug due to the larger diffusion barrier. However, at high pH, the nanogels were swollen and possessed a higher porosity, which enhanced the release of PrHy due to the reduction in the diffusion resistance. This is illustrated in Figure 5.29. For pH 5, the time to reach equilibrium was ~1.5 hours while for pH 8 the time required was ~4 hours. At pH 7.4, the -COOH groups will dissociate, thereby increasing the osmotic pressure inside the nanogels resulting in a higher swelling. Thus, more drugs will be released therefore it required more time to reach equilibrium. With P(MAA-co-MAA) spheres [Huang et al., 2000], polyacrylamide-g-guar gum nanogel [Soppimath et al., 2001] and PAA-g-EG hydrogels [Foss et al., 2004], the fractional release was higher at higher pH.

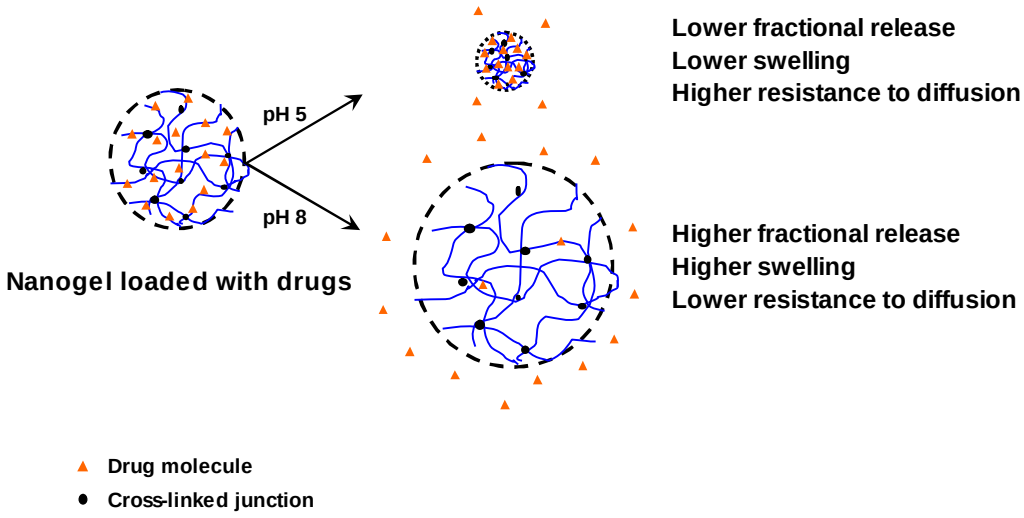

Figure 5.29 Schematic diagram of nanogels under different pHs.

The pH-responsive nanogels (HASE 50-50-4) loaded with 2.44 g drug/g polymer were characterized in diluted solution (0.1 wt%) at varying pH, ranging from 5 to 8 in 10 mM NaCl. The particle sizes were measured over a period of 24 hours as shown in Figure 5.30. The particle sizes were normalized by the size of nanogels with loading of 2.44 g

drug/g polymer. HASE 50-50-4 loaded with 2.44 g drug/g polymer possessed a R_h of ~81 nm and the pH of the solution for nanogels loaded with drugs was 7. The size of the particles varied depending on the pH of the dissolution medium and was found to swell at pH of 7.4 and 8 and de-swelled at pH of 5 and 6. The swelling and de-swelling of the particles was due to the presence of COOH groups being ionized and de-ionized at the prevailing pH respectively. Enhanced osmotic pressure exerted by counter-ions trapped inside the polymeric network caused the nanogels to swell while the reduction in the counter-ions concentration reduced the osmotic pressure leading to a de-swelling of the nanogels. The swelling and de-swelling of the nanogels did not change after the first 5 minutes, which suggested the fast response of the nanogels to changes in the external pH.

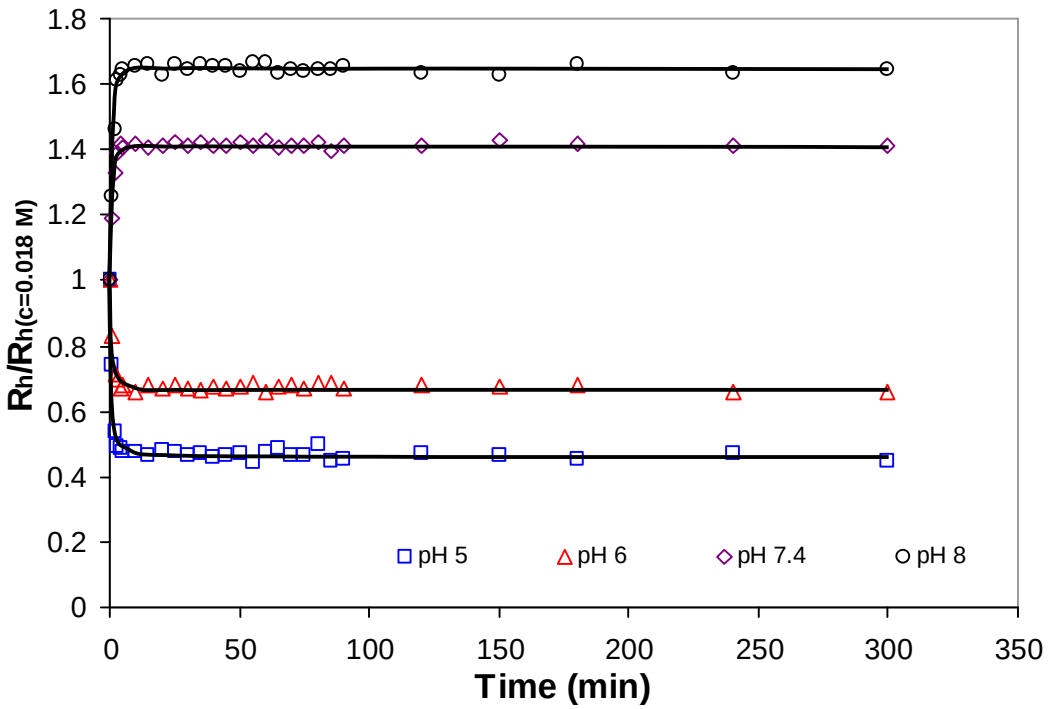

Figure 5.30 Particle size of HASE 50-50-4 nanogel loaded with 2.44 g drug/g polymer at varying pH.

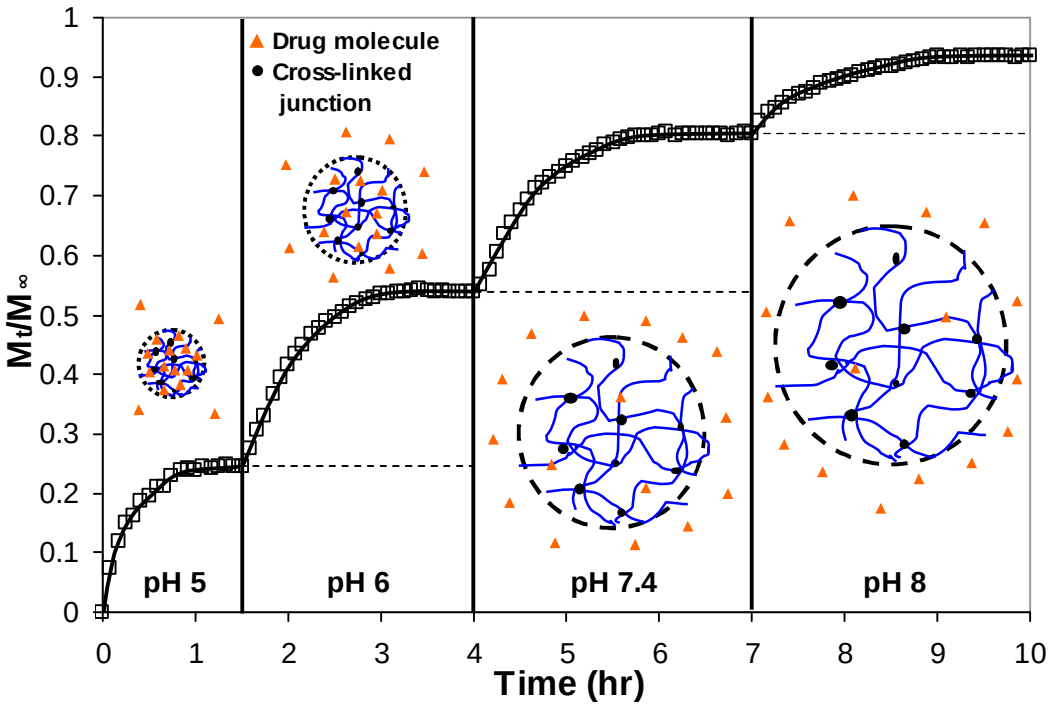

Figure 5.31 In-vitro release profile of PrHy from 0.1 wt% HASE 50-50-4 in a changing pH environment.

The normalized PrHy released profile in a changing pH environment was plotted in Figure 5.31 from PrHy loaded HASE 50-50-4 with a drug loading content of 2.44 g drug/g polymer. The first 1.5 hours of study was conducted at pH of 5 and the pH was increased to 6 and the release profile was monitored for 2.5 hours. The next 3 hours of the release was performed at pH of 7.4 and finally the pH was increased to 8 and the release was monitored for 3 hours. Data from Figure 5.31 showed that the amount of PrHy released increased from ~24% to ~54% when the pH was increased from 5 to 6 respectively and further increase in pH from 7.4 to 8 resulted in a further increase in release from ~80% to ~93% respectively. Since HASE 50-50-4 consisted of a pH responsive MAA segment, the pH of the medium will have an impact on the release behavior. The release of PrHy will depend on pH where an increase in pH will promote the release of PrHy. As shown in Figure 5.28, the maximum fraction of drug released at

pH of 5 was about 25% (open square in Figure 5.28) and by increasing the pH to 6, another 30% of the drugs could be released and this decreased to 26% when the pH was increased from 6 to 7.4. This reduction was likely to be attributed to the reduced concentration gradient difference of PrHy between the interior of the nanogels and the dissolution medium since some drugs had been released at pH of 5 and 6. Two comments should be made from the results reported in Figure 5.31. Firstly, the results demonstrated the viability of tuning the release profiles of drug from a pH-responsive nanogel system. The proportion of drug released can be controlled by manipulating the pH of the environment. Hence, it is possible to design a pH-dependent gradient release drug delivery system such that the active drugs could be released from the carrier in different regions of the physiological environment with different pH. This will result in extending the therapeutical period of the active drug and ensure that the targeted areas receive the right dosage of drugs. Secondly, the monitoring of amounts of drug released cannot be easily performed using the conventional dialysis membrane or centrifugation techniques. A continuous monitoring technique using the DSE reported here is the only practical method for measuring the concentration of drug released in an environment where the pH was continuously changed.

In Figure 5.32, the release profile of PrHy due to a step-change in pH was illustrated. The pH of the medium was changed from 5 to 7.4 and then back to 5. When the pH was changed from 5 ($\alpha = 0$) to 7.4 ($\alpha = 0.8$) at 0.5 hours, there was an increase in the amount of drugs released due to the increase in the porosity of the matrix. However, when the pH was reduced back to 5, there was a rapid increase over a short time and this was related to the release of PrHy near the surface of the nanogels as PrHy were being squeezed out from the nanogel matrix when the nanogels de-swelled. At the pH of 5, the nanogels

were in a more compact state, hence the rate and amount of PrHy released decreased at this pH regime. However, when the pH was again increased from 5 to 7.4 and the initial release rate was slower (compared to the behavior when the pH was decreased from 7.4 to 5) as the squeezing effect of the drug from the gel matrix was absent when the matrix swelled. There was a reduction in the absolute amount of PrHy released during the first and second 1.5 hours. This was attributed to a reduction in the concentration gradient difference of PrHy between the interior of the nanogels and medium, which was lower in the second 1.5 hours.

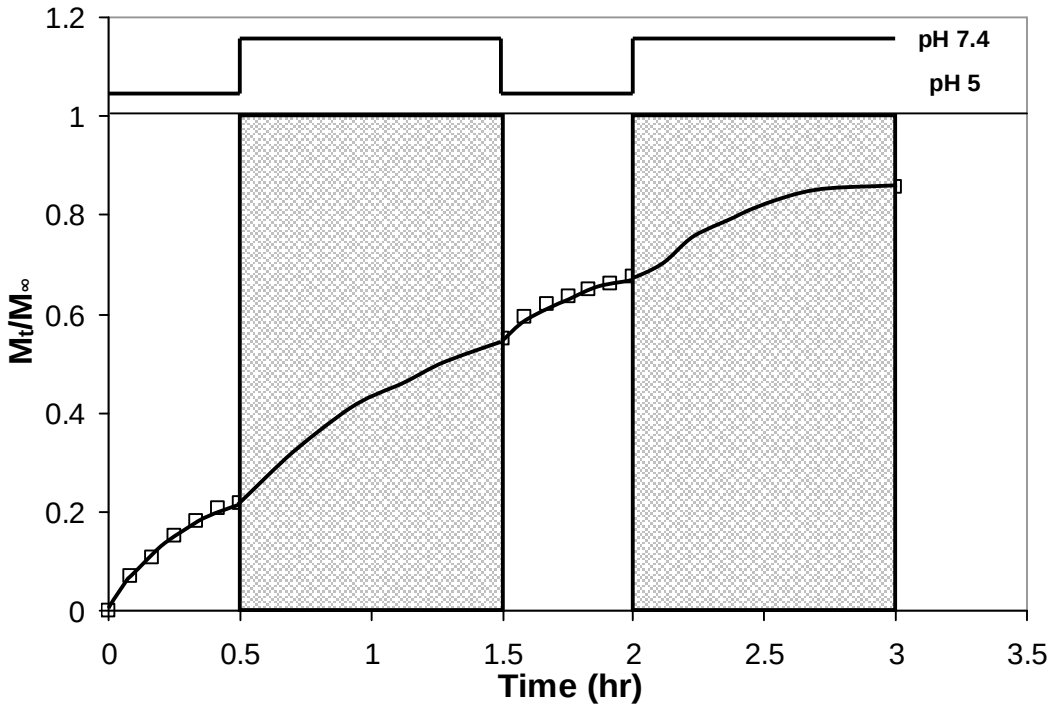

Figure 5.32 Step change in pH to induce variation in drug release for 0.1 wt% HASE 50-50-4 in 10 mM NaCl solution in 100-millilitre 10 mM NaCl solution.

5.4.3 Varying drug loading ratio

Drug release for 0.1 wt% HASE 50-50-4 with varying drug loading ratio was carried out in 100-millilitre 10 mM NaCl solution at pH 7.4. The results were plotted in Figure 5.33.

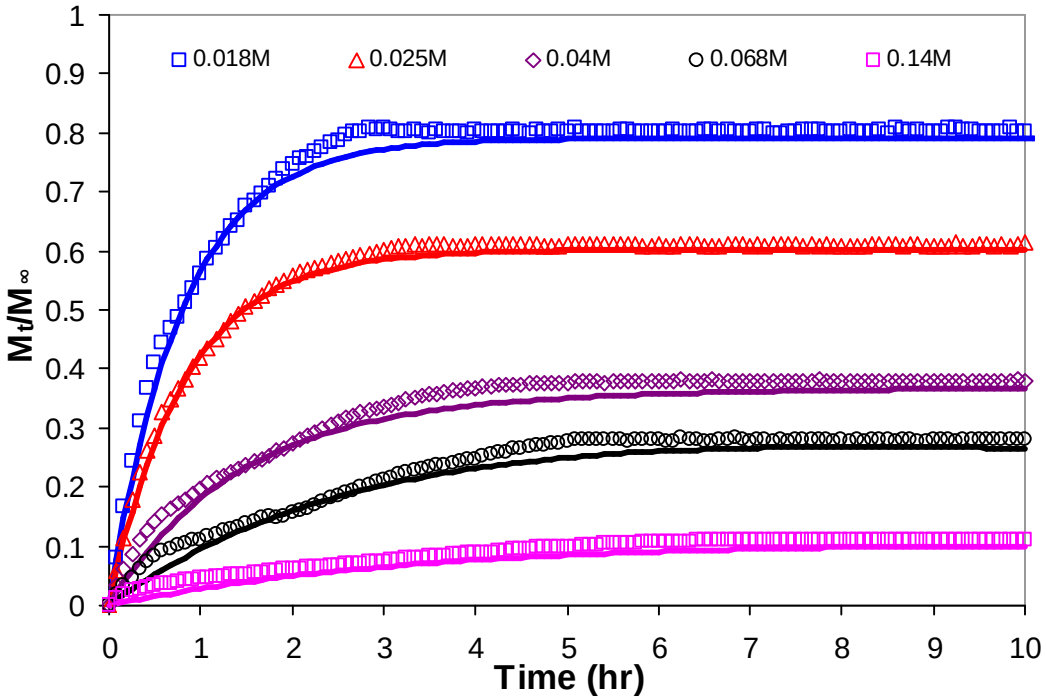

Figure 5.33 Release profile for 0.1 wt% HASE 50-50-4 in 100-millilitre 10 mM NaCl solution at pH 7.4 with varying drug loading ratio (a) 0.018 M (□), (b) 0.025 M (△), (c) 0.04 M (◇), (d) 0.068 M (○) and (e) 0.14 M (□) and theoretical fit of the Berens and Hopfenberg mathematical model taking into account drug diffusion and chain relaxation (solid lines).

With an increase in the amount of drug loaded, the fractional release will decrease. For example, at drug content of 0.018 M, the amount released was ~80% and decreased to ~11% for drug content of 0.14 M. When more drugs were loaded into the nanogels, this will cause the particles to become more compact induced by hydrophobic forces. Thus,

solvent molecules will not be able to penetrate into the nanogels to relax the nanogels to promote drug release. Since PrHy was mildly hydrophobic, the drug molecules aggregated within the nanogel matrix, resulting in a reduction in the release rate. Using polyacrylate with nifedipine [Benita et al., 1990], sulfopropyl dextran with doxorubicin [Liu et al., 2001] and poly(acrylamide-g-guar gum) with diltiazem [Toti and Aminabhavi, 2004], the fractional release was lowered when the drug loading was increased.

5.4.4 Varying cross-linking density

Drug release profiles obtained for 0.1 wt% MAA-EA nanogels containing 20 mole percent MAA with varying cross-linking density in 100-millilitre 10 mM NaCl at pH 7.4 is shown in Figure 5.34. Changing the cross-linking density will alter the porosity of the nanogels.

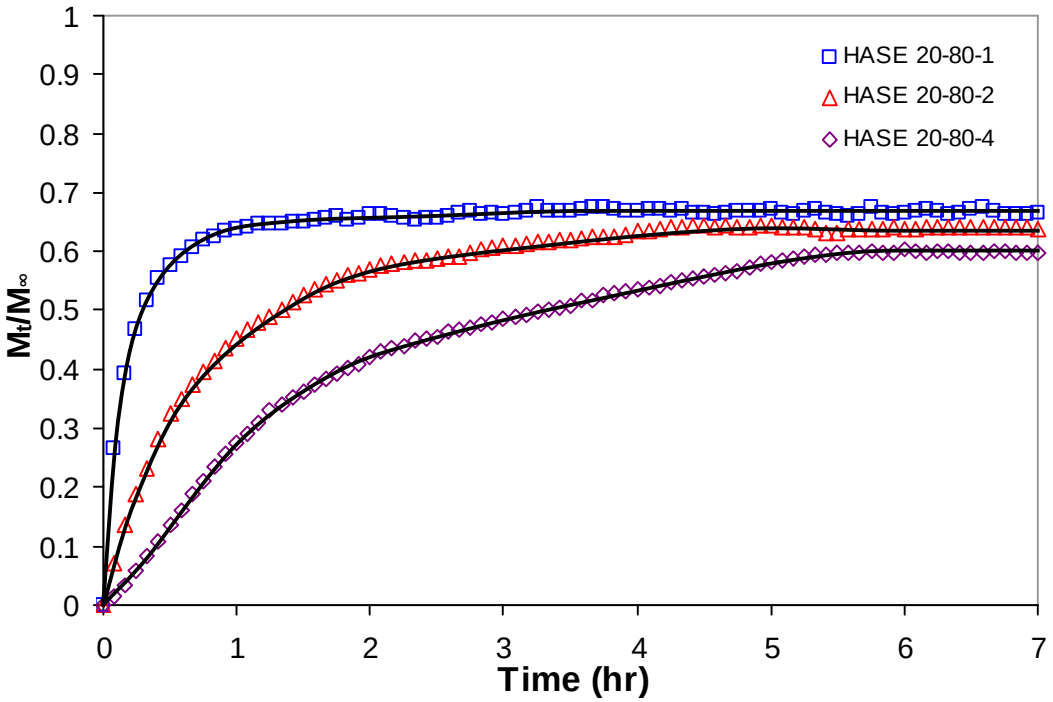

Figure 5.34 Release profile for 0.1 wt% MAA-EA nanogels containing 20 mole percent MAA with varying cross-linking density (a) HASE 20-80-1 (□), (b) HASE 20-80-2 (△) and (c) HASE 20-80-4 (◇) in 100-millilitre 10 mM NaCl solution at pH 7.4.

Nanogels with lower cross-linking density showed a faster release rate as compared to nanogels with higher cross-linking density. At lower cross-linking density, the network is loose with a greater hydrodynamic free volume. This will allow the chains to accommodate more solvent molecules resulting in larger swelling, thereby promoting the release of drugs, which correlated to the largest fractional release observed for HASE 20-80-1. HASE 20-80-1 possessed the steepest slope and fastest time to attain equilibrium as compared to HASE 20-80-2 and HASE 20-80-4. HASE 20-80-1 will have larger pore sizes due to a lower cross-linking density thus reducing the barrier effect to prevent drug molecules from diffusing out of the nanogels. By increasing the

cross-linking density, the nanogels became more rigid and the hydrodynamic free volume space will decrease. This resulted in a slower release rate and a lower fractional release. Since nanogels with lower cross-linking density are less rigid, the swelling rate will be faster thus increasing the rate of drug release. Similar results were obtained by Soppimath et al. using polyacrylamide-g-guar gum nanogel, Kurkuri and Aminabhavi using poly(acrylic acid) and poly(vinyl alcohol) cross-linked with glutaraldehyde pH sensitive microspheres and El-Sherbiny et al. using poly[N-acryloylglycine-chitosan] nanogels [Soppimath et al., 2001; Kurkuri and Aminabhavi, 2004; El-Sherbiny et al., 2005].

5.4.5 Varying MAA-EA molar ratio

Drug release profiles obtained for 0.1 wt% MAA-EA nanogels containing 4 wt% DAP with varying MAA-EA molar ratio in 100-millilitre 10 mM NaCl at pH 7.4 is shown in Figure 5.35. Through the changing of the amount of MAA groups present, the osmotic pressure will change thus the degree of swelling and porosity will be different.

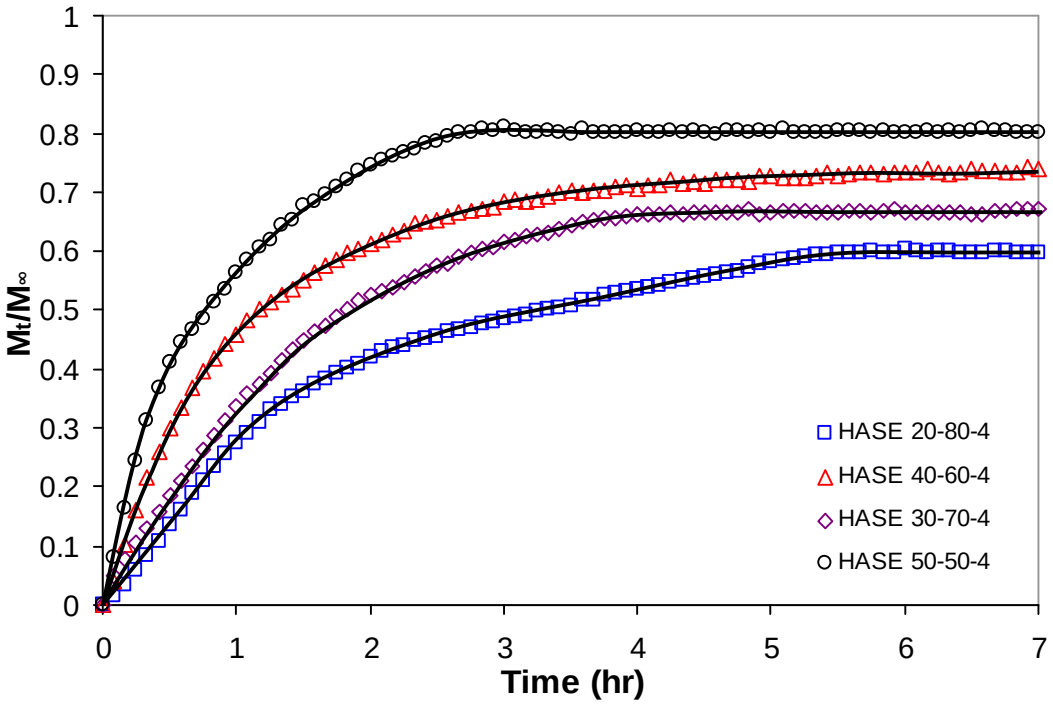

Figure 5.35 Release profile for 0.1 wt% MAA-EA nanogel containing 4 wt% DAP with varying MAA-EA molar ratio (a) HASE 20-80-4 (□), (b) HASE 30-70-4 (△), (c) HASE 40-60-4 (◇) and (d) HASE 50-50-4 (○) in 100-millilitre 10 mM NaCl solution at pH 7.4.

Nanogels with higher MAA-EA molar ratio have a higher fractional release and faster release rate. Nanogels with higher MAA-EA molar ratio will have higher water uptake capability due to the presence of more COOH groups. This will increase the matrix swelling capability as well as increasing the porosity within the nanogels, which reduces the barrier effect for the drug molecules to diffuse out of the nanogels. The swelling rate increased with more COOH groups leading to a faster release rate which can be seen from the steeper slope within the first hour. Similar results were obtained by Kim and Peppas using PMAA-g-EG hydrogel, Kurkuri and Aminabhavi using poly(acrylic acid) and poly(vinyl alcohol) cross-linked with glutaraldehyde pH sensitive microspheres and

El-Sherbiny et al. using poly[N-acryloylglycine-chitosan] nanogels [Kim and Peppas, 2003; Kurkuri and Aminabhavi, 2004; El-Sherbiny et al., 2005].

5.5 Mathematical modeling

Mathematical modeling plays an important role in elucidating the drug release mechanism, thus facilitating the development of new delivery systems by a systematic rather than trial and error method [Arifin et al., 2006]. Based on the physical or chemical characteristics of polymer, drug release mechanism from a polymer matrix can be categorized according to three main processes (systems) [Leong et al., 1987], namely, diffusion controlled, swelling controlled and erosion controlled. In a swelling controlled system (pH-responsive nanogels), the drug release is not only controlled by the diffusion of drugs from the polymeric matrix, but also by the polymer matrix disentanglement and dissolution (chain relaxation). The "anomalous transport" of drug released is often present in swelling controlled systems since both diffusion and chain relaxation occur together [Arifin et al., 2006].

The diffusion behavior of the drug from the interior of nanogels to the bulk solution can be mathematically described by Equation 5.3 [Frisch, 1969]:

$$\frac{\partial C}{\partial t} = \frac{\partial}{\partial x}\left[D\frac{\partial C}{\partial x} - vC \right] \tag{5.3}$$

where C is the concentration of solute, x is the diffusional path, D is the diffusion coefficient, v is the velocity of the solvent front and t is the time. This equation contains both the Fickian behavior, described by $D\frac{\partial C}{\partial t}$ and the Non-Fickian behavior given by vC.

To obtain a better approximation, an exact solution of Equation 5.3 was proposed by Berens and Hopfenberg [Enscore et al., 1977; Berens and Hopfenberg, 1978] having the form shown in Equation 5.4:

$$\frac{M_t}{M_\infty} = 1 - f_F\left[\frac{6}{p^2}\sum_{n=1}^{\infty}\frac{1}{n^2}\exp\left(-4p^2n^2Dt/d^2\right)\right] - f_R\exp(-kt) \qquad (5.4)$$

where D is the diffusion coefficient for the Fickian portion of the transport, k is the first-order relaxation constant, f_F and f_R are the fractions of sorption contributed by Fickian diffusion and chain relaxation respectively, d is the diameter of sphere and t is time. The above model describes the overall release behavior in terms of Fickian and non-Fickian contributions. This analysis can lead to the determination of diffusion coefficient (D), and characteristic relaxation time (τ), which is a reciprocal of k.

In this section, the importance of diffusion (f_F) and chain relaxation (f_R) was examined by fitting the release kinetic data to Equation 5.4. With the use of the DSE, the use of dialysis membrane was eliminated, thus the existence of relaxation contribution of drug release from the nanoparticles could be measured. Both Madeline and Peppas [Madeline and Peppas, 1999] and Soppimath et al. [Soppimath et al., 2001] could not fit the Berens and Hopfenberg equation (Equation 5.4) to all the experimental data to determine the values of f_F and f_R since the assumption at long times, solvent transport are dominated by non-Fickian term. There were insufficient experimental data points to fit the non-linear equation described by Equation 5.4, thus they ignored the first term of Equation 5.4. However, in the present study, the complete Berens and Hopfenberg model equation was fitted to more than 50 data points (compared to less than 10-15 data points in previous reported studies) to obtain both f_F and f_R as well as D and τ. When using Equation 5.4 to fit the kinetic data of between 10 to 15 data points, the R^2 values for the

fittings were all below 0.7, and since more than 50 data points were used in the present study, all fittings possessed a R^2 values exceeding 0.9.

The model fitting to the experimental data shown in Figures 5.27, 5.28 and 5.33 using the Berens and Hopfenberg model (Equation 5.4) was used to determine the parameters D, k, f_F and f_R in the model equation. The solid lines in Figures 5.27, 5.28 and 5.33 were the Berens and Hopfenberg model fitting using the non-linear least squares fitting routine of MATLAB. Excellent agreement between the experimental and predicted kinetic profiles was obtained in all cases. From the model fittings, f_F and f_R were found to vary with pH, [PrHy] loading and concentration gradient as shown in Figures 5.36a to 5.36c respectively. The parameter f_F was found to dominate the release process at high pH and concentration gradient and low PrHy loading as these factors either contributed to a swollen or more porous nanogel, which facilitated the diffusion process since the chains do not relax before the drug was released. However, at low pH and concentration gradient and high PrHy loading, f_R dominated. Under such circumstances, the nanogels assumed a compact structure, where the polymeric chains must relax before the diffusion of drugs could take place. Therefore, in the drug release process, the release of drugs from pH-responsive nanogels was governed by a combination of chain relaxation and diffusion processes and this will change depending on the characteristics of the gel network. [Note: such evidence may not be obvious if the release kinetic data were obtained using the conventional dialysis method as the dialysis membrane may have "filtered" the chain relaxation process of the nanogels.]

Based on the fittings from Berens and Hopfenberg model, the diffusion coefficient and characteristic relaxation time were as a function of pH, concentration gradient and initial

drug loading, where the results are illustrated in Figures 5.37 and 5.38 respectively. From Figure 5.37a, the diffusion coefficient decreased with increasing pH up to pH of 7 before increasing again. At low pH of 5 and 6, the high diffusion coefficient was due to the collapse of the nanogels resulting in the drugs being squeezed out. The nanogels swelled at pH greater than 7, which promoted the release of drugs that corresponded to a higher diffusion coefficient. The characteristic relaxation time decreased with increasing pH as shown in Figure 5.38a. With increasing pH, the polymeric chains were in a more relax state, therefore a low characteristic relaxation time was observed. An empirical relationship between diffusion coefficient or characteristic relaxation time and pH of the release medium is given below:

$$D = (0.81pH^2 - 11.32\,pH + 41.8)x10^{-15} \quad (5.5a)$$

$$t = 133882084.79\exp(-2.19\,pH)x10^5 \quad (5.5b)$$

Based on these relationships, it is possible to determine the diffusion coefficient and characteristic relaxation time at any arbitrary pH.

As shown in Figures 5.37b and 5.38b, the diffusion coefficient increased while the characteristic relaxation time decreased in proportion to the concentration gradient. With a larger concentration differences, the driving force for diffusion was greater and this enhanced the release of drugs leading to a larger diffusion coefficient. An empirical relationship between diffusion coefficient or characteristic relaxation time and concentration gradient difference (dx/dt) is shown as below:

$$D = 0.82\exp(0.09\frac{dx}{dt})x10^{-15} \quad (5.6a)$$

$$t = 245.99\exp(-0.19\frac{dx}{dt})x10^4 \quad (5.6b)$$

Based on these relationships, the diffusion coefficient and characteristic relaxation time at any arbitrary concentration gradient can be predicted.

From Figures 5.37c and 5.38c, the diffusion coefficient decreased while the characteristic relaxation time increased with increasing initial drug loading. Due to a more compact structure at higher drug loading, the nanogels cannot readily relax, and this increased the relaxation time and decreased the diffusion coefficient. The compact structure of the nanogels retarded the release of drugs, which significantly lowered the diffusion coefficient. An empirical relationship between diffusion coefficient or characteristic relaxation time and initial drug loading ([PrHy]) is shown as below:

$$D = 3.61\exp(-27.91[\mathrm{Pr}\,Hy])x10^{-15} \quad (5.7a)$$

$$t = 0.998\exp(15.8[\mathrm{Pr}\,Hy])x10^{6} \quad (5.7b)$$

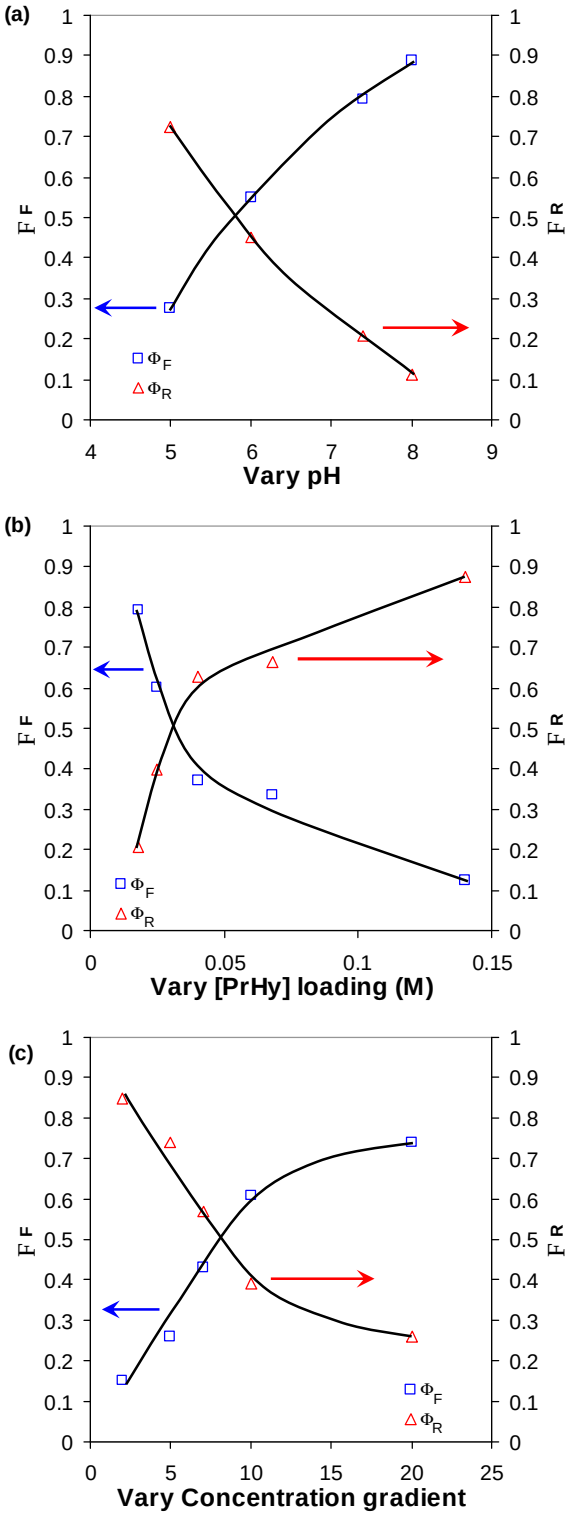

Figure 5.36 Dependence of ϕ_F and ϕ_R against (a) Vary pH, (b) Vary [PrHy] loading and (c) Vary concentration gradient obtained from the Berens and Hopfenberg model.

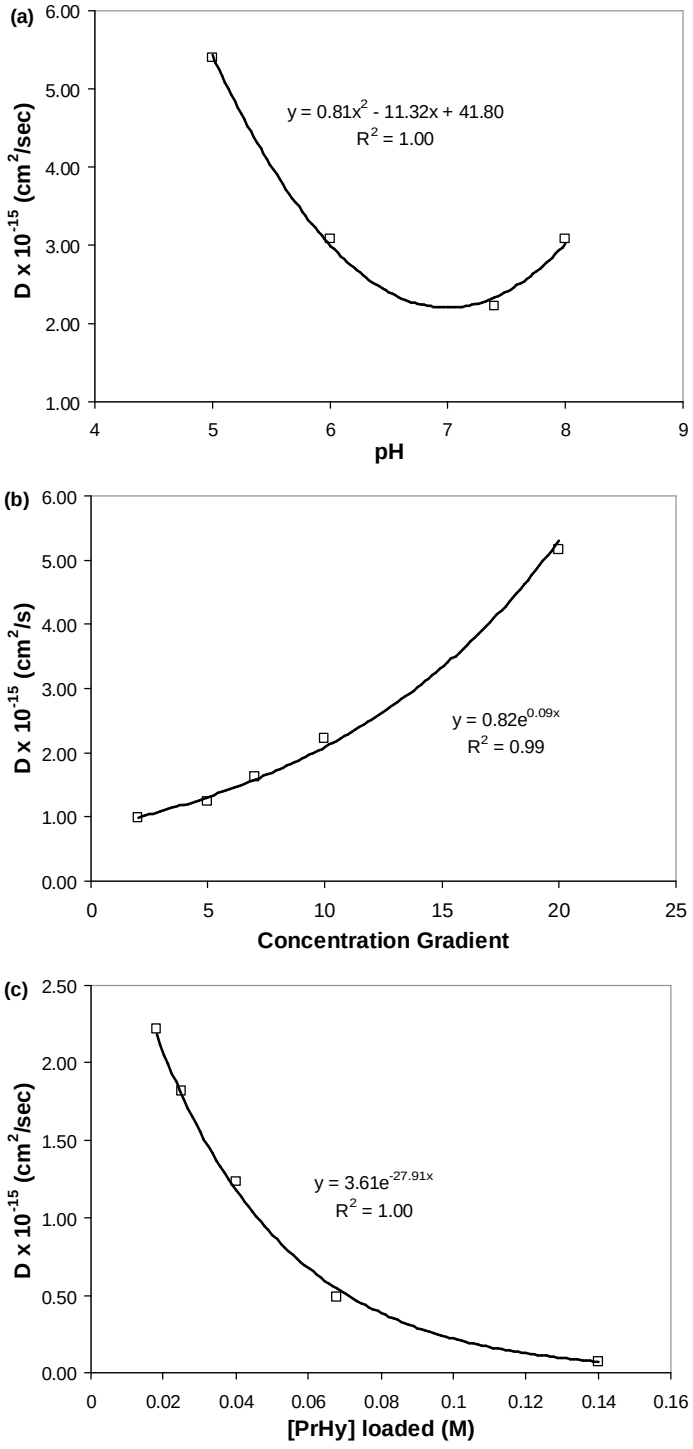

Figure 5.37 Dependence of the diffusion coefficient (D_o) of PrHy from nanogels particle on the (a) pH of the release medium (quadratic fit), (b) concentration gradient difference (exponential fit) and (c) initial drug loading (exponential fit).

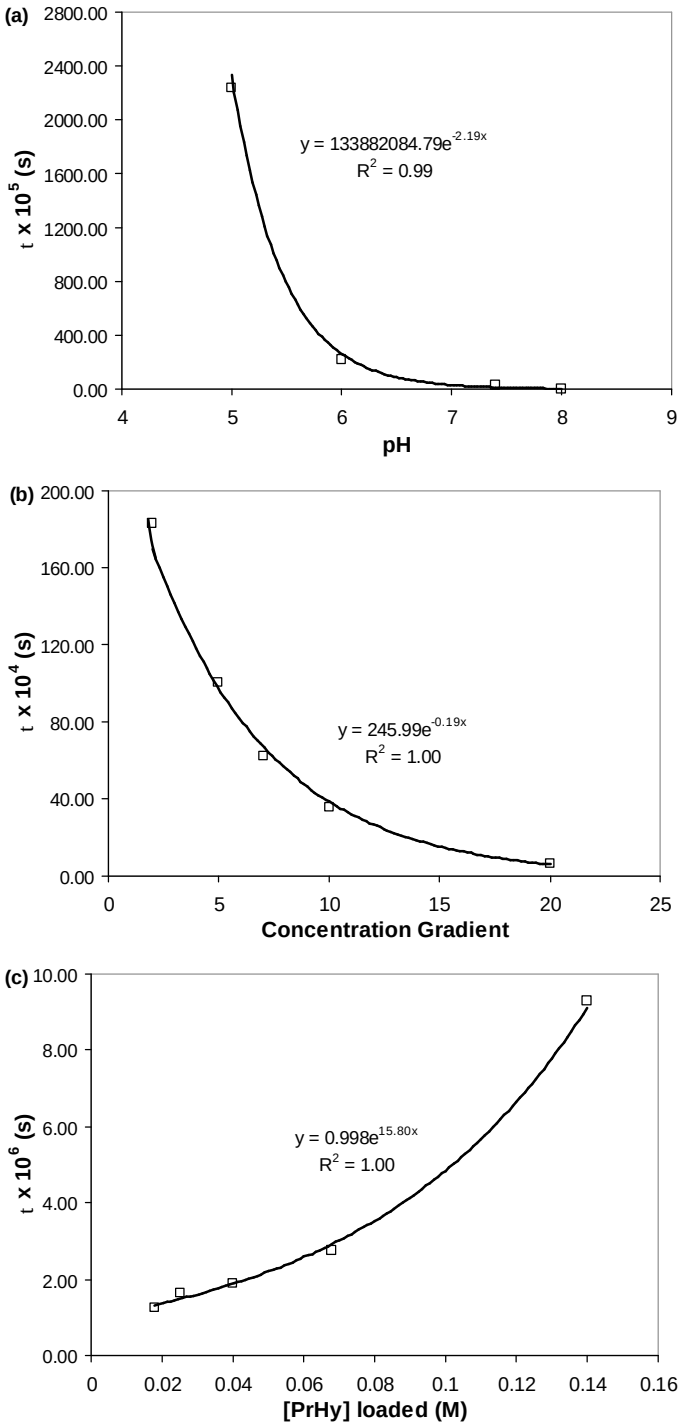

Figure 5.38 Dependence of the characteristic relaxation time (τ) of polymeric chains on the (a) pH of the release medium (exponential fit), (b) concentration gradient difference (exponential fit) and (c) initial drug loading (exponential fit).

5.6 Summary

Based on the titration, DLS and ζ-potential results, the MAA-EA nanogels would not undergo any conformational change and the particle size and ζ-potential at $\alpha = 0$ would be roughly the same due to the seeded emulsion polymerization technique.

R_h for nanogels would increase with an increase in α. This was due to the increase in osmotic pressure created by ionized carboxylate groups. However, with the increase in cross-linking density or the decrease in MAA content, R_h would decrease due to more chemical cross-linking to prevent swelling and lesser osmotic pressure with lower MAA content. All the R_h underwent a sharp transition point at $\alpha = 0.3$ as the osmotic pressure would be large enough to overcome the strong hydrophobic attraction between EA blocks. ζ-potential would become more negative with the increase in α until $\alpha = 0.3$ as more COOH groups were converted to COO^-. After the $\alpha = 0.3$ point, the increase in particle size would cause the mobility of the nanogels to be lowered thus ζ-potential would become less negative.

The particle size decreased with increasing salt concentration as the salt shielded the charges around the negatively charged carboxylate groups. Some of the Na^+ counter-ions from the salt would be able to penetrate into the porous nanogels and thereby expelling the Na^+ counter-ions from NaOH.

PrHy was loaded into MAA-EA nanogels via diffusion and hydrophobic interactions at $\alpha < 1$ due to the steric hindrance of the ethyl groups, which shielded the positive charge from the negatively charged carboxylate groups. However, at $\alpha = 1$, the drug diffused

into the MAA-EA nanogels and bound hydrophobically due to the deprotonation of PrHy.

The size of MAA-EA nanogels decreased with increasing drug loading due to the charge shielding effect on the negatively charged carboxylate groups by PrHy. With the addition of PrHy, there was a reduction in the polymer-solvent interactions as the nanogel environment became more polar. Therefore, the nanogels adopted a more compact conformation. The decrease in cross-linking density and increase in MAA-EA molar ratio enhanced the drug loading capability.

The DSE was found to be a good alternative to other techniques in determining the drug release profile of PrHy from MAA-EA nanogels. The released of PrHy under varying parameters: concentration gradient, pH, drug loading ratio, cross-linking density and MAA-EA molar ratio was studied. Parameters that encouraged the diffusion process of drugs from the interior to exterior of the nanogels would increase the fractional drug release. The amount of drugs release was found to increase with increasing concentration gradient difference, MAA-EA molar ratio and pH. However, the fractional release decreased with increasing cross-linking density and drug loading ratio. From the Berens and Hopfenberg model, during the drug release process, chain relaxation and diffusion played an important role in determining the amount of drugs being released. A step change in pH was conducted to mimic the physiological conditions during intravascular injection of drug delivery system and the drug electrode was able to monitor the release of drugs with changing pH adequately. The results demonstrated the viability of tuning the release profiles of drug from a pH-responsive nanogel system.

6.0 EFFECTS OF LAYER BY LAYER COATING ON PrHY RELEASE

Layer by layer (LBL) coating of polyelectrolytes on HASE 50-50-4 grafted with poly(ethylene glycol)methacrylate (PEGMA) was carried out in the presence of 0.1 M NaCl at pH 6. The coated nanogels did not show signs of aggregation and the swelling decreased with increasing number of polyelectrolyte layers. Poly(allylamine hydrochloride) (PAH) coated nanogels retained their colloidal stability up to pH 8, while poly(sodium 4-styrenesulfonate) (PSS) coated nanogels were stable at all pH.

Drug release using the coated nanogels was conducted using the procaine hydrochloride (PrHy) selective electrode. LBL coating of drug loaded nanogels resulted in reduced burst release phenomenon, which can extend the therapeutic range of the coated delivery system. The amount of drugs trapped in the delivery system increased correspondingly.

6.1 Characterization of MAA-EA nanogels grafted with PEGMA

^{1}H NMR was conducted to ensure the grafting was conducted successfully. From the ^{1}H NMR spectrum from MAA-DEA grafted with PEGMA (Figure 6.1a and b) [Tan et al., 2007] and comparing to the ^{1}H NMR spectrum for MAA-EA grafted with PEGMA (Figure 6.1c), the peak at 3.5 ppm correspond to the $-OCH_2$ from PEGMA.

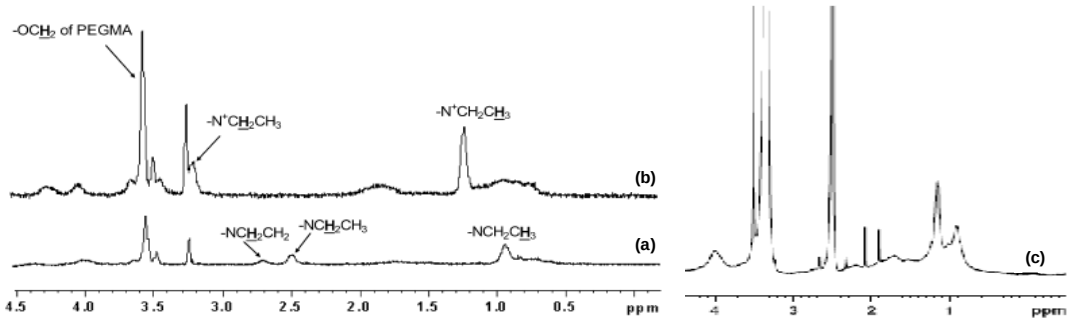

Figure 6.1 ^{1}H NMR spectrum for (a) 60M 40D 20P MAA-DEA microgel at pH 11 using NaOD/D_2O [Tan et al., 2007], (b) 60M 40D 20P MAA-DEA microgel at pH 2 using DCl/D_2O [Tan et al., 2007] and (c) HASE 50-50-4 nanogel grafted with PEGMA using DMSO.

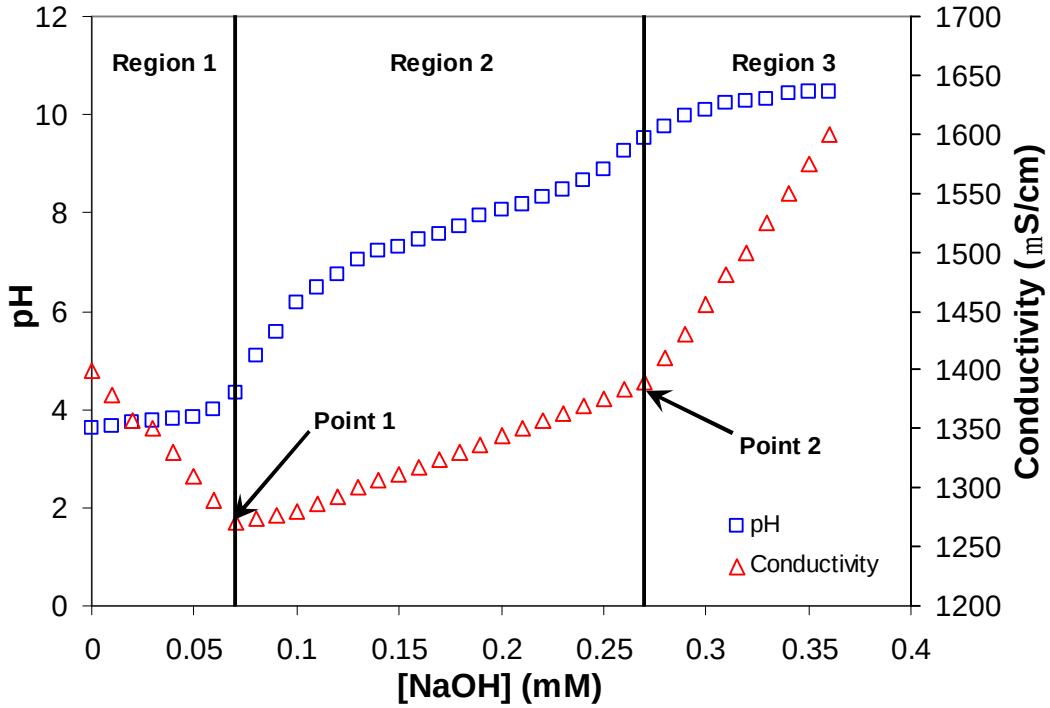

Figure 6.2 pH and conductivity titration of 0.1 wt% HASE 50-50-4 grafted with PEGMA with 1 M NaOH at 25 ^{o}C.

The pH and conductivity curves obtained from titrating 1 M NaOH into 0.1 wt% MAA-EA grafted with PEGMA in 10 mM NaCl solution is shown in Figure 6.2. Three

regions could be distinguished in Figure 6.2. Region 1 and 3 is where there is an excess of HCl and NaOH respectively. When the titration transited from Region 1 to 2, at Point 1, the onset of neutralization of COOH groups from MAA to COO^- occurred. This will continue until Point 2 was reached where all the COOH groups have been converted to COO^-. The pH curves increased progressively and did not exhibit any plateau over the entire course of titration. This might indicate that the nanogels did not undergo conformational transition throughout the entire titration. Based on the amount of NaOH used to neutralize the COOH groups on the MAA segments, the amount of COOH present was calculated. The targeted mole ratio of MAA:EA was 50:50 while the actual mole ratio was calculated to be 52:48.

6.2 Characterization of layer by layer coated nanogels

The optimum amount of PAH and PSS to be added into HASE 50-50-4 grafted with PEGMA is based on the particle size and ζ-potential of the coated products, where the chosen amount should have the maximum ζ-potential and minimum hydrodynamic radius (R_h). Particle size and ζ-potential graphs for the first to fifth layer plotted against ratio of the volume of PAH/PSS against volume of HASE 50-50-4 grafted with PEGMA are shown in Figure 6.3. For example, when a 30-millilitre nanogel solution was used, the volume of polyelectrolyte used was 3-millilitre assuming the ratio to be 0.1. The first, third and fifth layer consisted of PAH (positively charged) layer, while the second and fourth layer comprised of PSS (negatively charged) layer. From Figure 6.3a, the bare HASE 50-50-4 grafted with PEGMA possessed a R_h of ~47 nm and ζ-potential of ~-24 mV. When a ratio of 0.025 was used, R_h increased to ~294 nm and ζ-potential changed to ~+9.2 mV. The small amount of PAH added did not fully cover the surface of the

nanogels. This will create an unstable nanogel as indicated by the ζ-potential (below the stable region of ± 20 mV). Therefore aggregation between nanogels occurred leading to an increase in particle size. Since there were exposed areas not covered by PAH, these exposed areas could be attracted to another nanogel coated with PAH, which induced aggregation of the nanogels, as illustrated in Figure 6.5. Transmittance data is shown in Figure 6.4 and value for the transmittance decreased from ~87 to ~20% when a ratio of 0.025 was used, signifying the aggregation of nanogels. When a ratio greater than 0.025 was used, transmittance increased to ~83%, however high ratio should not be used as the cleaning process will become increasingly more difficult. Similar observations (signs of aggregation were evident) were seen in Figures 6.3b to 6.3e when small ratio was used. Therefore the optimum ratio of PAH used in the first, third and fifth layer should be 0.1, while the optimum ratio of PSS used in the second and fourth layer was 0.3.

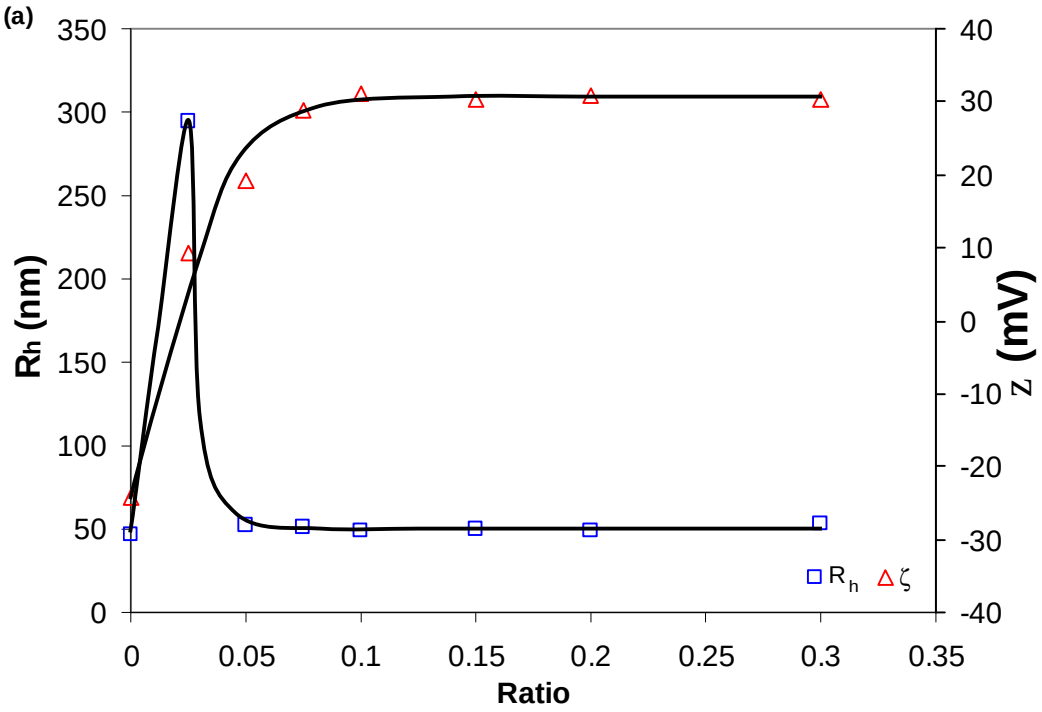

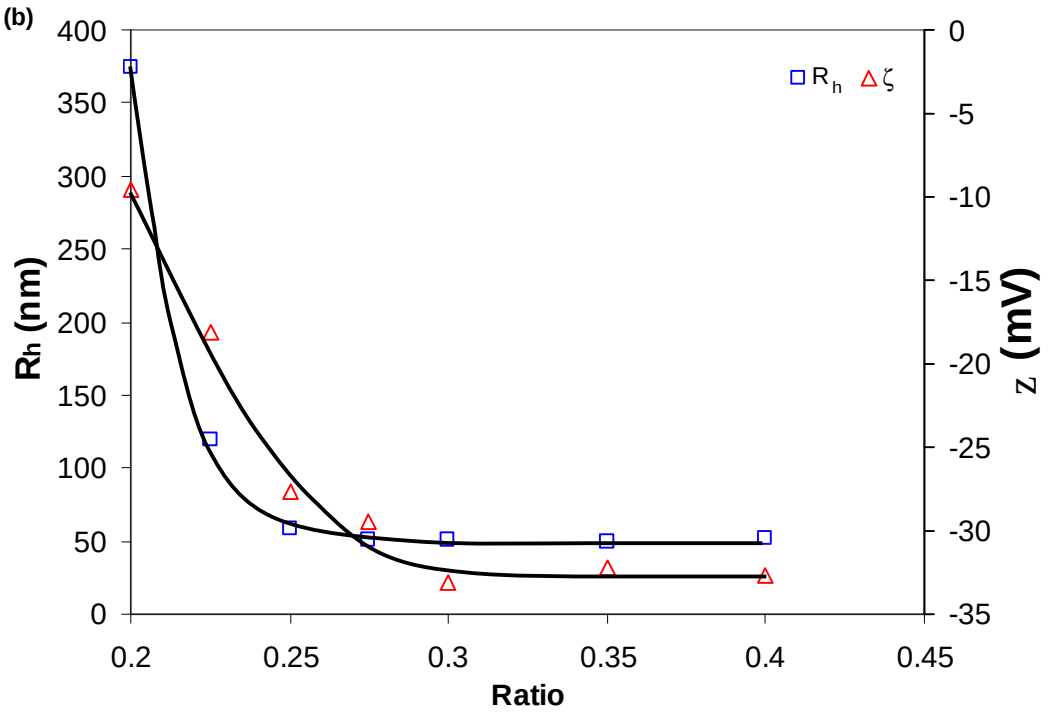

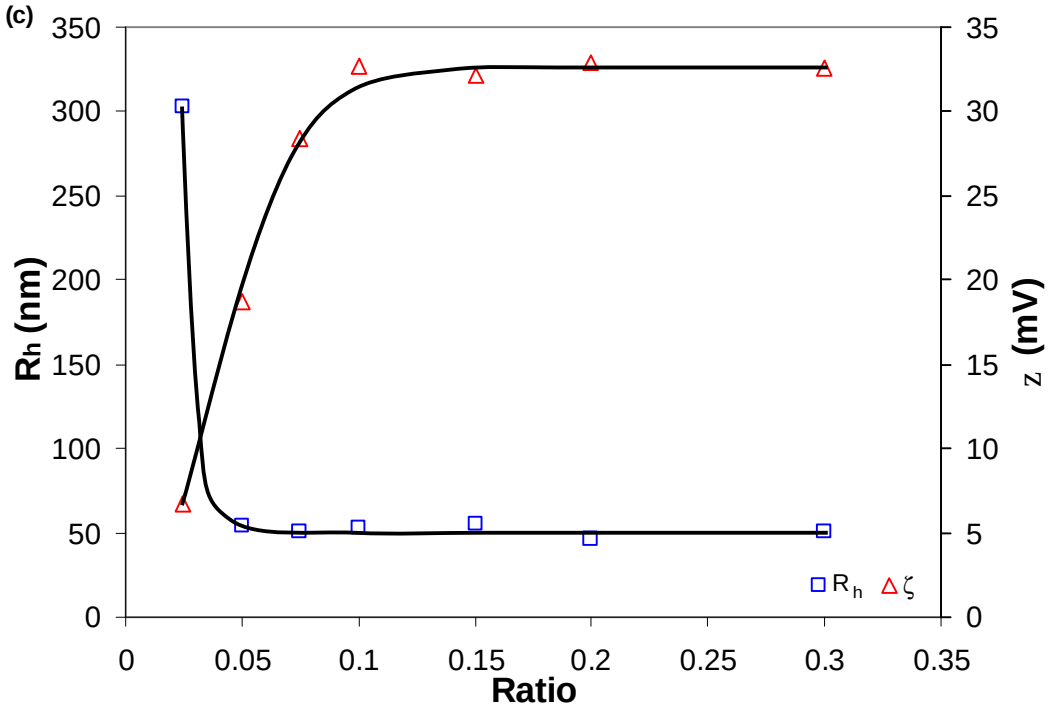

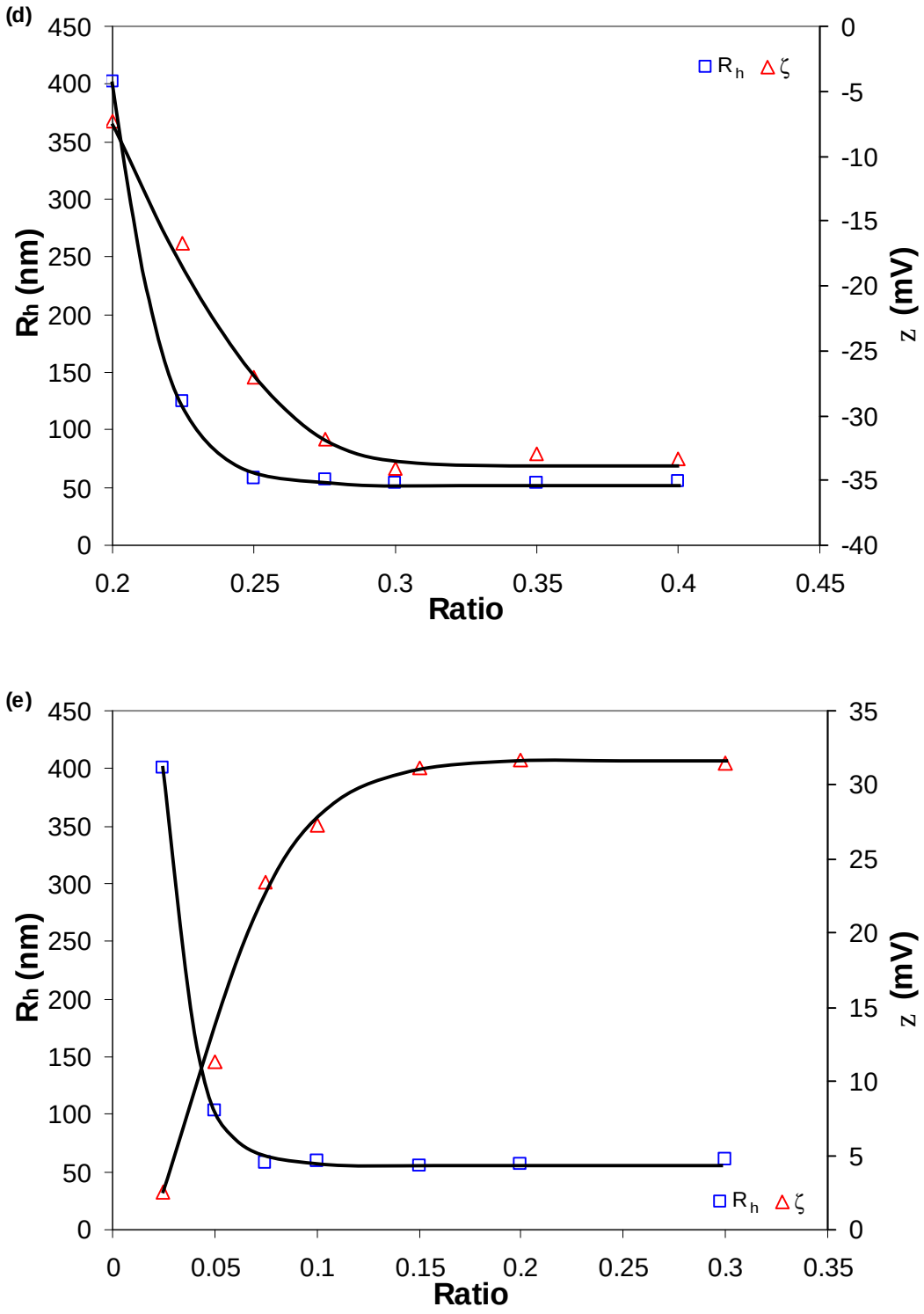

Figure 6.3 R_h and ζ-potential of (a) 1st layer, (b) 2nd layer, (c) 3rd layer, (d) 4th layer and (e) 5th layer against the ratio of volume of PAH/PSS to volume of HASE 50-50-4 grafted with PEGMA in 0.1 M NaCl at pH 6.

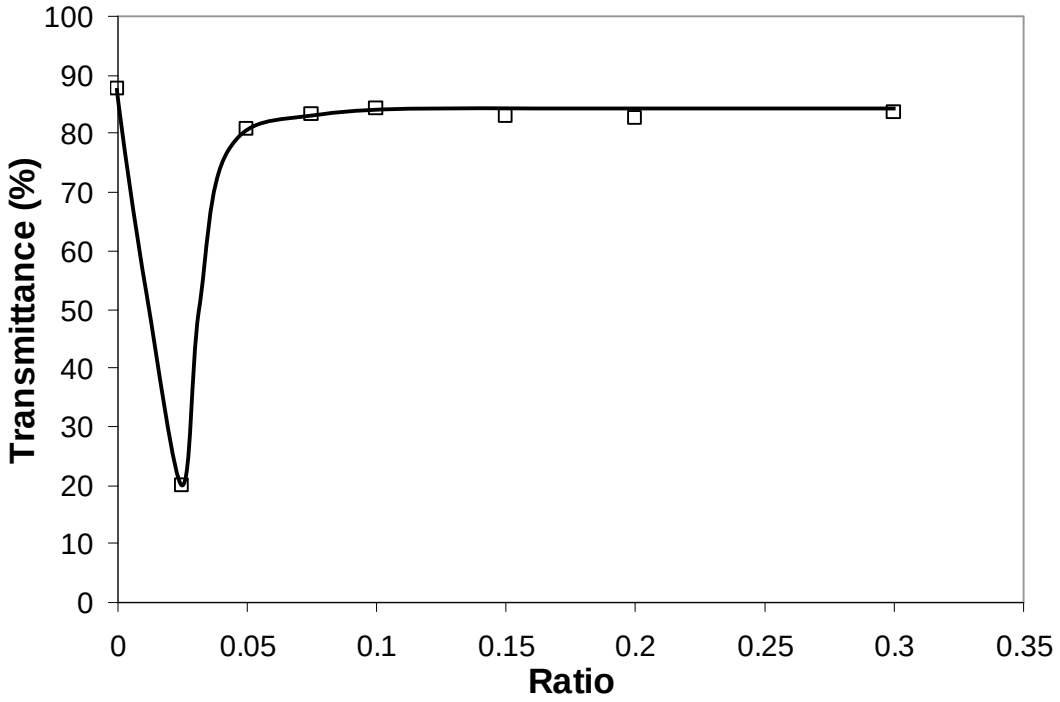

Figure 6.4 Transmittance for the first coated layer against the ratio of volume of PAH/PSS against volume of HASE 50-50-4 grafted with PEGMA in 0.1 M NaCl at pH 6.

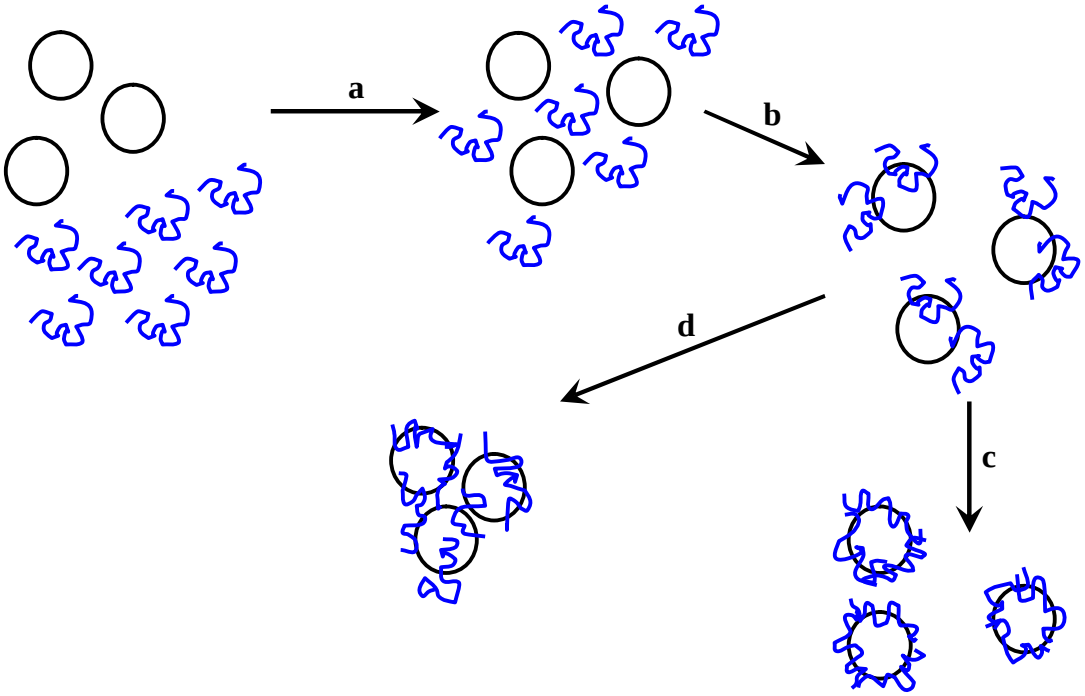

Figure 6.5 Schematic diagram of the stages involved in LBL coating of HASE 50-50-4 grafted with PEGMA (a) addition of polyelectrolytes into nanogels, (b) absorption of polyelectrolyte onto nanogels, (c) individually coated nanogels and (d) aggregation of nanogels (small ratio).

The experimental protocol involved the followings. Firstly, MAA-EA nanogels grafted with PEGMA were synthesized via the emulsion polymerization technique. PrHy was added to the nanogels and left to equilibrate overnight before LBL coating was performed. Alternating layers of PAH and PSS were deposited on the charged nanogels assisted by electrostatic attractive forces. With the addition of a single layer in 0.1 M NaCl at pH 6, approximately 2 nm of shell layer was deposited on the nanogel surface as shown in Figure 6.6. The bare nanogels without coating possessed a R_h of ~47 nm and with the addition of the first PAH layer, R_h increased to ~49 nm. After the fifth layer was deposited, the radius approached ~56 nm. From the small increment in dimension, no aggregation arising from chain bridging was evident. However, in the case of HASE

50-50-4 without any PEGMA grafts, aggregation occurred (result not shown). Figure 6.6 shows the dependence of ζ-potential on the layer number (L) of negatively charged MAA-EA grafted with PEGMA nanogels coated with PAH or PSS. The negatively charged (uncoated) MAA-EA grafted with PEGMA nanogels yielded a ζ-potential of ~-25 mV in 0.1 M NaCl pH 6 solution. Addition of cationic PAH produced a reversal in the ζ-potential from ~-25 to ~+32 mV. Subsequent addition of PSS onto the PAH coated nanogels produced a ζ-potential of ~-33 mV. Alternating ζ-potential (in sign) was observed with subsequent addition of PAH and PSS layers. The colloidal stability of coated nanogels was better than bare nanogels as evident from the larger magnitude of ζ-potential, which was probably due to the greater electrostatic and steric stabilization conferred on the nanogels with the addition of polyelectrolyte layers. Only ~20% of COOH groups were converted to COO^- at pH 6 and at this pH, PAH and PSS chains remained fully charged, which enhanced the stability of the coated nanogels.

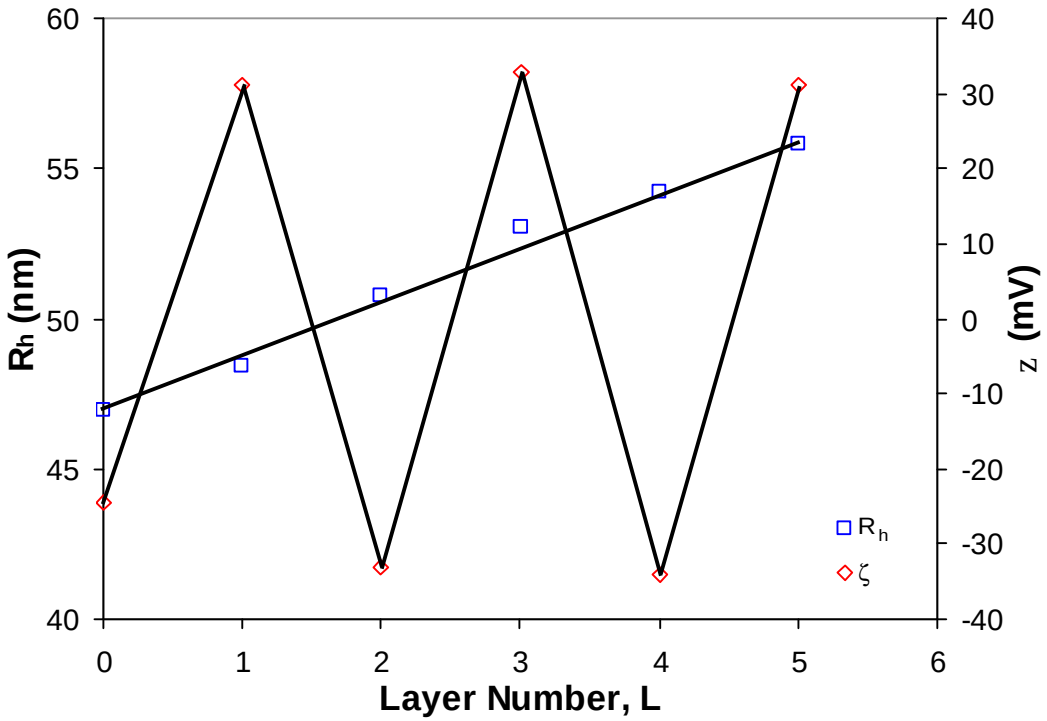

Figure 6.6 ζ-potential and R_h as a function of polyelectrolyte layer number (L).

The ζ-potential and particle size of coated nanogels were plotted as a function of pH in Figures 6.7 and 6.8 respectively. The ζ-potential of bare nanogel became more negative with increasing pH due to more COO^- groups and with further increase in pH, the ζ-potential became less negative due to the increasing size of the nanogels, which reduced the mobility of the nanogels and correspondingly the ζ-potential. Since the negative charges on the PSS are independent of pH, the ζ-potential for second and fourth layer remained constant despite changes in the pH. With increasing pH, more COOH groups were converted to COO^- and the particle size swelled due to the osmotic pressure induced by counter-ions A larger increase in particle size was evident after pH 6 when the osmotic pressure overcame the hydrophobic interactions of EA segments. The swelling was suppressed with additional polyelectrolyte layers. With the addition of a polyelectrolyte layer, neutralization of COOH groups was restricted, which reduced the

swelling of the coated nanogels. When the pH for the coated nanogels with one, three and five layers was increased from 4 to 10, the ζ-potential remained constant at ~+32 mV up to pH of 7, beyond which it decreased rapidly. From pH of 4 to 7, the corresponding degree of protonation for PAH was between 1 to 0.95, which decreased rapidly after pH of 7 as shown in Figure 6.10. The particle size of coated nanogels with one, three and five layers increased with pH due to osmotic pressure from counter-ions within the nanogels. Beyond pH 8, the ζ-potential decreased to less than +20 mV, which was within the unstable regime that induced aggregation of the coated nanogels. Under this condition, PAH chains began to detach from the coated nanogels and bridged two or more nanogels to form larger aggregates as indicated by the increased turbidity shown in Figure 6.8. A clearer picture of the particle sizes against the pH is shown in Figure 6.9.

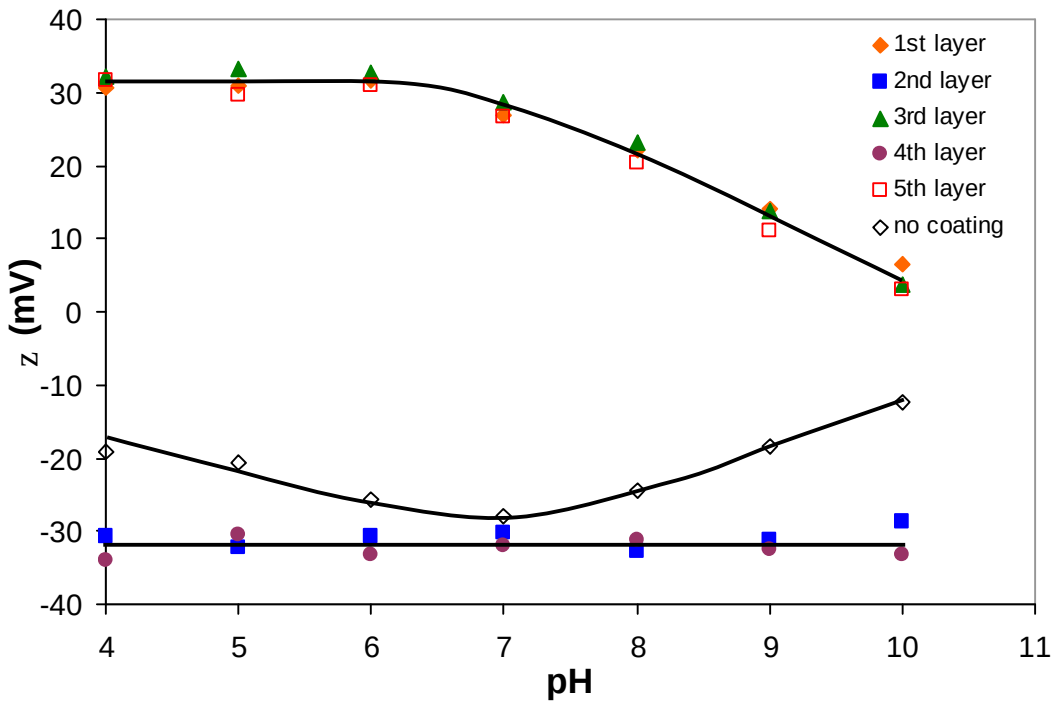

Figure 6.7 ζ-potential of the coated nanogels as a function of pH.

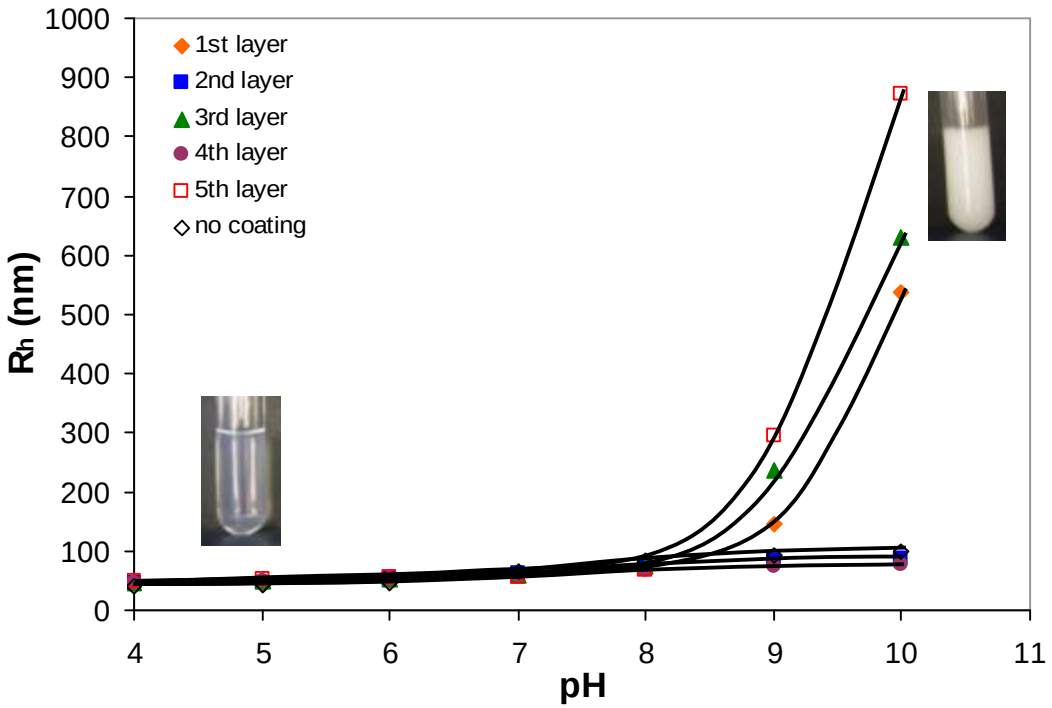

Figure 6.8 Particle size of the coated nanogels as a function of pH.

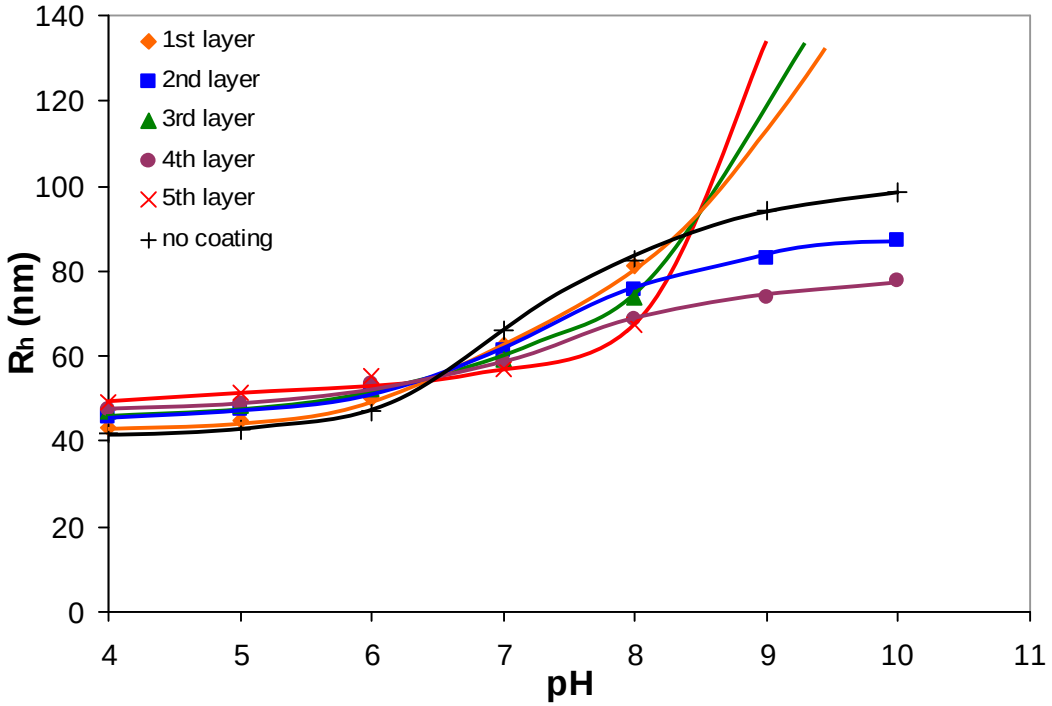

Figure 6.9 Particle size of the coated nanogels as a function of pH plotted from 0 to 140 nm.

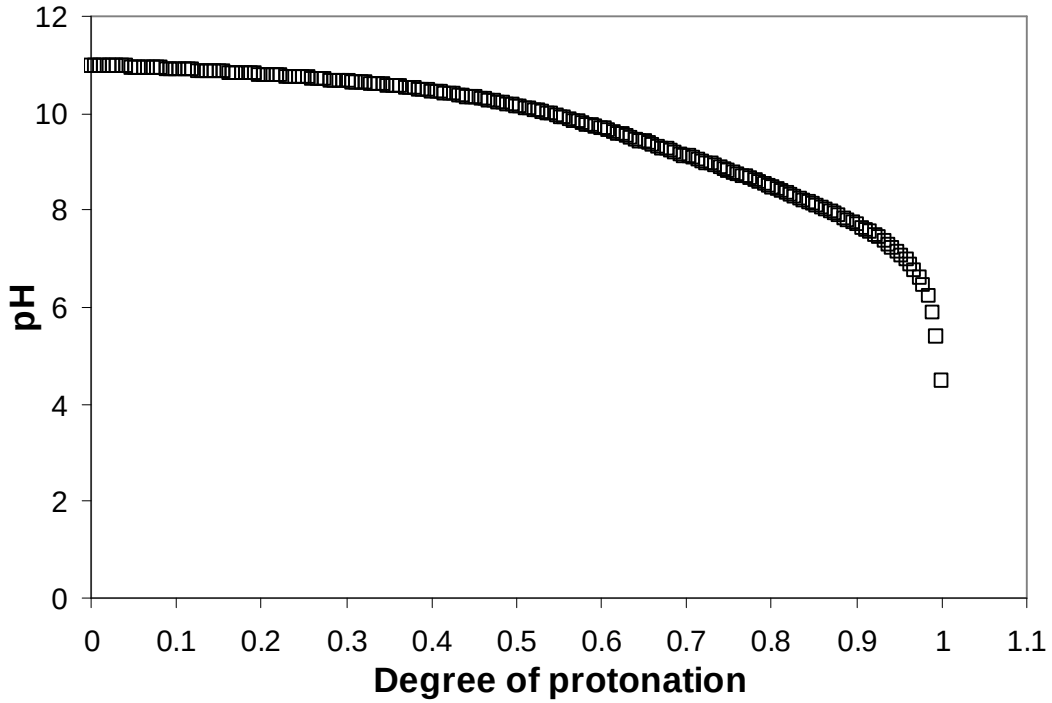

Figure 6.10 Titration data for 0.1 wt% PAH in 0.1 M NaCl plotted against the degree of protonation.

6.3 PrHy release from layer by layer coated nanogels

Nanoparticles are ideal systems for site specific delivery applications [Roman et al., 2004] and histological studies showed that particles at 100 nm could diffuse through the submucosal layers, while larger sized particles (500 nm–10 μm) were found to be concentrated within the epithelial lining of tissues [Arifin et al., 2006]. Due to the large surface to volume ratio, the release of drugs or proteins will be released rapidly as indicated by the undesirable initial burst release phenomenon. One strategy in addressing this problem is to develop a double walled composite particle with a less permeable outer shell comprising of a hydrophobic matrix for controlling the initial burst release [Arifin et al., 2006], however, this may not be the easiest route for limiting the initial burst release. In this study, the LBL technique was adopted, and through this strategy the initial burst release was alleviated and this technique offers potential advantages over the double walled composite particle system as;

(4) it is simple since it only involves electrostatic attraction between oppositely charged polyelectrolyte and the layer thickness can be generated with nanometer precision,

(5) it is more cost efficient and practical than to chemically modify the surface of nanoparticles and,

(6) the release process can be extended by manipulating the number of layers of polyelectrolyte.

Following a detailed physical characterization of the polyelectrolyte coated nanogels, the application of the coated nanogels to control the released of PrHy was demonstrated. The capability of the coated nanogels in slowing down or eliminating the initial burst release

associated with controlled release using nanoparticles was demonstrated. The nanogels were first loaded with 1.42 g of drug/g of polymer, which was then subjected to the LBL coating steps to achieve the desired layers of coatings as described earlier. This coated nanogels with drug (0.01 wt%) were placed in 100-millilitre of 10 mM NaCl solution at pH 7.4 at a temperature of 37 ^{o}C and the concentration of released PrHy was measured using the PrHy selective electrode as shown in Figure 6.11. Initial burst release of PrHy was present in the bare nanogel and one and two layers coated nanogels, which were related to the release of PrHy on the outer surface of uncoated nanogel. The burst release phenomenon was reduced and minimized with the addition of more polyelectrolyte layers on the nanogel. As evident from Figure 6.11, the initial steep slope at short times (signifying burst release) became gentler when the number of polyelectrolyte layers was increased. With more polyelectrolyte layers, the more accessible surface adhered PrHy molecules have to diffuse through the polyelectrolyte layers, therefore mitigating the burst release phenomenon. The time to attain the steady state drug concentration (τ_D) (indicated by the arrow on Figure 6.11) was increased as the number of coated layers was increased. Two factors contribute to this trend: (1) difference in size of swollen nanogel and (2) changes in the permeability. The swelling characteristic of coated nanogels with different polyelectrolyte layers is different as evident from Figure 6.9. Such differences in the swelling trend of coated nanogels alter the porosity and impact the diffusion of drug from the coated nanogel, resulting in a different kinetic release profiles. Nanogels with more polyelectrolyte layers swelled the least, resulting in a corresponding lower diffusion of drug. By increasing the number of coated polyelectrolyte layers, the diffusion of PrHy from the surface and interior of the coated nanogel decreased significantly, since the diffusion barrier for PrHy molecules was greatly increased. The

mechanism for the delayed and controlled release of drug from coated nanogel is depicted in Figure 6.12.

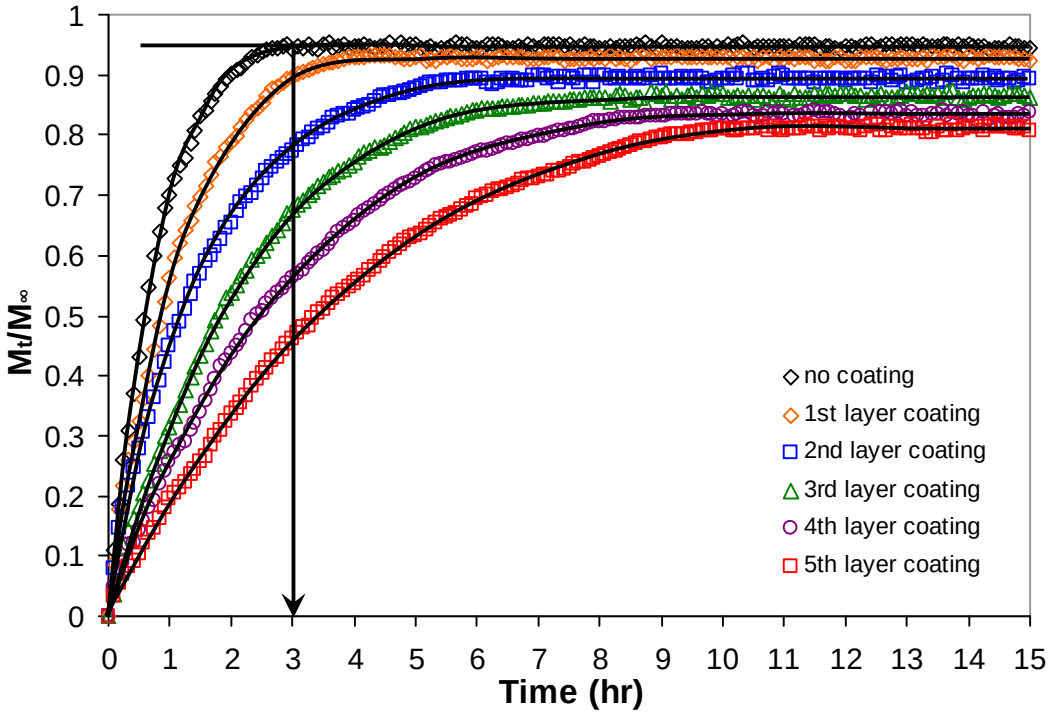

Figure 6.11 Release profiles for MAA-EA nanogels grafted with PEGMA and polyelectrolyte coated MAA-EA nanogels grafted with PEGMA in 100-millilitre 10 mM NaCl at pH 7.4.

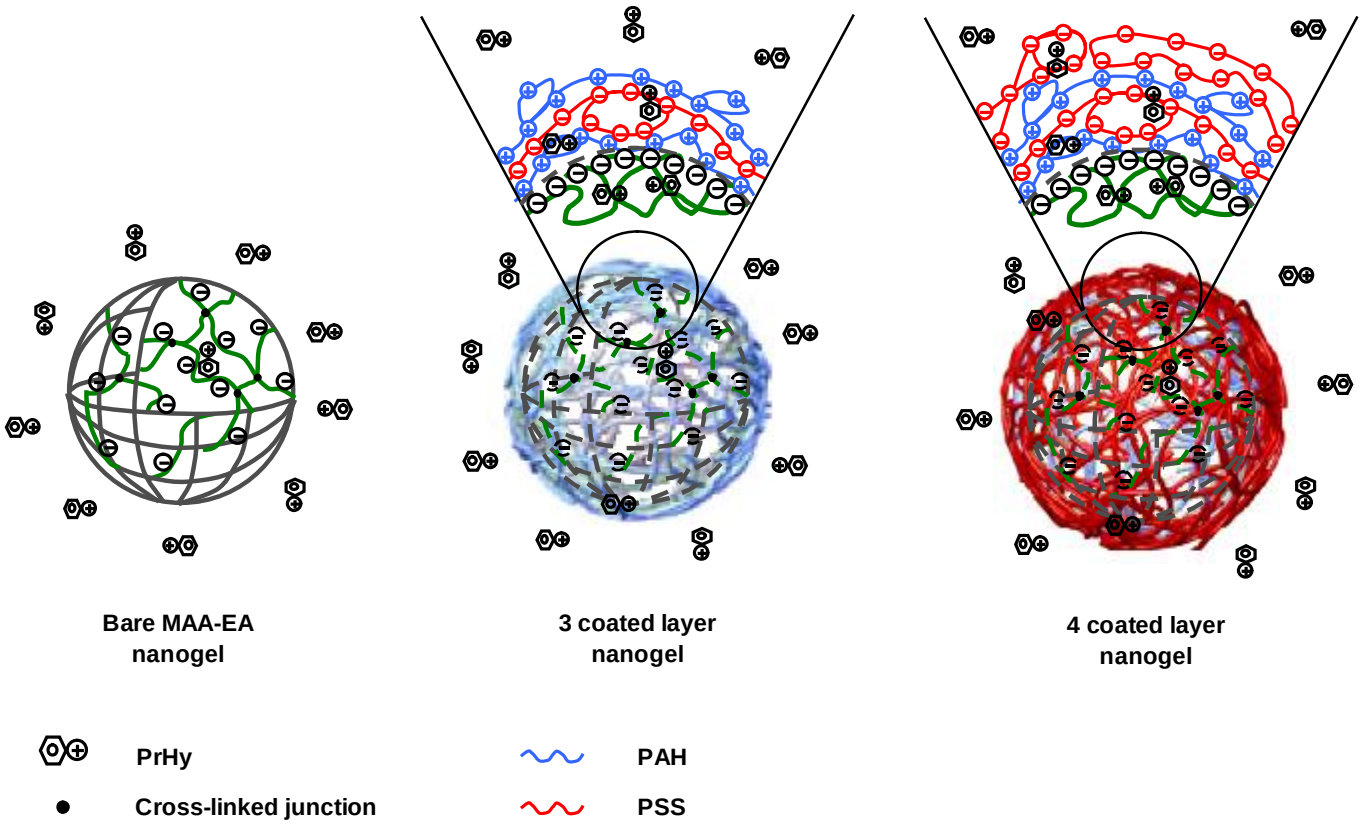

Figure 6.12 Scheme illustrating the drug release process for the bare and coated nanogels. (a) Bare nanogels drug release demonstrated high burst release due to surface adhered drugs, (b) 3 coated layer nanogels demonstrated a lowered burst release and prolonged sustained drug release as compared to the bare nanogels due to the reduced permeability and (c) 4 coated layer nanogels demonstrated very low burst release and prolonged sustained drug release as compared to 3 coated layer nanogels.

As illustrated in Figure 6.13, τ_D was linearly dependent on the number of polyelectrolyte layers, where it increased from ~3 to ~11 hrs when the polyelectrolyte layer was increased from 0 to 5 layers. This suggested that the diffusion process was controlled by the increase in layer thickness and the type of polyelectrolyte within the layer was not particularly important. A simple linear relationship between τ_D and the layer number of polyelectrolyte (L) was computed and shown in Equation 6.1. This simple relationship provided a useful guide in the design of coated nanogels for drug delivery applications as required by the therapeutic specifications of a treatment regime.

$$t_D = 1.73L + 2.93 \tag{6.1}$$

where τ_D is the time to achieve the steady state drug concentration (hrs) and L is the layer number of polyelectrolyte.

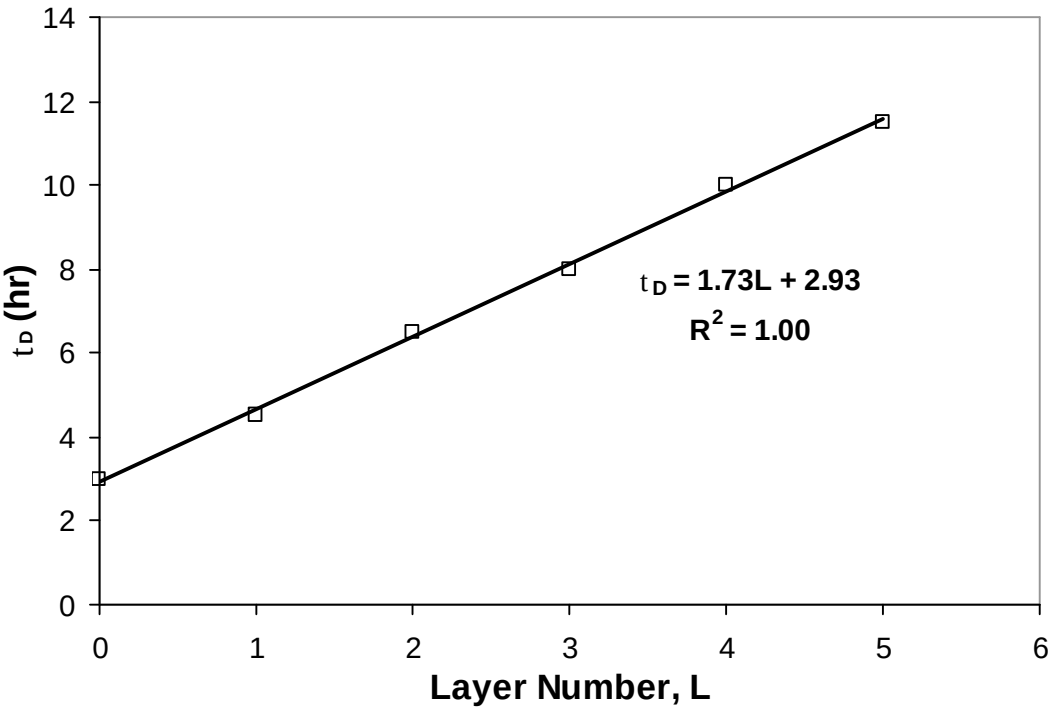

Figure 6.13 Time to attain the steady state drug concentration (τ_D) as a function of layer number of polyelectrolyte (L).

6.4 Mathematical modeling

Modeling of the results was carried out using the Berens and Hopfenberg [Enscore et al., 1977; Berens and Hopfenberg, 1978] model having the form shown in Equation 6.2:

$$\frac{M_t}{M_\infty} = 1 - f_F\left[\frac{6}{p^2}\sum_{n=1}^{\infty}\frac{1}{n^2}\exp\left(-4p^2n^2Dt/d^2\right)\right] - f_R\exp(-kt) \qquad (6.2)$$

where D is the diffusion coefficient for the Fickian portion of the transport, k is the first-order relaxation constant, f_F and f_R are the fractions of sorption contributed by Fickian diffusion and chain relaxation respectively, d is the diameter of sphere and t is time. The above model describes the overall release behavior in terms of Fickian and non-Fickian contributions. This analysis can lead to the determination of diffusion coefficient (D), and characteristic relaxation time (τ), which is a reciprocal of k.

The model fitting to the experimental data shown in Figure 6.14 using the Berens and Hopfenberg model (Equation 6.2) was used to determine the parameters D, k, f_F and f_R in the model equation. The solid lines in Figure 6.14 are the Berens and Hopfenberg model fitting using the non-linear least squares fitting routine of MATLAB. Excellent agreement between the experimental and predicted kinetic profiles was obtained in all cases. From the model fittings, f_F and f_R were found to vary with L as shown in Figure 6.15. The parameter f_F was found to dominate the release process at no or few layers of coating as these contributed to a swollen or more porous nanogel, which facilitated the diffusion process since the chains did not relax before the drug was released. However, with increasing layers of coatings, f_R dominated. Under such circumstances, the nanogels assumed a compact structure as neutralization of COOH groups was hindered,

where the polymeric chains must first relax before the diffusion of drugs could take place. Therefore, in the drug release process, the release of drugs from LBL coated nanogels was governed by a combination of chain relaxation and diffusion processes and this will change depending on the characteristics of the gel network.

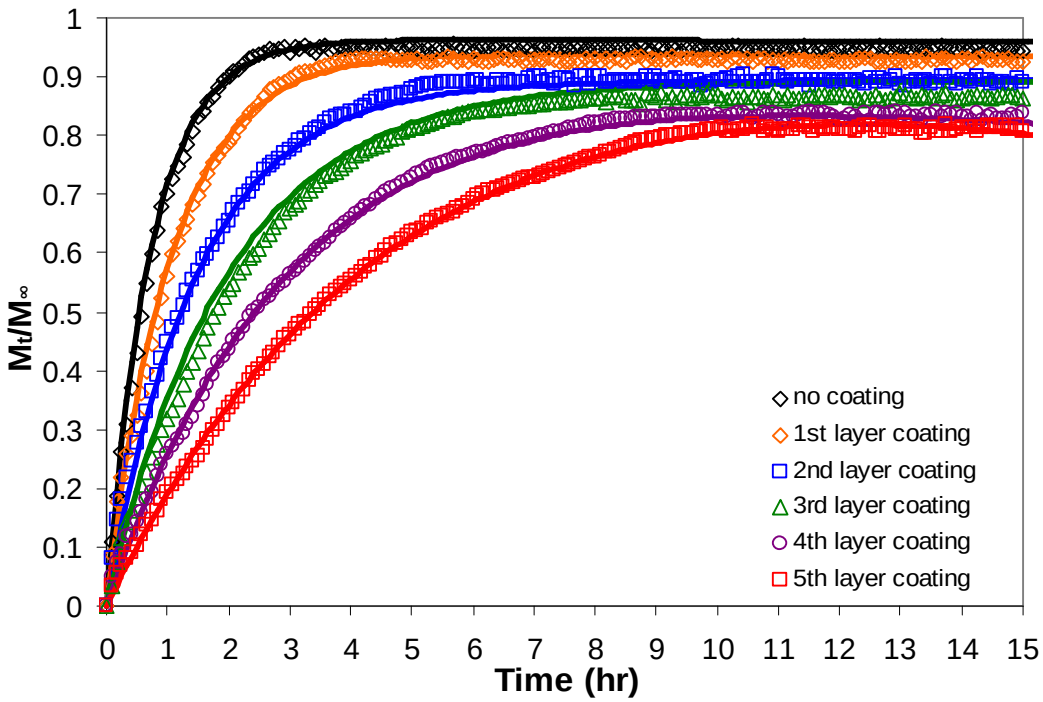

Figure 6.14 Release profile for 0.01 wt% HASE 50-50-4 grafted with PEGMA in 100-millilitre 10 mM NaCl solution at varying pH (a) no coating (◇), (b) 1st layer coating (◇), (c) 2nd layer coating (□), (d) 3rd layer coating (△), (e) 4th layer coating (○) and (f) 5th layer coating (□) and theoretical fit of the Berens and Hopfenberg mathematical model taking into account drug diffusion and chain relaxation (solid lines).

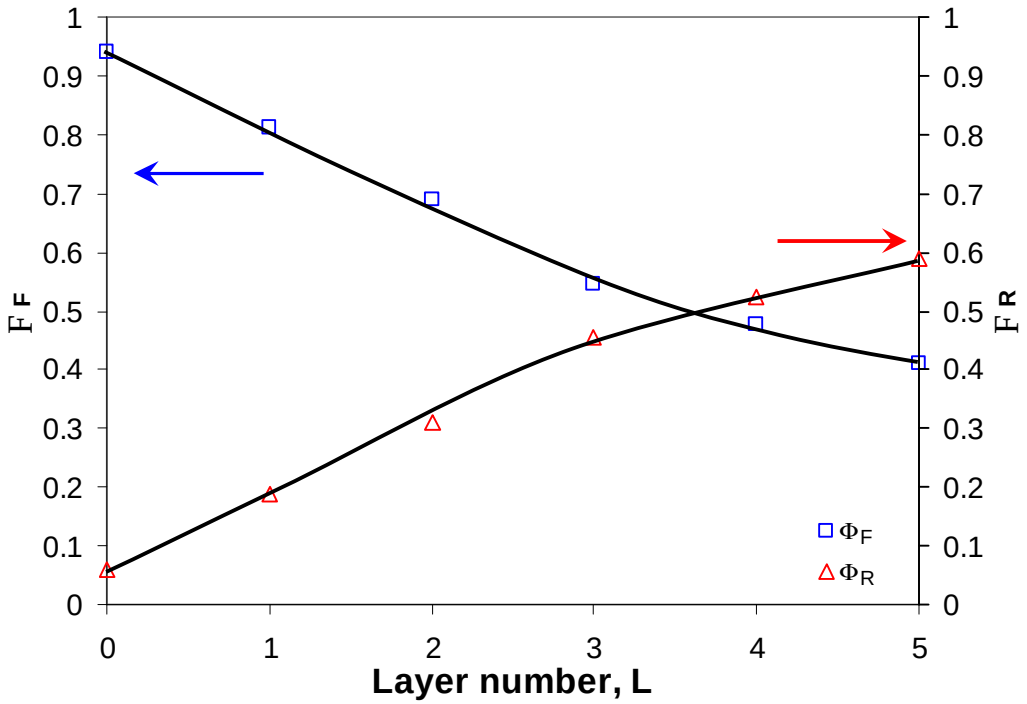

Figure 6.15 Dependence of ϕ_F and ϕ_R against layer number (L).

Based on the fittings from Berens and Hopfenberg model, the diffusion coefficient and characteristic relaxation time as a function of layer number of polyelectrolyte (L) are illustrated in Figures 6.16 and 6.17 respectively. From Figure 6.16, the diffusion coefficient decreased with increasing number of polyelectrolyte layers. Increasing the number of polyelectrolyte layers reduced the permeability of the nanogels, which lowered the diffusion coefficient. The characteristic relaxation time increased with increasing polyelectrolyte layers as shown in Figure 6.17. When the number of polyelectrolyte layers increased, the neutralization of COOH groups became more difficult, hence the swelling of the nanogel will take a longer time. An empirical relationship between diffusion coefficient or characteristic relaxation time and pH of the release medium is given below:

$$D = [1.91\exp(-0.95L)]x10^{-15} \quad (6.3a)$$

$$t = [45.32\exp(0.66L)]x10^{4} \quad (6.3b)$$

Based on these relationships, it is possible to determine the diffusion coefficient and characteristic relaxation time at any arbitrary polyelectrolyte layers.

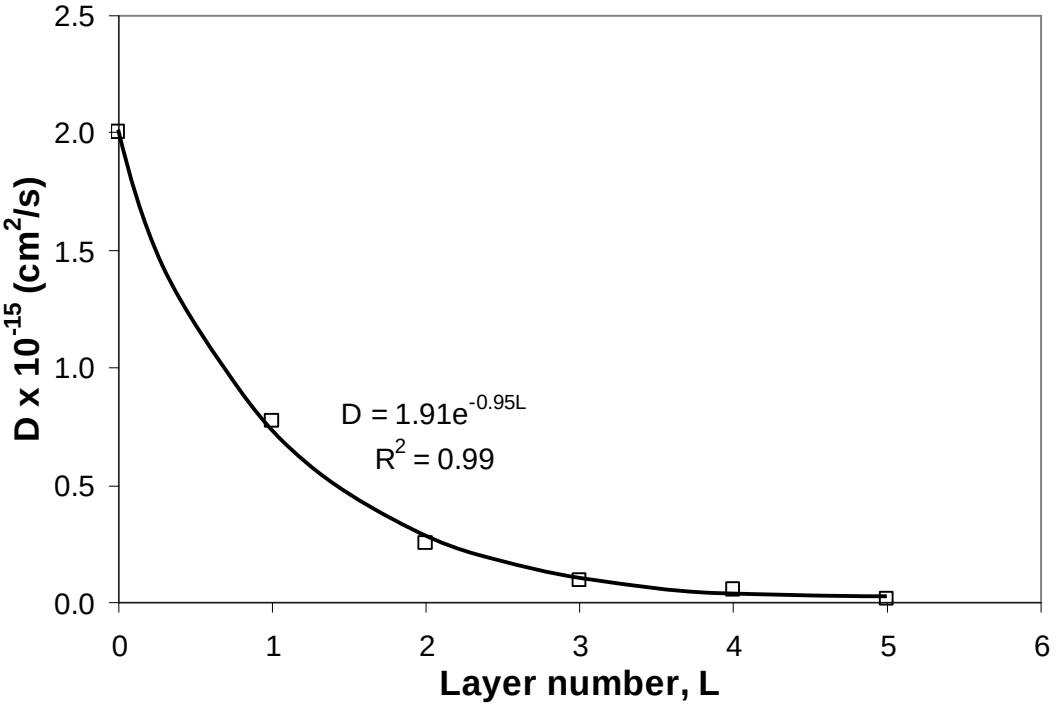

Figure 6.16 Dependence of the diffusion coefficient (D_o) of PrHy from nanogels grafted with PEGMA on the layer number of polyelectrolyte (L) (exponential fit).

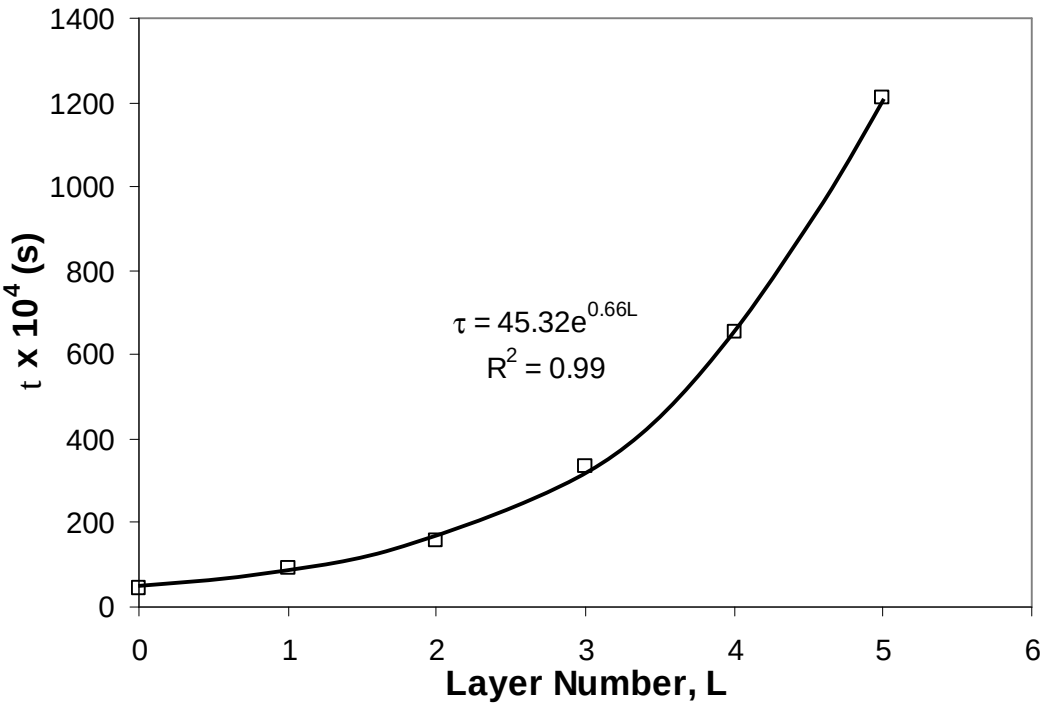

Figure 6.17 Dependence of the characteristic relaxation time (τ) of polymeric chains on the on the layer number of polyelectrolyte (L) (exponential fit).

6.5 Summary

Successful preparation of coated nanogels grafted with PEGMA with encapsulated drugs using the LBL approach was demonstrated. The initial burst release behavior observed in nanoparticles was minimized and eliminated by the introduction of several polyelectrolyte layers. Through this LBL approach, the permeability of nanogels was altered and with each additional polyelectrolyte layer, τ_D increased linearly with L. The swelling behavior of coated nanogels decreased with increasing polyelectrolyte layers resulting in a slower release of drugs. The colloidal stability of coated nanogel was maintained up to pH 8 for PAH coated system, while it was always maintained at all pH for PSS coated system. LBL coating of responsive nanogel provided solutions in the use of nanoparticles in drug delivery applications, where the high initial burst release and short therapeutic time range were overcome. The findings in the present study provided a useful guide in the design of coated responsive nanogels for controlled drug delivery applications. From the Berens and Hopfenberg model, during the drug release process, chain relaxation and diffusion played an important role in determining the amount of drugs being released.

7.0 EFFECT OF T_g ON PrHy RELEASE

Three different nanogels with different glass transition temperature (T_g) were synthesized via the emulsion polymerization technique. The swelling behavior (microscopic) of the pH-responsive nanogels was studied at various pHs. The pH and conductivity curves as a function of degree of neutralization (α) exhibited a well-defined equivalence point corresponding to the complete neutralization of MAA groups at $\alpha = 1$. The actual molar ratio of monomers in the nanogels was very close to the targeted value and the slight deviation was within experimental error of 2%. Nanogel and drug solutions of desired concentrations were prepared from stock solutions for isothermal titration calorimetric, zeta potential and laser light scattering studies. Through these characterizations, the drug binding mechanism of PrHy to the three nanogels were studied and changes in particle sizes at different drug loading ratio were investigated. The binding mechanism provided useful insights into the release behavior.

Drug release was carried out with varying parameters: pH and T_g, using the drug selective electrode. Modeling with an existing Berens and Hopfenberg model was carried out to gain insights into the diffusion and chain relaxation behavior during the release process.

7.1 Characterization of nanogels

7.1.1 Glass transition temperature

Glass transition temperature (T_g) for the three nanogels were calculated based on Fox's equation:

$$\frac{1}{T_g} = \frac{w}{T_{g1}} + \frac{1-w}{T_{g2}} \tag{7.1}$$

where T_g is the glass transition temperature of the nanogels, subscript 1 and 2 represent the two different monomers and w is the weight percent of each monomer used. The Fox equation is commonly used to describe the composition dependence of T_g of ideal copolymers or polymer blends, where strong interactions are absent [Boileau et al., 2002]. Based on the studies by Okubo et al. [Okubo et al., 2004], the T_g of MMA-MAA, MMA-BMA and MMA-EA emulsion, calculated from Fox's equation agreed well with the DSC results. The T_g calculated from Fox's equation for 50MAA-50EA, 50MAA-50BMA and 50MAA-50MMA nanogels were 67.8, 83.0 and 153.6 ^oC respectively while T_g measured by DSC were 64.4, 85.9 and 157.2 ^oC respectively. The T_g for the three nanogels are shown in Table 7.1 to 7.3.

Table 7.1 T_g calculated from Fox's equation for 50MAA-50EA.

Name of nanogel	MAA (wt%)	EA (wt%)	T_g (^oC)	T_g (MAA) (^oC)	T_g (EA) (^oC)
50MAA-50EA	0.536	0.464	67.8	228	-24

Table 7.2 T_g calculated from Fox's equation for 50MAA-50BMA.

Name of nanogel	MAA (wt%)	BMA (wt%)	T_g (^oC)	T_g (MAA) (^oC)	T_g (BMA) (^oC)
50MAA-50BMA	0.377	0.623	83.0	228	30

Table 7.3 T_g calculated from Fox's equation for 50MAA-50MMA.

Name of nanogel	MAA (wt%)	MMA (wt%)	T_g (^oC)	T_g (MAA) (^oC)	T_g (MMA) (^oC)
50MAA-50MMA	0.464	0.536	153.6	228	105

7.1.2 Potentiometric titration studies

The pH and conductivity curves obtained from titrating 1 M NaOH into 0.1 wt% 50MAA-50EA, 50MAA-50BMA and 50MAA-50MMA nanogels in 10 mM NaCl solution are shown in Figure 7.1. The mole ratio of MAA to other comonomer was 50:50 with a cross-linked density of 4 wt%. In Figure 7.1, the pH and conductivity were plotted against degree of neutralization (α).

There was a sharp increase in pH values from ~4 to 6.2 in the range of $\alpha \sim 0$ to $\alpha \sim 0.1$ for all the three different nanogel samples. Thereafter, the pH curves increased progressively until the neutralization process was completed at $\alpha = 1$ and did not exhibit any plateau over the entire course of neutralization. This might indicate that the nanogels did not undergo conformational transition throughout the neutralization process. The sharp increase in pH at low α was due to the strong acid-base interaction caused by the

neutralization of small amounts of sulfate (-SO_3H) groups introduced from the initiator during synthesis. This is a typical phenomenon for synthetic polyacid and is observed in many studies on surface charges of such colloidal particles [Wang, 2004].

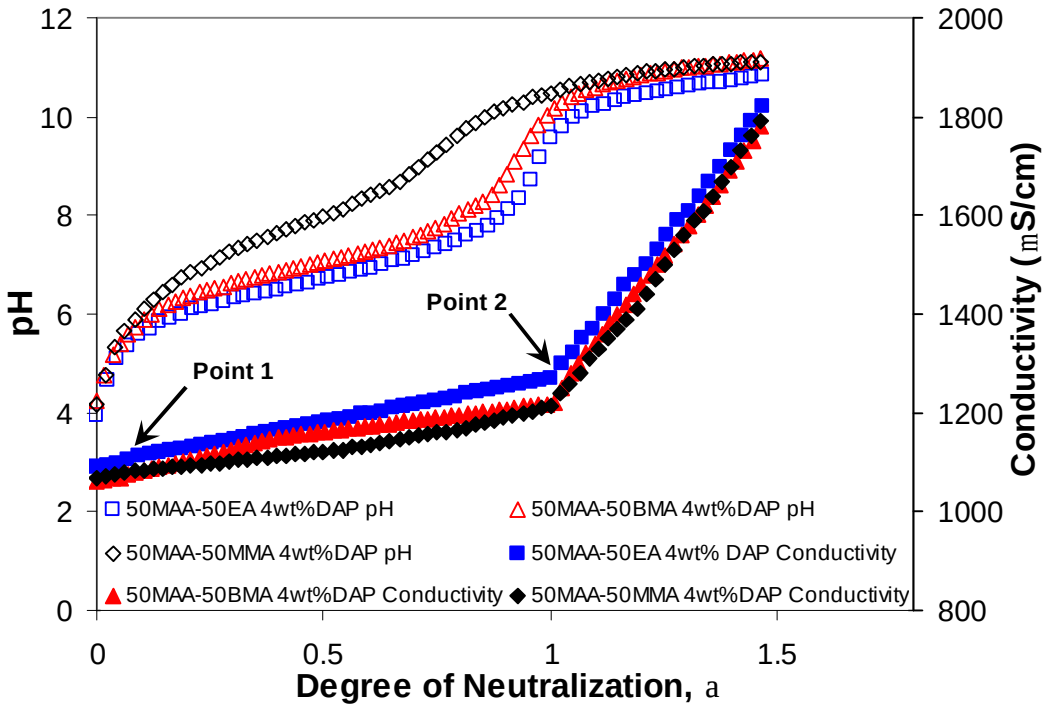

Figure 7.1 pH (open symbols) and conductivity curves (closed symbols) for 0.1 wt% (a) MAA-EA nanogels (□, ■), (b) MAA-BMA nanogels (△, ▲) and (c) MAA-MMA nanogels (◇, ◆) in 10 mM NaCl solution.

For the conductivity curves, two distinct equivalence points (Points 1 and 2) as indicated by the arrows can be observed. The first equivalence point (Point 1) corresponded to the sharp increase in pH at $\alpha \sim 0.1$, which is due to the strong acid-base neutralization of small amounts of sulfate (-SO_3H) groups introduced from the initiator. The second equivalence point (Point 2) at $\alpha = 1$ was due to the complete neutralization of MAA groups and beyond this point the conductivity increased progressively with the addition

of excess NaOH. The conductivity curves leveled off with an increase in glass transition temperature (T_g) (EA < BMA < MMA), that correlated to the reduction in particle mobility for polymers with higher T_g. The values of the conductivity over the course of neutralization were fairly identical showing that the H^+ ions from COOH in the nanogels possessed analogous diffusion velocity that was independent of cross-linked density suggesting that the nanogels possessed comparable size and molecular weight. Based on the amount of NaOH used to neutralize the COOH groups present in the nanogels, the actual mol% could be determined, where the actual mole ratio of MAA:EA, MAA:BMA, and MAA:MMA were 53:47, 52:48 and 48:52 respectively.

The potentiometric titration of polyelectrolyte solution can be treated as the negative logarithm of the apparent dissociation constant (pK_a) described by Henderson-Hasselbalch equation:

$$pK_a = pH + \log\left(\frac{1-a}{a}\right) \tag{7.2}$$

and pK_a can be obtained from the measured pH and α value and is the sum of two terms:

$$pK_a = pK_0 + 0.4343\frac{dG_{el}}{RTda} \tag{7.3}$$

where pK_0 is the intrinsic dissociation constant independent of α, R is the universal gas constant and T is the absolute temperature and G_{el} is the electrostatic Gibbs energy. G_{el} is not the free energy change of the neutralization process but the energy required to overcome the strong electrostatic force for extracting a proton from a charged polyion [Wang et al., 2005]. The pK_0 values were obtained by extrapolating the titration curves to $\alpha = 0$.

ΔG_{el} can be derived from graphical integration based on Equation 7.4:

$$\Delta G_{el} = 2.30RT\int_0^1 [pK_a - pK_0]da \quad (7.4)$$

where pK_α is the dissociation constant at any given α value and pK_0 is the intrinsic dissociation constant.

Figure 7.2 shows the dependence of pK_α on α for the titration of the three nanogels samples. The electrostatic Gibbs energy for deprotonating COOH groups of MAA segments was determined by integrating the area under the curve and subtracting the area under pK_0. The pK_α showed a progressive increment for all three nanogels. At low α, the hydrophobic interactions between the polymeric chains hindered the deprotonation of COOH groups. Therefore, highly ionized polymer chains are required to accumulate sufficient Coulombic repulsion to overcome the hydrophobic attraction between polymeric segments in order to swell the polymer particles. With increasing charge density on the nanogels, COOH groups on MAA segments were progressively deprotonated. Hence the nanogels began to swell due to the increase the osmotic pressure, which facilitated the deprotonation of COOH to COO^- groups. Since 50MAA-50MMA has the highest T_g among the three, the swelling ratio was the smallest, where the deprotonation of COOH to COO^- groups was restricted resulting in the large pK_α values. 50MAA-50BMA was more hydrophobic compared to 50MAA-50EA as BMA has an additional $–CH_2CH_2$ group compared to EA. The increase in hydrophobicity will hinder the deprotonation of COOH groups. With progressive protonation of the polymeric chains, sufficient electrostatic forces were needed to be generated to overcome the hydrophobic interactions resulting in the swelling of the nanogels that will promote and facilitate the further deprotonation of COOH groups.

The pK_0 and ΔG_{el} values for the three nanogels are summarized in Table 7.4, where the pK_0 was determined by extrapolating α to zero. The values of ΔG_{el} increased from 3.78 to 6.04 kJ/mol when T_g for the nanogels was increased. This indicated that more energy was needed to extract protons from COOH groups in high T_g nanogels (50MAA-50MMA). The dissociation of COOH groups present in MAA segments is dominated by the swelling ratio and hydrophobic interaction between polymeric chains instead of electrostatic attraction between H^+ and COO^-.

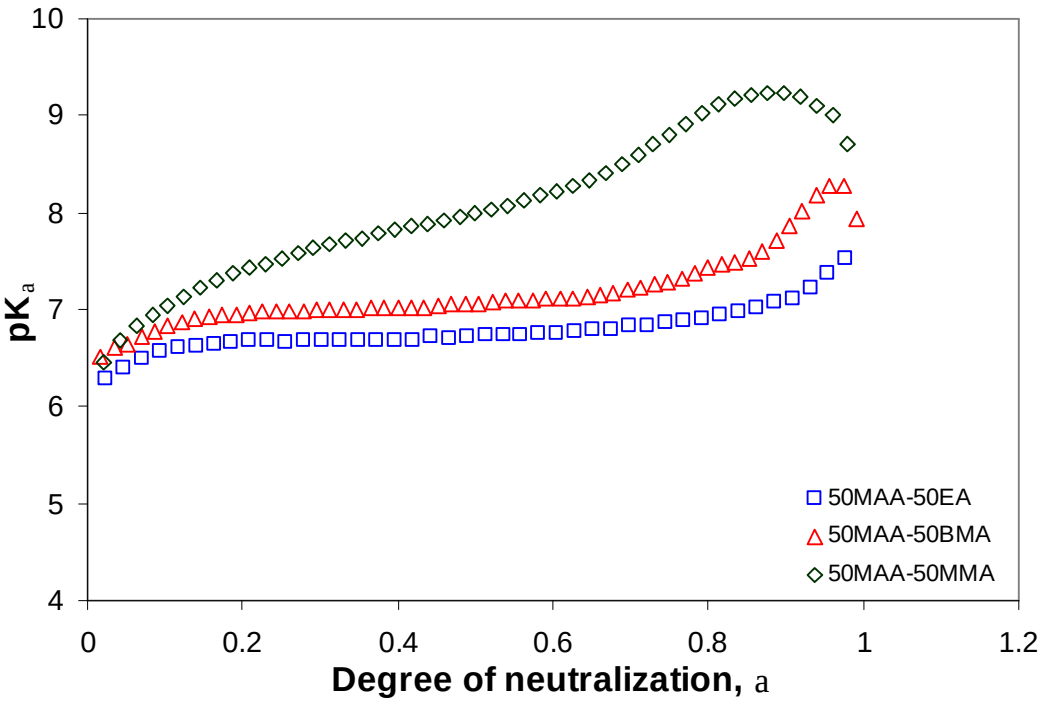

Figure 7.2 pK_α curves for 0.1 wt% (a) 50MAA-50EA nanogels (□), (b) 50MAA-50BMA nanogels (△) and (c) 50MAA-50MMA nanogels (◇) in 10 mM NaCl solution at 25 ^oC.

Table 7.4 Values of pK_0 and ΔG_{el} for the three nanogels in 10 mM NaCl solution at 25 ^oC.

Name of nanogel	**Tg (^oC)**	**pK_0**	**DG_{el} (kJ/mol)**
50MAA-50EA	67.8	6.08	3.78
50MAA-50BMA	83.0	6.53	4.17
50MAA-50MMA	153.6	5.97	6.04

Potentiometric titration (Figure 7.3) was carried out using 0.1 wt% 50MAA-50BMA at 10 and 25 ^oC in 10 mM NaCl solution. Similar to Figure 7.1, two transition points were observed. Point 1 corresponds to the acid-base titration of strong acid groups ($-SO_3H$) while Point 2 represents the end of neutralization of the COOH groups of MAA segments. However, in the case of 10 ^oC, the pH curve was higher than 25 ^oC indicating that deprotonation of COOH groups at 10 ^oC was more difficult. At 10 ^oC, the polymeric chains were less mobile and the ability to swell was lower thus restricting the accessibility of protons on COOH groups. This is illustrated in the pK_α curves shown in Figure 7.4, where the pK_α curve for 10 ^oC was higher than 25 ^oC.

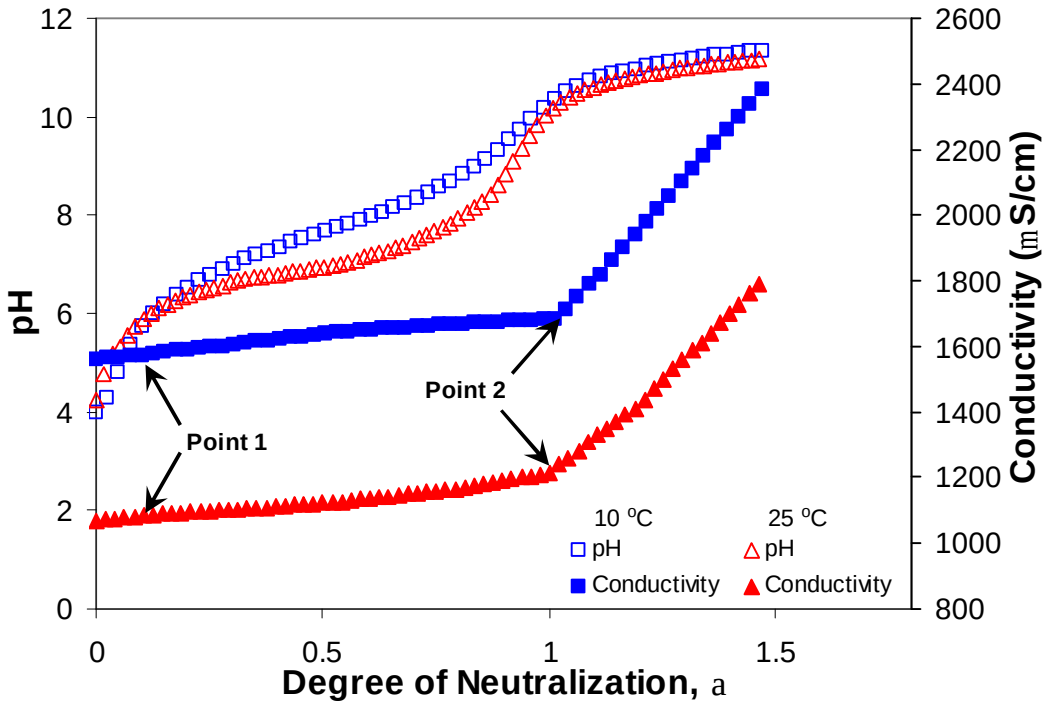

Figure 7.3 pH and conductivity curves for 0.1 wt% 50MAA-50BMA in 10 mM NaCl at (a) 10 °C (□, ■) and (b) 25 °C (△, ▲).

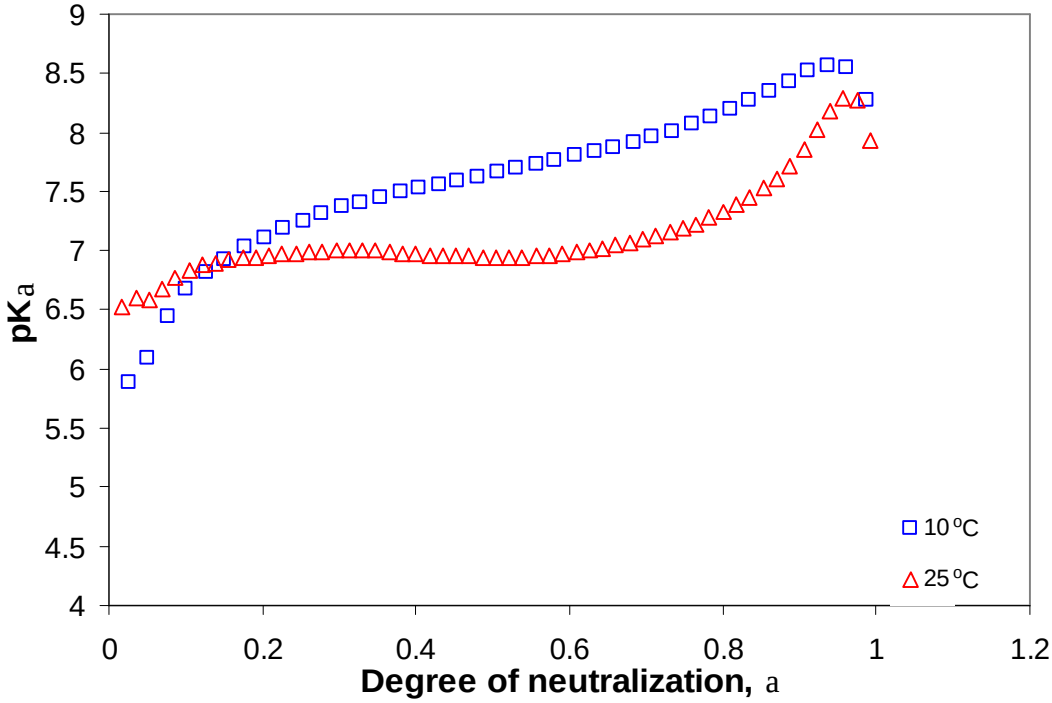

Figure 7.4 pK_α curves for 0.1 wt% 50MAA-50BMA in 10 mM NaCl at (a) 10 °C (□) and (b) 25 °C (△).

Table 7.5 Values of pK_0 and ΔG_{el} for 50MAA-50BMA in 10 mM NaCl solution at 10 and 25 ^oC.

Temperature (^oC)	**pK_0**	**DG_{el} (kJ/mol)**
10	5.5	4.50
25	6.53	4.17

By extrapolating pK_a curves and performing graphical integration using Equation 7.4, the pK_0 and ΔG_{el} values can be determined. The pK_0 and ΔG_{el} values for 50MAA-50BMA at 10 and 25 ^oC are summarized in Table 7.5. When the temperature was decreased from 25 to 10 ^oC, ΔG_{el} increased from 4.17 to 4.50 kJ/mol, which suggested that more energy was required to extract protons from 50MAA-50BMA at a lower temperature as the polymeric chains are less mobile, making the protons less accessible.

7.1.3 Particle size characterization

The particle sizes of 0.1 wt% pH-responsive 50MAA-50EA, 50MAA-50BMA and 50MAA-50MMA nanogels in 10 mM NaCl solution for α ranging from 0 to 1 are shown in Figure 7.5. In the unneutralized state (α = 0), 50MAA-50EA, 50MAA-50BMA and 50MAA-50MMA possessed R_h of ~42, ~58 and ~67 nm respectively. The difference in the particle size could be due to the different chain rigidity as MMA has a T_g of ~105 ^oC compared to ~30 ^oC for BMA and ~-24 ^oC for EA. Since the polymerization was carried out at 80 ^oC, only MMA possessed a T_g, greater than the polymerization temperature, which inhibits the chains during polymerization. The R_h displayed a continuous increase with increasing α from 0 to 1 as indicated in Figure 7.5. As dissociation of MAA groups

progressed, increasing charges within the nanogels induced electrostatic repulsions produced a swelling of the particles. The enhanced osmotic pressure exerted by counter-ions trapped inside the nanogels also contributed to the increase in R_h.

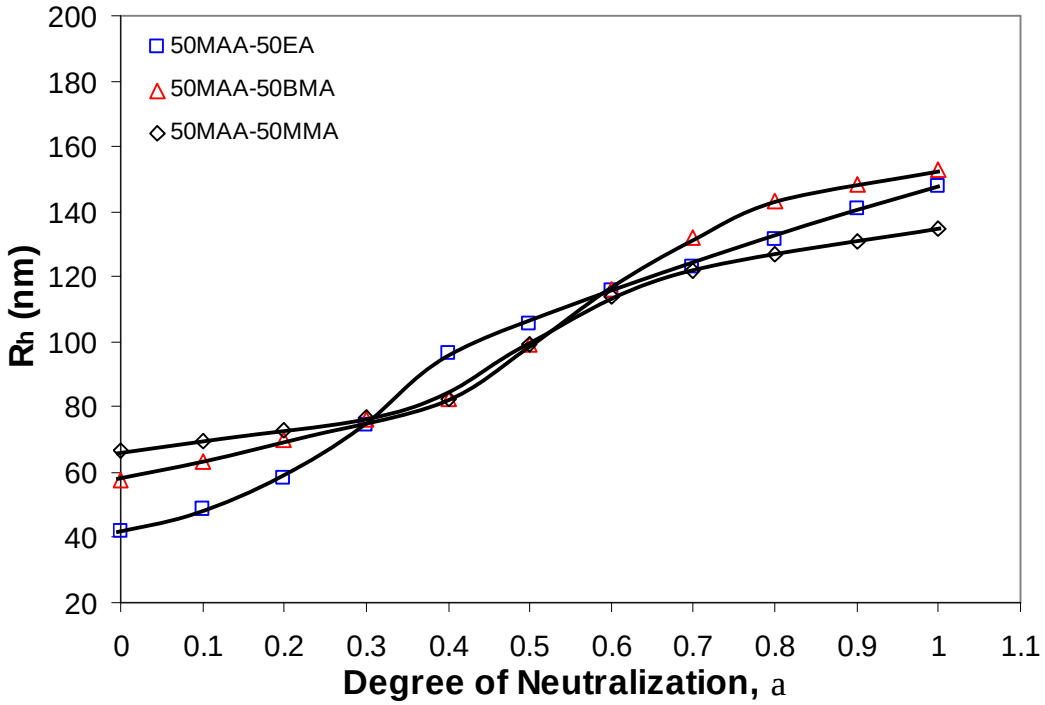

Figure 7.5 Dependence of hydrodynamic radius (R_h) on degree of neutralization (α) for 0.1 wt% (a) 50MAA-50EA (□), (b) 50MAA-50BMA (△) and (c) 50MAA-50MMA (◇) nanogels in 10 mM NaCl solution.

The swelling ratio (SR) as defined by Equation 7.5:

$$SR = \frac{R_h}{R_{h(a=0)}} \tag{7.5}$$

for the three nanogels were plotted in Figure 7.6, where R_h is the hydrodynamic radius at any α and $R_{h\,(\alpha=0)}$ is the hydrodynamic radius at $\alpha = 0$. The swelling ratio decreased with increase in T_g. For example at $\alpha = 1$, swelling ratio for 50MAA-50EA is ~3.52, ~2.64 for

50MAA-50BMA and ~2.03 for 50MAA-50MMA. With the increase in T_g, polymeric chain rigidity is increased, which limits the swelling capability of the nanogels.

The R_h values deviated more when α exceeded 0.3 for 50MAA-50EA and α exceeded 0.4 for 50MAA-50BMA and 50MAA-50MMA. The hydrophobic attraction between the EA blocks reduces the swelling of 50MAA-50EA at $\alpha \leq 0.3$, whereas the osmotic pressure caused by counter-ions attracted to the carboxylate groups will produce a sudden increase in R_h after $\alpha = 0.3$. Therefore, a transition region of nanogels caused by the competition of these two types of interactions was observed at $\alpha = 0.3$. At $\alpha \leq 0.3$, the increment in R_h was smaller due to the osmotic pressure exerted by counter-ions and the electrostatic repulsion between carboxylate groups are insufficient in overcoming the strong hydrophobic attraction between EA blocks. When α was increased beyond 0.3, the osmotic pressure could overcome the hydrophobic attraction, which caused the R_h to increase rapidly. Hydrophobic attraction between BMA blocks and MMA blocks and higher chain rigidity of BMA and MMA prevents the swelling of 50MAA-50BMA and 50MAA-50MMA respectively below $\alpha = 0.4$ and beyond this point, the osmotic pressure exceeded the hydrophobic attraction and caused the nanogels to increase rapidly. There was a delay in the transition point as hydrophobic interaction of BMA required a larger osmotic pressure to induce the observed swelling. The solubility of BMA and EA is 0.6 g/L and 1.5 g/L in 20 ^oC water respectively. The increase in hydrophobicity enhanced the hydrophobic attraction between BMA blocks and more COOH groups must be ionized before the osmotic pressure can overcome this attractive force. Although the hydrophobicity of MMA and EA are more or less similar (MMA has a solubility of 1.6 g/L in 20 ^oC water), the transition point for 50MAA-50MMA was slightly delayed due to the more rigid MMA chains since the T_g of MMA blocks is higher. The osmotic pressure

must overcome both the chain rigidity and hydrophobic attraction before swelling of the nanogel occurs.

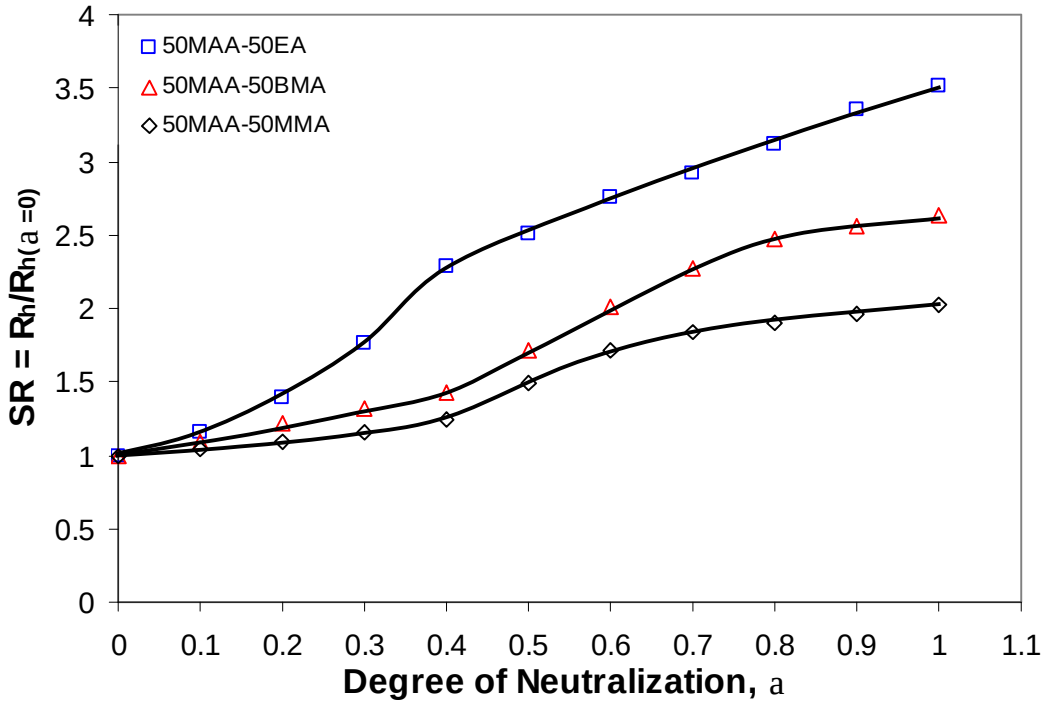

Figure 7.6 Swelling ratio (SR) for (a) 50MAA-50EA (□), (b) 50MAA-50BMA (△) and (c) 50MAA-50MMA (◇) nanogels in 10 mM NaCl solution.

7.1.4 z-potential studies

The ζ-potential of 0.1 wt% pH-responsive 50MAA-50EA, 50MAA-50BMA and 50MAA-50MMA nanogels in 10 mM NaCl solution is shown in Figure 7.7. The ζ-potential generally became more negative with increasing α before becoming less negative after $\alpha = 0.3$ for 50MAA-50EA and $\alpha = 0.4$ for both 50MAA-50BMA and 50MAA-50MMA. The ζ-potential becomes more negative with increasing α as more COOH are ionized to COO^- groups, which increased the surface charge of the nanogels.

After the transition point at $\alpha = 0.3$ for 50MAA-50EA and $\alpha = 0.4$ for both 50MAA-50BMA and 50MAA-50MMA, ζ-potential became less negative due to the increasing size of nanogels, which reduced the mobility of nanogels and correspondingly the ζ-potential.

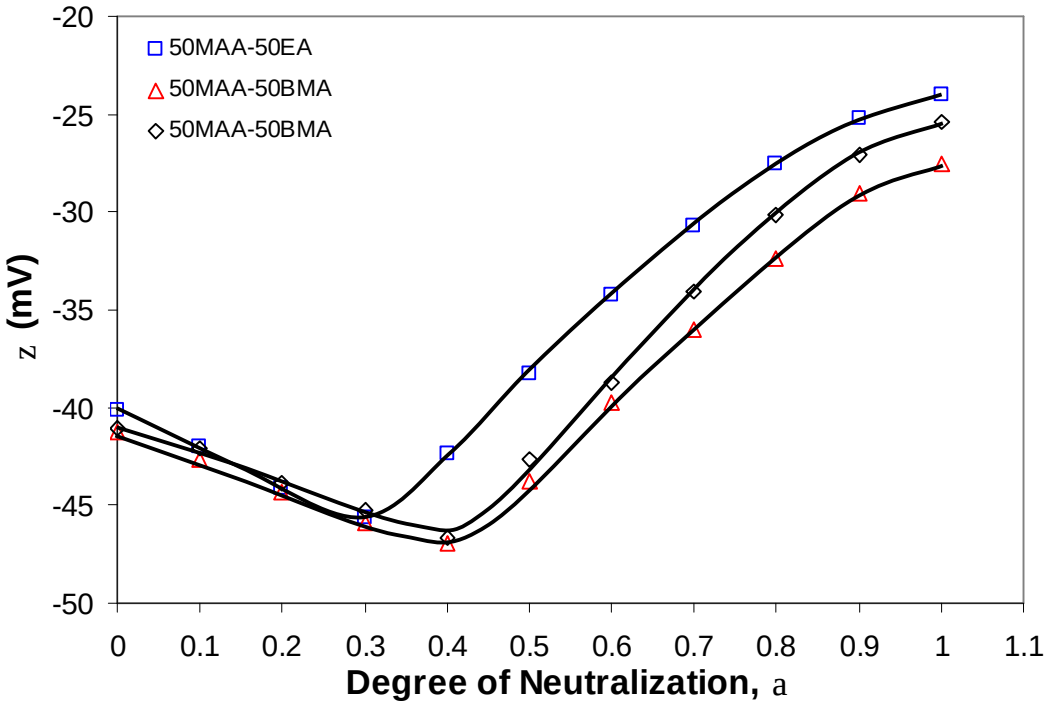

Figure 7.7 Dependence of ζ-potential on degree of neutralization (α) for 0.1 wt% (a) 50MAA-50EA (□), (b) 50MAA-50BMA (△) and (c) 50MAA-50MMA (◇) nanogels in 10 mM NaCl.

7.1.5 Molecular weight analysis

Static light scattering were conducted to determine the molecular weight (M_w) and second virial coefficient (A_2) for the three nanogels at $\alpha = 1$. The Zimm plot (based on Equation 2.28) for 50MAA-50EA, 50MAA-50BMA and 50MAA-50MMA is shown in

Figure 7.8 to 7.10 respectively. The three nanogels have M_w and A_2 of 3.64 x 10^6, 4.08 x 10^6 and 3.80 x 10^6 g/mol and 3.87 x 10^{-5}, 3.45 x 10^{-5} and 3.90 x 10^{-5} cm^3mol/g^2 respectively. The M_w for the three nanogels were identical, which suggested that the seeded emulsion polymerization process was well-controlled, where an in-situ seed product with approximately similar number of monomer units (hence similar M_w) were cross-linked together to produce a compact particle consisting of several polymer chains. All three nanogels showed a positive A_2 at $\alpha = 1$, which indicated the particle-solvent interaction was favorable due to the dissociated COOH groups. However, 50MAA-50BMA possessed the lowest A_2 as BMA was the most hydrophobic monomer, which was less soluble in water. Both 50MAA-50EA and 50MAA-50MMA possessed similar A_2 as the hydrophobicity of EA and MMA were the same.

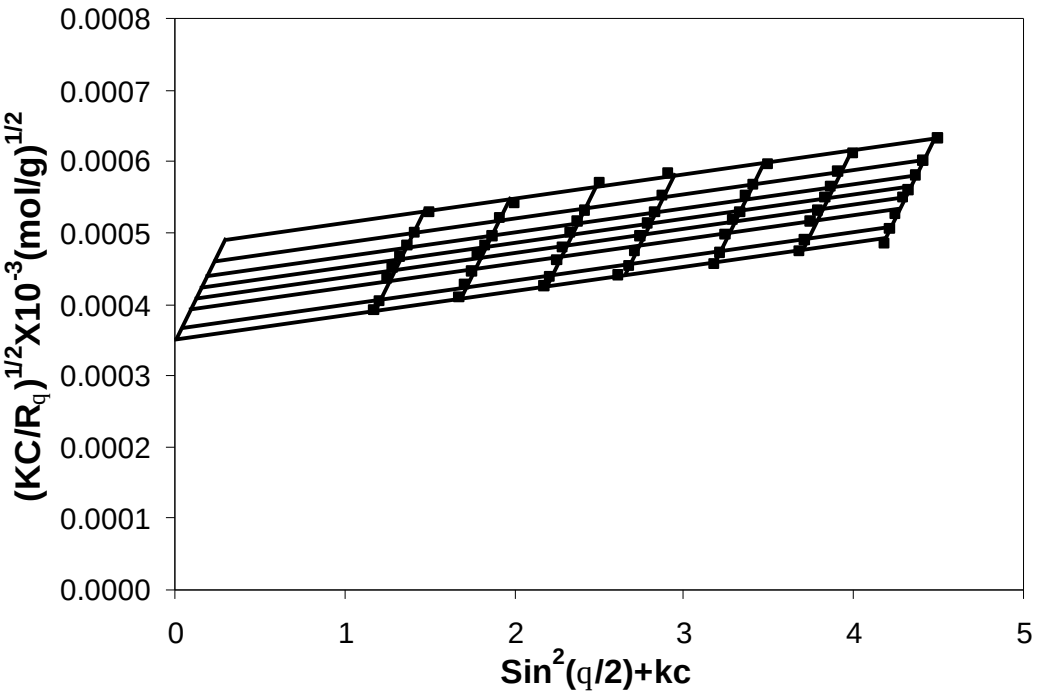

Figure 7.8 Zimm plot for 50MAA-50EA at $\alpha = 1$ where the nanogel concentration is changed from 0.2 to 0.8 mg/ml.

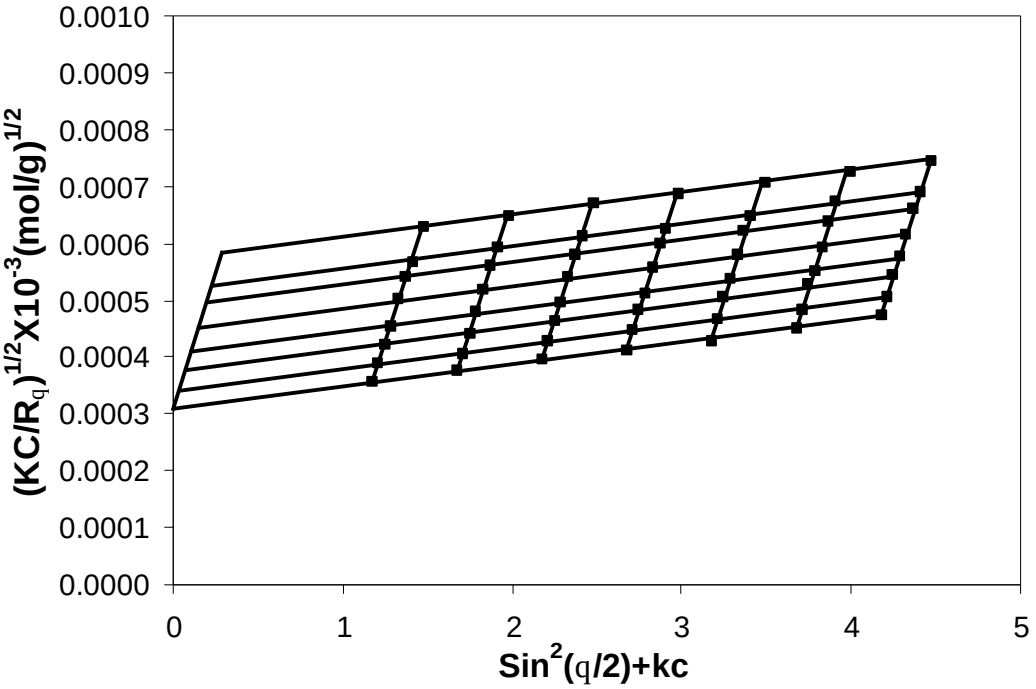

Figure 7.9 Zimm plot for 50MAA-50BMA at $\alpha = 1$ where the nanogel concentration is changed from 0.2 to 0.8 mg/ml.

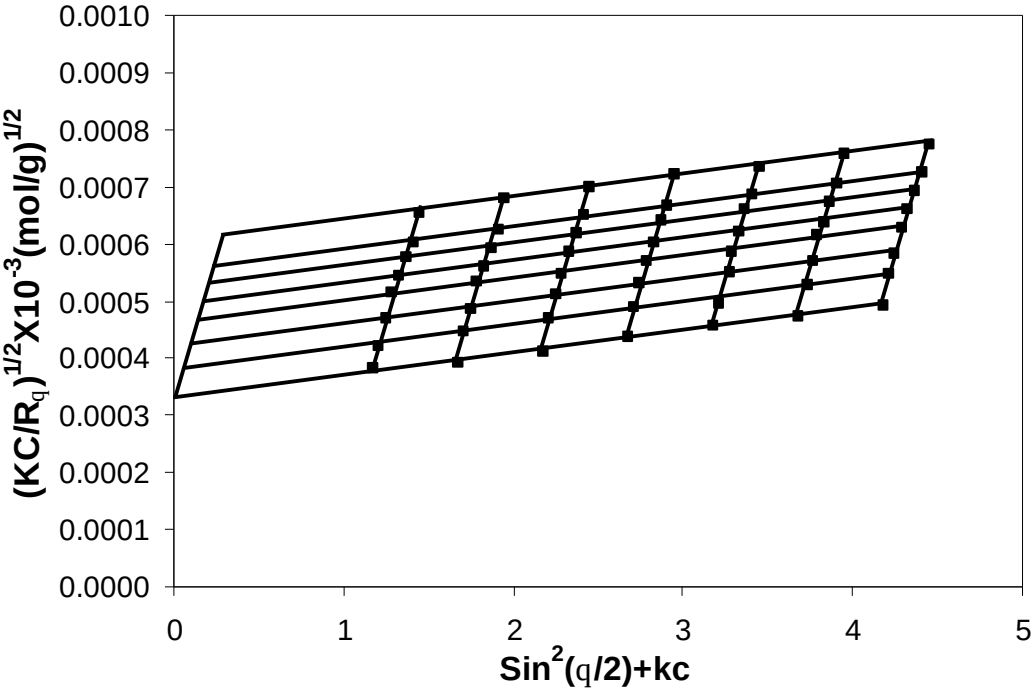

Figure 7.10 Zimm plot for 50MAA-50MMA at $\alpha = 1$ where the nanogel concentration is changed from 0.2 to 0.8 mg/ml.

7.2 Drug interactions with nanogels

The differential enthalpy curves for titrating 0.6 M PrHy into partially neutralized ($\alpha = 0.3$, $\alpha = 0.5$ and $\alpha = 1$) 0.1 wt% 50MAA-50EA, 50MAA-50BMA and 50MAA-50MMA in 10 mM NaCl is shown in Figures 7.11 to 7.13 respectively. From Figure 7.11, the titration results showed no electrostatic binding between the negatively charged COO^- groups and positively charged PrHy even when the pH was lowered from pH 9 ($\alpha = 1$) to pH 6.9 ($\alpha = 0.5$) or pH 6.3 ($\alpha = 0.3$), which significantly lowered the concentration of unprotonated PrHy. This is probably due to the steric hindrance from the two ethyl groups around N^+. The two ethyl groups hindered the accessibility of positively charged N^+ to negatively charged COO^- ions. From Figure 7.12, when the pH was lowered from pH 10.2 ($\alpha = 1$) to pH 7.1 ($\alpha = 0.5$) or pH 6.6 ($\alpha = 0.3$), the enthalpy remained almost constant even when the amount of unprotonated PrHy was reduced. This suggests that there is no electrostatic binding between COO^- and PrHy. Similarly, in Figure 7.13, when the pH was lowered from pH 10.5 ($\alpha = 1$) to pH 8 ($\alpha = 0.5$) or pH 7.2 ($\alpha = 0.3$), the enthalpy remained the same. The differences in enthalpy at similar α for the three nanogels were due to the different state of protonation of PrHy. For example, at $\alpha = 1$, the pH for 50MAA-50EA, 50MAA-50BMA and 50MAA-50MMA was 9, 10.2 and 10.5 respectively. At a higher pH, more PrHy will be in the unprotonated state therefore a higher enthalpy was observed due to the stronger hydrophobic interactions.

The concentration at which the enthalpy approached zero (~20 mM in Figure 7.11, ~25 mM in Figure 7.12 and ~15 mM in Figure 7.13) was almost identical for all α, suggesting that the binding of PrHy onto the nanogels is not related to electrostatic attraction. When the interaction is electrostatic, the concentration at which the enthalpy

goes to zero will be different due to the differences in number of binding sites on negatively charged MAA segments. The observed variations in the concentration of PrHy needed to saturate the nanogels were related to the hydrophobicity and size of nanogels. Since BMA is more hydrophobic than EA, more PrHy molecules can be partitioned to 50MAA-50BMA, thus a higher concentration is needed to saturate the nanogels. In the case of MMA and EA (almost the same hydrophobicity), the difference could be due to the difference in the size of the nanogel. No hydrogen bonding occurred between PrHy and the nanogels as the enthalpy recorded in Figures 7.11 to 7.13 remained essentially constant when α was reduced from 1 to 0.3. Through the reduction in α, more COOH groups are present and hydrogen bonding should be stronger but the result in Figures 7.9 to 7.11 did not show this trend. The ethyl groups surrounding the N^+ induce a steric hindrance that inhibited formation of hydrogen bonding.

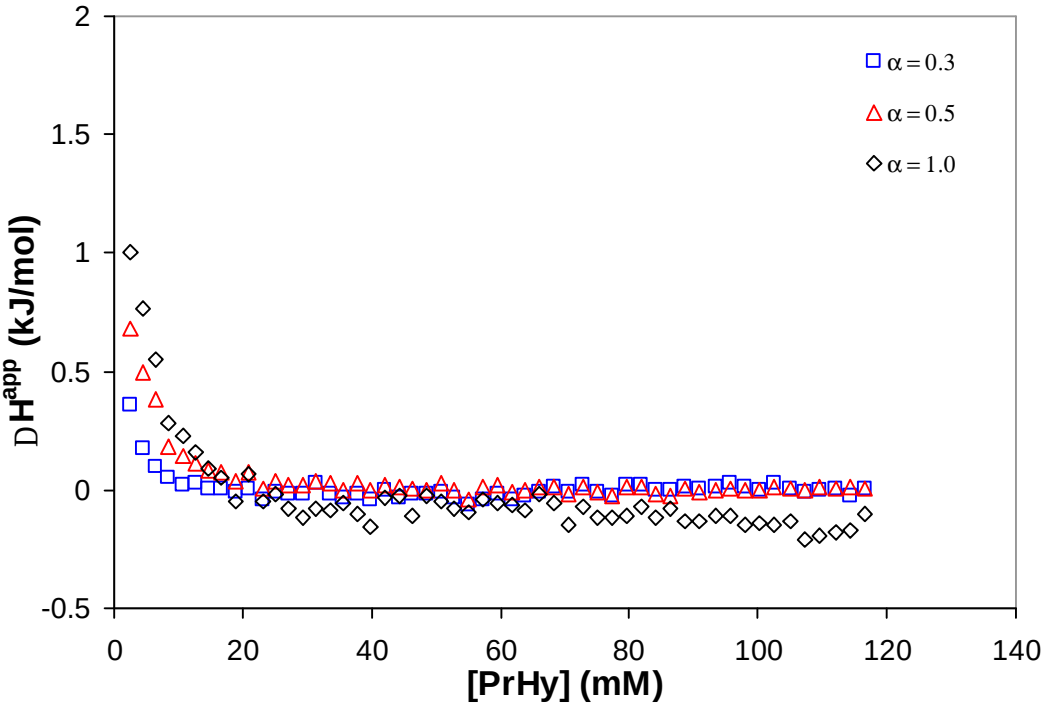

Figure 7.11 Differential enthalpy curves for titrating 0.6 M PrHy into 0.1 wt% 50MAA-50EA at varying α in 10 mM NaCl solution at 25 °C.

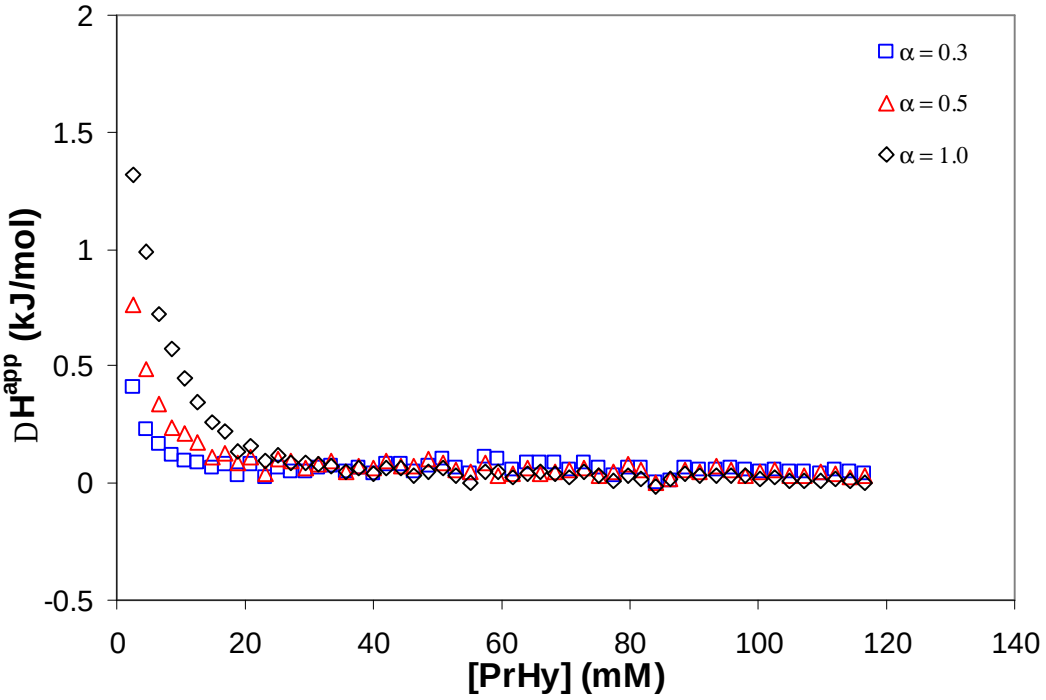

Figure 7.12 Differential enthalpy curves for titrating 0.6 M PrHy into 0.1 wt% 50MAA-50BMA at varying α in 10 mM NaCl solution at 25 °C.

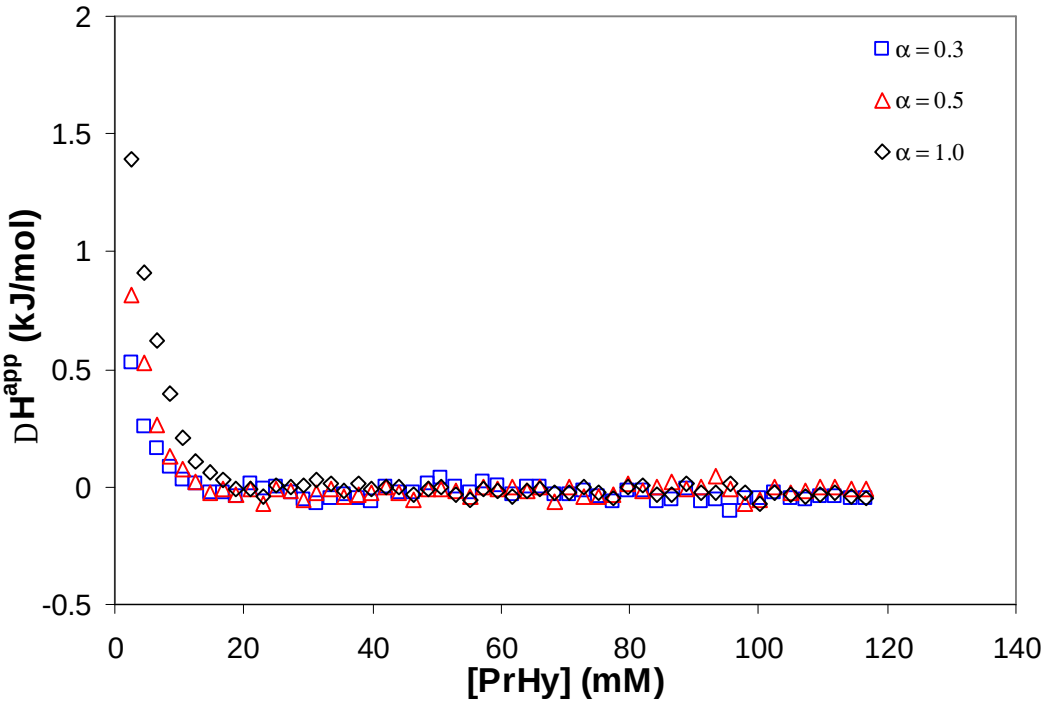

Figure 7.13 Differential enthalpy curves for titrating 0.6 M PrHy into 0.1 wt% 50MAA-50MMA at varying α in 10 mM NaCl solution at 25 ^{o}C.

The differential enthalpy curves for titrating 0.6 M PrHy solution into fully neutralized (α = 1) 0.1 wt% 50MAA-50EA, 50MAA-50BMA and 50MAA-50MMA in 10 mM NaCl solution at varying temperature are shown in Figures 7.14 to7.16. As the temperature was increased from 25 to 50 ^{o}C, ΔH increased, which was attributed to the enthalpy changes associated with an increase in the hydrophobic environment. This in turn resulted in a stronger hydrophobic interaction between PrHy and nanogels. The difference in concentration between the interior and exterior of the nanogels will drive the drugs into the nanogels, where the drug molecules will interact hydrophobically with the polymeric chains.

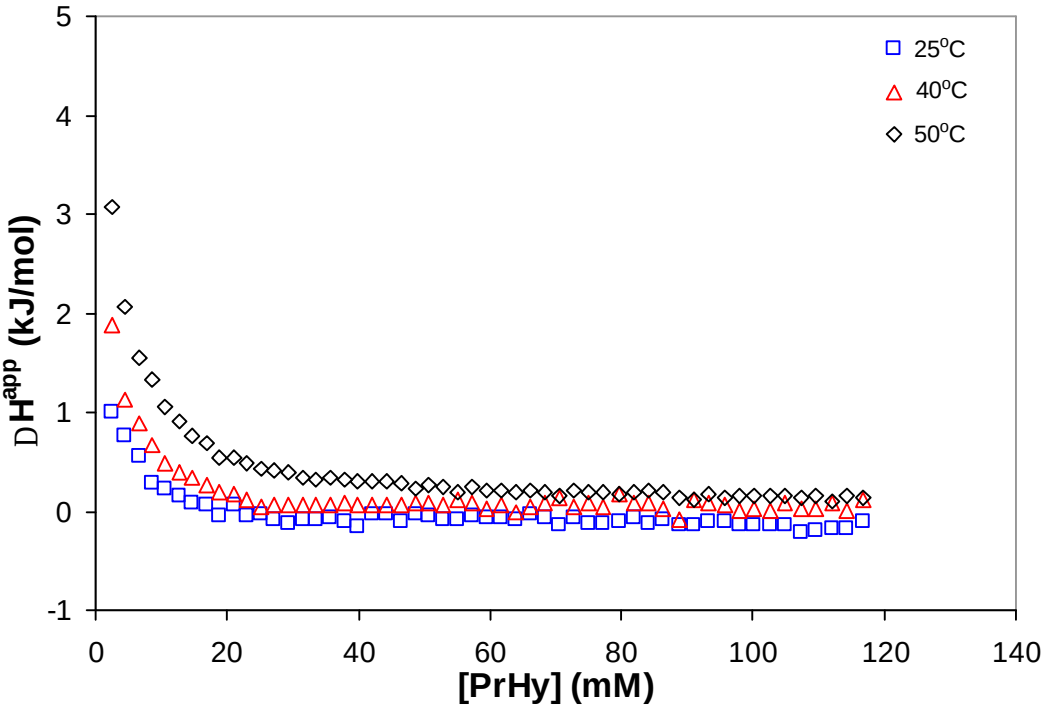

Figure 7.14 Differential enthalpy curves for titrating 0.6 M PrHy into 0.1 wt% 50MAA-50EA in 10 mM NaCl solution at varying temperature.

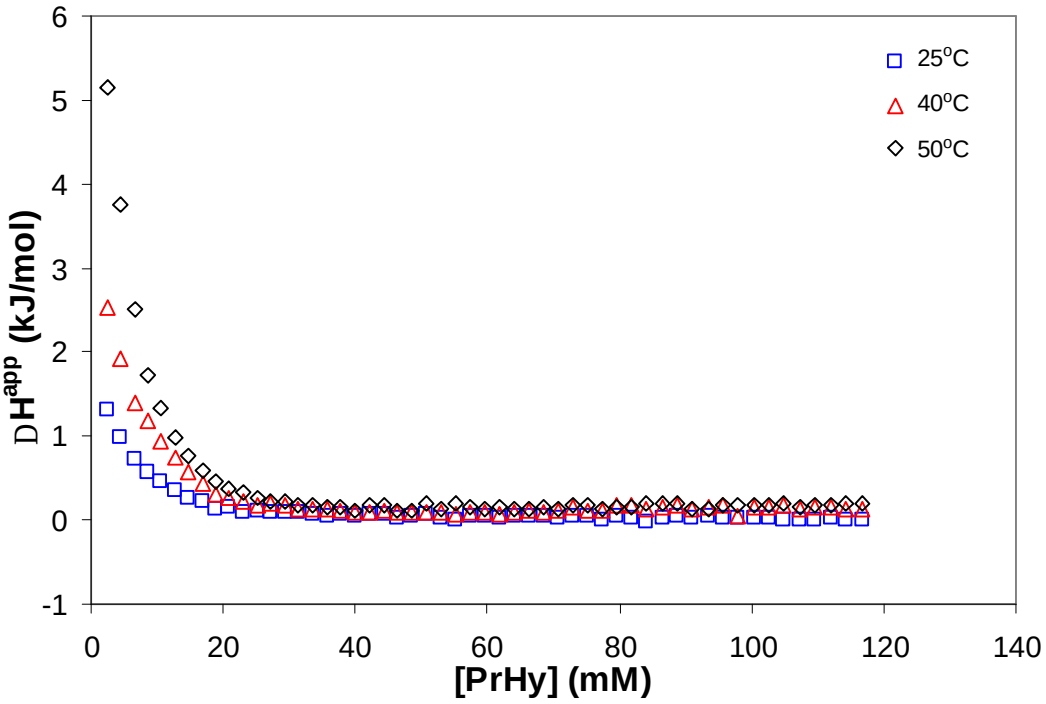

Figure 7.15 Differential enthalpy curves for titrating 0.6 M PrHy into 0.1 wt% 50MAA-50BMA in 10 mM NaCl solution at varying temperature.

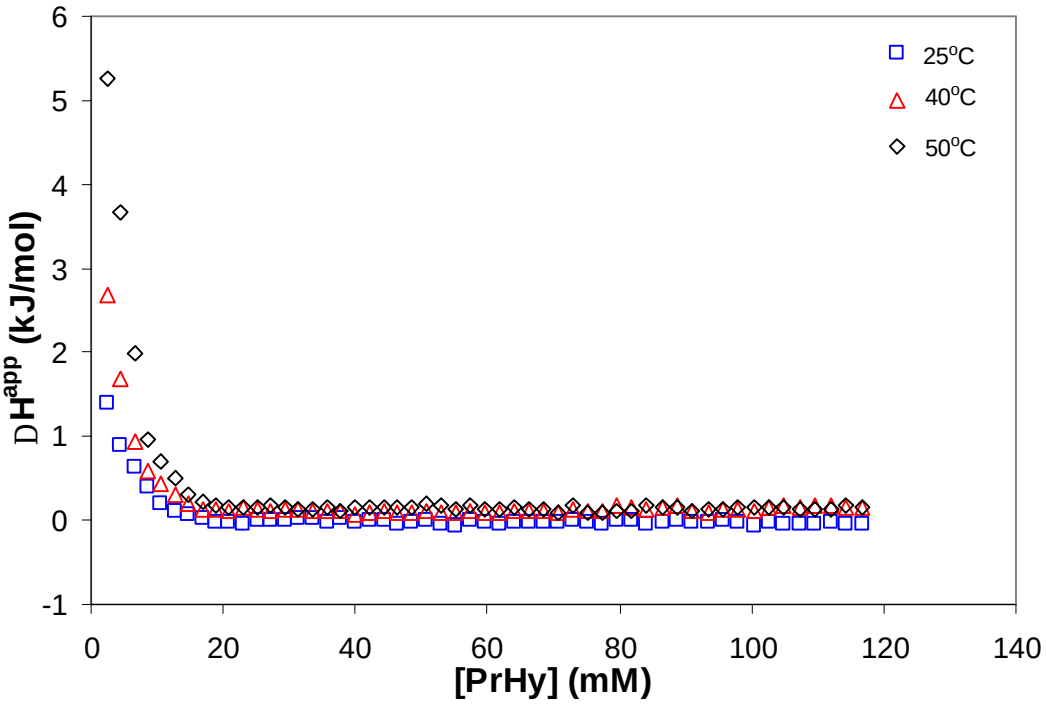

Figure 7.16 Differential enthalpy curves for titrating 0.6 M PrHy into 0.1 wt% 50MAA-50MMA in 10 mM NaCl solution at varying temperature.

7.3 Variation in particle sizes and z-potential with drug concentration

The effect of varying drug concentration on particle sizes for 50MAA-50EA, 50MAA-50BMA and 50MAA-50MMA is shown in Figure 7.18. The hydrodynamic radius (R_h) at varying drug concentration was normalized against the hydrodynamic radius of each nanogel in the absence of drugs at $\alpha = 1$ ($R_{h\,(c=0)}$).

The relationship between the relaxation rates of Γ and q^2 for 0.1 wt% 50MAA-50EA, 50MAA-50BMA and 50MAA-50MMA in 10 mM NaCl and 0.04 M PrHy solution are shown in Figure 7.17a to 7.17c respectively. All the decay functions decreased with increasing scattering angles. The relaxation rates exhibited q^2 dependence confirming that the decay corresponded to translational diffusion. The translational diffusion coefficients were obtained from the slope of Figure 7.17a to 7.17c and based on Stokes-Einstein relationship, where the R_h of the particle was calculated.

The drug loading capability for 50MAA-50EA, 50MAA-50BMA and 50MAA-50MMA was compared at a drug content of 0.018 M and shown in Table 7.6. There was an increase in loaded drug when BMA was used in the polymerization and a smaller amount was observed for nanogels with MMA segments. The higher hydrophobicity of BMA (solubility of BMA is 0.6 g/L in 20 ^{o}C water) enhanced the partitioning of more PrHy molecules resulting in a higher drug loading. There is a reduction in drug loading for 50MAA-50MMA nanogels as the swelling ratio is the smallest yielding a lower porosity, which increases the diffusion barrier. For future drug release studies, the same drug loading ratio will be used.

Table 7.6 Results of drug loading capability for 50MAA-50EA, 50MAA-50BMA and 50MAA-50MMA in 10 mM NaCl.

Name of nanogel	Loading (g of drug/g of polymer)
50MAA 50EA	2.44
50MAA 50BMA	2.53
50MAA 50MMA	2.30

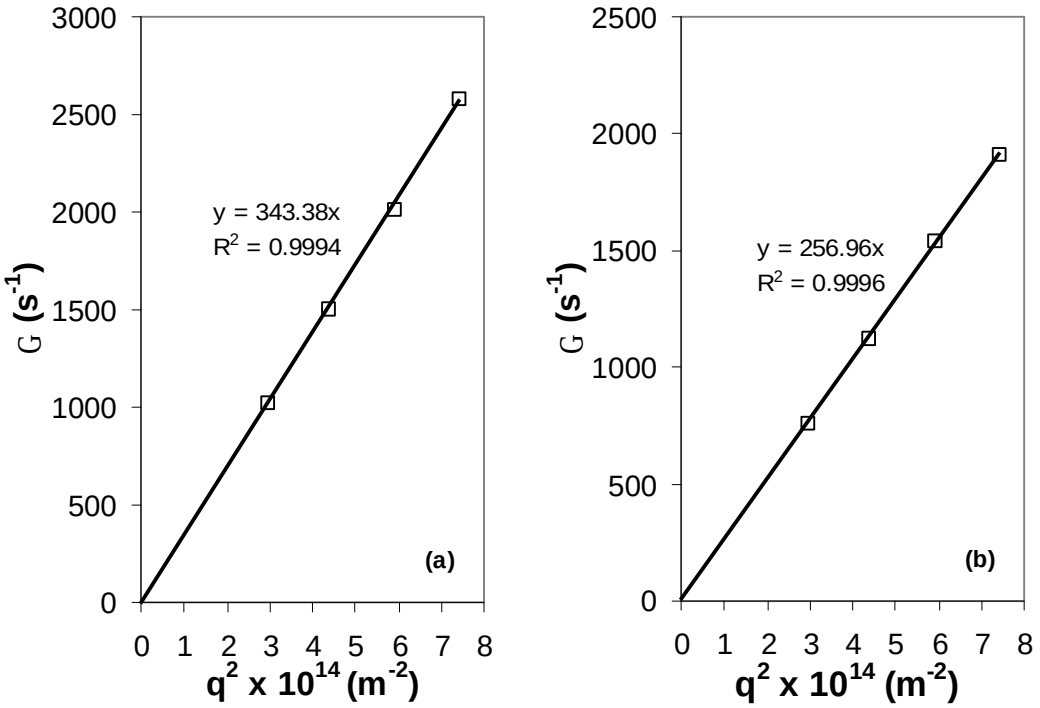

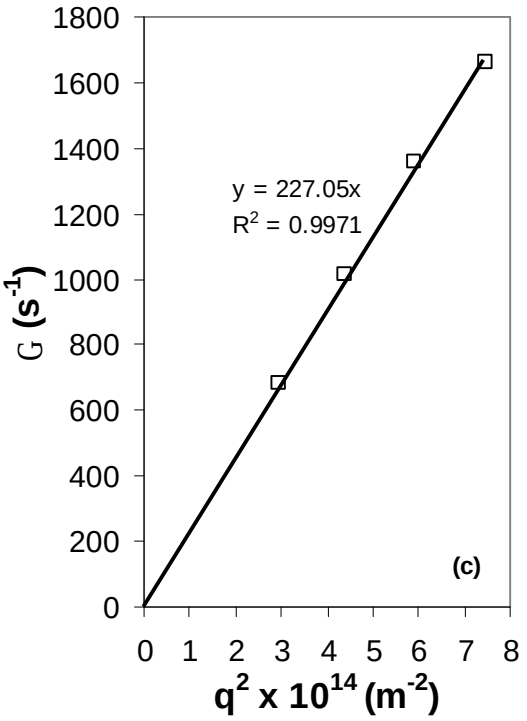

Figure 7.17 The relationship of Γ and q^2 for 0.1 wt% (a) 50MAA-50EA, (b) 50MAA-50BMA and (c) 50MAA-50MMA in 10 mM NaCl and 0.04 M PrHy solution.

Based on Figure 7.18, the particle sizes decreased with increasing drug concentration. As more drugs are incorporated to the nanogels, the resultant shielding effect on the charged groups present in the nanogels will increase. This shielding will result in a reduction of the internal charge repulsion between ionized MAA groups, and there will also be a concomitant reduction in the polymer-solvent interactions as the overall effect of drug loading produced a less polar environment within the nanogels due to the hydrophobicity of PrHy, which produced a more compact nanogel structure. Similar trends have been observed by Lopez and co-workers [Lopez et al., 2005] and Bromberg [Bromberg, 1998]. As shown in Figure 7.18, 50MAA-50BMA has the lowest ratio ($R_h/R_{h\,(c\,=\,0)}$) as the drug loading was the highest. With more PrHy loaded to the nanogels, the reduction of

the internal charge repulsion will be lowest and the hydrophobic characteristics within the nanogels will be greatly increased, resulting in a more compact nanogel structure. 50MAA-50MMA has the lowest swelling ratio that corresponded to the lowest porosity among the three nanogels, resulting in the smallest amounts of PrHy loaded, and the lowest reduction in particle size. The slope for 50MAA-50BMA (indicated by (a) in Figure 7.18) was the steepest, compared to 50MAA-50EA (indicated by (b) in Figure 7.18), and 50MAA-50MMA (indicated by (c) in Figure 7.18), as the gradient of the slope is a function of drug loading capability. A higher loading capability will result in a more hydrophobic nanogel, which induced a more significant reduction in the particle size.

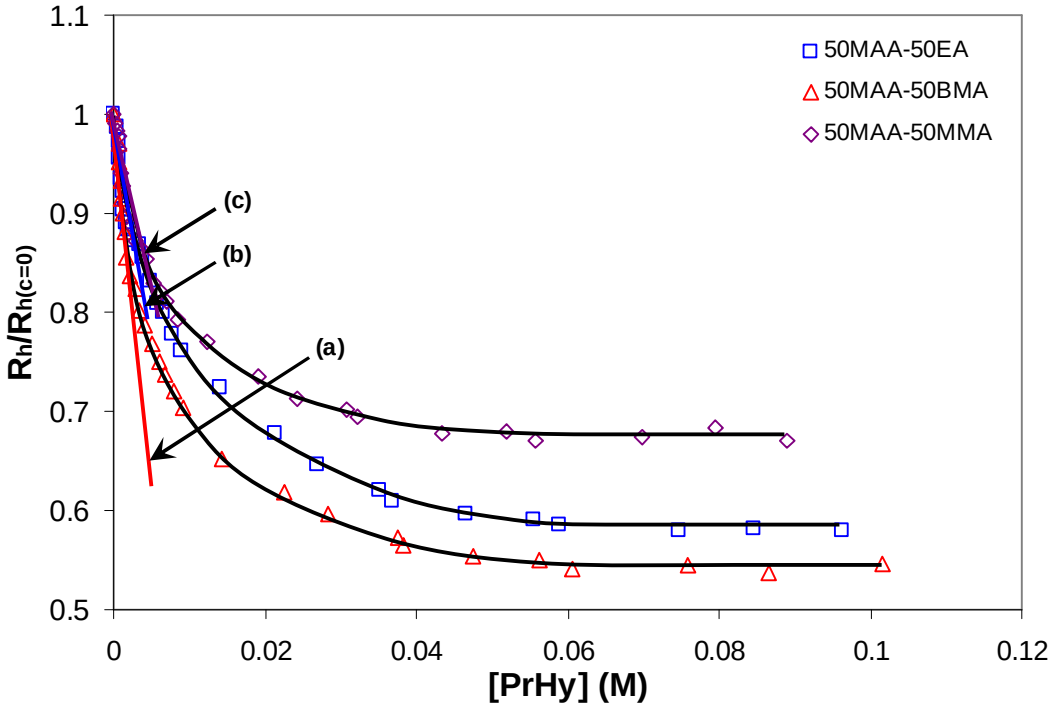

Figure 7.18 Dependence of the ratio of hydrodynamic radius with drugs (R_h) normalized with hydrodynamics radius without drug at $\alpha = 1$ ($R_{h\,(c=0)}$) on [PrHy] for 50MAA-50EA, 50MAA-50BMA and 50MAA-50MMA in 10 mM NaCl solution.

The ζ-potential became more negative with increasing concentration of loaded PrHy as shown in Figure 7.19. As the particle size became smaller, the mobility and hence the ζ-potential of the nanogels increased.

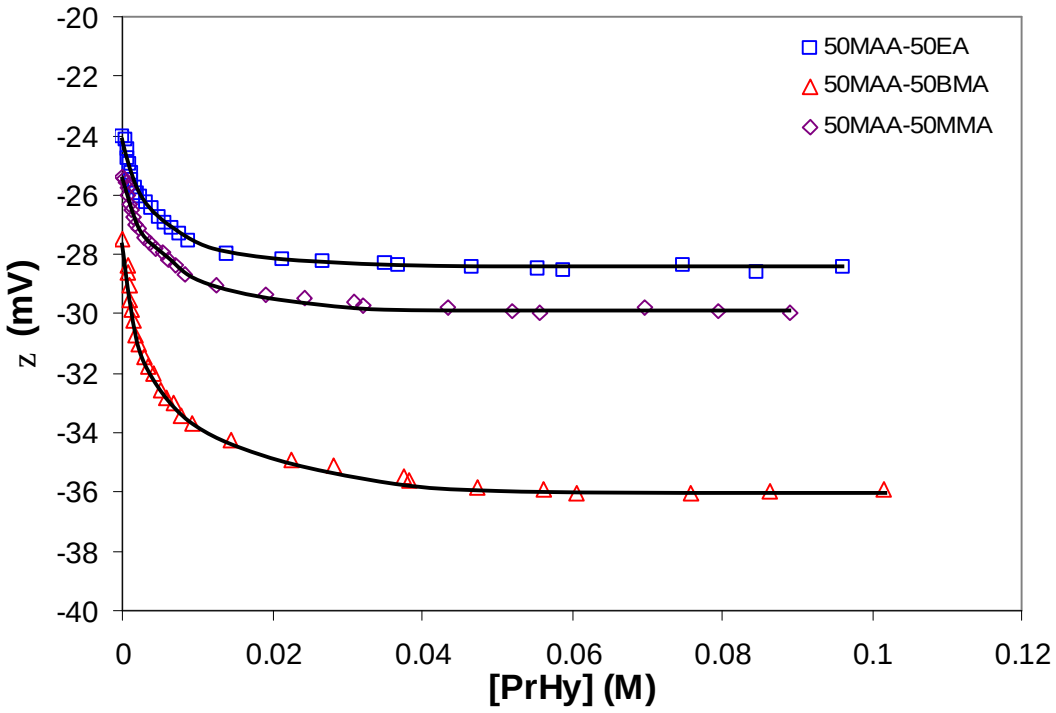

Figure 7.19 Dependence on the ζ-potential on [PrHy] for 50MAA-50EA, 50MAA-50BMA and 50MAA-50MMA in 10 mM NaCl solution.

7.4 Effect of varying parameters on the release kinetics of PrHy

7.4.1 Varying pH

In-vitro release studies were performed at varying pHs, namely at pH of 5, 6, 7.4 and 8 using 0.1 wt% 50MAA-50EA loaded with 2.44 g of drug/g of polymer, 0.1 wt% 50MAA-50BMA loaded with 2.53 g of drug/g of polymer and 0.1 wt% 50MAA-50MMA loaded with 2.30 g of drug/g of polymer in 100-millilitre 10 mM NaCl solution at 37 ^{o}C. The release profiles are shown in Figures 7.20 to 7.22 respectively.

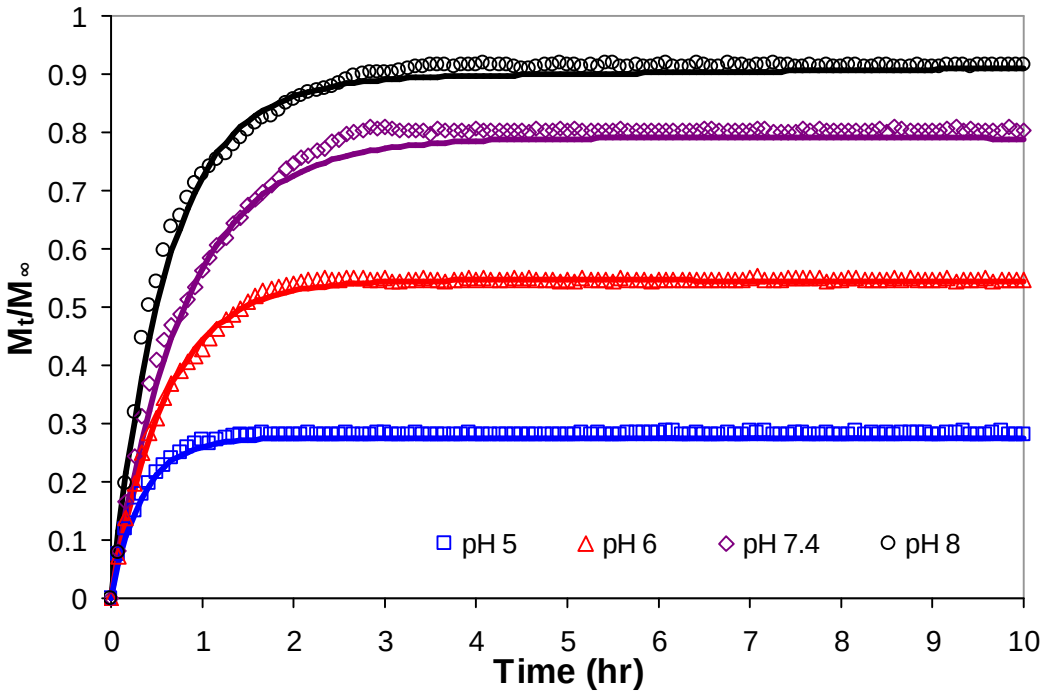

Figure 7.20 Release profile for 0.1 wt% 50MAA-50EA in 100-millilitre 10 mM NaCl solution at varying pH (a) pH 5 (□), (b) pH 6 (△), (c) pH 7.4 (◇) and (d) pH 8 (○) and theoretical fit of the Berens and Hopfenberg mathematical model taking into account drug diffusion and chain relaxation (solid lines).

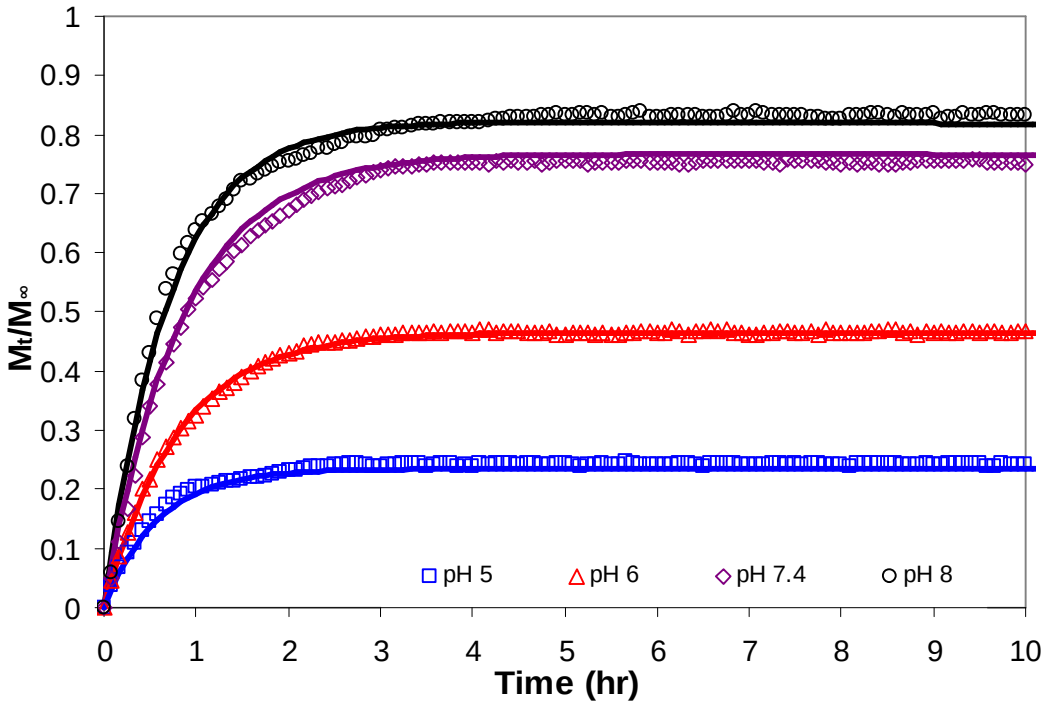

Figure 7.21 Release profile for 0.1 wt% 50MAA-50BMA in 100-millilitre 10 mM NaCl solution at varying pH (a) pH 5 (□), (b) pH 6 (△), (c) pH 7.4 (◇) and (d) pH 8 (○) and theoretical fit of the Berens and Hopfenberg mathematical model taking into account drug diffusion and chain relaxation (solid lines).

From Figures 7.20 to 7.22, all three nanogels have a higher release and longer time to reach steady state at high pH. For example, the percentage of PrHy released at pH 8 using 50MAA-50EA was ~90% compared to ~30% at pH 5. The degree of neutralization (α) was 0.9 at pH 8 and 0.0 at pH 5, and the difference in the amounts of PrHy released was due to the different degrees of neutralization of COOH groups. At low pH, the nanogels possessed a compact structure and a lower porosity, which resulted in a lower release of drug due to the larger diffusion barrier. However, at high pH, the nanogels were swollen and possessed a higher porosity, which enhanced the release of PrHy due to the reduction in the diffusion resistance, which is illustrated in Figure 7.23. At pH 5,

the time to reach equilibrium is ~1.5 hours while for pH 8 the time required is ~4 hours. At pH 8, the COOH groups will dissociate, thereby increasing the osmotic pressure inside the nanogels resulting in a higher swelling. Thus, more drugs will be released therefore requiring a longer time to reach equilibrium. Using P(MAA-co-MAA) spheres [Huang et al., 2000], polyacrylamide-g-guar gum nanogel [Soppimath et al., 2001], and PAA-g-EG hydrogels [Foss et al., 2004] also showed that at higher pH, the fractional release was higher.

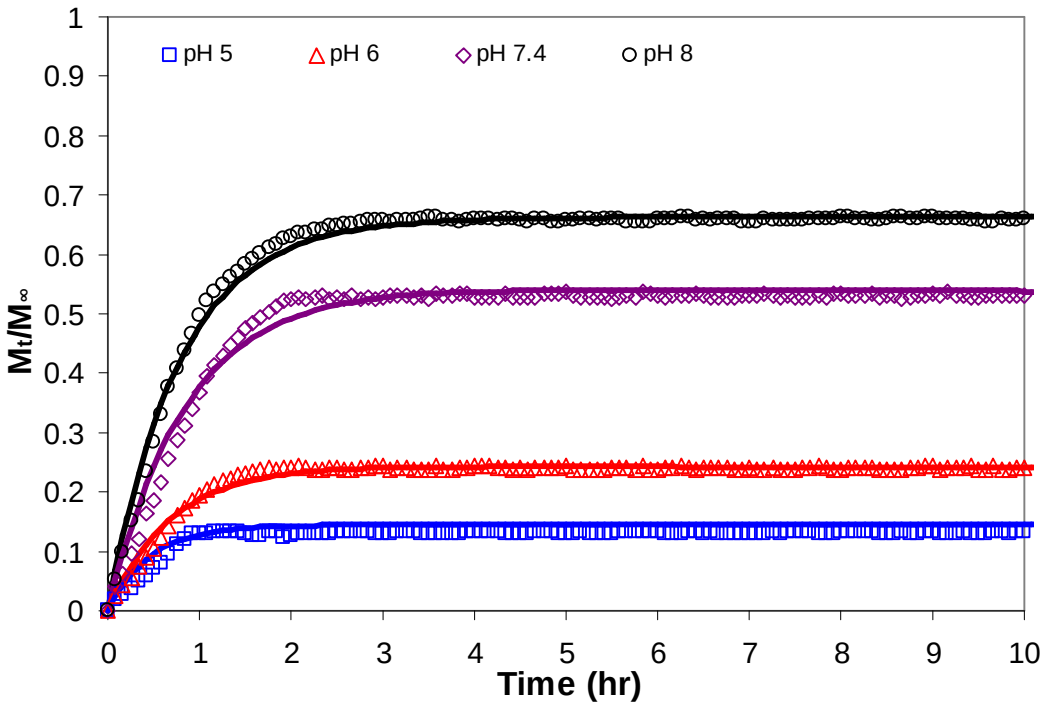

Figure 7.22 Release profile for 0.1 wt% 50MAA-50MMA in 100-millilitre 10 mM NaCl solution at varying pH (a) pH 5 (□), (b) pH 6 (△), (c) pH 7.4 (◇) and (d) pH 8 (○) and theoretical fit of the Berens and Hopfenberg mathematical model taking into account drug diffusion and chain relaxation (solid lines).

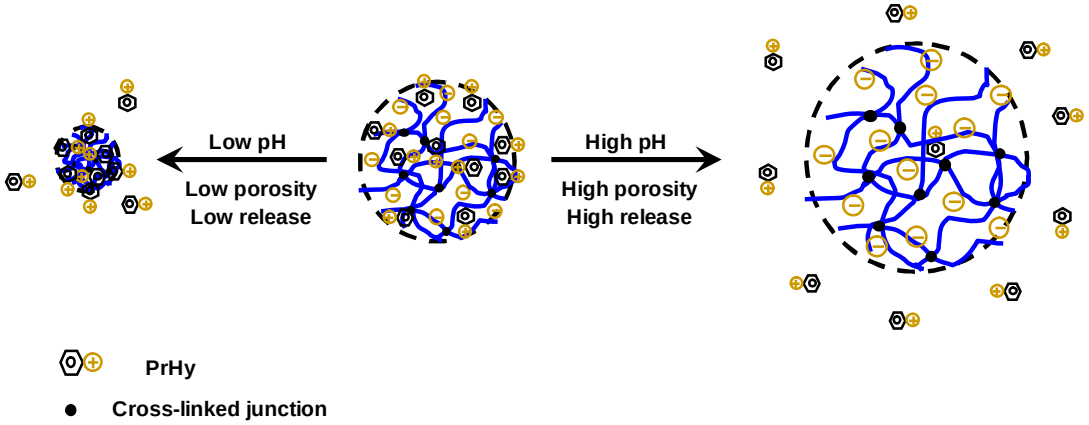

Figure 7.23 Schematic diagram of nanogels under different pHs.

7.4.2 Varying T_g of nanogels

Drug release for 0.1 wt% 50MAA-50EA, 50MAA-50BMA and 50MAA-50MMA at α = 0.05, 0.2 and 0.5 was carried out in 100-millilitre 10 mM NaCl solution at 37 ^{o}C. The results were plotted in Figures 7.24 to 7.26 respectively. All the releases were conducted at the same α to determine the effects of nanogel's T_g on the release behavior. The maximum α that could be conducted was 0.5, which corresponded to pH 8 for 50MAA-50MMA, since beyond pH 8 the drug electrode was not stable as shown in Figure 4.5.

All the release profiles shown in Figures 7.24 to 7.26 possessed a similar trend, with 50MAA-50EA exhibiting the highest release followed by 50MAA-50BMA and 50MAA-50MMA. In Figure 7.24, the release was conducted at α = 0.02, where 50MAA-50EA and 50MAA-50MMA possessed the highest and lowest release profiles respectively. Since the T_g of 50MAA-50EA is the lowest (67.8 ^{o}C as compared to 153.6 ^{o}C for 50MAA-50MMA), the chains are more flexible with a higher swelling

capability as shown in Figure 7.6. With the higher swelling capability, the porosity will be higher thus more PrHy could be release resulting in a longer time to attain the equilibrium condition, i.e. ~2 hours for 50MAA-50EA compared to ~1.75 hours for 50MAA-50MMA. However, 50MAA-50BMA possessed the longest time to achieve equilibrium drug concentration as BMA was more hydrophobic than both EA and MMA, which induced a stronger hydrophobic interaction with PrHy.

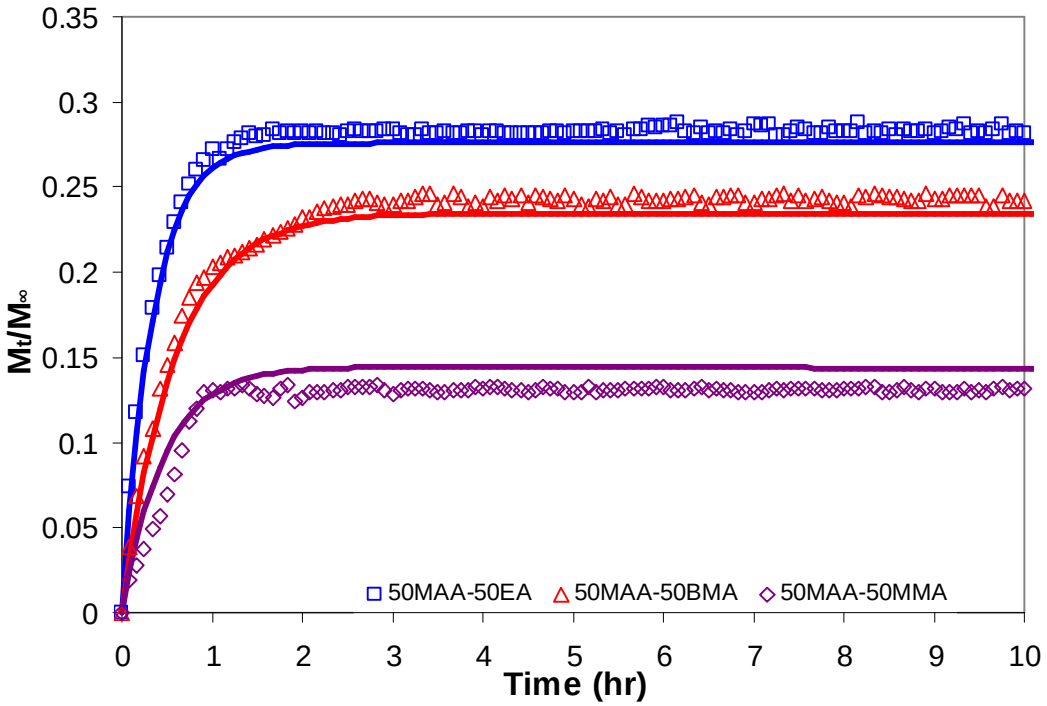

Figure 7.24 Release profile for 0.1 wt% α = 0.05 (a) 50MAA-50EA (□), (b) 50MAA-50BMA (△) and (c) 50MAA-50MMA (◇) in 100-millilitre 10 mM NaCl solution and theoretical fit of the Berens and Hopfenberg mathematical model taking into account drug diffusion and chain relaxation (solid lines).

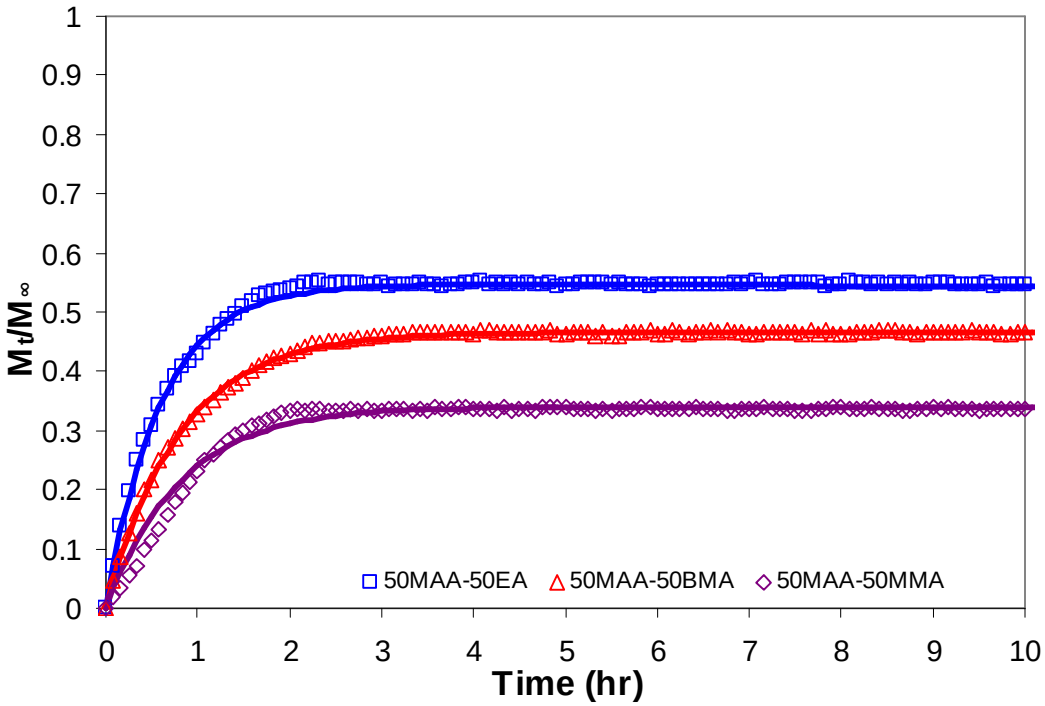

Figure 7.25 Release profile for 0.1 wt% α = 0.2 (a) 50MAA-50EA (□), (b) 50MAA-50BMA (△) and (c) 50MAA-50MMA (◇) in 100-millilitre 10 mM NaCl solution and theoretical fit of the Berens and Hopfenberg mathematical model taking into account drug diffusion and chain relaxation (solid lines).

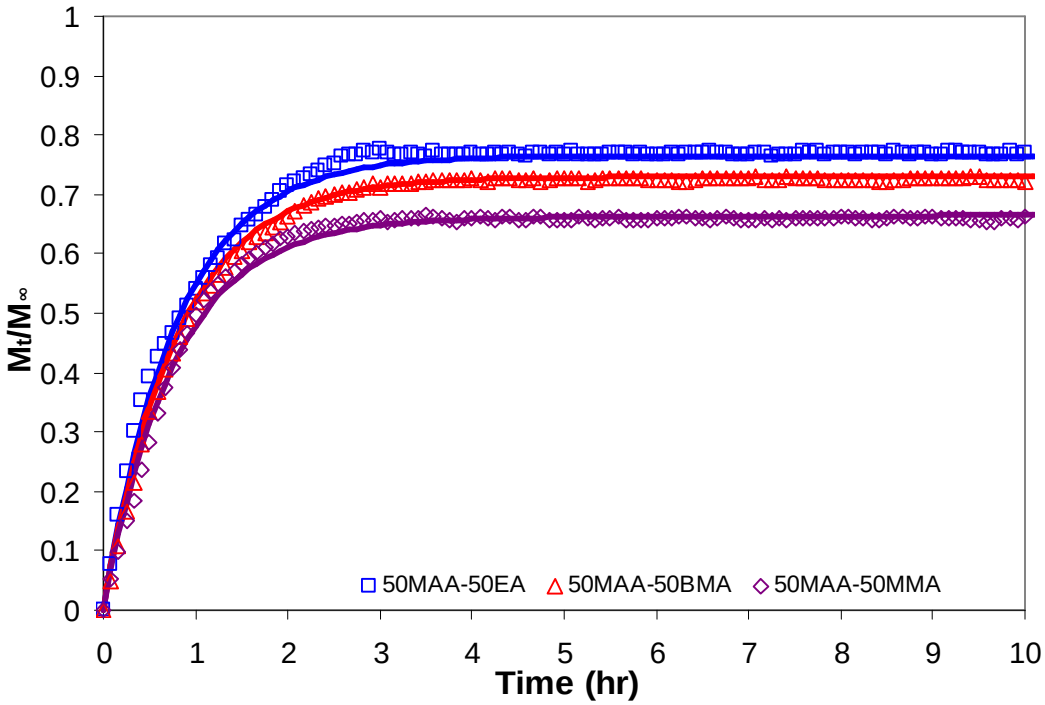

Figure 7.26 Release profile for 0.1 wt% α = 0.5 (a) 50MAA-50EA (□), (b) 50MAA-50BMA (△) and (c) 50MAA-50MMA (◇) in 100-millilitre 10 mM NaCl solution and theoretical fit of the Berens and Hopfenberg mathematical model taking into account drug diffusion and chain relaxation (solid lines).

7.5 Mathematical modeling

Berens and Hopfenberg model [Enscore et al., 1977; Berens and Hopfenberg, 1978] having the form shown in Equation 7.6 was used to model the experimental data:

$$\frac{M_t}{M_\infty} = 1 - f_F\left[\frac{6}{p^2}\sum_{n=1}^{\infty}\frac{1}{n^2}\exp\left(-4p^2n^2Dt/d^2\right)\right] - f_R\exp(-kt) \qquad (7.6)$$

where D is the diffusion coefficient for the Fickian portion of the transport, k is the first-order relaxation constant, f_F and f_R are the fractions of sorption contributed by Fickian diffusion and chain relaxation respectively, d is the diameter of sphere and t is time. The above model describes the overall release behavior in terms of Fickian and non-Fickian contributions. This analysis can lead to the determination of diffusion coefficient (D) and characteristic relaxation time (τ), which is a reciprocal of k.

The model fitting to the experimental data shown in Figures 7.20 to 7.22 and 7.24 to 7.26 using the Berens and Hopfenberg model (Equation 7.6) was used to determine the parameters D, k, f_F and f_R in the model equation. The solid lines in Figures 7.20 to 7.22 and 7.24 to 7.26 are the Berens and Hopfenberg model fitting using the non-linear least squares fitting routine of MATLAB. Excellent agreement between the experimental and predicted kinetic profiles was obtained in all cases. From the model fittings, f_F and f_R were found to vary with pH and T_g of nanogels as shown in Figures 7.27 and 7.28 respectively. The parameter f_F was found to dominate the release process at high pH and lower T_g nanogels as these factors either contributed to a swollen or more porous nanogel, which facilitated the diffusion process since the chains did not relax before the drug was released. However, at low pH and high T_g nanogels, f_R dominated. Under such circumstances, the nanogels assumed a compact structure, where the polymeric chains

must relax before the diffusion of drugs could take place. Therefore, in the drug release process, the release of drugs from pH-responsive nanogels was governed by a combination of chain relaxation and diffusion processes and this will change depending on the characteristics of the gel network.

Based on the fittings from Berens and Hopfenberg model, the diffusion coefficient and characteristic relaxation time as a function of pH for the three nanogels are illustrated in Figures 7.29 and 7.30 respectively. All three nanogels showed similar decreasing trend in the diffusion coefficient before increasing again. From Figure 7.29a, the diffusion coefficient decreased with increasing pH up to pH 7 before increasing again. At low pH of 5 and 6, the high diffusion coefficient was due to the collapse of the nanogels resulting in the drugs being squeezed out. The nanogels swelled at pH greater than 7, which promoted the release of drugs that corresponded to a higher diffusion coefficient. There is a delay in the minimum pH before the increase in the diffusion coefficient when the T_g of the nanogels was increased. For example, 50MAA-50EA was at pH 7, 50MAA-50BMA was at pH 7.2 and 50MAA-50MMA is at pH 7.4. This is mostly likely due to the difference in chain rigidity as all the three nanogels have different T_g. Since 50MAA-50MMA has the highest T_g, the ability to swell will be delayed as shown in Figure 7.6. Osmotic pressure must be able to overcome all the hydrophobic interactions and chain rigidity before swelling can take place. The stronger hydrophobicity in 50MAA-50BMA could be another reason for the delay in swelling. The characteristic relaxation time decreased with increasing pH as shown in Figure 7.30. With increasing pH, the polymeric chains were in a more relax state, therefore a low characteristic relaxation time was observed. An empirical relationship between diffusion coefficient or

characteristic relaxation time and pH of the release medium for 50MAA-50EA, 50MAA-50BMA and 50MAA-50MMA respectively is given below:

50MAA-50EA:

$$D = (0.81pH^2 - 11.32\,pH + 41.8)x10^{-15} \quad (7.7a)$$

$$t = 1.34x10^8 \exp(-2.19\,pH)x10^5 \quad (7.7b)$$

50MAA-50BMA:

$$D = (0.35pH^2 - 4.96\,pH + 19.67)x10^{-15} \quad (7.8a)$$

$$t = 1.40x10^8 \exp(-2.12\,pH)x10^5 \quad (7.8b)$$

50MAA50MMA:

$$D = (0.32pH^2 - 4.85\,pH + 19.09)x10^{-15} \quad (7.9a)$$

$$t = 6.88x10^7 \exp(-1.95\,pH)x10^5 \quad (7.9b)$$

Based on these relationships, it is possible to determine the diffusion coefficient and characteristic relaxation time at any arbitrary pH.

As shown in Figures 7.31 and 7.32, the diffusion coefficient decreased while the characteristic relaxation time increased in relation to T_g when the release kinetic was evaluated at different α. 50MAA-50MMA possessed the lowest diffusion coefficient and highest relaxation time regardless of α, while 50MAA-50EA has the highest diffusion coefficient and lowest relaxation time. This is due to the inability to swell since the nanogel possesses a higher T_g and higher difficulty to relax the polymeric chains.

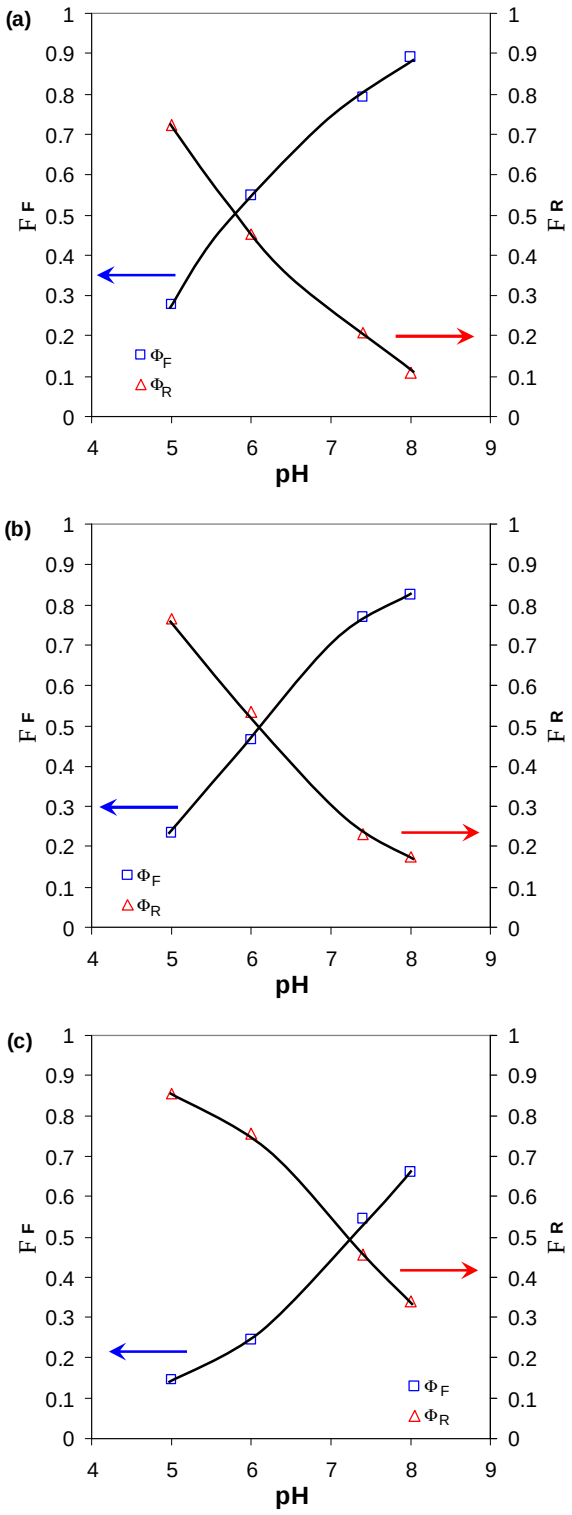

Figure 7.27 Dependence of ϕ_F and ϕ_R against varying pH (a) 50MAA-50EA, (b) 50MAA-50BMA and (c) 50MAA-50MMA obtained from the Berens and Hopfenberg model.

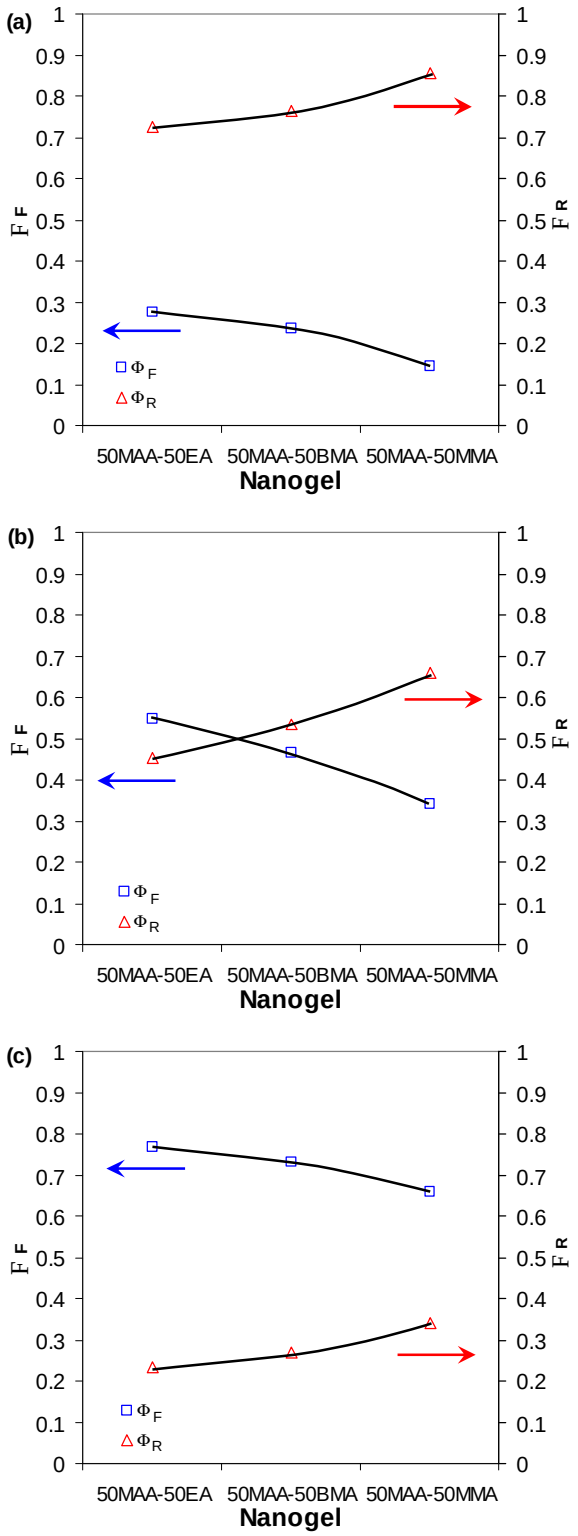

Figure 7.28 Dependence of ϕ_F and ϕ_R against varying nanogels with varying T_g (a) α = 0.05, (b) α = 0.2 and (c) α = 0.5 obtained from the Berens and Hopfenberg model.

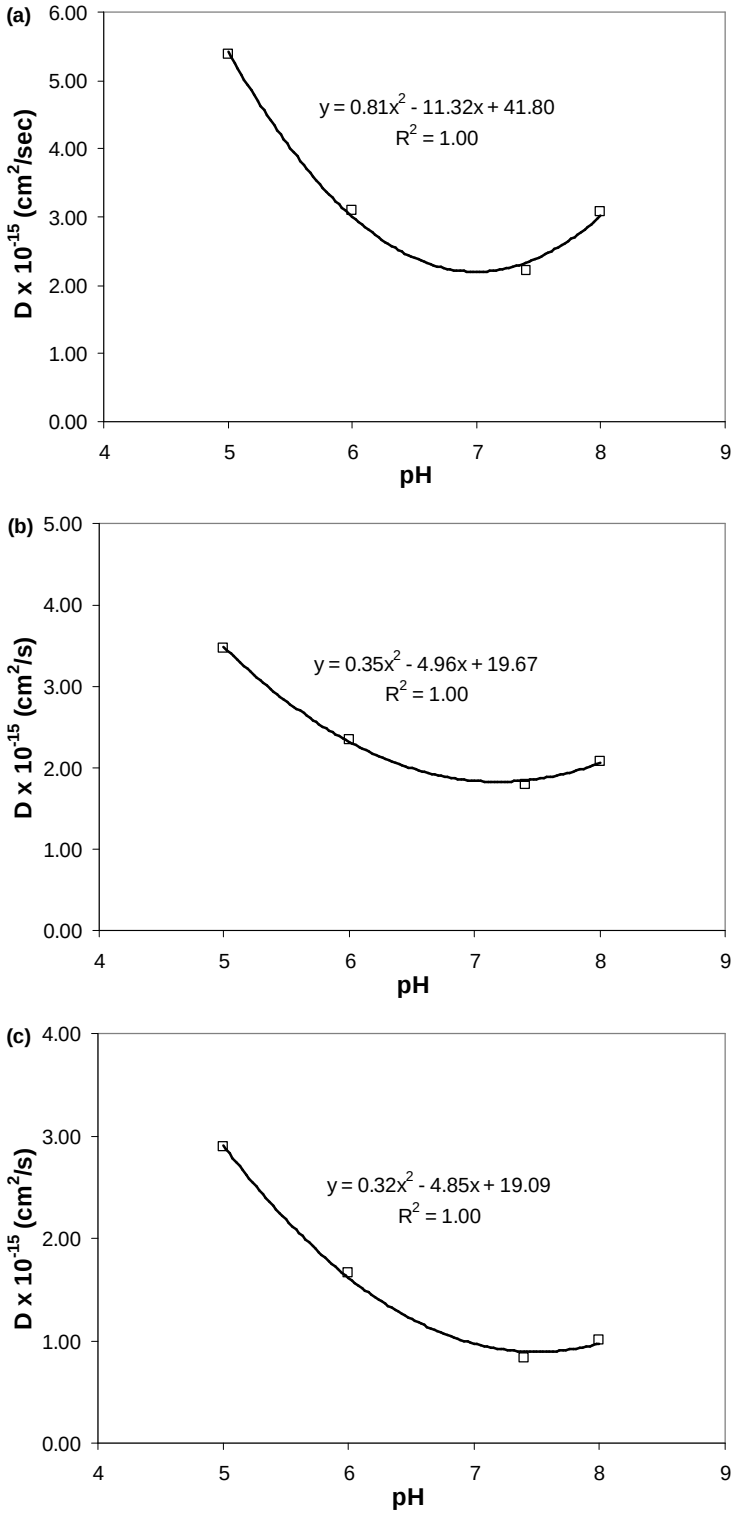

Figure 7.29 Dependence of the diffusion coefficient (D_o) of PrHy from varying pH using (a) 50MAA-50EA (quadratic fit), (b) 50MAA-50BMA (quadratic fit) and (c) 50MAA-50MMA (quadratic fit).

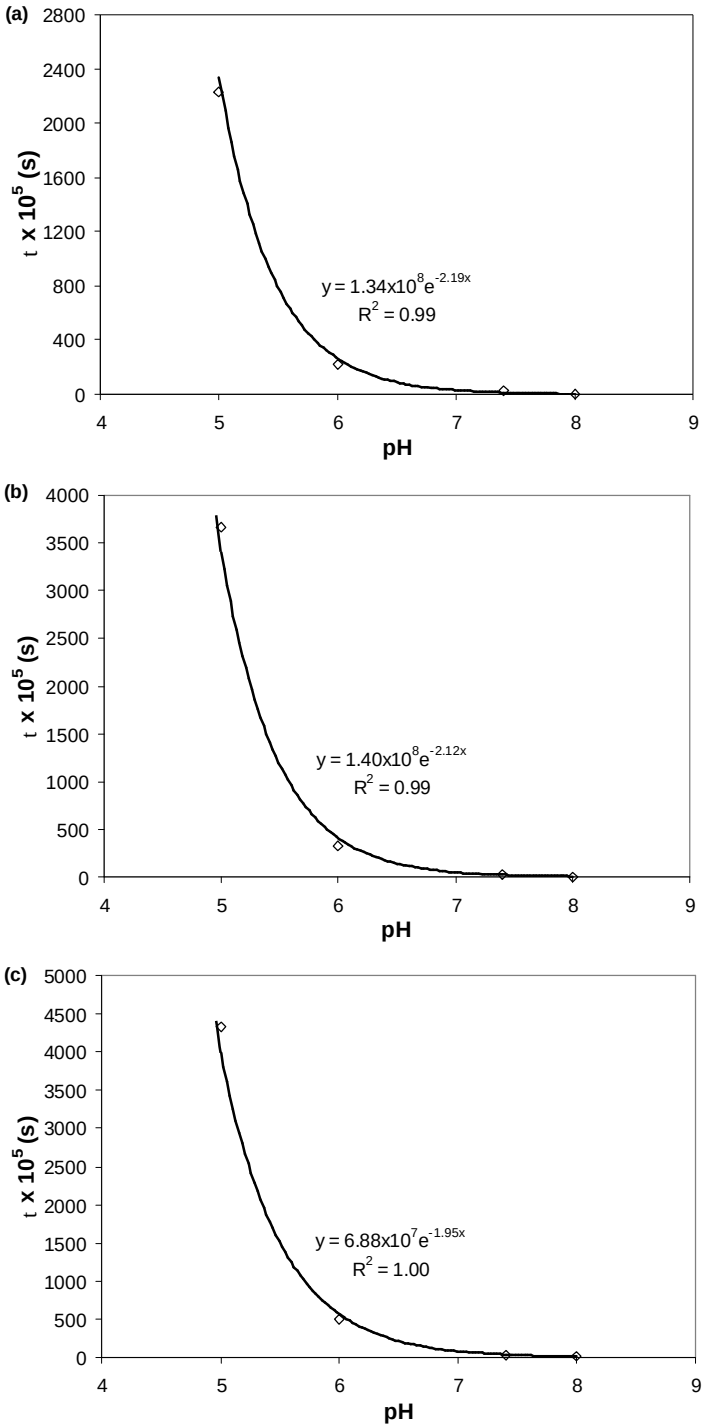

Figure 7.30 Dependence of the characteristic relaxation time (τ) of polymeric chains at varying pH on (a) 50MAA-50EA (exponential fit), (b) 50MAA-50BMA (exponential fit) and (c) 50MAA-50MMA (exponential fit).

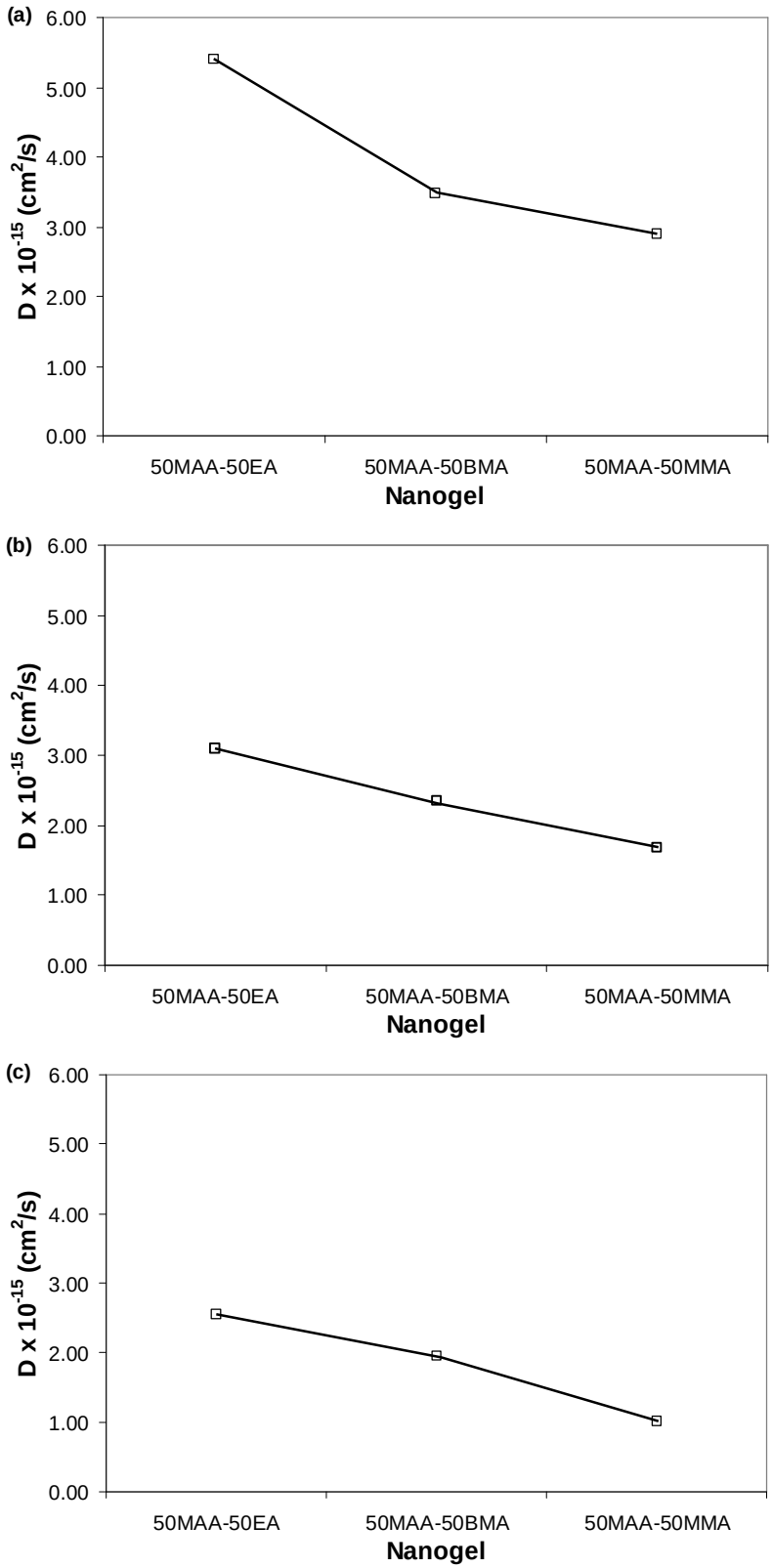

Figure 7.31 Dependence of the diffusion coefficient (D_o) of PrHy from varying nanogels with varying T_g using (a) $\alpha = 0.05$, (b) $\alpha = 0.2$ and (c) $\alpha = 0.5$.

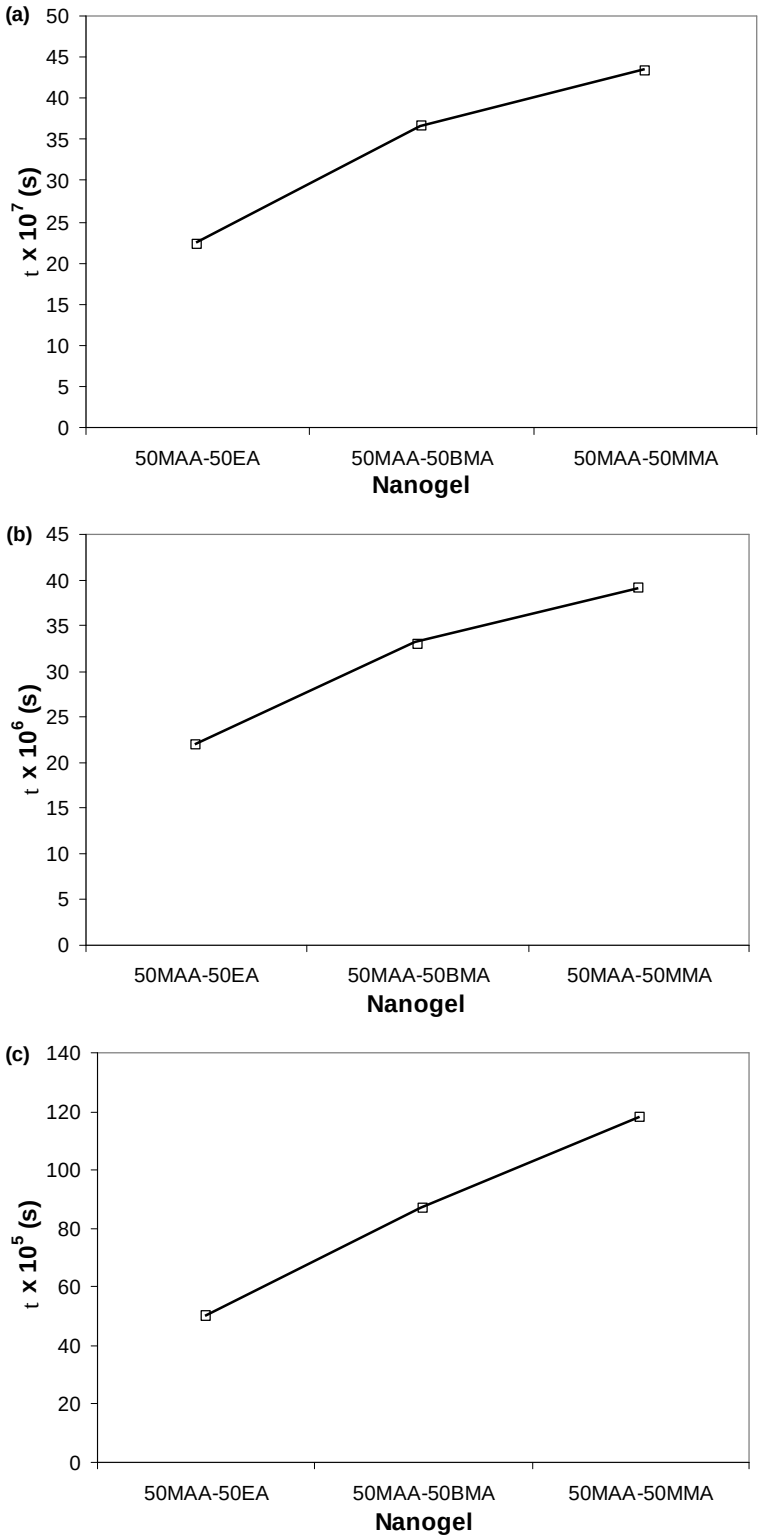

Figure 7.32 Dependence of the characteristic relaxation time (τ) of polymeric chains from varying nanogels with varying T_g on (a) $\alpha = 0.05$, (b) $\alpha = 0.2$ and (c) $\alpha = 0.5$.

7.6 Summary

The R_h for nanogels increased with α, which was due to the increase in osmotic pressure created by ionized carboxylate groups. However, with the increase in T_g, the swelling ratio decreased due to higher chain rigidity. 50MAA-50EA underwent a sharp transition at α = 0.3 as the osmotic pressure exceeded the hydrophobic attraction between EA blocks. However, there was a delay in the transition point for 50MAA-50BMA and 50MAA-50MMA due to a greater hydrophobic interaction between BMA segments and higher chain rigidity respectively. ζ-potential became more negative with increasing α as more COOH were converted to COO^- groups. After the transition point, the increase in particle size reduced the mobility of the nanogels, hence the ζ–potential became less negative.

PrHy was loaded into the nanogels via diffusion and hydrophobic interactions at $\alpha < 1$ due to the steric hindrance of ethyl groups, which shielded the positive charges from the negative carboxylate groups. However, at α = 1, the drug diffused into the nanogels and bound hydrophobically due to the deprotonation of PrHy.

The size of the nanogels decreased with increasing drug loading due to the charge shielding effect on the negatively charged carboxylate groups by PrHy. With the addition of PrHy, there was a reduction in the polymer-solvent interactions as the nanogel environment became more polar, where the nanogels adopted a more compact conformation. The increase in T_g reduced the drug loading capability but not in the case of 50MAA-50BMA as the higher hydrophobicity will induce higher drug loading.

The release of PrHy under varying parameters: pH and T_g was studied. Parameters that promoted the diffusion process of drugs from the interior to exterior of the nanogels would increase the fractional drug release. The amount of drugs release was found to increase with pH and nanogels with lower T_g. From the Berens and Hopfenberg model, during the drug release process, chain relaxation and diffusion played an important role in determining the amount of drugs being released.

8.0 INTERACTIONS AND RELEASE PROFILES OF MAA-EA NANOGELS AND IMI

Nanogel and drug solutions of desired concentrations were prepared from stock solutions for isothermal titration calorimetric, ζ-potential and laser light scattering studies. Through these characterizations, the drug binding mechanism of IMI to MAA-EA nanogels (two series of pH-responsive nanogels, namely varying cross-linking (DAP) densities and molar ratio of acidic groups (MAA)) and the changes in particle sizes at different drug loading ratio were investigated, and the binding mechanism provides insights on the release behavior.

Drug release was carried out with varying parameters: pH, salt concentration, cross-linking density and MAA-EA molar ratio, using the drug selective electrode (DSE).

8.1 Drug interactions with MAA-EA nanogels

The differential enthalpy curves for titrating 20 mM IMI solution into pH 7 0.1 wt% MAA-EA nanogels containing 20 mole percent MAA with varying cross-linking density in 10 mM phosphate buffer (PB) solution and pH 7 0.1 wt% MAA-EA nanogels cross-linked with 4 wt% DAP with varying MAA-EA molar ratio in 10 mM PB solution are shown in Figures 8.1 and 8.2 respectively. In both figures, the enthalpy was plotted against the concentration of IMI.

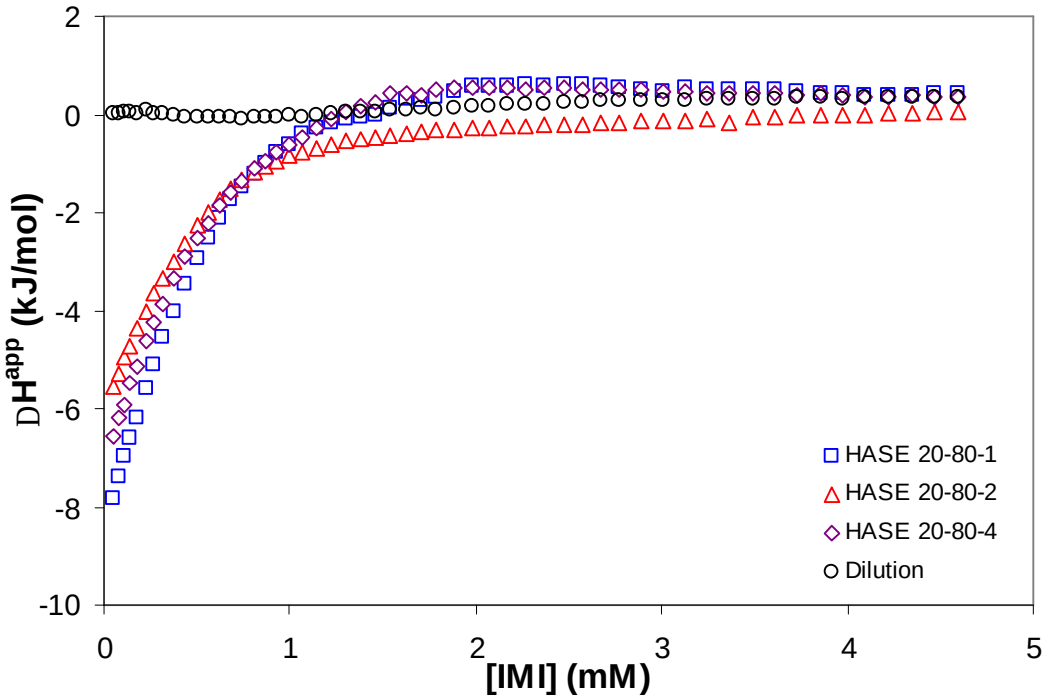

Figure 8.1 Differential enthalpy curves for titrating 20 mM IMI into 0.1 wt% MAA-EA nanogels containing 20 mole percent MAA with varying cross-linking density in 10 mM PB solution at 25 ^{o}C.

From Figure 8.1, the enthalpy profiles for titrating IMI into different nanogels with varying cross-linking density and dilution curve (titrating IMI into 10 mM PB solution) were different. The interaction between the drug and nanogels is electrostatic attraction. However, further confirmation (varying α and varying NaCl concentration testes) would be needed. The enthalpies profiles for HASE 20-80-1, HASE 20-80-2 and HASE 20-80-4 were similar to each other as the amount of COO^- groups present in the nanogels were identical. Besides the electrostatic attractions between negatively charged nanogels and positively charged IMI, hydrogen bonding and hydrophobic interaction are also present.

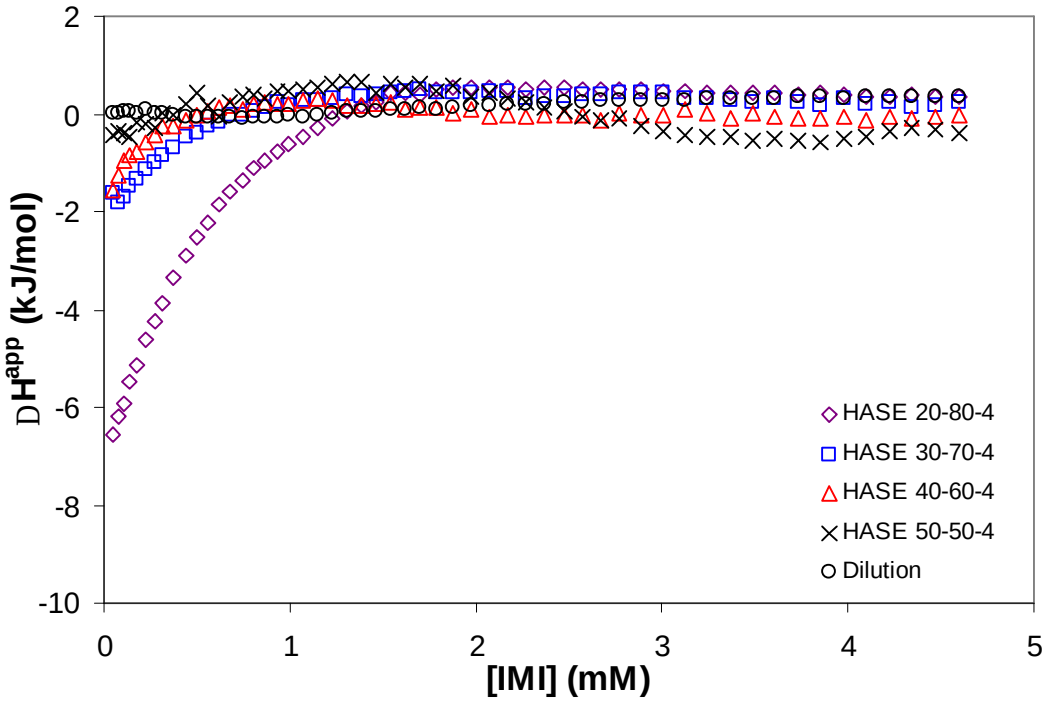

Figure 8.2 Differential enthalpy curves for titrating 20 mM IMI into 0.1 wt% MAA-EA nanogel cross-linked with 4 wt% DAP with varying MAA-EA molar ratio in 10 mM PB solution at 25 ^{o}C.

From Figure 8.2, the enthalpy profiles for titrating IMI into the nanogels were different from the dilution curves and the difference was due to the electrostatic attraction between the negatively charged COO^- groups and positively charged IMI. The enthalpy profile for HASE 20-80-4 was higher than HASE 30-70-4, HASE 40-60-4 and HASE 50-50-4. The observed results were due to higher ΔH generated by hydrophobic interaction between IMI and hydrophobic segments of the nanogels. HASE 20-80-4 possessed the most hydrophobic segments (EA segments) and hydrophobic interaction was the strongest.

The differential enthalpy curves for titrating 20 mM IMI into partially neutralized ($\alpha = 0$, $\alpha = 0.1$ and $\alpha = 0.6$) 0.1 wt% HASE 20-80-1 in 10 mM PB is shown in Figure 8.3, where

α = 0, 0.1 and 0.6 correspond to pH 4, 5.5 and 7 respectively. Based on Figure 8.3, the titration results revealed that electrostatic binding was present between negatively charged COO^- groups and positively charged IMI. The enthalpy increased and the concentration of IMI needed to attain saturation increased with α. The concentration needed to attain saturation increased from ~1 to ~3 mM when α was increased from 0 to 0.6 respectively. A higher concentration of IMI was required to achieve saturation as more COOH groups were ionized at higher pH (higher α). However, at lower α, the gradient was steeper at the initial stage as fewer IMI molecules were deprotonated compared to higher α.

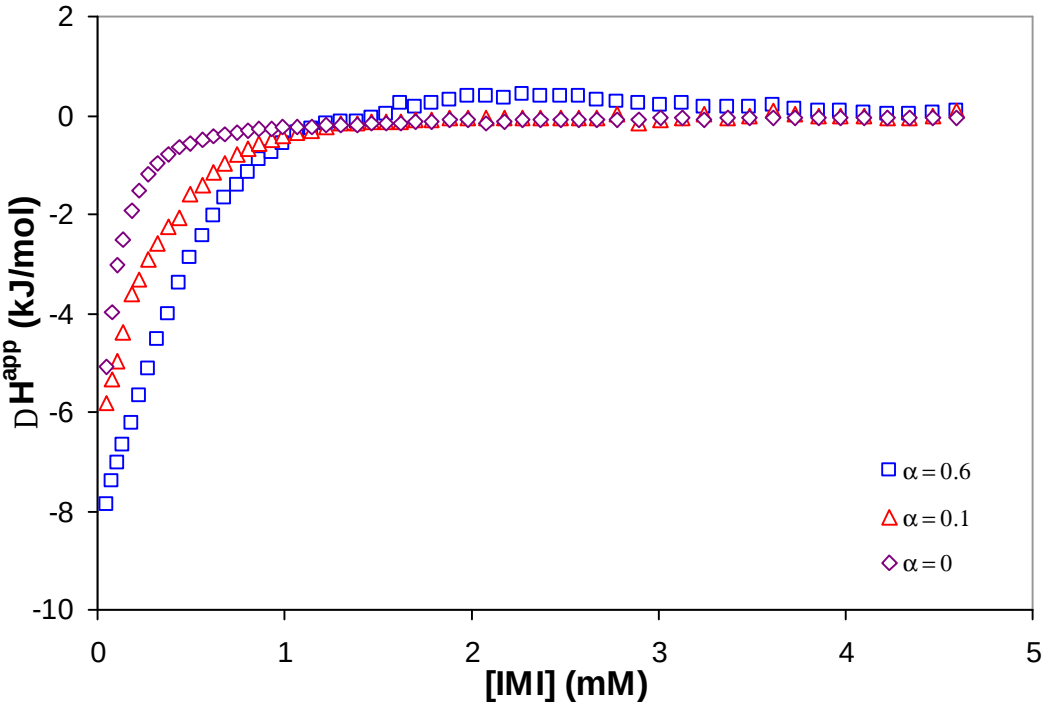

Figure 8.3 Differential enthalpy curves for titrating 20 mM IMI to HASE 20-80-1 at varying degree of neutralization (α) in 10 mM PB solution at 25 ^oC.

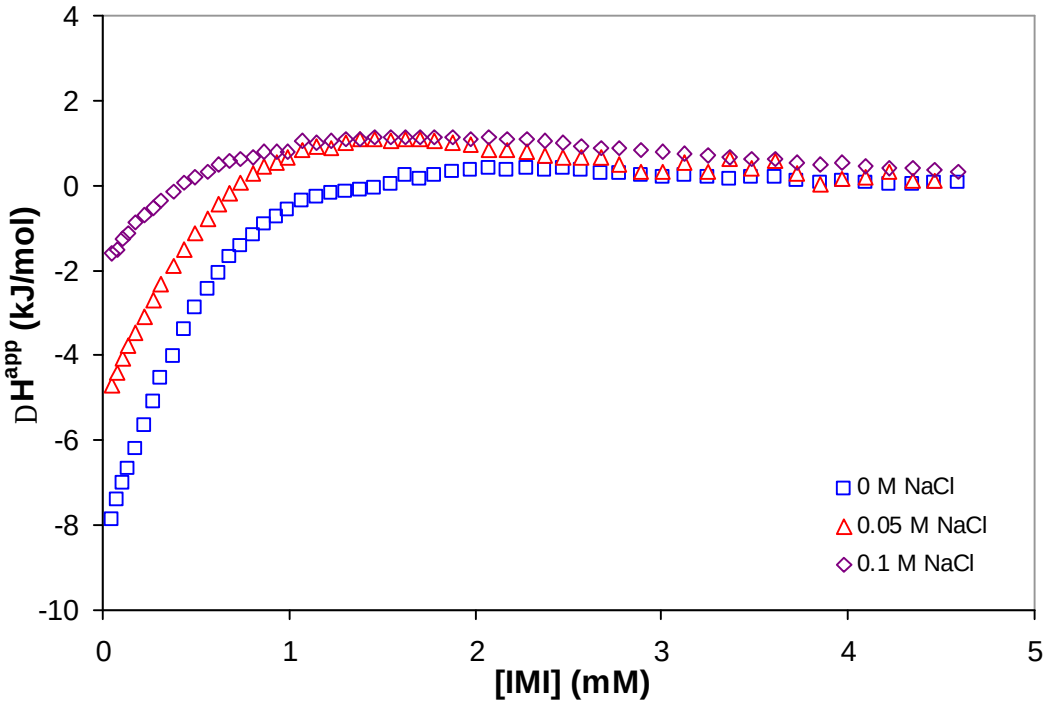

Figure 8.4 Differential enthalpy curves for titrating 20 mM IMI to HASE 20-80-1 at varying NaCl concentration in 10 mM PB solution at 25 ^{o}C.

The differential enthalpy curves for titrating 20 mM IMI into 0.1 wt% HASE 20-80-1 in 10 mM PB (pH 7) at varying NaCl concentrations (0, 0.05 and 0.1 M) are shown in Figure 8.4. The height of the exothermic peak varied inversely with NaCl concentration, indicating the binding was weakened by NaCl, which suppressed the electrostatic binding between the MAA and IMI. With the addition of salt, the Coulombic attractive force between the nanogels and IMI was screened, where the electrostatic binding was significantly weakened and consequently the concentration of IMI required to attain saturation decreased from ~3 mM at 0 M to 2 mM at 100 mM NaCl. Similar results were obtained by Wang and Tam when positively charged DoTab was titrated to negatively charged PAA [Wang and Tam, 2002]. Based on the results from Figures 8.1 to 8.4, the interaction between IMI and MAA-EA nanogels was electrostatic.

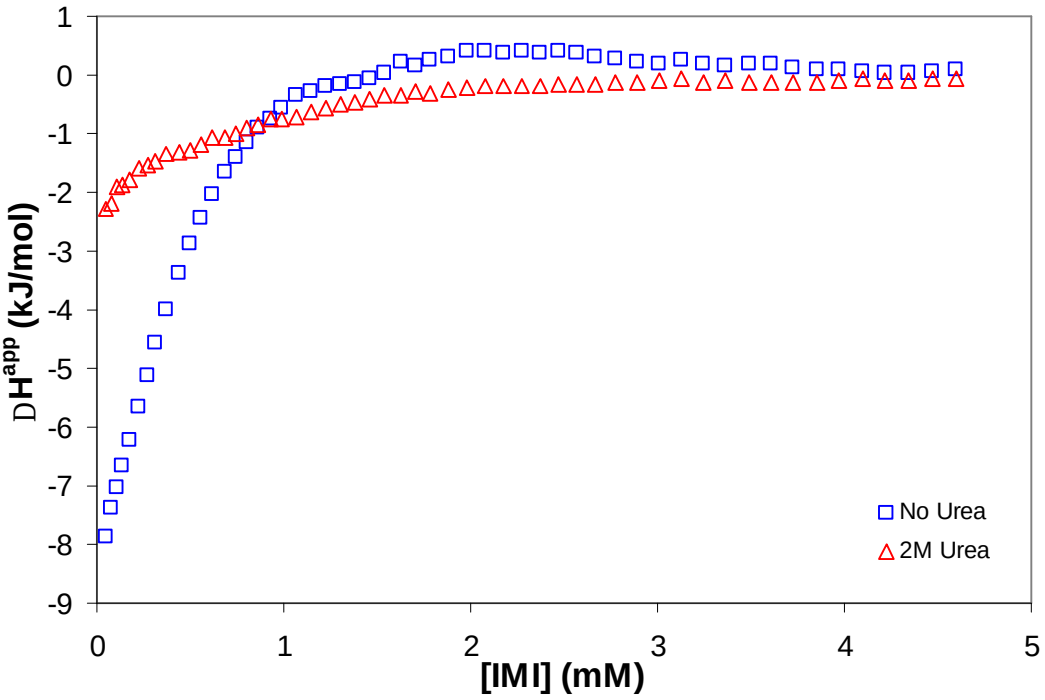

Figure 8.5 Differential enthalpy curves for titrating 20 mM IMI to HASE 20-80-1 at varying urea concentration in 10 mM PB solution at 25 ^{o}C.

The differential enthalpy curves for titrating 20 mM IMI into 0.1 wt% HASE 20-80-1 in 10 mM PB (pH 7) at varying urea concentrations (0 and 2 M) is shown in Figure 8.5. Urea is known to inhibit hydrogen bonding between two interacting components due to the presence of two NH_2 groups in a urea molecule. From Figure 8.5, the enthalpy curve for the addition of urea was less negative compared to without urea. This reduction in ΔH was caused by the reduction of hydrogen bonding between IMI and COOH segments in the nanogels. However, the concentration of IMI needed to attain saturation (~3 mM) remained the same for both cases as there was no change in the amount of COO^- groups with the addition of urea.

The differential enthalpy curves for titrating 20 mM IMI solution into 0.1 wt% HASE 20-80-1 in 10 mM PB solution (pH 7) at varying temperatures are shown in Figure 8.6. When the temperature was increased from 25 to 50 ^{o}C, the value of ΔH increased, which can be attributed to the enthalpy changes associated with an increase in the hydrophobic environment. As a result, a stronger hydrophobic interaction between IMI and MAA-EA nanogels was formed. Therefore, IMI was loaded to the nanogels through long range electrostatic attraction and followed by both hydrogen bonding and hydrophobic interaction.

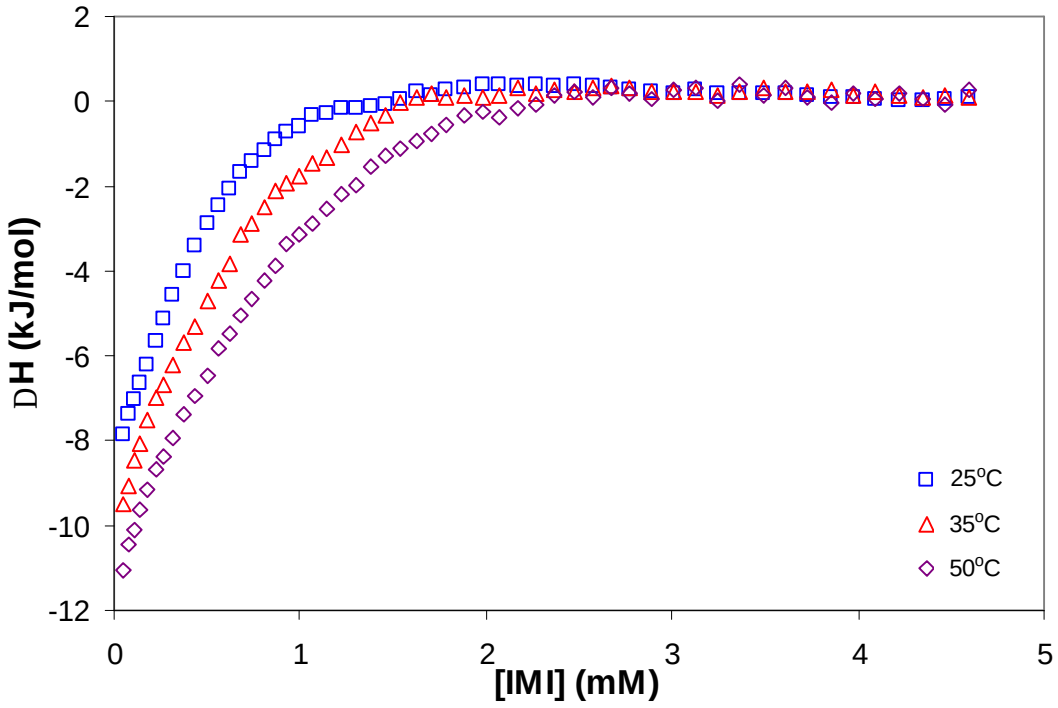

Figure 8.6 Differential enthalpy curves for titrating 20 mM IMI into 0.1 wt% HASE 20-80-1 in 10 mM PB solution at varying temperature.

8.2 Variation in particle sizes and z-potential with drug concentration

The effect of varying drug concentration on particle sizes with nanogels containing 20 mole percent MAA cross-linked with varying cross-linking density and nanogels with 4 wt% DAP and varying MAA-EA molar ratio is shown in Figures 8.8 and 8.14 respectively. The hydrodynamic radius (R_h) at varying drug concentration was normalized against the hydrodynamic radius of each nanogel in the absence of drugs at $\alpha = 1$ ($R_{h\,(c=0)}$).

The relationship between relaxation rates, Γ, and q^2 for 0.1 wt% HASE 20-80-1, HASE 20-80-2, HASE 20-80-4, HASE 30-70-4, HASE 40-60-4 and HASE 50-50-4 in 10 mM PB and 1 mM IMI solution are shown in Figures 8.7a to 8.7f respectively. All the decay functions decreased with increasing scattering angles. The relaxation rates exhibited q^2 dependence confirming that the decay is that of translational diffusion. The translational diffusion coefficients were obtained from the slope of Figures 8.7a to 8.7f and based on Stokes-Einstein relationship the R_h of the particle was calculated. R_h for HASE 20-80-1, HASE 20-80-2, HASE 20-80-4, HASE 30-70-4, HASE 40-60-4 and HASE 50-50-4 was found to be 87.9, 97.0, 123.8, 71.5, 40.9 and 56.6 nm respectively.

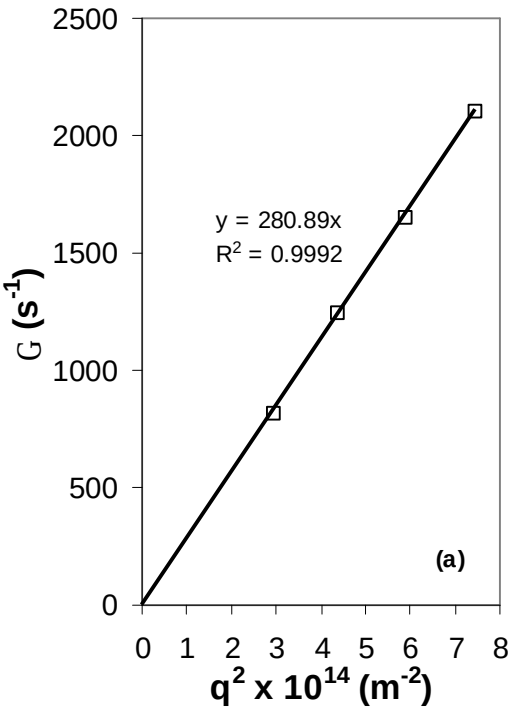

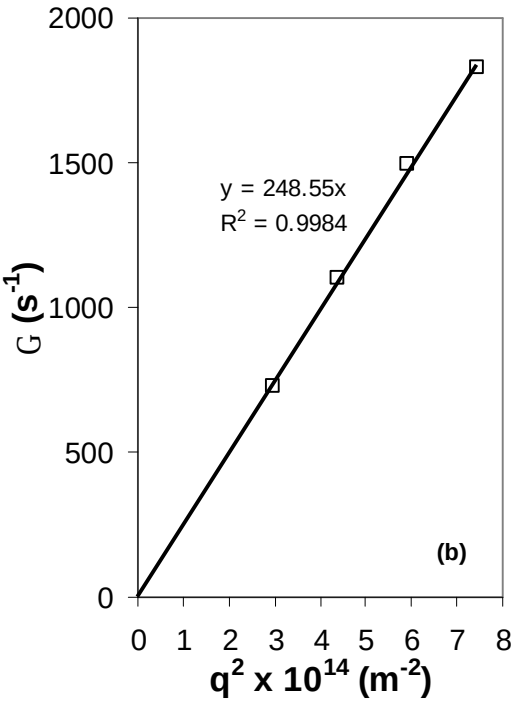

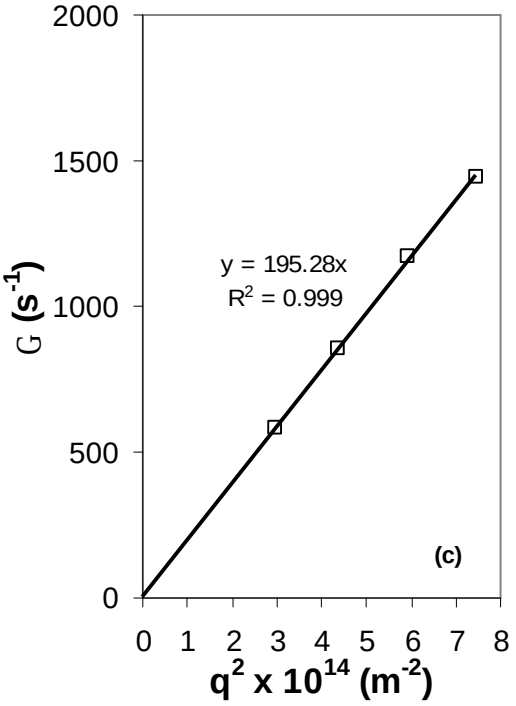

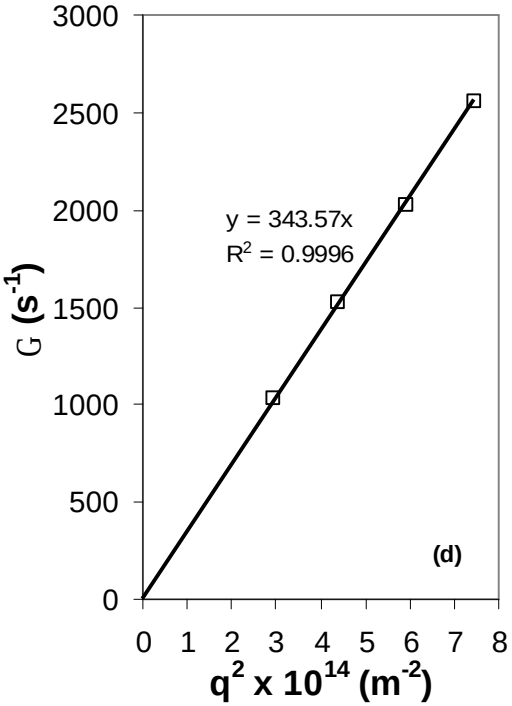

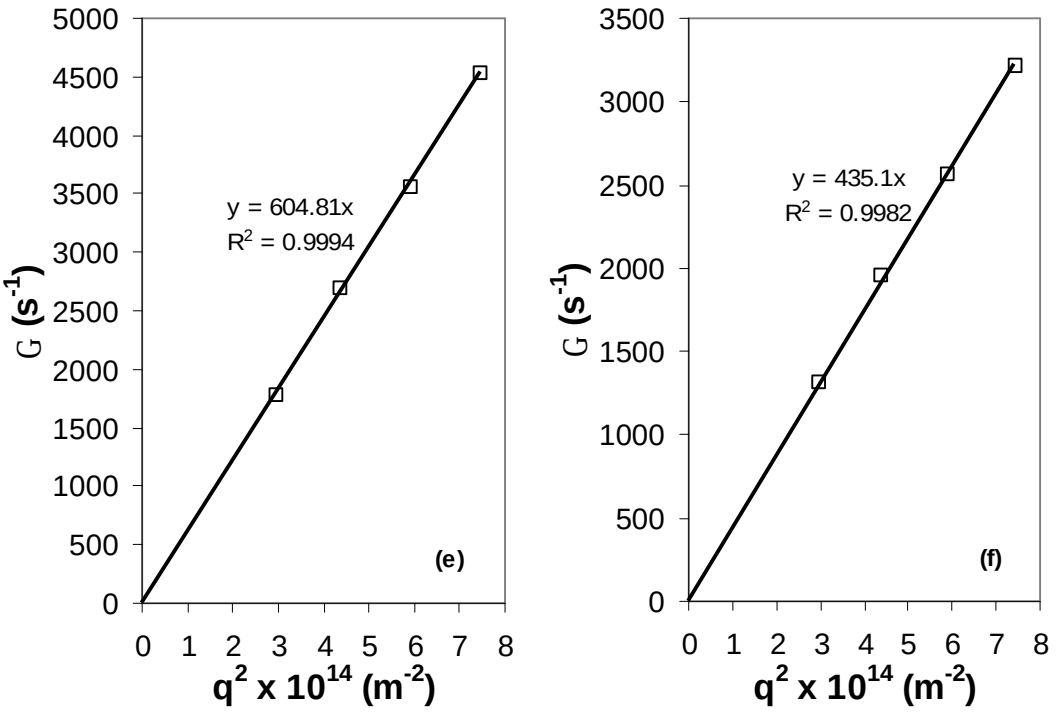

Figure 8.7 The relationship of Γ and q^2 for 0.1 wt% (a) HASE 20-80-1, (b) HASE 20-80-2, (c) HASE 20-80-4, (d) HASE 30-70-4, (e) HASE 40-60-4 and (f) HASE 50-50-4 in 10 mM PB and 1 mM IMI solution.

Based on Figures 8.8 and 8.14, the particle sizes decreased initially at low IMI concentration before it increased greatly at higher IMI loaded concentration due to aggregation of IMI loaded nanogels. When small amounts of IMI was electrostatically bound to COO^- groups, a charge shielding effect will reduce the size of the nanogels due to a reduction of the internal charge repulsion between ionized MAA groups (Figure 8.12). There will also be a concomitant reduction in the polymer-solvent interactions as the overall effect of drug loading produced a less polar environment within the nanogels due to the hydrophobicity of IMI and the reduction in ζ-potential (Figure 8.11), which produced a more compact nanogel structure. Similar trends were observed by Lopez et al. [Lopez et al., 2005] and Bromberg [Bromberg, 1998]. Beyond a critical drug concentration (0.25 mM IMI for HASE 20-80-1, 0.07 mM IMI for HASE 20-80-2 and

0.006 mM IMI for HASE 20-80-4), the particle size increased significantly, which is likely to be due to aggregation of IMI loaded nanogels. The IMI on the surface of the nanogels could interact hydrophobically with another particle to produce a larger aggregate (Figure 8.9). From the Transmission Electron Microscopy (TEM) monographs shown in Figure 8.10c, aggregation of individual IMI loaded nanogels was evident. As shown in Figure 8.8, HASE 20-80-4 began to aggregate at a lower IMI concentration, and HASE 20-80-4 swelled the least due to the higher cross-linked density. Because of the lower swelling, the porosity will be lower resulting in more IMI on the surface of the nanogels, which enhances the aggregation of the nanogels.

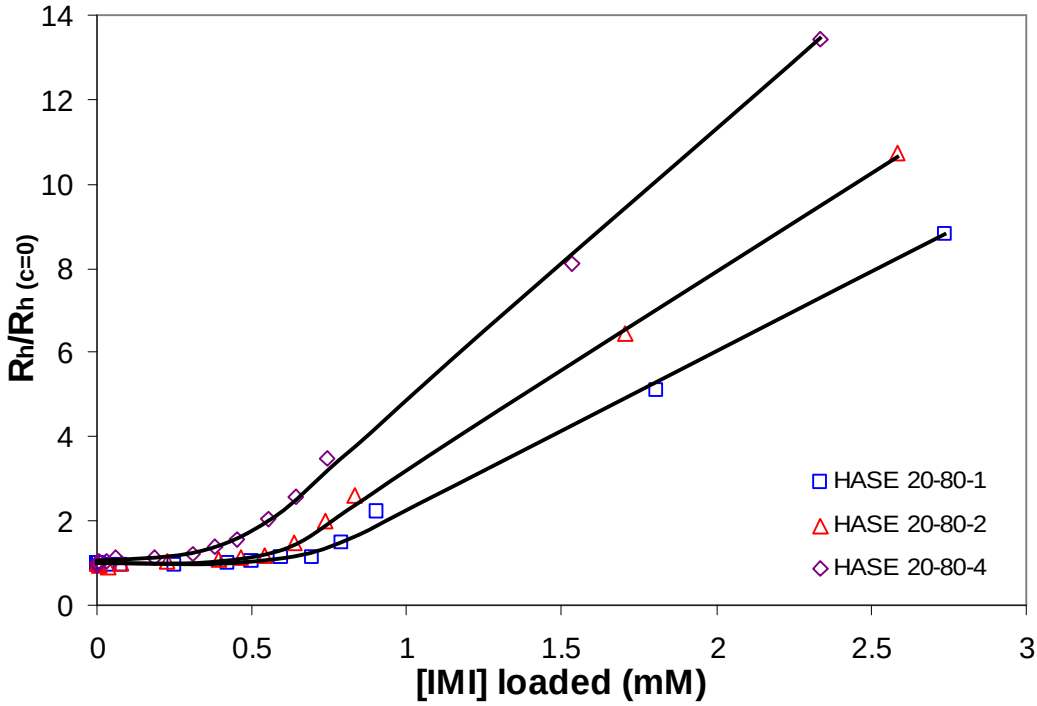

Figure 8.8 Dependence of the ratio of hydrodynamic radius with drugs (R_h) normalized with hydrodynamics radius without drug at pH 7 ($R_{h\ (c=0)}$) on [IMI] loaded for nanogels with 20 mole percent MAA with varying cross-linking density in 10 mM PB solution.

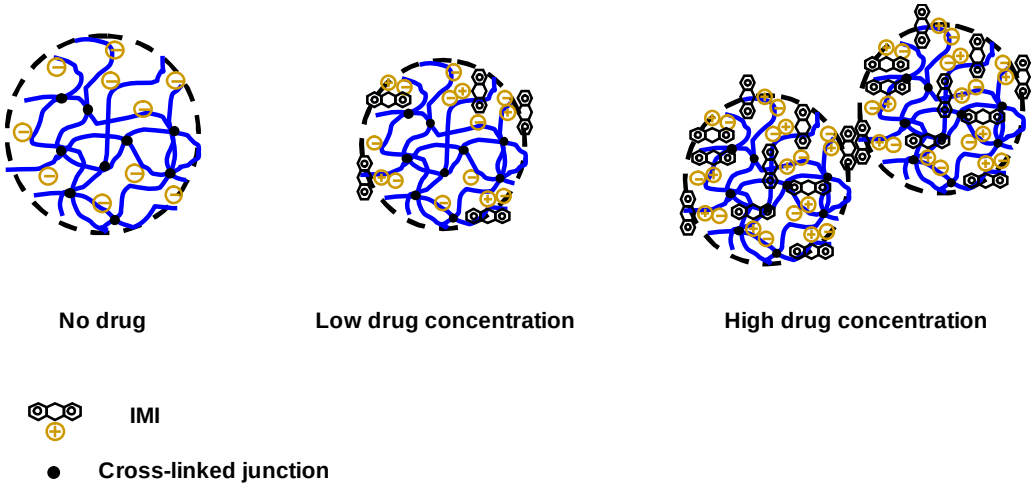

Figure 8.9 Schematic diagram on the drug loading situation at both low and high drug concentration.

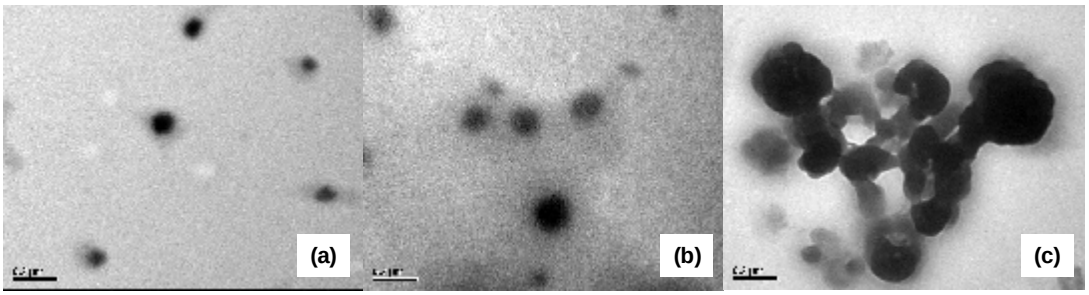

Figure 8.10 Morphology of (a) HASE 20-80-1 without IMI, (b) HASE 20-80-1 with 0.008 mM IMI (low drug concentration) and (c) HASE 20-80-1 with 2.7 mM IMI (high drug concentration).

The ζ-potential became less negative with increasing concentration of IMI before ζ-potential decreased sharply at the critical drug concentration (0.25 mM IMI for HASE 20-80-1, 0.07 mM IMI for HASE 20-80-2 and 0.006 mM IMI for HASE 20-80-4) as shown in Figure 8.11. The electrostatic attraction between positively charged IMI and negatively charged COO^- reduced the amounts of negative charges on the MAA-EA nanogels and made the ζ-potential less negative. After the critical concentration,

ζ-potential became more negative due to the aggregation of nanogels where the amount of negative charges present in the aggregated particles will increase. Similar to Figure 8.8, the ζ-potential for HASE 20-804 became more negative at an earlier drug concentration as there were more IMI on/near the surface of the nanogels, which promoted an earlier aggregation of the nanogels.

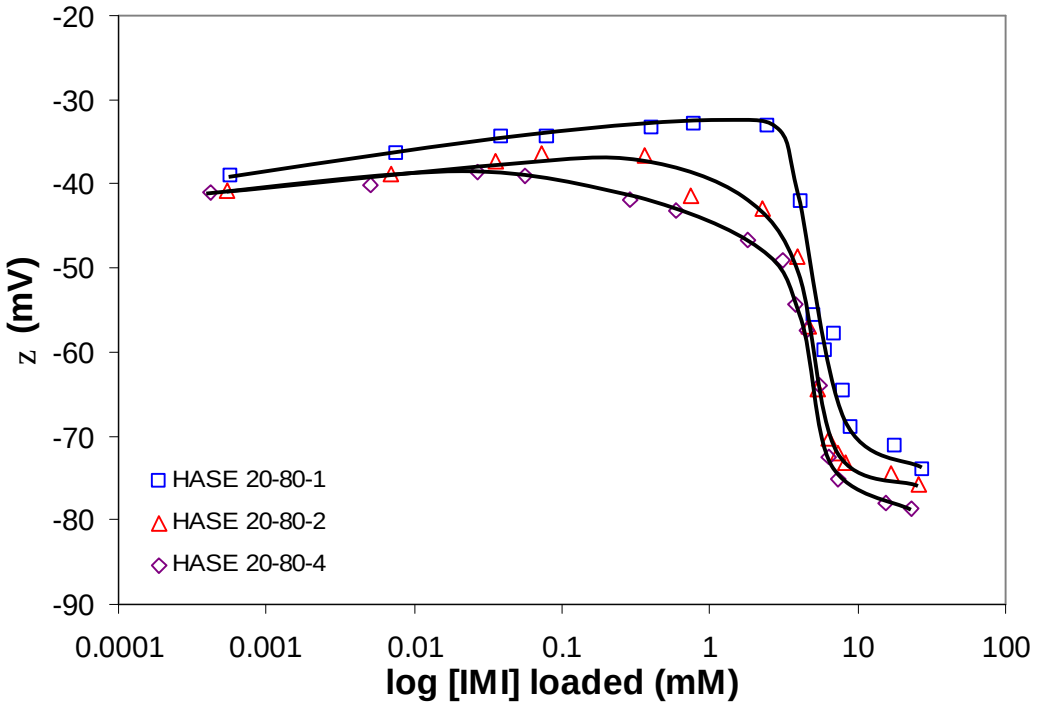

Figure 8.11 Dependence on the ζ-potential on [IMI] loaded for nanogels with 20 mole percent MAA with varying cross-linking density in 10 mM PB solution.

By re-plotting the results in Figures 8.8 and 8.11 together for 0 to 0.5 mM IMI (Figure 8.12), the effect of charged shielding by IMI molecules that reduced the particle size was clearly evident. The critical concentration of loaded IMI that produced a larger particle size corresponded to the turn in ζ-potential. Aggregation in the nanogels will increase the

amounts of COO^- groups present yielding a more negative ζ-potential. The rest of the nanogels exhibited similar trend as Figure 8.12 and will not be shown.

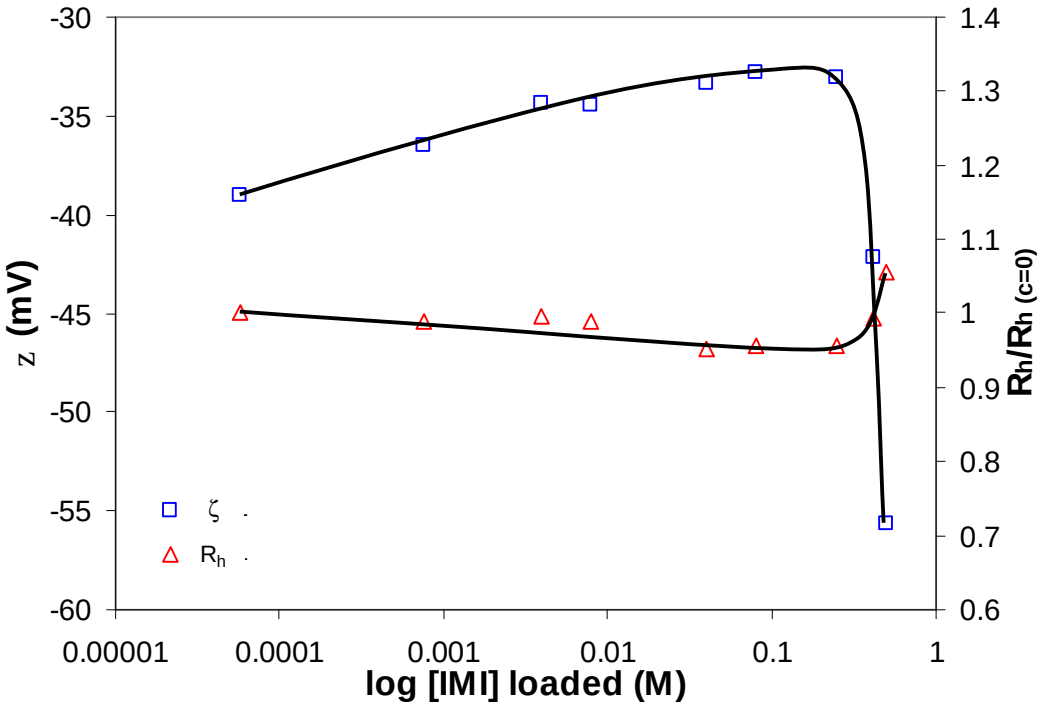

Figure 8.12 Dependence on the (a) ζ-potential and (b) ratio of hydrodynamic radius with drugs (R_h) normalized with hydrodynamics radius without drug at pH 7 ($R_{h\ (c=0)}$) on [IMI] loaded (0 to 0.5 mM IMI) for HASE 20-80-1 in 10 mM PB solution.

Turbidity results for the IMI loaded in the 20 mole percent MAA and varying cross-linking density nanogels are shown in Figure 8.13. The transmittance generally possessed decreasing trend due to the compact structure of the nanogels as more IMI was loaded. The transmittance for HASE 20-80-1 was higher than HASE 20-80-2 and HASE 20-80-4 as the nanogels could swell more due to the lower cross-linked density. At low IMI loaded concentration, the transmittance value for the 3 nanogels were identical as

this was also evident from the pictures, where similar clarity could be seen. The small reduction in size at low IMI loaded concentration will not cause the transmittance to change much. However, at higher IMI loaded concentration, transmittance was found to deviate more for the 3 nanogels. With higher IMI loaded concentration, the size change will be more significant and the reduction in transmittance was higher.

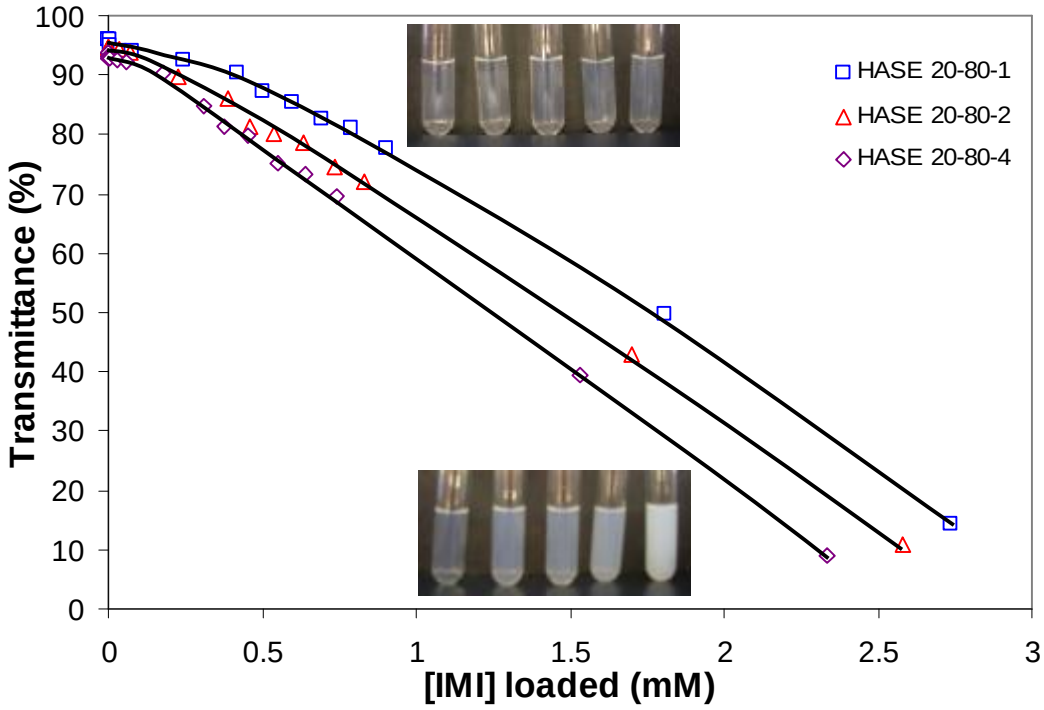

Figure 8.13 Dependence on the transmittance on [IMI] loaded with 20 mole percent MAA with varying cross-linking density in 10 mM PB solution.

The drug loading capacity of the 20 mole percent MAA and varying cross-linking density nanogels was compared at a drug content of 1 mM. The loading capacity of drugs showed a decreasing trend with increasing cross-linking density as shown in Table 8.1. Similar trend was observed by Kurkuri and Aminabhavi using poly(acrylic acid) and poly(vinyl alcohol) cross-linked with glutaraldehyde pH sensitive microspheres [Kurkuri and Aminabhavi, 2004]. The increase in cross-linking density will cause the nanogels to

become more rigid, which reduces the free volume within the polymer matrix, resulting in a lower drug loading capacity.

Table 8.1 Results of drug loading capacity and particle size of 20 mole percent MAA and varying cross-linking density nanogels.

Name of nanogel	Loading (g of drug/g of polymer)	Particle size, R_h (nm)
HASE 20-80-1	0.286	89.7
HASE 20-80-2	0.264	97.0
HASE 20-80-4	0.236	123.8

As shown in Figure 8.14, the particle size decreased due to charge shielding effect and beyond the critical concentration (0.006 mM IMI for HASE 20-80-4, 0.47 mM for HASE 30-70-4, 0.84 mM for HASE 40-60-4 and 2.66 mM for HASE 50-50-4), the particle aggregated resulting in a larger size. The hydrophobic interaction between the surface adhered drugs exceeded the electrostatic repulsion between nanogels, and this induced the aggregation of the nanogels. HASE 20-80-4 began to aggregate and precipitated first compared to HASE 30-70-4, HASE 40-60-4 and HASE 50-50-4. HASE 20-80-4 has the least amounts of charged groups thus is least stable in a hydrophobic environment while HASE 50-50-4 (having the most charged groups) will be the most stable, and the aggregation and precipitation of HASE 50-50-4 will be delayed.

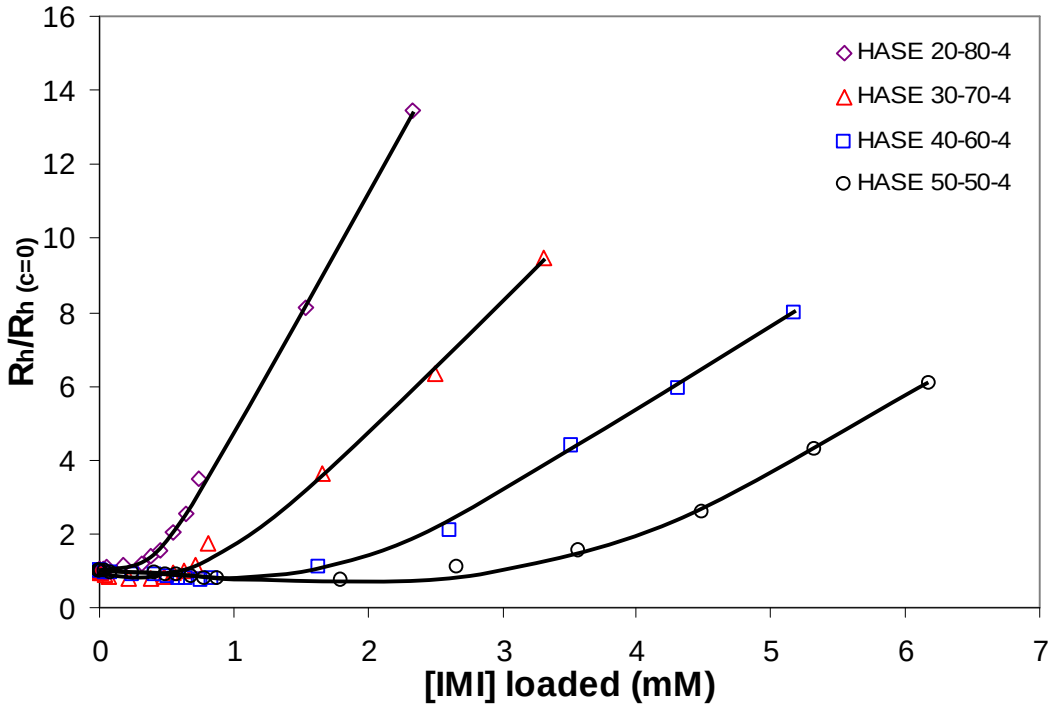

Figure 8.14 Dependence of the ratio of hydrodynamics radius with drugs (R_h) normalized with hydrodynamics radius without drug at pH 7 ($R_{h\ (c=0)}$) on [IMI] loaded for nanogels with 4 wt% DAP with varying MAA-EA molar ratio in 10 mM PB solution.

The ζ-potential decreased and became more negative before the critical concentration as shown in Figure 8.15. Charge shielding and aggregation of IMI loaded nanogels will cause the ζ-potential to change respectively. The turning point where the ζ-potential became more negative coincides with the IMI concentration when the particle size began to increase. The drop in ζ-potential for HASE 20-80-4 is the most gradual as the amount of COO^- groups present is the least. A small amount of IMI loaded will cause an obvious change in ζ-potential before the particles become more hydrophobic and aggregate.

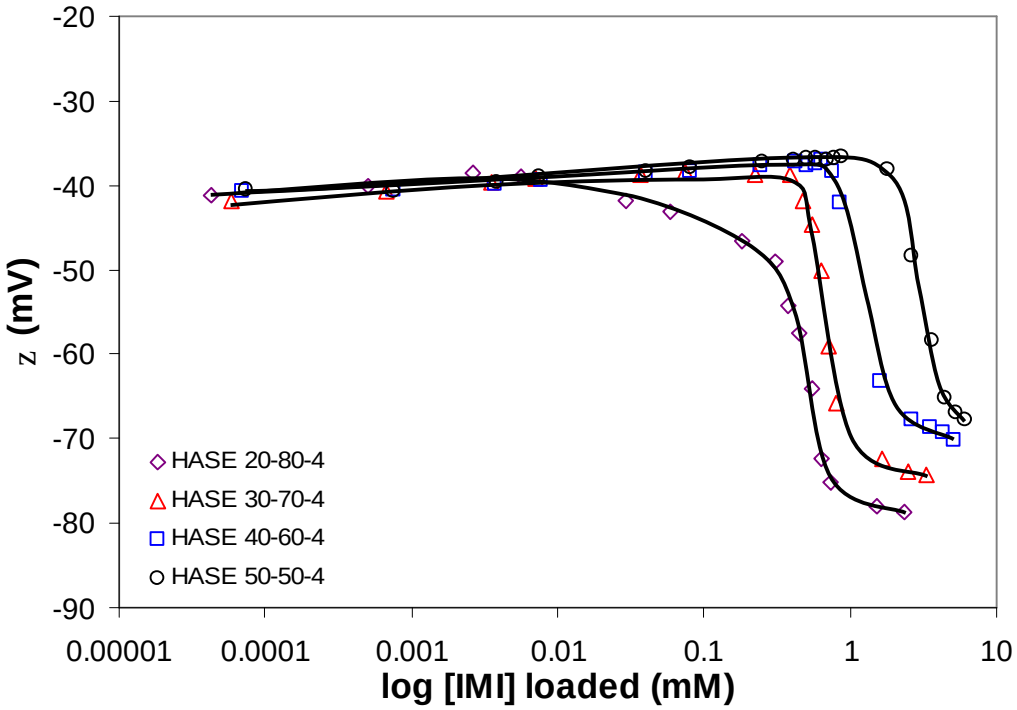

Figure 8.15 Dependence on the ζ-potential on [IMI] loaded for nanogels with 4 wt% DAP with varying MAA-EA molar ratio in 10 mM PB solution.

Turbidity studies from the IMI loaded nanogels for nanogels with 4 wt% DAP and varying MAA-EA molar ratio is shown in Figure 8.16. Transmittance generally has a decreasing trend due to the compact structure of the nanogels as more IMI was loaded. This will lower the porosity and allow less light to pass through. The transmittance for HASE 50-50-4 is the highest as the nanogels have more MAA segments. The higher content of MAA will increase the swelling ability and increase the porosity. At low IMI loaded concentration, the transmittance values for the 4 nanogels are the same due to small reduction in size at low IMI concentration. However, at higher IMI concentration, transmittance was found to deviate more for the 4 nanogels. With higher IMI loaded concentration, the size change will be more significant and the drop in transmittance is higher.

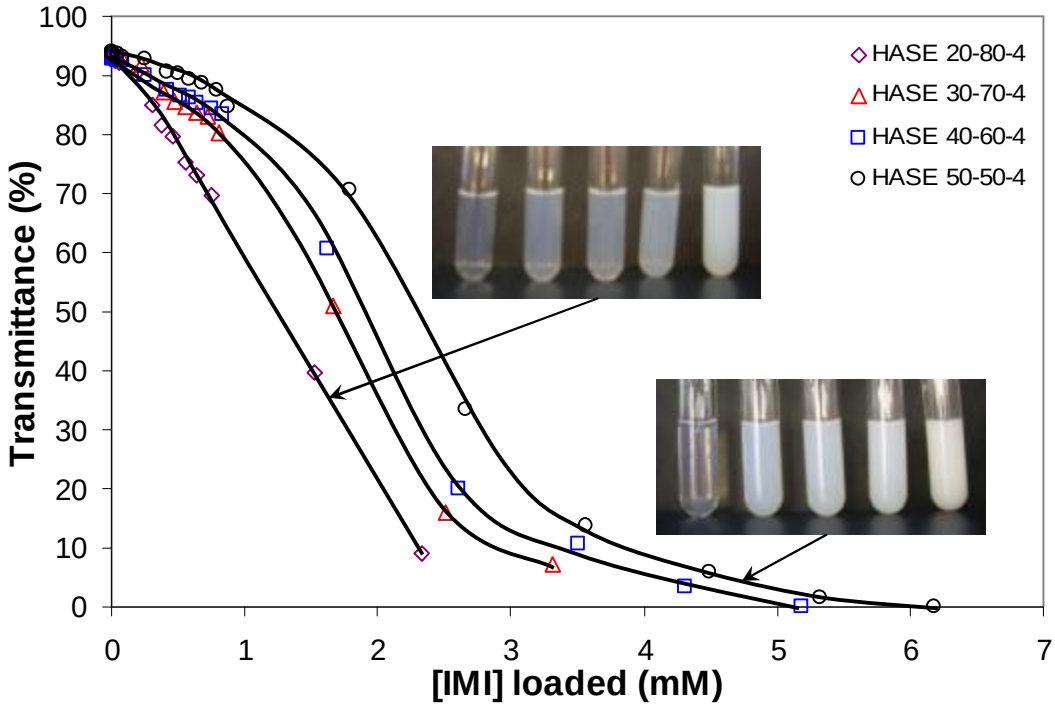

Figure 8.16 Dependence on the transmittance on [IMI] loaded for nanogels with 4 wt% DAP with varying MAA-EA molar ratio in 10 mM PB solution.

Table 8.2 Results of drug loading capability and particle size for nanogels with 4 wt% DAP with varying MAA-EA molar ratio at an added drug concentration of 1 mM.

Name of nanogel	Loading (g of drug/g of polymer)	Particle size, R_h (nm)
HASE 20-80-4	0.236	123.8
HASE 30-70-4	0.255	71.5
HASE 40-60-4	0.265	40.9
HASE 50-50-4	0.277	56.6

The drug loading capacity for nanogels with 4 wt% DAP and varying MAA-EA molar ratio was compared at an added drug concentration of 1 mM. The loading capacity of

drugs showed an increasing trend with increasing MAA content as shown in Table 8.2. Similar trend was observed by Kurkuri and Aminabhavi using poly(acrylic acid) and poly(vinyl alcohol) cross-linked with glutaraldehyde pH sensitive microspheres [Kurkuri and Aminabhavi, 2004]. The increase in MAA content will allow the nanogels to attract more positively charged IMI and the ability to swell more will increase the porosity and thus promote loading.

8.3 Effect of varying parameters on IMI release

8.3.1 Varying pH

In-vitro release studies were performed at varying pHs, namely at pH 4, 5, 6 and 7.4, where the release kinetics are shown in Figure 8.17. The drug release was conducted with 0.1 wt% HASE 50-50-4 loaded with 0.277 g drug/g polymer in 30-millilitre 10 mM PB solution.

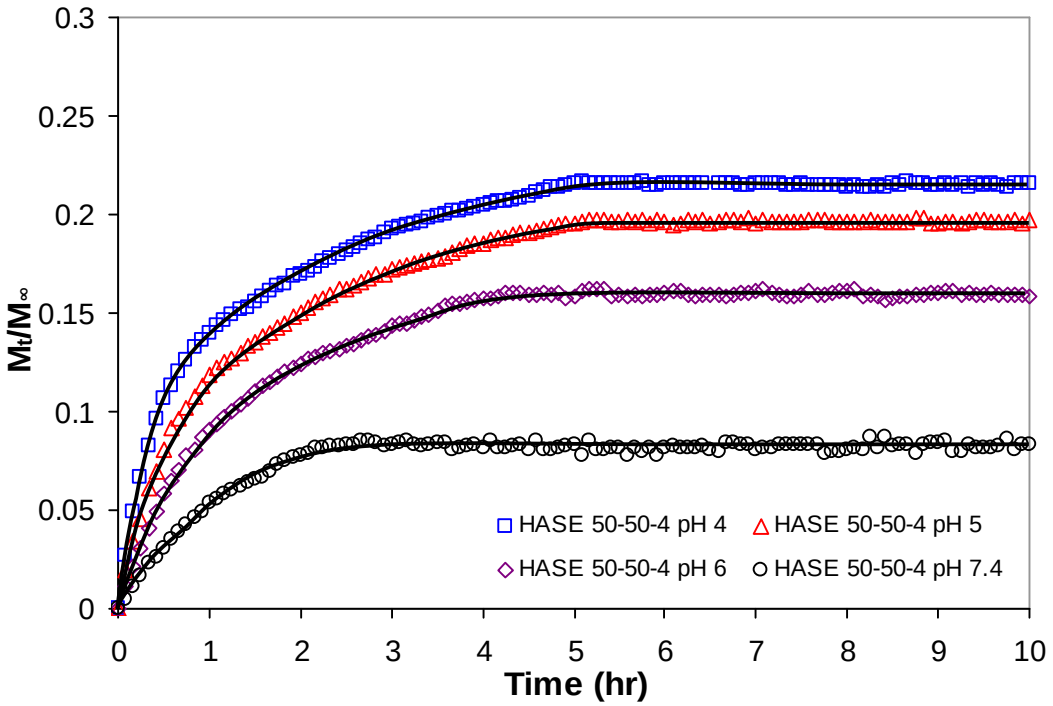

Figure 8.17 Release profile for 0.1 wt% HASE 50-50-4 in 30-millilitre 10 mM PB solution at varying pH (a) pH 4 (□), (b) pH 5 (△), (c) pH 6 (◇) and (d) pH 7.4 (○).

$$COO^{-}IMI^{+} + HCl \rightarrow COOH + IMI^{+} \qquad (8.1)$$

The amount of IMI released at pH 4 was ~23% compared to ~8% at pH 7.4. The greater release at lower pH is most likely due to the protonation of COO^- to COOH (Equation 8.1), which releases positively charged IMI from the negatively charged COO^- groups as the groups become uncharged. At high pH, the COO^- groups remain negatively charged thus the positively charged IMI molecules are bound to the nanogels as illustrated in Figure 8.18. On the average, the IMI loaded nanogels (Figure 8.17) took a longer time to attain the maximum released as compared to PrHy loaded nanogels (Figure 5.28). The stronger interaction between IMI and MAA-EA nanogel (electrostatic and hydrophobic interaction and hydrogen bonding) as compared to PrHy and MAA-EA nanogel (hydrophobic interaction) could be the reason for the longer time needed. This MAA-EA system will be able to deliver two different kinds of drugs, which are bound electrostatically, hydrophobically and via hydrogen bonding. Therefore with a single drug delivery system (MAA-EA nanogels), many types of cationic drug could be loaded and released.

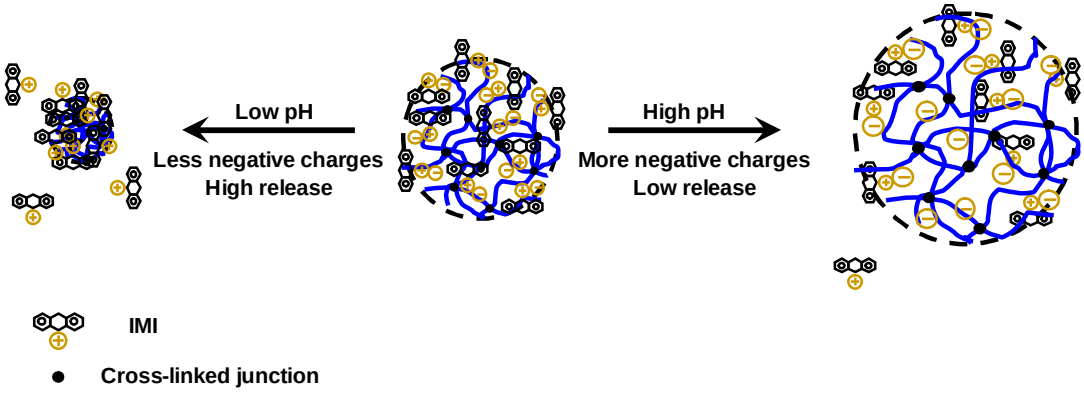

Figure 8.18 Schematic diagram of nanogels under different pH.

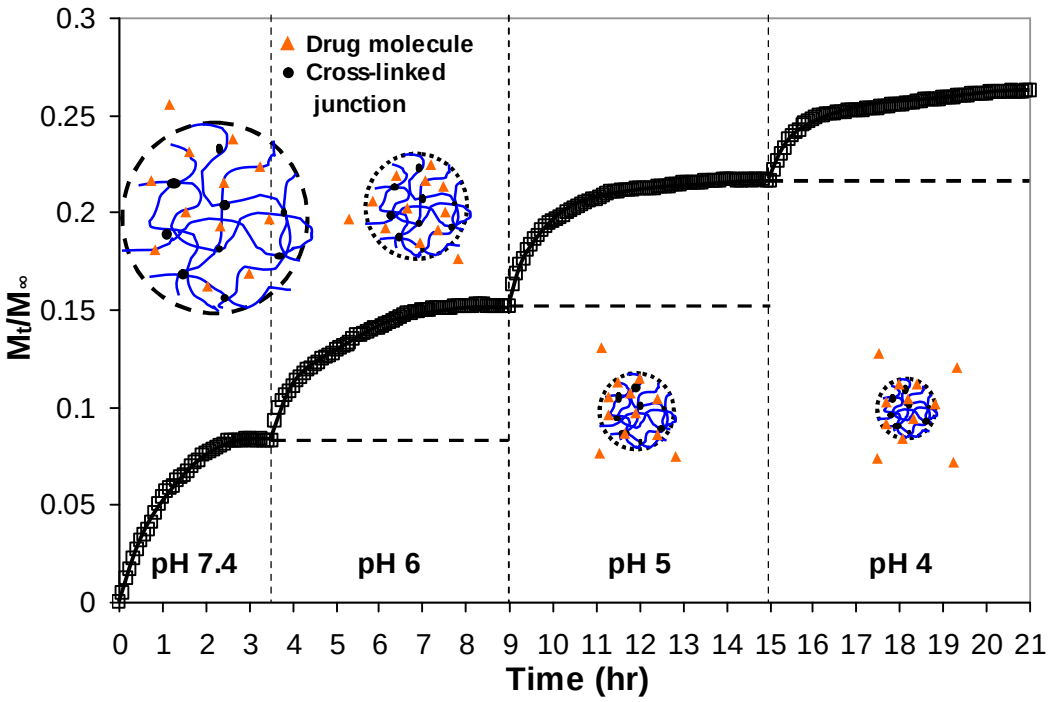

Figure 8.19 In-vitro release profile of IMI from 0.1 wt% HASE 50-50-4 in a changing pH environment.

The normalized IMI released profile under a step change in pH was plotted in Figure 8.19 from IMI loaded HASE 50-50-4 nanogel. The first 3.5 hours of study was conducted at pH of 7.4 and the pH was decreased to 6 and the release profile was monitored for 5.5 hours. The next 6 hours of the release was performed at pH 5 and finally the pH was decreased to 4 and the release was monitored for 6.5 hours. Data from Figure 8.19 showed that the amount of IMI released increased from ~8% to ~15% when the pH was decreased from 7.4 to 6 respectively and further decrease in pH from 5 to 4 resulted in a further increase in release from ~22% to ~26% respectively. Since the HASE 50-50-4 nanogels consisted of pH-responsive MAA segments, the pH of the medium will have an impact on the release behavior. The release of IMI will depend on pH where a decrease in pH will promote the release of IMI. As shown in Figure 8.19, the maximum fraction of drug released at pH of 7.4 was about ~8% (open circle in Figure

8.17) and by decreasing the pH to 6, another ~8% of the drugs could be released, and this decreased to ~5% when the pH was decreased from 5 to 4. This reduction was likely to be attributed to the reduced concentration gradient difference of IMI between the interior of the nanogel and the dissolution medium since some drugs had been released at pH 5. Three comments should be made from the results reported in Figures 5.31 and 8.19. Firstly, the results demonstrated the viability of tuning the release profiles of drug released from a pH-responsive nanogel system. The proportion of drug release can be controlled by manipulating the pH of the environment. Hence, the possibility to design a pH-dependent gradient release drug delivery system such that the active drugs could be released from the carrier in different regions of the physiological environment having different pHs. This will result in extending the therapeutical period of the active drug and ensure that the targeted areas receive the right dosage of drugs. Secondly, the interaction between drug and drug delivery nano-carriers will determine the release patterns and the effective therapeutical period of the nano-carriers and is possible to design drug delivery system for better interaction with drugs to have a better control during the release. Thirdly, the monitoring of the amounts of drug released cannot be easily performed using the conventional dialysis membrane or the centrifugation techniques. A continuous monitoring technique using the drug selective electrode system reported here is the only practical method for measuring the concentration of drug release in an environment where the pH is continuously changed.

8.3.2 Varying NaCl concentrations

Drug release for 0.1 wt% HASE 50-50-4 was carried out in 30-millilitre 10 mM PB solution at pH 5 at varying NaCl concentration, and the results were plotted in Figure 8.20.

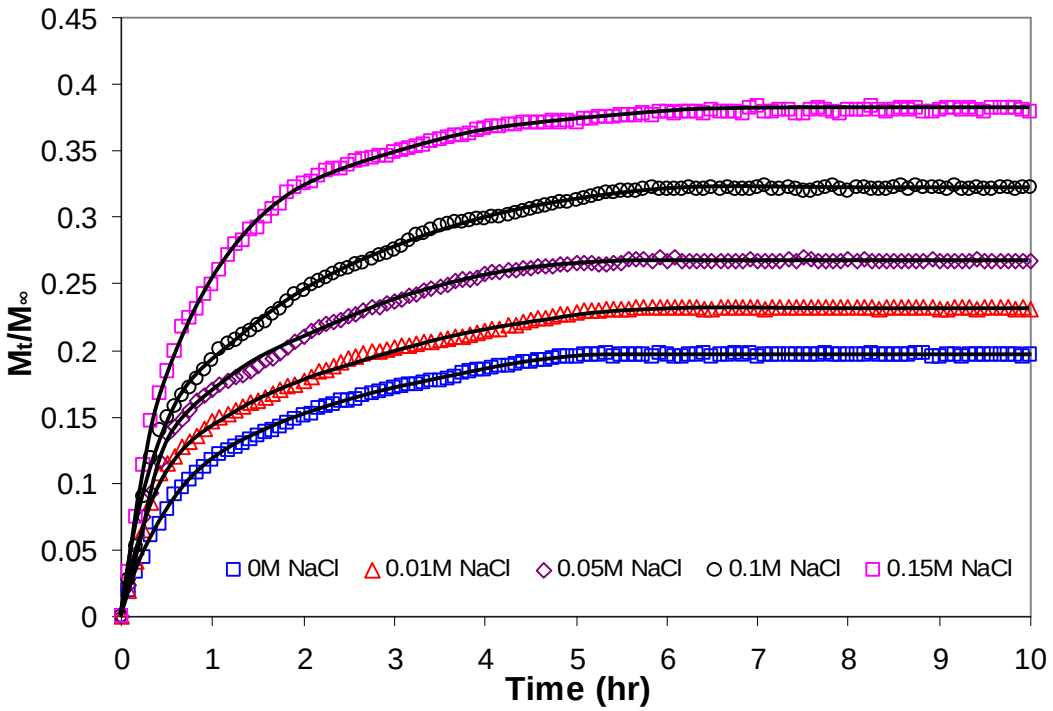

Figure 8.20 Release profile for 0.1 wt% HASE 50-50-4 in 30-millilitre 10 mM PB solution at pH 5 with varying NaCl concentration (a) 0 M (□), (b) 0.01 M (△), (c) 0.05 M (◇), (d) 0.1 M (○) and (e) 0.15 M (□).

$$COO^{-}IMI^{+} + Na^{+}Cl^{-} \rightarrow COO^{-}Na^{+} + IMI^{+}Cl^{-} \qquad (8.2)$$

With an increase in the NaCl concentration in the release medium (10 mM PB at pH 5), the fractional release will increase. For example, at NaCl concentration of 0 M, the

amount released was ~20% and increased to ~38% for NaCl concentration of 0.15 M. Since Na^+ and Cl^- are very small ions, Na^+ ions can displace the IMI from the nanogels as shown in Equation 8.2. Theoretically, one Na^+ ion can have a one to one displacement with the IMI molecule (Figure 8.21). Therefore, there will be an increase in release of IMI when the concentration of NaCl in the release medium was increased. The time to achieve equilibrium increased with increasing NaCl concentration. At a higher NaCl concentration, the nanogels will be in a more compact state therefore a longer time will be needed for the loosely bound IMI to be released.

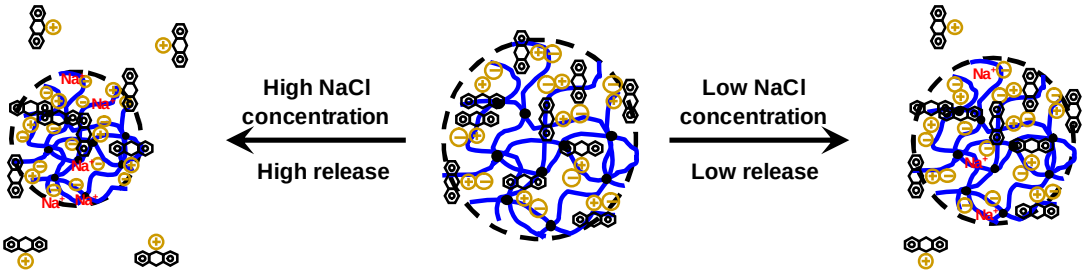

Figure 8.21 Schematic diagram of nanogels under different NaCl concentrations.

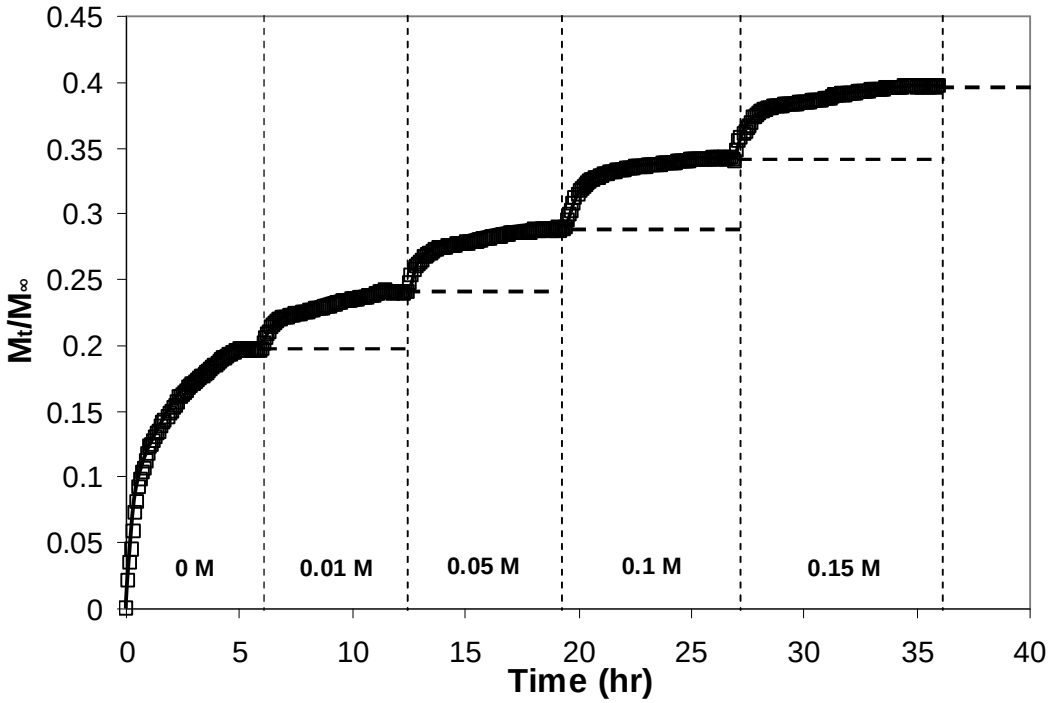

Figure 8.22 In-vitro release profile of IMI from 0.1 wt% HASE 50-50-4 in a changing NaCl concentration environment.

The normalized IMI released profile under step change in NaCl concentration was plotted in Figure 8.22 from IMI loaded HASE 50-50-4 nanogels at pH 5. The first 6 hours of study was conducted at 0 M NaCl and the NaCl concentration was increased to 0.01 M and the release profile was monitored for 6.5 hours. The next 7 hours of the release was performed at 0.05 M NaCl. Then the release was conducted in 0.1 M NaCl for 7.5 hours and finally the NaCl was increased to 0.15 M and the release was monitored for 9 hours. Data from Figure 8.22 showed that the amount of IMI released increased from ~20% to ~24% when the NaCl concentration was increased from 0 to 0.01 M respectively and further increase in NaCl concentration from 0.05 to 0.1 to 0.15 M resulted in a further increase in the release from ~29% to ~34% to ~40% respectively. Since the IMI was loaded electrostatically to HASE 50-50-4, the concentration of NaCl will have an impact on the release behavior. The release of IMI

will depend on NaCl concentration where an increase in NaCl will promote the release of IMI.

8.3.3 Varying cross-linking density

Drug release profiles obtained for 0.1 wt% MAA-EA nanogels containing 20 mole percent MAA with varying cross-linking density in 30-millilitre 10 mM PB at pH 5 is shown in Figure 8.23. The effect of changing the cross-linking density will change the porosity of the nanogels.

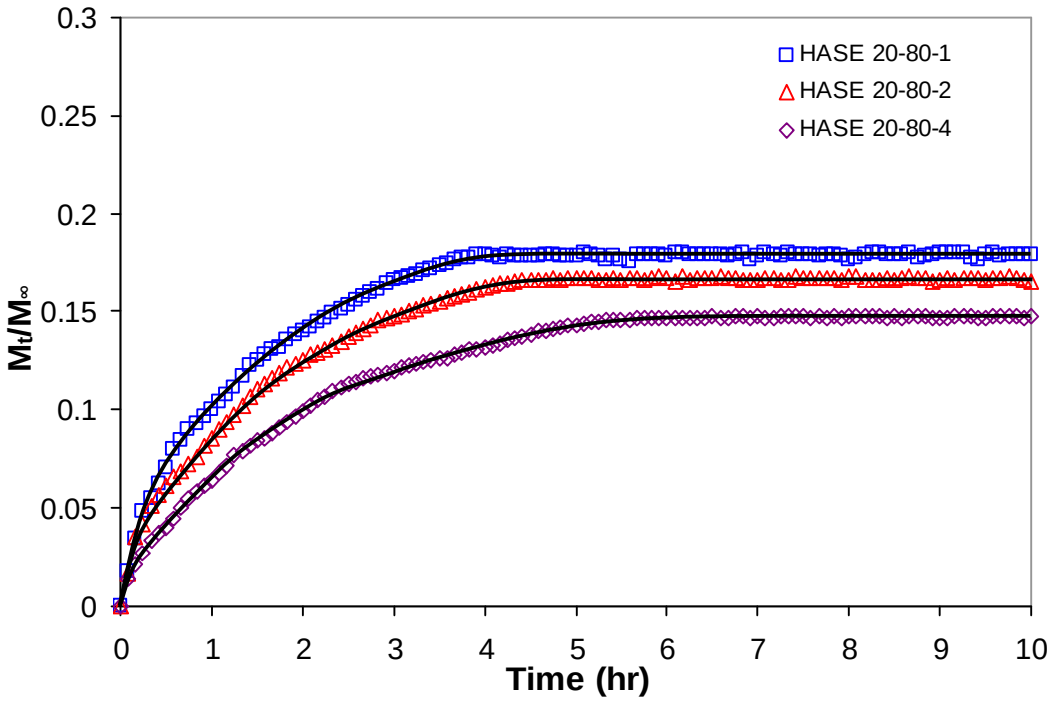

Figure 8.23 Release profile for 0.1 wt% MAA-EA nanogels containing 20 mole percent MAA with varying cross-linking density (a) HASE 20-80-1 (□), (b) HASE 20-80-2 (△) and (c) HASE 20-80-4 (◇) in 30-millilitre 10 mM PB solution at pH 5.

Nanogels with lower cross-linking density exhibited a faster release rate compared to nanogels with higher cross-linking density. At lower cross-linking density, the network is loose and possesses a greater hydrodynamic free volume. This will allow the chains to accommodate more solvent molecules resulting in a higher swelling, which will promote a higher fractional release of drugs as evident in HASE 20-80-1. HASE 20-80-1 has the steepest slope and fastest time to attain equilibrium compared to HASE 20-80-2 and HASE 20-80-4. HASE 20-80-1 will have larger pore sizes due to a lower cross-linking density, which reduces the diffusion barrier for the drug molecules to diffuse from the nanogels. By increasing the cross-linking density, the nanogels became more rigid and the hydrodynamic free volume decreased, which resulted in a slower release rate and lower fractional release. Since nanogels with lower cross-linking density are less rigid, the swelling rate will be faster thus increasing the rate of drug release. Similar results were obtained by Soppimath et al. using polyacrylamide-g-guar gum nanogel, Kurkuri and Aminabhavi using poly(acrylic acid) and poly(vinyl alcohol) cross-linked with glutaraldehyde pH sensitive microspheres and El-Sherbiny et al. using poly[N-acryloylglycine-chitosan] nanogels [Soppimath et al., 2001; Kurkuri and Aminabhavi, 2004; El-Sherbiny et al., 2005].

8.3.4 Varying MAA-EA molar ratio

Drug release profiles obtained for 0.1 wt% MAA-EA nanogels containing 4 wt% DAP and varying MAA-EA molar ratio in 30-millilitre 10 mM PB at pH 5 is shown in Figure 8.24. By changing the amounts of MAA groups, the osmotic pressure will change thus the degree of swelling and porosity will be different.

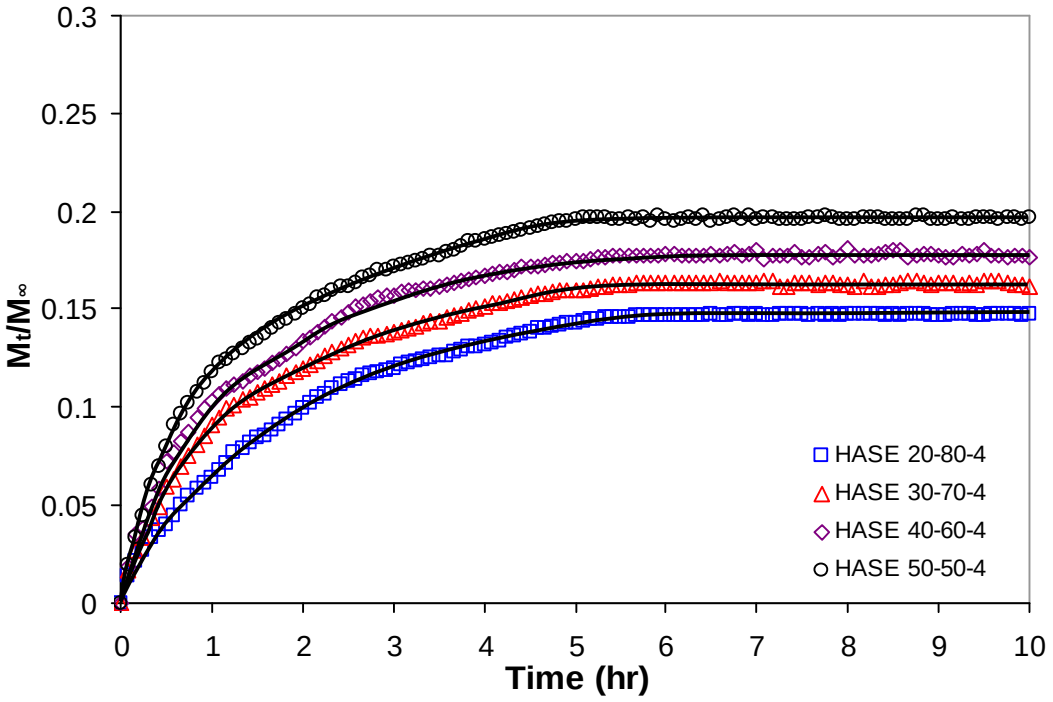

Figure 8.24 Release profile for 0.1 wt% MAA-EA nanogel containing 4 wt% DAP with varying MAA-EA molar ratio (a) HASE 20-80-4 (□), (b) HASE 30-70-4 (△), (c) HASE 40-60-4 (◇) and (d) HASE 50-50-4 (○) in 30-millilitre 10 mM PB solution at pH 5.

Nanogels with higher MAA-EA molar ratio have a higher fractional release and faster release rate. Nanogels with higher MAA-EA molar ratio will have higher water uptake capacity due to the presence of more COOH groups. This will increase the matrix swelling capacity as well as increasing the porosity of the nanogels. The swelling rate increased with more COOH groups leading to a faster release rate as evident from the steeper slope in Figure 8.24. Similar results were obtained by Kim and Peppas using PMAA-g-EG hydrogel, Kurkuri and Aminabhavi using poly(acrylic acid) and poly(vinyl alcohol) cross-linked with glutaraldehyde pH sensitive microspheres and El-Sherbiny et

al. using poly[N-acryloylglycine-chitosan] nanogels [Kim and Peppas, 2003; Kurkuri and Aminabhavi, 2004; El-Sherbiny et al., 2005].

8.4 Summary

IMI was loaded to the MAA-EA nanogels through electrostatic attraction, hydrogen bonding and hydrophobic interaction. There was no change in the enthalpy profile when the cross-linking density was changed as the amount of MAA groups remained the same. However, when the amount of MAA groups was increased, the enthalpy decreased as there was a reduction in hydrophobic interaction. MAA-EA nanogels could load and release two different kinds drugs, which were bound electrostatically, hydrophobically and via hydrogen bonding. Therefore with a single drug delivery system (MAA-EA nanogels), many types of cationic drug could be loaded and released.

The particle size of the MAA-EA nanogels decreased at low IMI concentration due to charge shielding, and increased when aggregation of nanogels loaded IMI occurred. The reduction in cross-linking density, and increased in MAA-EA molar ratio enhanced the drug loading capability.

The release of IMI under varying parameters: pH, NaCl concentration in release medium, cross-linking density and MAA-EA molar ratio was studied. Parameters that disrupted the electrostatic attraction would increase the fractional drug release. The amount of drugs release was found to increase with increasing NaCl concentration in the release medium and MAA-EA molar ratio. However, the fractional release would decrease with increasing pH and cross-linking density. A continuous monitoring of the release profiles at step changes in pH and NaCl concentration was conducted using the drug selective electrode. The viability of tuning the release profiles of drug released from a pH-responsive nanogel system by changing the pH and NaCl concentration was

demonstrated. The interaction between drug and drug delivery nano-carriers would determine the release patterns, and knowing the effective therapeutical period of the nano-carriers, could lead to a better designed drug delivery system for better interaction with drugs to have a better control during the release.

9.0 CONCLUSIONS

The characteristics of pH-responsive nano-colloidal systems consisting of methacrylic acid-ethyl acrylate (MAA-EA), methacrylic acid-butyl methacrylate (MAA-BMA) and methacrylic acid-methyl methacrylate (MAA-MMA) cross-linked with di-allyl phthalate (DAP) were synthesized for drug delivery applications. Neutralization of acid groups increased the osmotic pressure exerted by counter-ions trapped in the polymeric network against the ions in bulk solution, which was responsible for the swelling.

In Chapter 4, a novel technique in utilizing a drug selective electrode for studying drug release profiles was proposed. Two drug selective membranes, procaine hydrochloride (PrHy) and imipramine hydrochloride (IMI), was constructed through the variations in amount of ion-exchangers to solvent mediator to drug complex. These membranes exhibited excellent reproducibility and stability, which are important for usage as a detection device in drug delivery application. With the addition of ion-exchanger, the sensitivity and Nernstian response improved due to the added stability, and increase in electroactive site carriers for transferring ions. However, deviations from linear response occurred at high concentrations due to the aggregation of drug molecules. The pK_a value of PrHy and IMI obtained by the drug electrode was similar to those reported in literature. There was a limited range of pH, which the drug electrodes produced a stable response. At pH > 8.5, drug molecules would be deprotonated and at pH < 3, large amount of H^+ ions would interfere with the results.

In Chapters 5 and 8, the ability of MAA-EA nanogels to deliver drugs that were bound by hydrophobic, electrostatic or hydrogen bonding interactions was demonstrated. These different kinds of interactions will result in different release profiles and hence would be important in the design of a delivery carrier, where the released of drugs could be triggered by pH changes. The interaction between PrHy and MAA-EA nanogels was driven by hydrophobic forces, while IMI partitioned to the MAA-EA nanogels induced by electrostatic interaction and hydrogen bonding. The amount of drugs loaded would be affected by cross-linking density and MAA-EA molar ratio. An increase in MAA-EA molar ratio or decrease in cross-linking density will promote drug loading. Drug release was conducted under varying parameters: concentration gradient, cross-linking density, MAA-EA molar ratio, pH and drug loading ratio. The amount of drugs release was found to increase with increasing concentration gradient difference, MAA-EA molar ratio and pH. A higher concentration gradient would increase the driving force to expel the loaded drugs while an increase in MAA content or pH would decrease the diffusion barrier. For the release of IMI, at a lower pH, the release would be higher as electrostatic interaction was weakened. The fractional release decreased with increasing cross-linking density and drug loading ratio. The increase in cross-linking density increased the diffusion barrier while an increase in drug loading would make the nanogel more hydrophobic that reduced the access of the solvent molecules to the drugs. A step change in pH was conducted and the drug selective electrode (DSE) was able to monitor the release of drugs with changing pH. The results demonstrated the viability of tuning the release profiles of drug from a pH-responsive nanogel system. Berens and Hopfenberg model was successfully fitted to the kinetic data and the role of chain relaxation (f_R) and diffusion process (f_F) was distinguished for drug release from a pH-responsive nanogel.

Successful preparation of coated nanogels with encapsulated drugs using the layer by layer (LBL) approach was documented in Chapter 6. The initial burst release behavior observed in nanoparticles was minimized and eliminated by the introduction of several polyelectrolyte layers. Through this LBL approach, the permeability of nanogels was altered and with each additional polyelectrolyte layer, the time to achieve the steady state drug concentration (τ_D) increased linearly with polyelectrolyte layer (L). The swelling behavior of coated nanogels decreased with increasing polyelectrolyte layers resulting in a slower release of drugs. The colloidal stability of coated nanogel was maintained up to pH 8 for PAH coated system, while it was always maintained at all pH for PSS coated system. LBL coating of pH-responsive nanogels provided solution in the use of nanoparticles in drug delivery applications, where the high initial burst release and short therapeutic time range were overcome. The findings provide a useful guide in the design of coated responsive nanogels for controlled drug delivery applications.

Nanogels with varying glass transition temperature (T_g) (MAA-EA, MAA-BMA and MAA-MMA) were used to study the effects of T_g on the release of PrHy (Chapter 7). The swelling ratio was found to be lowered when chain rigidity is high (high T_g). There is a delay in the transition point, where osmotic pressure exceeded the hydrophobic attraction between polymer segments and chain rigidity to significantly swell the nanogels. Drug loading was proportional to the hydrophobicity of monomers and inversely proportional to T_g. The higher T_g would lower the swelling thus reducing the porosity of the nanogels, which would increase the diffusion barriers. The release of PrHy under varying parameters: pH and T_g was studied. Parameters that encourage the diffusion process of drugs from the interior to exterior of the nanogels would increase the fractional drug release. The amount of drugs release was found to increase with pH and

nanogels with lower T_g as the increase in pH and lowering of T_g would decrease the diffusion barrier.

10.0 RECOMMENDATIONS FOR FUTURE WORK

The significant breakthrough in this current study is the development of a drug selective electrode (DSE) to obtain the drug release profile for the release of procaine hydrochloride (PrHy) and imipramine hydrochloride (IMI) from pH-responsive drug carriers. From the experimental results, the validity and ability of the electrode to determine the drug release profile suitable for the fitting of the Berens and Hofenberg model was demonstrated. With these findings, a more sensitive and Nernstian response drug electrode could be produced by making variations to the ion exchangers or additives and solvent mediators or plasticizers. Different ion exchangers like sodium tetrakis [3, 5-bis(trifluoromethyl)phenyl] borate (NaTFPB) and potassium tetrakis(p-chlorophenyl) borate (KTpCIPB) would be used. Tris(2-ethylhexyl) trimellitate (TEHT) and dioctyl phthalate (DOP) are possible solvent mediators to be varied in the investigation.

Through the layer by layer (LBL) coating, the burst release could be either lowered or eliminated and the release of drugs could be prolonged as a function of the number of coated layers. Based on this finding, a mixture of drugs could be incorporated at different layers leading to different release rates to match therapeutic requirements. For example, a drug that is not needed regularly could be located nearer the matrix of the drug carrier while other drugs could be incorporated nearer the surface of the coated particles. In this way, a mixture of drugs could be released at different rates with a single dosage of drug carriers. Biodegradable polyelectrolytes could be used to coat the drug carriers and various drugs could be loaded at different layers to achieve a controlled release.

Polyampholyte MAA-DEA nanogels, which can be protonated or deprotonated to obtain positive or negative charge respectively, can be used to deliver proteins. As proteins could be negatively or positively charged, the MAA-DEA nanogels will be very useful in loading and releasing proteins. The molar ratio of MAA to DEA could be varied to control the isoelectric point (IEP) to match the IEP of the proteins and loading and releasing of proteins could be achieved.

REFERENCES

Aboul-Enein, H. Y., Sun, X. X. (2000). "A novel ion selective PVC membrane electrode for determination of propranolol in pharmaceutical formulation." **Analusus.,** 28, 855-858.

Abrol, S., Solomon, D. H. (1999). "Studies on microgels: 4. The effect of solvent on the synthesis of t-butylstyrene-divinylbenzene microgels by anionic polymerization." **Polymer.,** 40, 6583-6589.

Alizadeh, N., Mehdipour, R. (2002). "Drug-selective electrode for ketamine determination in pharmaceutical preparations and electrochemical study of drug with BSA." **Journal of Pharmaceutical & Biomedical Analysis.,** 30, 725-731.

Antipov, A. A., Sukhorukov, G. B. (2004). "Polyelectrolyte multilayer capsules as vehicles with tunable permeability." **Advances in Colloid and Interface Science.,** 111, 49-61.

Antonietti, M., Bremsr, W., Schmidt, M. (1990). "Microgels: Model polymers for the cross-linked state." **Macromolecules.,** 23, 3796-3805.

Antionietti, M., Pakula, T., Bremser, W. (1995). "Rheology of small spherical polystyrene microgels: A direct proof for a new transport mechanism in bulk polymers besides reputation." **Macromolecules.,** 28, 4227-4233.

Arifin, D. Y., Lee, L. Y., Wang, C. H. (2006). "Mathematical modeling and simulation of drug release from microspheres: Implications to drug delivery systems." **Advanced Drug Delivery Reviews,** 58, 1274-1325.

Barnes, H. A. (1989). **An introduction to rheology.** London, Elsevier.

Bartsch, E., Frenz, V., Baschnagel, J., Schartel, W., Sillescu, H. (1997). "The glass transition dynamics of polymer micronetwork colloids. A mode of coupling analysis." **J. Chem. Phys.,** 106, 3743-3756.

Benee, L., Snowden, M. J., Chowdhry, B. Z. (2002). **Encyclopedia of advanced materials.** New York, Wiley.

Benita, S., Barkai, A., Pathak, Y. V. (1990). "Effect of drug loading extent on the in vitro release kinetic behaviour of nifedipine from polyacrylate microspheres." **Journal of Controlled Release.,** 12, 213-222.

Berens, A. R., Hopfenberg, H. B. (1978). "Diffusion and relaxation in glassy polymer powders: 2. Separation of diffusion and relaxation parameters." **Polymer.,** 19, 489-496.

Boileau, S., Bouteiller, L., Foucat, E., Lacoudre, N. (2002). "Stable low molecular weight glasses based on mixtures of bisphenol-A and bispyridines." **Journal of Materials Chemistry.,** 12, 195–199.

Bolle, T. (1993). Microemulsion polymerization of 1,4-divinylbenzene and styrene., University of Stuttgart.

Borrega, R., Cloitre, M., Betremieux, I., Ernst, B., Leibler, L. (1999). "Concentration dependence of the low-shear viscosity of polyelectrolyte micro-networks: From hard spheres to soft microgels." **Europhys. Lett.,** 47, 729-735.

Bouklouze, A. A., El Jammal, A., Vire, J. C., Patriarche, G. J. (1992). "Comparative study of three polymeric membrane electrodes selective to tizanidine." **Analytica Chimica Acta.,** 257, 41-48.

Bromberg, L. (1998). "Properties of aqueous solution and gels of poly(ethylene oxide)-b-poly(propylene oxide)-b-poly(ethylene oxide)-g-poly(acrylic acid)." **J. Phys. Chem. B,** 102, 10736-10744.

Brown, W. (1993). **Dynamics Light Scattering - the Method and Some Applications.** Boston, Clarendon Press.

Bruce, A., Bray, D., Lewis, J., Raff, M., Roberts, K., Watson, J. D. (1994). **Molecular Biology of the Cell.** New York, Garland.

Burke, S. E., Barrett, C. J. (2004). "pH-dependent loading and release behavior of small hydrophilic molecules in weak polyelectrolyte multilayer films." **Macromolecules.,** 37, 5375-5384.

Carothers, W. H. (1931). "Polymerization." **Chem. Rev.,** 8, 353-426.

Caruso, F., Caruso, R. A., Möhwald, H. (1998). "Nanoengineering of inorganic and hybrid hollow spheres by colloidal templating." **Science.,** 282, 1111-1114.

Caruso, F., Lichtenfeld, H., Donath, E., Möhwald, H. (1999). "Investigation of electrostatic interactions in polyelectrolyte multilayer films: Binding of anionic fluorescent probes to layers assembled onto colloids." **Macromolecules.,** 32, 2317-2328.

Chen, L. W., Yang, B. Z., Wu, M. L. (1997). "Synthesis and kinetics of microgel in inverse emulsion polymerization of acrylamide." **Progree in Organic Coatings.,** 31, 393-399.

Chu, B. (1991). **Laser Light Scattering - Basic Principles and Practice.** Boston, Academic Press.

Clarke, J., Vincent, B. (1981). "Stability of non-aqueous microgel dispersions in the presence of free polymer." **J. Chem. Soc. Faraday Trans.,** 77, 1831-1843.

Cloitre, M., Borrega, R., Monti, F., Leibler, L. (2003). "Structure and flow of polyelectrolyte microgels: from suspensions to glasses." **C. R. Physique.,** 4, 221-230.

De Geest, B. G., Déjugnat, C., Verhoeven, E., Sukhorukov, G. B., Jonas, A. M., Plain, J., Demeester, J., De Smedt, S. C. (2006). "Layer-by-layer coating of degradable microgels for pulsed drug delivery." **Journal of Controlled Release.,** 116, 159-169.

Decher, G. (1997). "Fuzzy nanoassemblies: Toward layered polymeric multicomposites." **Science.,** 277, 1232-1237.

Eichenbaum, G. M., Kiser, P. F., Dobrynin, A. V., Simon, S. A., Needham, D. (1999). "Investigation of the swelling response and loading of ionic microgels with drugs and proteins: The dependence on cross-link density." **Macromolecules.,** 32, 4867-4878.

Eichenbaum, G. M., Kiser, P. F., Shah, D., Simon, S. A., Needham, D. (1999). "Investigation of the swelling response and drug loading of ionic microgels: The dependence on functional group composition." **Macromolecules.,** 32, 8996-9006.

El-Sherbiny, I. M., Lins, R. J., Abdel-Bary, E. M., Harding, D. R. K. (2005). "Preparation, characterization, swelling and in-vitro drug release behaviour of poly[N-acryloylglycine-chitosan] interpolymeric pH and thermally-responsive microgel." **European Polymer Journal.,** 41, 2584-2591.

Enscore, D. J., Hopfenberg, H. B., Stannett, V. T. (1977). "Effect of particle size on the mechanism controlling n-hexane sorption in glassy polystyrene microspheres." **Polymer.,** 18, 793-800.

Flory, P. J. (1941). "Molecular size distribution in three dimensional polymers. I. Gelation." **J. Am. Chem. Soc.,** 63, 3083-3090.

Flory, P. J. (1953). **Principles of Polymer Chemistry.** New York, Cornell University Press.

Foss, A. C., Goto, T., Morishita, M., Peppas, N. A. (2004). "Development of acrylic-based copolymers for oral insulin delivery." **European Journal of Pharmaceutics and Biopharmaceutics.,** 57, 163-169.

Frank, M., Burchard, W. (1991). "Microgels by intramolecular crosslinking of poly(allylamine) single chains." **Makromol. Chem. Rapid Commun.,** 12, 645-652.

Frisch, H. L. (1969). "Diffusion in glassy polymer." **Journal of Polymer Science.,** 7, 879-887.

Fu, B., Yun, J. H., Wahr, J., Meyerhoff, M. E., Yang V. C. (1996). "Polyionic drug-sensitive membrane electrodes: principles and practice." **Advances Drug Delivery Reviews.,** 21, 215-223.

Funasaki, N., Hada, S. (1980). "Coexistence of two kinds of mixed micelles." **Journal of Physcial Chemistry.,** 84, 736-744.

Funke, W. E., Okay, O., Joos-Muller, B. (1998). "Microgels intramolecularly cross-linked macromolecules with a globular structure." **Advances in Polymer Science.,** 136, 140-234.

Graham, N. B., Mao, J. (1996). "Microgels Part 2. Solution polymerization using a urethane setpgrowth mechanism." **Colloids and Surfaces A: Physicochemical and Engineering Aspects.,** 118, 211-220.

Govender, T., Stolnik, S., Garnett, M. C., Illum, L., Davis, S. S. (1999). "PLGA nanoparticles prepared by nanoprecipitation: drug loading and release studies of a water soluble drug." **Journal of Controlled Release.,** 57, 171-185.

Guo, L. (1997). Rheology of alkali-soluble associative polymer in aqueous solution. School of Mechanical and Production Engineering. Singapore, Nanyang Technological University.

Hemminger, W. (1994). **Calorimetric Methods. Calorimetry and Thermal Analysis of Polymers.** New York, Hanser Publishers**,** 17.

Hirsjärvi, S., Peltonen, L., Hirvonen, J. (2006). "Layer-by-layer polyelectrolyte coating of low molecular weight poly(lactic acid) nanoparticles." **Colloids and Surfaces B: Biointerfaces.,** 49, 93-99.

Homola, A., James, R. O. (1977). "Preparation and characterization of amphoteric polystyrene lattices." **Journal of Colloid and Interface Science.,** 59, 123-134.

Huang, J., Kao, H., Wu, X. Y. (2000). "The pH-dependent biphasic release of azidothymidine from a layered composite of PVA disks and P(MMA/MAA) spheres." **Journal of Controlled Release.,** 67, 45-54.

Huang, L., Somasundaran, P. (1993). "Changes in micelles compositions and monomer concentrations in mixed surfactant solutions." **Langmuir.,** 9, 5790-5795.

Hunter, R. J. (2001). **Foundations of colloid science.** New York, Oxford University Press Inc.

Katsu, T., Mori, Y., Furuno, K., Gomita, Y. (1999). "Mexiletine-sensitive membrane electrode for medical application." **Journal of Pharmaceutical and Biomedical Analysis.,** 19, 585-593.

Khalil, S., Kelzieh, A., Ibrahim, S. A. (2003). "Ion-selective electrode for the determination of prazosin in tablets." **Journal of Pharmaceutical & Biomedical Analysis.,** 33, 825-829.

Kim, B., Peppas, N. A. (2003). "In vitro release behavior and stability of insulin in complexation hydrogels as oral drug delivery carriers." **International Journal of Pharmaceutics.,** 266, 29-37.

Kiser, P. F., Wilson, G., Needham, D. (2000). "Lipid-coated microgels for the triggered release of doxorubicin." **Journal of Controlled Release.,** 68, 9-22.

Kjoniksen, A. L., Nystrom, B., Iversen, C., Nakken, T., Palmgren, O., Tande, T. (1997). "Viscosity of dilute aqueous solutions of hydrophobically modified chitosan and its unmodified analogue at different conditions of salt and surfactant concentrations." **Langmuir.,** 13, 4948-4952.

Koppel, D. E. (1972). "Analysis of Macromolecular Polydispersity in Intensity Correlation Spectroscopy: The method of Cumulants." **J. Chem. Phys.,** 57, 4814-4820.

Kositaz, M. J., Bohne, C., Alexandridis, P., Hatton, T. A., Holzwarth, J. F. (1999). "Dynamics of micro- and macrophase separation of amphiphilic block copolymers in aqueous solution." **Macromolecules.,** 32, 5539-5551.

Kumacheva, E., Rharbi, Y., Winnik, M. A., Guo, L., Tam, K. C., Jenkins, R. D. (1997). "Fluorescence studies of an alkaline swellable associative polymer in aqueous solution." **Langmuir.,** 13, 182-186.

Kumar, M. N. V. R., Kumar, N., Domb, A.J., Arora, M. (2002). "Pharmaceutical polymeric controlled drug delivery systems." **Advances in Polymer Science.,** 160, 45-117.

Kurkuri, M. D., Aminabhavi, T. M. (2004). "Poly(vinyl alcohol) and poly(acrylic acid) sequential interpenetrating network pH-sensitive microspheres for the delivery of diclofenac sodium to the intestine." **Journal of Controlled Release.,** 96, 9-20.

Langer, R. (2001). "Drug delivery: Drugs on target." **Science.,** 293, 58-59.

Leong, K. W., Langer, R. (1987). "Polymeric controlled Drug Delivery." **Advanced Drug Delivery Reviews,** 1, 199-233.

Liu, Z., Cheung, R., Wu, X. Y., Ballinger, J. R., Bendayan, R., Rauth, A. M. (2001). "A study of doxorubicin loading onto and release from sulfopropyl dextran ion-exchange microspheres." **Journal of Controlled Release.,** 77, 213-224.

Lopez, V. C., Hadgraft, J., Snowden, M. J. (2005). "The use of colloidal microgels as a transdermal drug delivery system." **International Journal of Pharmaceutics.,** 292, 137-147.

Madeline, T.-L., Nikolaos, A. Peppas (1999). "Molecular design and in vitro studies of novel pH-sensitive hydrogels for the oral delivery of calcitonin." **Macromolecules.,** 32, 6646-6651.

Makayssi, A., Lemordant, D., Treiner, C. (1993). "Structural change and micellar composition in aqueous solution of binary cationic surfactant mixtures as deduced from cross-flow ultrafiltration experiments." **Langmuir.,** 9, 2808-2813.

Mathiowitz, E. (1999). **Encyclopedia of controlled drug delivery**, John Wiley and Sons.

Matsummura, Y., Iwai, K. (2005). "Synthesis and thermo-respomsive behavior of fluorescent labeled microgel particles based on poly(N-isopropylacryamide) and its related polymers." **Polymer.,** 46, 10027-10034.

Neyret, S., Vincent, B. (1997). "The properties of polyampholyte microgel particles prepared by microemulsion polymerization." **Polymer.,** 38, 6129-6134.

Noggle, J. H. (1996). **Physics Chemistry.** New York, Harpercollins Colledge Publisher.

Okay, O., Funke, W. (1990). "Anionic dispersion polymerization of 1,4-divinylbenzene." **Macromolecules.,** 23(2623-2628).

Okay, O., Funke, W. (1990). "Steric stabilization of reactive microgels from 1, 4-divinylbenzene." **Makromol. Chem. Rapid Commun.,** 11, 583-587.

Okubo, M., Inoue, M., Suzuki, T., Kouda, M. (2004). "Effect of hydrophilicity of polymer particles on their glass transition temperatures in the emulsion state." **Colloid Polymer Science.,** 282, 1150-1154.

Pelton, R. H., Chibante, P. (1986). "Preparation of aqueous latices with N-isopropylacrylamide." **Colloids Surf.,** 20, 247-256.

Pillay, V., Fassihi, R. (1999). "In vitro release modulation from crosslinked pellets for site-specific drug delivery to the gastrointestinal tract. I. Comparison of pH-responsive drug release and associated kinetics." **Journal of Controlled Release.,** 59, 229-242.

Pungor, E. (1998). "The theory of Ion-Selective Electrodes." **Anal. Sci.,** 14, 249-256.

Richards, J. H. (1985). **The role of polymer permeability in the control of drug release. Polymer permeability.** J. Comyn. London, Elsevier**,** 217-267.

Ritger, P. L., Peppas, N. A. (1987). "A simple equation for description of solute release II. Fickian and anomalous release from swellable devices." **Journal of Controlled Release.,** 5, 37-42.

Rodriquez, B. E., Wolfe, M. S. (1994). "Nonuniform swelling of alkali swellable microgels." **Macromolecules.,** 27, 6642-6647.

Roman, R. A., Naik, A., Kalia, Y. N., Guy, R. H., Fessi, H. (2004). "Skin penetration and distribution of polymeric nanoparticles." **Journal of Controlled Release.,** 99, 53-62.

Rong, X. (2001). Equilibrium studies of aqueous surfactant systems containing additives. Institute for Materials Research. Salford, UK, University of Salford.

Sahoo, S. K., De Tapas, K., Ghosh, P. K., Maitra, A. (1998). "pH- and thermo-senisitive hydrogel nanoparticles." **Journal of Colloid and Interface Science.,** 206, 361-368.

Saunders, B. R., Crowther, H. M., Vincent, B. (1997). "Poly[(methyl methacrylate)-co-(methacrylic acid)] microgel particles: Swelling control using pH, cononsolvency and osmotic deswelling." **Macromolecules.,** 30, 482-487.

Saunders, B. R., Vincent, B. (1999). "Microgel particles as model colloids: theory, properties and applications." **Advances in Colloid Interface Science.,** 80, 1-25.

Sen, M., Yakar, A., Guven, O. (1999). "Determination of average molecular weight between cross-links from swelling behaviours of diprotic acid-containing hydrogels." **Polymer.,** 40, 2969-2974.

Senel, S., Isik-Yruksoy, B., Cicek, Tuncel, A. (1997). "Thermoresponsive N-isopropylacryamide-vinylpyrrolidone copolymer by radiation polymerization." **J. Appl. Polym. Sci.,** 64, 1775-1784.

Shahrokhian, S., Hamzahloei, A., Bagherzadeh, M. (2002). "Chromium(III) porphyrin as a selective ionophore in a salicylate-selective membrane electrode." **Anal. Chem.,** 74, 3312-3320.

Shashoua, V. A., Beaman, R. G. (1958). "Microgel: An idealized polymer molecule." **J. Polym Sci.,** 33, 101-117.

Sieglaff, C. L. (1963). "Viscosity and swelling behaviour of lightly cross-linked microgels." **Polymer.,** 4, 281-284.

Soppimath, K. S., Kulkarni, A. R., Aminabhavi, T. M. (2001). "Chemically modified polyacrylamide-g-guar gum-based crosslinked anionic microgels as pH-sensitive drug delivery systems: preparation and characterization." **Journal of Controlled Release.,** 75, 331-345.

Srinivasan, K., Rechnitz, G. A. (1969). "Selectivity studies on liquid membrane, ion-selective electrodes." **Anal. Chem.,** 41(10), 1203-1208.

Stefan, R. I., Aboul-Enein, H. Y. Baiulescu, G. E. (1996). "Amiodarone-selective membrane electrode." **Sensors and Actuators B.,** 37, 141-144.

Sutani, K., Kaetsu, I., Uchida, K., Matsubara, Y. (2002). "Stimulus responsive drug release from polymer gel. Controlled release of ionic drug from polyampholyte gel." **Radiation Physics and Chemistry.,** 64, 331-336.

Takisawa, N., Hall, D. G., Wyn-Jones, E., Brown, P. (1988). "The construction and characteristics of drug-selective electrodes." **J. Chem. Soc. Faraday Trans. 1.,** 84, 3059-3070.

Tan, B. H., Tam, K. C., Lam, Y. C., Tan, C. B. (2004). "Microstructure and rheology of stimuli-responsive nano-colloidal systems - effect of ionic strength." **Langmuir.,** 20, 11380-11386.

Tan, B. H., Tam, K. C., Lam, Y. C., Tan, C. B. (2005). "Microstructure and rheology of stimuli-responsive nano-colloidal systems - effect of cross-linker density." **Advances in Colloid and Interface Science.,** 113, 111-120.

Tan Maureen, B. H. (2004). Dynamics and microstructure of pH-responsive nano-colloidal particles. School of Mechanical and Production Engineering. Singapore, Nanyang Technological University.

Tang, Z., Wang, Y., Podsiadlo, P., Kotov, N. A. (2006). "Biomedical applications of layer-by-layer assembly: From biomimetics to tissue engineering." **Advanced Materials.,** 18, 3203-3224.

Tjipto, E., Quinn, J. F., Caruso, F. (2005). "Assembly of multilayer films from polyelectrolytes containing weak and strong acid moieties." **Langmuir.,** 21, 8785-8792.

Toti, U. S., Aminabhavi, T. M. (2004). "Modified guar gum matrix tablet for controlled release of diltiazem hydrochloride." **Journal of Controlled Release.,** 95, 567-577.

Vytras, K. (1989). "The use of ion-selective electrodes in the determination of drug substances." **Journal of Pharmaceutical & Biomedical Analysis.,** 7(7), 789-812.

Wang, C., Tam, K. C., Jenkins, R. D., Bassett, D. R. (2000). "Potentiometric titration and dynamic light scattering of hydrophobically modified alkali soluble emulsion (HASE) polymer solutions." **J. Phys. Chem. Chem. Phys.,** 2, 1967-1972.

Wang, C., Tam, K. C. (2002). "New insights on the interaction mechanism within oppositely charged polymer/surfactant systems." **Langmuir.,** 18, 6484-6490.

Wang, C. (2004). Association behaviors of amphiphilic polyelectrolytes and interactions between oppositely charged polymer and surfactants. School of Mechanical and Production Engineering. Singapore, Nanyang Technological University.

Wang, C., Tam, K. C., Tan, C. B. (2005). "Dissolution and swelling behaviors of random and cross-linked methacrylic ccid-ethyl acrylate copolymers." **Langmuir.,** 21, 4191-4199.

Warr, G. G., Grieser, F., Healy, T. W. (1983). "Composition of mixed micelles of polydisperse nonionic surfactants." **Journal of Physcial Chemistry.,** 87, 1220-1223.

Watanabe, K., Okada, K., Oda, H., Furuno, K., Gomita, Y., Katsu, T. (1995). "New cocaine-selective membrane electrode." **Analytica Chimica Acta.,** 316, 371-375.

Werff, V. D., Kruif, C. G. (1989). "Hard-sphere colloidal dispersions: The scaling of rheological properties with particle size, volume fraction and shear rate." **J. Rheology.,** 33, 421-454.

Wiseman, T., Williston, S., Brandts, J., Lin, L. (1989). "Rapid measurement of binding constants and heats of binding using a new titration calorimeter." **Analytical Biochemistry.,** 179, 131-137.

Wolfe, M. S., Scopazzi, C. (1989). "Influence of cross-linking density on microgel interaction." **J. Colloid Interface Sci.,** 133, 265-282.

Xiong, X. Y., Tam, K. C., Gan, L. H. (2001). "Release kinetics of hydrophobic and hydrophilic model drugs from Pluronic F127/poly(lactic acid) nanoparticles." **Journal of Controlled Release.,** 103, 73-82.

Yang, M., Cui F., You, B., Wang, L., Yue, P., Kawashima, Y. (2004). "A novel pH-dependent gradient-release delivery system for nitrendipine. II. Investigations of the factors affecting the release behaviors of the system." **International Journal of Pharmaceutics.,** 286, 99-109.

Zhang, Y., Zhu, W., Wang, B., Ding, J. (2005). "A novel microgel and associated post-fabrication encapsulation technique of protein." **Journal of Controlled Release.,** 105, 260-268.

APPENDIX A

Values of the parameters corresponding to the Berens and Hopfenberg model at different coated layers.

Berens and Hopfenberg model:

$$\frac{M_t}{M_\infty} = 1 - f_F\left[\frac{6}{p^2}\sum_{n=1}^{\infty}\frac{1}{n^2}\exp\left(-4p^2n^2Dt/d^2\right)\right] - f_R\exp(-kt)$$

where D is the diffusion coefficient for the Fickian portion of the transport, k is the first-order relaxation constant, f_F and f_R are the fractions of sorption contributed by Fickian diffusion and chain relaxation respectively, d is the diameter of sphere and t is time. This analysis can lead to the determination of diffusion coefficient (D), and characteristic relaxation time (τ), which is a reciprocal of k.

d (nm)	f_F	f_R	**D (cm^2/s)**	t **(s)**
No coating				
122	0.94	0.06	2×10^{-15}	4.44×10^5
1st layer coating				
126	0.81	0.19	7.72×10^{-16}	9.34×10^5
2nd layer coating				
130	0.69	0.31	2.5×10^{-16}	1.58×10^6
3rd layer coating				
134	0.55	0.45	9.55×10^{-17}	3.35×10^6
4th layer coating				
139	0.48	0.52	5.61×10^{-17}	6.54×10^6
5th layer coating				
145	0.41	0.59	1.49×10^{-17}	1.21×10^7